An Experimental Study of Ionising Collisions Between Metastable Helium and Various Atoms and Molecules

By

Joseph Henry Sanderson

A thesis submitted for the degree of Doctor of Philosophy

of

The University of London

1991

ProQuest LLC.
789 East Eisenhower Parkway
P.O. Box 1346
Ann Arbor, MI 48106 – 1346

Abstract

This thesis presents a study of chemi-ionisation reactions involving the two metastable states of helium $He(2^3S)$ and $He(2^1S)$ with Ar, CO_2, N_2O, CH_4, C_2H_2, and NH_3, also of $He(2^3S)$ with SF_6. The experimental techniques developed to measure both the relative total ionisation cross sections and the branching ratios for the different reactions is described, and a theoretical analysis is carried out in the case of collisions between helium atoms in both metastable states and argon.

The relative variation of total ionisation cross section with velocity is carried out using the time-of-flight technique in a computer controlled experiment. The metastable atom source produces a wide velocity distribution (1 - 20 kms^{-1} or 0.02 - 8 eV). A newly-designed quench lamp enables the removal of fast $He(2^1S)$ metastable atoms from the beam. In every case except that of Ar + $He(2^1S)$ in the range 1 - 5 kms^{-1} measurements with helium atoms in the $He(2^1S)$ state are the first to be made. The measurements made for $He(2^3S)$ with N_2O and SF_6 are also completely new. To make measurements using $He(2^1S)$ the quench lamp is pulsed giving time-of-flight distributions with and without $He(2^1S)$ information. Measurements with only the $He(2^3S)$ state are subtracted from measurements with both states in order to determine the contribution from the $He(2^1S)$ state. The computer control is essential to store this information simultaneously, but the process is by necessity slow and involves an appreciable amount of time in which data is not being recorded.

To measure branching ratios for the different chemi-ionisation reactions as a function of collision velocity, a time-of-flight mass spectrometer is used to separate the different product ions. The pulsed quench lamp is used again in conjunction with computer control to record metastable atom time-of-flight distributions and ionisation time-of-flight spectra so that the variation of the ion branches with velocity can be seen. As with the relative ionisation cross sections, the $He(2^1S)$ data is new except in the case of argon. The $He(2^3S)$ data is also new in the case of N_2O and SF_6.

Various interaction potentials for Ar+$He(2^3S)$ and Ar+$He(2^1S)$ have been used to calculate theoretical ionisation cross sections for comparison with the present experimental data. The potentials have been modified to find the best fit to the present experimental data, and the general applicability of the new potentials has been assessed.

For my loving and supportive parents

Acknowledgements

To Dr Tony Smith for inviting me to join the group, for his supervision and help with the writing of this thesis.

To Dr Roy Newell and Dr Sid Corrigan for their helpful suggestions.

To Mr Ivan Rangué and Mr Ted Oldfield for their indispensable expert help in the design and construction of new apparatus.

To Mr Brian Humm for constructing and repairing numerous quench lamps.

To Dr Nigel Mason, Dr Wyndham Johnstone, Ms Sarah Barnett, Ms Joan Furlong for their encouragement and advice.

To Ms Lisa Harmey for her moral support and help with the graphs in this thesis.

To the SERC for a postgraduate studentship.

Contents

	Page
Abstract	2
Acknowledgements	4
List of figures	9
List of tables	12
Chapter 1 Introduction	13
1.1 Background	13
1.2 Present aims and thesis content	14
Chapter 2 Theoretical approach to Penning ionisation	16
2.1 Introduction	16
2.2 The two potential model	16
2.3 Limitations of the two potential model	20
2.4 Calculation of classical cross sections	20
2.5 Refinements to classical theory	23
2.6 The simplified analytical theory	24
Chapter 3 Experiments with metastable helium	26
3.1 Introduction	26
3.2 Stationary afterglow experiments	26
3.3 Flowing afterglow experiments	27
3.4 Beam experiments	29
3.4.1 Gas cell experiments	29

3.4.2 Simple crossed beam experiments 31
3.4.3 Crossed beam experiments incorporating time-of-flight 32
3.4.4 Crossed beam differential scattering experiments 34
3.4.5 Crossed beam Penning-ionisation-electron-spectroscopy experiments 36

Chapter 4 Experimental method and apparatus 41

4.1 Introduction and general experimental arangement 41

4.1.1 The vacuum system 42

4.2 The metastable atom beam and target beam 43

4.2.1 Construction of the metastable atom beam sourse 43
4.2.2 Cathode preparation 47
4.2.3 Operation and charactoristics of the source 47
4.2.4 Production of metastable He(2^1S) 49
4.2.5 Maximising the metastable atom beam intensity 50
4.2.6 The target beam 54

4.3 The quench lamp 56

4.3.1 Introduction 56
4.3.2 The quenching process 56
4.3.3 Lamp performance 58
4.3.4 The new quench lamp 62
4.3.5 Comparison of new and old lamps 63

4.4 Utilising He(2^1S) and He(2^3S) 64

4.5 Total ionisation cross section measurement 68

4.5.1 The TOF system and metastable atom detection 68
4.5.2 The photon masking circuit 68
4.5.3 The TOF mass spectrometor 70
4.5.4 Data recording for total ionisation cross sections and high count rate corrections 75
4.5.5 Data analysis 78

4.6 Branching ratios 82

4.6.1 Data collection and analysis 82
4.6.2 Detection efficiencies 84

4.7 Correction for the thermal motion of target atoms 87

Chapter 5 Results and discussion 90

5.1 Introduction 90

5.2 Ar + $He(2^3S)$ 93

5.3 Ar + $He(2^1S)$ 94

5.3 CO_2 + $He(2^3S)$ 95

5.4 CO_2 + $He(2^1S)$ 96

5.5 N_2O + $He(2^3S)$ 96

5.6 N_2O + $He(2^1S)$ 97

5.7 CH_4 + $He(2^3S)$ 97

5.8 CH_4 + $He(2^1S)$ 98

5.9 C_2H_2 + $He(2^3S)$ 98

5.10 C_2H_2 + $He(2^1S)$ 99

5.11 NH_3 + $He(2^3S)$ 99

5.12 NH_3 + $He(2^1S)$ 100

5.13 SF_6 + $He(2^3S)$ 100

Chapter 6 Comparison of theoretical and experimental results for collisions of $He(2^3S)$ and $He(2^1S)$ with Ar 136

6.1 Introduction 136

6.2 Fitting procedure 138

6.3 Comparison of theoretical and experimental results for $He(2^3S)$+Ar 138

6.4 Comparison of theoretical and experimental results for $He(2^1S)$+Ar 146

6.5 Approximate cross sections 150

Chapter 7 Conclusions and suggestions for further work 153

7.1 Conclusion 153

7.2 Possible improvements and suggestions for improvements and further work 154

Appendices

1	Recalculation of the constants C, B and D	156
2	Relay logic circuit	158
3	Photo-detector circuit	158
4	TOF logic circuit with photon mask	159
5	Detector supply circuits	160
6	TOF3	161
7	HIGHCOUNT	167
8	CROSCAL	169
9	CROSS2	174
10	TOFM1	177
11	BRCAL	182
12	OLTP	185
13	BRUTRP	186
14	SISKA	188
15	HAB77	190
16	MARTIN	192
17	CRS	194
18	FUNCTN	196

References 198

List of figures

Figure		Page
2.1	Two potential model of chemi-ionisation	17
3.1	Flowing afterglow apparatus of Schmeltekopf and Fehsenfeld (1971)	27
3.2	Gas cell apparatus of Jerram and Smith (1985)	30
3.3	Crossed beam apparatus of West et al (1975)	32
3.4	Crossed beam apparatus of Pesnelle et al (1975) incorporating TOF	33
3.5	Crossed beam apparatus of Brutschy et al (1976) for measuring elastic scattering cross sections	35
3.6	Differential elastic scattering cross for Ar + He(2^3S) at several energies	35
3.7	Crossed beam apparatus for PIES	36
3.8	Ejected electron energy distribution for Ar + He(2^1S)	38
3.9	Repulsive potential model for Ar + He(2^3S)	38
3.10	Attractive potential model for H_2O + He(2^3S)	39
3.11	Ejected electron energy distribution for H_2O + He^*	39
4.1	Schematic diagram of the apparatus	42
4.2a	Cross section through the metastable atom source designed and built by Trujillo (1975)	45
4.2b	Photograph of metastable atom source	46
4.3a	Metastable atom TOF distribution after several hours	49
4.3b	Metastable atom TOF distribution with new cathode	49
4.4a	Metastable beam intensity versus source pressure	53
4.4b	Pressure in the source versus pressure in tank T1	53
4.5	Comparison of new and old metastable atom intensity	55
4.6	The energy levels of helium	57
4.7	The quench lamp used by Harper (1977)	59
4.8	Variation of quenching efficiency with velocity	61
4.9	Variation of q(v) with quench lamp increased in length by a factor of 3	61
4.10	The new lamp shown next to an old lamp for scale	63
4.11a	Singlet to triplet ratio for new and old lamp	65
4.11b	Improvement in quenching efficiency (q)	65
4.12	Data recording cycle	67
4.13	Start pulse	69
4.14	Cross section through the interaction region	71
4.15a	Cross section through the multi-channel plate mounting	72
4.15b	Photograph of multi-channel plate mounting	73
4.16a,b,c	Correction of photon peak shape by HIGHCOUNT program	79
4.17a,b	Cross sections calculated from corrected and uncorrected TOF distributions	80
4.18a	Detection efficiencies for positive ions and electrons	86
4.18b	Variation of combined detection efficiency with mass	86

5.1	Energy resolution of experiment	92
5.2	Total ionisation cross section for Ar + $He(2^3S)$	103
5.3	Branching ratio for Ar + $He(2^3S)$	103
5.4	Total ionisation cross section for Ar + $He(2^1S)$	105
5.5	Branching ratio for Ar + $He(2^1S)$	105
5.6	Total ionisation cross sections for Ar + $He(2^1S)$ and $He(2^3S)$	106
5.7	Total ionisation cross section for CO_2 + $He(2^3S)$	108
5.8	Branching ratio for CO_2 + $He(2^3S)$	108
5.9	Total ionisation cross section for CO_2 + $He(2^1S)$	110
5.10	Branching ratio for CO_2 + $He(2^1S)$	110
5.11	Total ionisation cross section cross sections for CO_2 + $He(2^1S)$ and $He(2^3S)$	111
5.12	Total ionisation cross section for N_2O + $He(2^3S)$	113
5.13	Branching ratio for N_2O + $He(2^3S)$	113
5.14	Total ionisation cross section for N_2O + $He(2^1S)$	115
5.15	Branching ratio for N_2O + $He(2^1S)$	115
5.16	Total ionisation cross section cross sections for N_2O + $He(2^1S)$ and $He(2^3S)$	116
5.17	Total ionisation cross section for CH_4 + $He(2^3S)$	118
5.18	Branching ratio for CH_4 + $He(2^3S)$	118
5.19	Total ionisation cross section for CH_4 + $He(2^1S)$	120
5.20	Branching ratio for CH_4 + $He(2^1S)$	120
5.21	Total ionisation cross section cross sections for CH_4 + $He(2^1S)$ and $He(2^3S)$	121
5.22	Total ionisation cross section for C_2H_2 + $He(2^3S)$	123
5.23	Branching ratio for C_2H_2 + $He(2^3S)$	123
5.24	Total ionisation cross section for C_2H_2 + $He(2^1S)$	125
5.25	Branching ratio for C_2H_2 + $He(2^1S)$	125
5.26	Total ionisation cross section cross sections for C_2H_2 + $He(2^1S)$ and $He(2^3S)$	126
5.27	Total ionisation cross section for NH_3 + $He(2^3S)$	128
5.28	Branching ratio for NH_3 + $He(2^3S)$	128
5.29	Total ionisation cross section for NH_3 + $He(2^1S)$	130
5.30	Branching ratio for NH_3 + $He(2^1S)$	130
5.31	Total ionisation cross section cross sections for NH_3 + $He(2^1S)$ and $He(2^3S)$	131
5.32	Total ionisation cross section for SF_6 + $He(2^3S)$	133
5.33	Branching ratio for SF_6 + $He(2^3S)$	133
6.1	Real part of interaction potentials for Ar + $He(2^3S)$	139
6.2	Coupling width Γ for Ar + $He(2^3S)$	140
6.3	Theoretical total ionisation cross sections for Ar + $He(2^3S)$	142
6.4	Theoretical total ionisation cross sections for Ar + $He(2^3S)$ with Γ saturating	142
6.5	Real part of interaction potentials for Ar + $He(2^1S)$	144
6.6	Coupling width Γ for Ar + $He(2^1S)$	144
6.7	Theoretical total ionisation cross sections for Ar + $He(2^1S)$	147
6.8	Theoretical total ionisation cross sections for Ar + $He(2^1S)$ with Γ saturating	147

6.9	Variation of turning point with angular momentum	148
6.10a,b	Variation of cross section with angular momentum	149
6.11	Log-log plot of cross section against energy for collisions with $He(2^3S)$	151
6.12	Log-log plot of cross section against energy for collisions with $He(2^1S)$	152

Appendix

1	Metastable atom count rate as a function of quench lamp current	157
2	Relay logic circuit	158
3	Optical switch circuit	158
4	TOF logic circuit with photon mask	159
5	Detector supply circuits	160

List of Tables

Table		Page
4.1	Comparison of metastable atom sources	50
4.2	Probability of detecting more than one metastable atom	77
4.3	Detection efficiencies	85
5.1	Normalisation errors	101
5.2	Relative cross section and branching ratio for $He(2^3S)+Ar$	102
5.3	Relative cross section and branching ratio for $He(2^1S)+Ar$	103
5.4	Relative cross section and branching ratio for $He(2^3S)+CO_2$	107
5.5	Relative cross section and branching ratio for $He(2^1S)+CO_2$	109
5.6	Relative cross section and branching ratio for $He(2^3S)+N_2O$	112
5.7	Relative cross section and branching ratio for $He(2^1S)+N_2O$	114
5.8	Relative cross section and branching ratio for $He(2^3S)+CH_4$	117
5.9	Relative cross section and branching ratio for $He(2^1S)+CH_4$	119
5.10	Relative cross section and branching ratio for $He(2^3S)+C_2H_2$	122
5.11	Relative cross section and branching ratio for $He(2^1S)+C_2H_2$	124
5.12	Relative cross section and branching ratio for $He(2^3S)+NH_3$	127
5.13	Relative cross section and branching ratio for $He(2^1S)+NH_3$	129
5.14	Relative cross section and branching ratio for $He(2^3S)+SF_6$	132
5.15	Single energy branching ratio measurements for $He(2^3S)$	134
5.16	Single energy branching ratio measurements for $He(2^1S)$	135

Chapter 1
Introduction

1.1 Background to the present research

Ionisation by metastable helium atoms is an important process both in natural and man-made plasmas. Helium is a major constituent of many planetary and stellar atmospheres and is present in the interstellar medium (Rees et al 1968). The metastable levels present in helium are important in the production of a population inversion in some lasers, for example He-Ne and He-Cd (Webb 1976). Also metastable atoms give rise to energy loss in experimental fusion reactors because they cannot be contained by magnetic fields.

The interaction of metastable helium with many gases has been studied experimentally for many years (chapter 2) and the theoretical approach has been developed to apply to the case of argon (chapters 3 and 6).

The two electrons of helium combine according to the LS-coupling rule and so the 1s2s lowest excited state gives rise to 2^1S and a 2^3S atomic states. These singlet and triplet states are both metastable; the transition to the 1^1S ground state is optically forbidden by the parity change rule and the $\Delta L = \pm 1$ selection rule. In addition to this the 2^3S state is also forbidden to decay by the $\Delta S = 0$ rule. The lifetimes of the 2^3S and 2^1S states are 9×10^3s and 2×10^{-2}s respectively as measured by Woodsworth and Moos (1975).

Because of the large excitation energies of the two metastable states, 19.8eV for He(2^3S) and 20.6eV for He(2^1S), collisions with atoms and molecules may lead to ionisation of the target at any collision velocity. In most cases more than one ionisation process is possible:

$He^* + AB \rightarrow He + AB^+ + e^-$	Penning ionisation	(1.1)
$He^* + AB \rightarrow HeAB^+ + e^-$	Associative ionisation	(1.2)
$He^* + AB \rightarrow He + A^+ + B + e^-$	Dissociative ionisation	(1.3)
or $\rightarrow He + B^+ + A + e^-$		
$He^* + AB \rightarrow HeA^+ + B + e^-$	Associative-dissociative	(1.4)
or $\rightarrow HeB^+ + A + e^-$	ionisation	

where A and B are fragments of a molecule and may be atoms, or molecules in their own

right. Any combination of these processes may be available for a given target; collectively the processes are known as chemi-ionisation.

Penning (1927) observed the reaction (Equation 1.1) in his studies of the effects of small amounts of impurities in rare gas discharges and in 1934 he published the first indirect cross section measurement. However it was not until 1966 that the study of chemi-ionisation became precise and widespread, with the first experimental measurements of ejected electron energy distributions by Čermák. The theory of chemi-ionisation was developed by Nakamura (1969) and Miller (1970), (chapter 2) and a large number of absolute ionisation cross sections were measured by Schmeltekopf and Fehsenfeld (1970) using the flowing afterglow technique (chapter 3). This prompted the development of a wide range of beam techniques in the following years to measure absolute and relative total ionisation cross sections and differential elastic cross sections. The techniques of West et al (1975), Pesnelle et al (1975), Brutschy and Haberland (1977) and Jerram (1985) are described in chapter 2. The results of these experiments show that total ionisation cross sections can be strongly dependent on collision velocity, and some large differences may occur in the triplet and singlet cross sections. Far more work has been carried out with the triplet than with the singlet metastable atoms.

1.2 Present aims and thesis content

A detailed description of theoretical and experimental advances in the field of chemi-ionisation is given in chapters 2 and 3 respectively. The present work described in chapter 4 is intended to follow on directly from that described above, particularly that of Jerram (1985), and to extend it by making relative total ionisation cross section measurements over a wide velocity range (1 - 20 kms^{-1}) for both singlet and triplet metastable atoms.

Both $He(2^1S)$ and $He(2^3S)$ are used as the reagent in collision with various atoms and molecules (Ar, CO_2, N_2O, CH_4, C_2H_2, and NH_3). In the case of SF_6 only enough data could be accumulated for $He(2^3S)$ data to be recorded.

These targets have been chosen for a number of reasons: Ar because it has been extensively studied theoretically and will therefore allow measured ionisation cross sections to be compared to those calculated theoretically; carbon dioxide (CO_2), nitrous oxide (N_2O), methane (CH_4) and ammonia (NH_3) are all present in the atmosphere of the earth and other

planets; sulphur hexaphluoride (SF_6) is much used in the electrical industry; and acetylene (C_2H_2) is a combustible fuel. They are expected to interact with helium in a number of ways. CO_2, N_2O and C_2H_2 are expected to show a weak interaction, because of their intermediate polarisability. CH_4 and SF_6 are symmetrical molecules and should show argon-like repulsive interactions. Ammonia is very reactive and should show a much stronger interaction than any of the other molecules.

With the singlet state, except for the case of argon, no previous relative measurements have been made. In the triplet case previous measurements have been made (except in the cases of N_2O and SF_6), but the collision velocity range has been extended in the present experiment.

In addition to the total ionisation cross sections measured, the branching ratios for the reactions shown in Equation 1.1-1.4 are measured over a wide velocity range (1-14kms^{-1}), again using both singlet and triplet metastable species.

In chapter 5 the results are tabulated and presented graphically with relative total ionisation cross sections normalised to absolute measurements. Comparisons with other experimental work are made where possible, and conclusions about the interaction potential characteristics for each target species are made.

In chapter 6 the classical approach described in chapter 2 is used with theoretical interaction potentials derived by several authors to calculate total ionisation cross sections for Ar + He(2^1S) and Ar + He(2^3S). These cross sections are compared with the present measured ionisation cross sections and the interaction potentials adjusted to give the best fit. The interaction potentials are examined to find which best represents the present experimental results. The extent to which changes to the potentials has reduced their relevance to differential data, for which they were originally constructed, is also assessed. The approximate cross section technique of Illenberger and Niehaus (1975) is also used to examine all measured ionisation cross sections at intermediate collision velocities.

In chapter 7 the results are summarised, conclusions are drawn from the present work, and ideas are put forward for improvements to the present experiment and future research.

Chapter 2

Theoretical approach to Penning ionisation

2.1 Introduction

A metastable rare gas atom has a more open electronic structure than a ground state atom and therefore its electron orbitals can overlap and interact with those of a target particle, causing ionisation. The ionisation cross section for a target particle with a metastable atom is affected by their separations and the time taken in the collision. Both of these factors are determined by the potential experienced by the particles as they approach and as they move apart. To calculate a theoretical Penning ionisation cross section, therefore, it is necessary to have a knowledge of these potentials.

2.2 The two potential model

The two potential curve model developed by Herman and Čermák (1966) is the basis of all subsequent theoretical treatments such as Katsuura (1965), Mori (1966 and 1969), Nakamura(1969, 71, 75 and 76), Hickman et al (1977a and b), and most importantly Miller (1970, 72 and 77) whose approach is closely followed later in the chapter.

Figure 2.1 shows schematically the two potential curve model for ionisation. Before ionisation the reactant particles X^* and AB form an excited quasi-molecule XAB^* and after form an ionised quasi-molecule XAB^+. Penning ionisation is caused by an autoionising transition between two adiabatic potential curves $V^*(R)$ and $V^+(R)$, shown in the following reaction

$$\begin{array}{c} X^*+AB \rightarrow [X^*AB] \rightarrow [XAB^+ + e^-] \rightarrow X+AB^+ + e^- \\ V^*(R) \rightarrow V^+(R) \end{array} \qquad (2.1)$$

The probability of ionisation per unit time P(R) is related to the 'energy width' $\Gamma(R)$ of $V^*(R)$ by

$$P(R) = \frac{\Gamma(R)}{\hbar} \qquad (2.2)$$

$\Gamma(R)$ and $V^*(R)$ combine to form an initial state complex or optical potential $W^*(R)$

Energy (arb units)

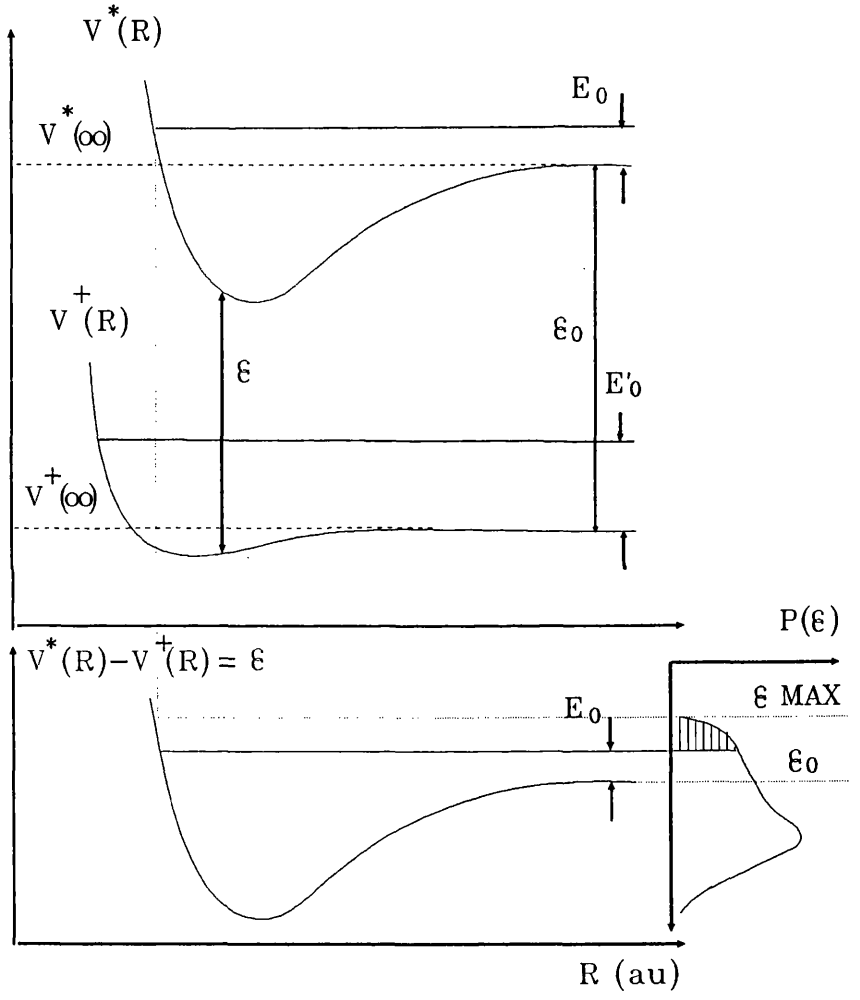

Figure 2.1 Two potential model of chemi-ionisation

given by

$$W^*(R) = V^*(R) - i\frac{\Gamma(R)}{2} \tag{2.3}$$

The energy of the particles before collision is given in Figure 2.1 by the upper horizontal line giving a relative kinetic energy of E_0, The energy after collision is given by the lower horizontal line with a relative kinetic energy of E_0'. Ionisation takes place by a vertical transition obeying the Born-Oppenheimer approximation, which is to say that the transition is instant with internuclear separation and kinetic energy equal immediately before and after ionisation. The values of E_0 and E_0' may be different because of the possibility of conversion of internal energy to translational energy. The total energy E is conserved giving the relation

$$E = V^*(R) + E_0 = V^+(R) + E_0' + \epsilon \tag{2.4}$$

where ϵ, the electron energy, is the difference between the energy of the initial and final quasi-molecular states at a fixed internuclear distance (the Frank-Condon principle). The final energy of the collision particles can be derived from this expression to give

$$E_0' = E_0 + [V^*(\infty) - V^+(\infty)] - \epsilon \tag{2.5}$$

From this relation it can be seen that if the difference in the asymptotic potentials plus the initial energy is less than the electron energy ϵ, then the final energy E_0' is negative and a bound state is formed. This is known as associative ionisation. If E_0' is greater than zero then the particles are not bound together and Penning ionisation occurs. Associative ionisation can only occur if the potential $V^+(R)$ contains a well deep enough to support a bound state, for example in the case of the interaction of argon with metastable helium where both species of ion are formed. The branching ratio has been measured in this work and also by Jerram (1985) and Pesnelle et al (1975). Because the electron energy is fixed as a consequence of the Frank-Condon principle and the asymptotic potentials are also fixed, it can be seen from Equation 2.5 that the amount of associative ionisation must decrease with increasing initial energy E_0. Above a certain energy, associative ionisation does not occur. This pattern is observed in the experiments carried out in this work. In

the case of $He(2^3S)$ + Ar no associative ionisation is observed above a kinetic energy of 0.7eV and in the case of $He(2^1S)$ + Ar none is observed above 0.2 eV, in good agreement with the experiment of Pesnelle et al (1975).

The Frank-Condon principle is represented clearly by

$$\epsilon = V^*(R_i) - V^+(R_i) \tag{2.6}$$

where R_i is the internuclear separation at ionisation. The important consequence of this is that the energy of an ejected electron gives useful information about the two quasi-molecular potentials. The study of the ejected electron was originated by Čermák (1966 a,b and c). Subsequent Penning ionisation electron spectroscopy or PIES has been carried out by many experimenters notably by Niehaus and his collaborators (Fuchs and Niehaus (1968), Hotop and Niehaus (1969a,b) Hotop et al (1969), Niehaus (1973). Figure 2.1 shows graphically, from a plot of electron energy versus internuclear separation, and an electron energy distribution curve of the type derived by the technique of PIES, the relative proportion of Penning ionisation to associative ionisation (shaded region) for the system. Also shown is ϵ_0 the energy of an electron ejected at large separation (effectively no collision takes place and $E_0 = E_0'$). This value is equal to the energy of an electron ejected due to photoionisation by a photon of energy equal to the metastable excitation energy of the projectile particle.

In the two potential model for Penning ionisation the origin of the ejected electron is not significant. The electron may come from a direct process where the target electron is ejected, or indirectly in which it is ejected from the projectile. If $He(2^1S)$ is the projectile both methods of ionisation are possible from the Wigner spin conservation rule, but if $He(2^3S)$ is the projectile then only the indirect method is allowed. Hotop and Niehaus (1969) first suggested that the ejected electron originates from the projectile even if the direct method is allowed, a proposal which is widely accepted now. Equation 2.7 shows the indirect process which involves electron exchange.

$$He^*(2^3S)\,[\uparrow\uparrow] + AB[\uparrow\downarrow] \rightarrow He(1^1S)\,[\uparrow\downarrow] + AB^+[\uparrow] + e^-[\uparrow] \tag{2.7}$$

An electron from the outer shell of the target atom AB is exchanged into the incomplete

1s shell of the helium atom filling the shell so that the electron in the 2s shell is ejected. The process leaves the helium atom in the ground state and the target molecule ionised. Experiments with spin polarised He(2^3S) (such as done by Keliher et al (1975a and b) and Hodge et al (1979)) have confirmed this process.

2.3 Limitations of the two potential model

The two potential model is too simplistic for describing anything but the most simple cases, such as collisions between metastable helium and atoms such as argon and simple molecules. The theory can only describe collisions between metastable atoms and ground state atoms. It is also essential that the metastable energy of the projectile is greater than the ionisation potential of the target. This is the case for most atoms and molecules interacting with metastable helium, which has a large metastable energy (19.8 eV for He(2^3S) and 20.6 eV for He(2^1S)). Neon has an ionisation energy (21.6 eV) above the metastable energy of both helium species and is thus not ionised by thermal energy helium metastable atoms.

In order for the Born-Oppenheimer approximation to be applicable, the collision energy must be small. This allows two adiabatic potential energy curves to describe the two states in the system. The two curves must be isolated allowing no transitions to other adiabatic potentials. This is a big difficulty in the case of molecular targets for which there will in fact be many adiabatic curves such as those which describe the formation of ground state helium and excited state target species $(AB^+)^*$. In the case of molecular targets there is also the possibility of vibrational, rotational and chemical reactions such as dissociative ionisation and associative-dissociative ionisation taking place. In addition the non-spherical shapes of most molecules means that the potential experienced by the projectile particle is dependent on the orientation of the target molecule. The complex interaction potential must therefore be replaced by a potential surface. The hydrogen molecule has been considered by several theoreticians, notably Cohen and Lane (1976) who have produced a theoretical potential surface, but their calculated total ionisation cross section is in poor agreement with the experimental work of Jerram and Smith (1985).

2.4 Calculation of classical cross sections

In order to calculate the total ionisation cross section as a function of collision energy it is first necessary to devise a theoretical interaction potential. As has been stated above, this

is a particularly difficult process for a molecular target, but can be achieved considerably more easily for a simple target such as argon because the potential is spherically symmetrical. Chapter 6, in which some theoretical cross sections are calculated for the He^* + Ar system, describes in detail the construction of such spherically symmetric potentials from the experimental study of differential scattering of helium from argon. However, it is not necessary to have constructed an interaction potential in order to derive an expression for the total ionisation cross section in terms of the interaction energy and a hypothetical potential. The technique used by Miller (1970) is described below.

Miller (1970) has derived expressions for the total ionisation cross sections using classical, semiclassical and quantum mechanical treatments. His classical treatment starts from the assumption of a spherically symmetrical interaction potential, the radial motion can be treated separately at each value of angular momentum $l\hbar$. It is necessary to find an expression for $P_l(R)$ in terms of $V^*(R)$ and $\Gamma(R)$, where $P_l(R)dR$ is the probability density function of leakage to the continuum occurring in the region of internuclear separation between R and R + dR. The value of the function $P_l(R)$ at R is different for the particles moving together and moving apart. $P_l(R)$ is therefore defined as either P_l^{in} or P_l^{out}. The expression derived by Miller (1970) is

$$P_l^{in}(R)\,dR = \left[1-\int_R^{\infty} P_l^{in}(R')\,dR'\right]\frac{\Gamma(R)}{\hbar v_l(R)}\,dR \qquad (2.8)$$

The expression in brackets represents the probability that ionisation has not taken place in the region between R and infinity. The remainder of the equation is simply Equation 2.2, the probability of ionisation at R, multiplied by the time spent in the interval R to R + dR given by $dR/v_l(R)$. The radial velocity $v_l(R)$ is given by

$$v_l(R) = v_0\left[1-\frac{V^*(R)}{E_0}-\frac{l(l+1)\hbar^2}{2\mu E_0 R^2}\right]^{\frac{1}{2}} \qquad (2.9)$$

where v_0 is the collision velocity, E_0 is the asymptotic collision energy and μ is the reduced mass of the system. In order to solve Equation 2.8 it must first be turned into a differential equation

$$P_l^{in}(R) = \frac{\Gamma(R)}{\hbar v_l(R)}\exp\left[-\int_R^{\infty}\frac{\Gamma(R')}{\hbar v_l(R')}\,dR'\right] \qquad (2.10)$$

Using the same principle an expression for P_1^{out} is derived

$$P_1^{out}(R)\,dR = \left[1-\int_{R_0}^{\infty} P_1^{in}(R')\,dR' - \int_{R_0}^{R} P_1^{out}(R')\,dR'\right]\frac{\Gamma(R)}{\hbar V_1(R)}\,dR \qquad (2.11)$$

where R_0 is the classical turning point, the largest value of R for which $v_1(R) = 0$. The brackets now contain the probability that ionisation has not taken place on the inward path from infinity to R_0 or on the outward path from R_0 to R. Equation 2.11 is solved to give

$$P_1^{out}(R) = \frac{\Gamma(R)}{\hbar V_1(R)}\exp\left[-\int_{R_0}^{\infty}\frac{\Gamma(R')}{\hbar V_1(R')}\,dR' - \int_{R_0}^{R}\frac{\Gamma(R')}{\hbar V_1(R')}\,dR'\right] \qquad (2.12)$$

The total probability of ionisation occurring on the inward and outward paths is given by the following expressions

$$\int_{R_0}^{\infty} P_1^{in}(R)\,dR = 1-\exp\left[-\int_{R_0}^{\infty}\frac{\Gamma(R)}{\hbar V_1(R)}\,dR\right] \qquad (2.13)$$

$$\int_{R_0}^{\infty} P_1^{out}(R)\,dR = \exp\left[-\int_{R_0}^{\infty}\frac{\Gamma(R)}{\hbar V_1(R)}\,dR\right]\times\left[1-\exp\left(\int_{R_0}^{R}\frac{\Gamma(R)}{\hbar V_1(R)}\,dR\right)\right] \qquad (2.14)$$

The total probability of ionisation occurring at separation R is

$$P_1 = P_1^{in}(R) + P_1^{out}(R) \qquad (2.15)$$

which is the sum of the probabilities of ionisation at R on the inward and outward paths, and the total probability of ionisation during the collision P_1 is

$$P_1 = \int_{R_0}^{\infty} P_1(R)\,dR \qquad (2.16)$$

The final result then is

$$P_l = 1-\exp\left[-2\int_{R_0}^{\infty} \frac{\Gamma(R)}{\hbar V_l(R)}\,dR\right] \qquad (2.17)$$

which is the sum of 2.13 and 2.14. To determine the total cross section at velocity v_0 the probability of ionisation must be summed over all l to give

$$\sigma_0^{tot} = \left(\frac{\pi}{k_0^2}\right)\sum_l (2l+1)\,P_l \qquad (2.18)$$

where k_0 is given by

$$k_0 = \left[\frac{2\mu\,[E_0 - V_0(\infty)]}{\hbar^2}\right]^{\frac{1}{2}} \qquad (2.19)$$

The dependence of k_0 on E_0 is very important because in the low energy region it causes the cross section to decrease rapidly with increasing energy (Burdensky et al 1981). The cross section begins to increase again above 20 meV because collisions penetrate to lower internuclear separation. Thus R_0 decreases and so the probability of ionisation increases. The probability of ionisation saturates eventually and the cross section begins to decline again. This behaviour is observed experimentally for many systems (chapter 5).

2.5 Refinements to classical theory

Miller (1970) has derived a semi-classical expression for the total ionisation cross section. The major difference between the classical and semi-classical approaches is the replacement of probabilities with probability amplitudes, that is to say the magnitude of the probability squared. The total ionisation cross section in terms of the S matrix, which possesses a phase as well as a probability, is

$$\sigma_0^{tot} = \left(\frac{\pi}{k_0^2}\right)\sum_l (2l+1)\,|S_l|^2 \qquad (2.20)$$

In this semi-classical case interference terms are present in the summation. These have very little effect on the total ionisation cross section at the collision energies in the present experiment. Because of its relative simplicity the classical approach is used in chapter 6 to calculate the total ionisation cross sections for argon with both metastable species of

helium. Burdensky et al (1981) have made measurements below 1 meV, a region in which resonances are predicted by the semi-classical calculations of Brutschy et al (1976). The semi-classical approach is very useful in calculating the differential cross sections, either for elastic or inelastic scattering. The differential cross section is calculated from the modulus squared of the scattering amplitude given by

$$\sigma(\theta) = |f(\theta)|^2 \; ; \quad f(\theta) = (2ik)^{-1}\sum_l (2l+1) S_l P_l(\cos\theta) \qquad (2.21)$$

The quantum mechanical approach is unnecessary in the present experiment for the same reason as the semi-classical approach, but is useful (as is the semi-classical approach) for the calculation of differential cross sections and to compare with the classical calculations of low energy total ionisation cross sections.

2.6 The simplified analytical theory

Illenberger and Niehaus (1974) have identified an energy region in the ionisation cross section in which certain approximations may be made to Equation 2.17. There are two conditions for the applicability of these approximations. Firstly the collision energy $E_0 >> \Delta^*$ where Δ^* is the well depth of V^*, the real part of the potential curve. Secondly $P_l << 1$ where P_l is the ionisation efficiency per collision. The first condition implies that only collisions which penetrate to the repulsive region of the interaction need be considered. The second condition ensures that collisions in the region where P_l and the total ionisation cross section saturates are not included. The energy range implied by these conditions is between 20 meV and 100 meV.

The major simplification made is the replacement of the angular momentum l by a continuous function including the impact parameter b and k_0 previously defined in Equation 2.19

$$bk_0 = l + \frac{1}{2} \qquad (2.22)$$

With P(b) small, Equation 2.17 can be expanded to give

$$P(b) = 2\int_{R_0}^{\infty} \frac{\Gamma(R)}{\hbar v(b,R)}\, dR \qquad (2.23)$$

Now the total ionisation cross section defined in Equation 2.18 can also be turned into an integral:

$$\sigma(E) = 2\pi\int_{0}^{\infty} P(b)\, b\, db \qquad (2.24)$$

Substituting P(b) into Equation 2.24 and integrating over b leaves an integral over R only

$$\sigma(E) = \int_{R_0}^{\infty} \frac{4\pi r^2 \Gamma(R)}{\sqrt{\frac{2}{\mu}(E_0 - V^*(R))}}\, dR \qquad (2.25)$$

V^* is simplified to the same functional form as Γ (Equation 2.26) because only the repulsive region is used in this analysis.

$$V^*(R) = C\exp(-\frac{R}{D}) \qquad \Gamma(R) = A\exp(-\frac{R}{B}) \qquad (2.26)$$

The integation can now be performed to give

$$\sigma(E_0) = 2A(\frac{\mu}{2B})^{\frac{1}{2}}(BD\pi)^{\frac{3}{2}}(\ln\frac{E_0}{C})^2(\frac{E_0}{C})^{\frac{D}{B}-\frac{1}{2}} \qquad (2.27)$$

It is now possible for a log-log plot of cross section against energy to yield a gradient value approximately equal to D/B-1/2. The aim of this treatment is simply to gain information about the shape of the coupling width Γ from the already deduced shape of the real part of the interaction potential. In chapter 6 this simple theory will be tested using the present experimental data.

Chapter 3

Experiments with metastable helium

3.1 Introduction

In this section a brief review of the more important and relevant experiments performed up to the present is given. The merits of the various methods are compared, as are their problems.

3.2 Stationary afterglow experiments

The use of gaseous discharges is the oldest method of gaining information about the ionisation by metastable atoms. Observations have usually been made of the afterglow of the discharge. The experiments are of two main types, stationary and flowing afterglow studies.

The stationary afterglow method is simple in principle. A discharge is struck momentarily in a mixture of a rare gas and a reagent gas, and the concentrations of excited atoms in the rare gas is monitored as they decay. By a detailed analysis of the continuity equation which describes this decay, the rate constant k for different reactions can be determined. The cross section σ is related to k by the following relation

$$k = \int_0^\infty v\sigma(v)\, f(v)\, dv \qquad (3.1)$$

where v is the relative velocity, and f(v) is the velocity distribution function at v.

The concentration of metastables is generally measured by illuminating the gas with a resonance lamp and observing the absorption of line radiation by transitions of known oscillator strength. For example Benton et al (1962) observed the concentration of $He(2^3S)$ and $He(2^1S)$ by monitoring the 3^3P-2^3S (388nm) and the 3^1P-2^1S (501.6nm) lines respectively.

The major problems with these experiments are in determining absolutely the quantity of reagent gas present in the plasma, the quantity is usually small and measurement is further complicated by the presence of impurities, which outgas from the walls of the container. The importance of this second factor is dependent on the pressure at which the experiments are performed. Pulsed electrolysis experiments, for example, in which the plasma is produced by electron bombardment, are performed at atmospheric pressure. In these experiments the problems are reduced by the high pressure but errors may occur because second and third order reactions may become important.

3.3 Flowing afterglow experiments

Developed by Ferguson, Schmeltekopf and Fehsenfeld (1969) primarily for atmospheric ion-molecule reaction studies and widely applied by Schmeltekopf and Fehsenfeld (1970) the flowing afterglow method is a development which has allowed the total quenching constants for metastable helium by many reagent gases to be measured. Some of the inherent problems with the stationary afterglow system are solved by striking the discharge in a fast-moving gas.

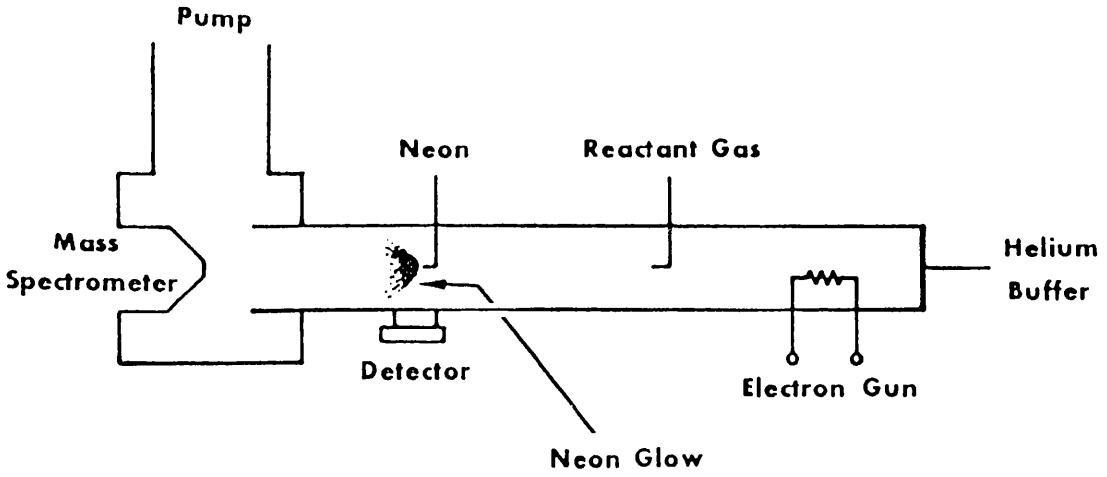

Figure 3.1 Flowing afterglow apparatus of
Schmeltikopf add Fehsenfeld (1970)

Figure 3.1 shows the system described by Schmeltekopf and Fehsenfeld (1970). The discharge is struck in a gas at 0.4 torr and with a velocity of 8×10^3cm s^{-1}. The flow rate is much greater than the rate of outgassing and so there is no problem associated with contamination of the buffer gas, as in the stationary afterglow method. An electron gun

is used to produce a discharge, to produce the triplet state an acceleration of 100eV at 2mA is used. This produces strong ionisation and results in the conversion of $He(2^1S)$ to $He(2^3S)$ by superelastic collisions with free electrons. In order to produce singlet metastables the electron gun is operated at an acceleration lower than the ionisation potential of helium, so that excess free electrons are not present. Metastables are produced in the discharge region and are transported along the tube. The reagent is added further along the tube, and because of this separation from the discharge, the reagent is in the ground state.

Further along the tube the concentrations of metastables can be measured by a variety of methods. In the experiment shown neon is added to the gas flow. The neon is immediately excited into different radiating states. Depending on which metastable does the exciting either 568.98 nm (from $Ne+He(2^1S)$), or 703.24nm, (from $Ne+He(2^3S)$) radiation is emitted. The absolute determination of the intensity of these lines allows the concentration of both metastable species to be measured.

The quenching constant k can be determined from the following relation.

$$\ln(X^*) = \ln(X^*_0) - D - \frac{Bkl}{\bar{v}} Y \qquad (3.2)$$

in this X^* is the concentration of metastables at the point of detection, X^*_0 is the initial concentration, D is the coefficient of diffusion for metastables to the tube walls, l is the distance between the point at which the reagent is added and the detection region, Y is the reagent concentration, and $\bar{v}$ is the mean buffer gas velocity. The constant B is pressure dependant and corrects for the variation of buffer gas velocity across the tube diameter. By varying Y a plot of $\ln(X^*)$ against Y will be a straight line with a gradient equal to $Bkl/\bar{v}$.

The problems with this method are firstly the difficulty in determining the parameters D, B and the effective length l. B and l are dependent on the individual flow characteristics of each apparatus. The other disadvantages of the flowing afterglow method are that large amounts of expensive gas are used and that secondary reactions may distort the results. Nevertheless most of these difficulties can be largely overcome and much useful data has been obtained.

3.4 Beam experiments

The major advantage of beam experiments over the flowing afterglow studies is the ability to study reactions individually and in more detail. It is possible to measure the ionisation cross section σ in Equation 3.1 at a single velocity, rather than the quenching rate constant k which is integrated over all velocities. Both the ejected electrons and the positive ions are available for study. It is therefore possible to measure the ionisation cross sections for associative and dissociative reactions as well as examining the Penning ionisation electron spectrum. In addition, it is possible to measure the angular distribution of scattered metastable atoms and product ions.

Beam experiments are of two types, gas cell and crossed beam arrangements. Gas cell experiments are most useful for making absolute measurements of ionisation cross sections. Crossed beam apparatuses are more flexible but are less capable of making absolute measurements.

3.4.1 Gas cell experiments

The gas cell technique was developed by Sholette and Muschlitz (1962) and was the first technique developed to measure the absolute total ionisation cross section of rare gases by metastable helium. The technique has been further developed by many experimenters including several in the present author's laboratory such as Dunning and Smith (1971) and Jerram and Smith (1985), whose experimental set-up is shown in Figure 3.2.

Jerram and Smith's apparatus is as follows. The metastable beam source is a constricted-arc hot-cathode type designed by Trujillo (1975) with a wide velocity output (a more detailed analysis of the variety of sources used by experimenters is presented in chapter 4). The velocity selector designed by Trujillo (1975) is used to produce a metastable atom beam of variable velocity. A helical quench lamp of the Hotop et al (1969) type is used to remove singlet metastables from the beam (see chapter 4.3).

The gas cell, shown in some detail in Figure 3.2, is a sophisticated detector consisting of an outer earthed box and an inner box which can be biased positively or negatively and connected to either the slats or grid. Gas is admitted to the cell and the pressure carefully monitored by a calibrated Pirani gauge. Currents due to the metastable flux J are measured

at the monitor grid and currents due to positive ions I_g are measured at the fine grid. The electron current I_s, due to ionisation of the reagent gas and the emission of secondary electrons from the back face of the gas cell is measured at the slats. A computer is used to record and average the outputs from two electrodes connected to the monitor grid and slats.

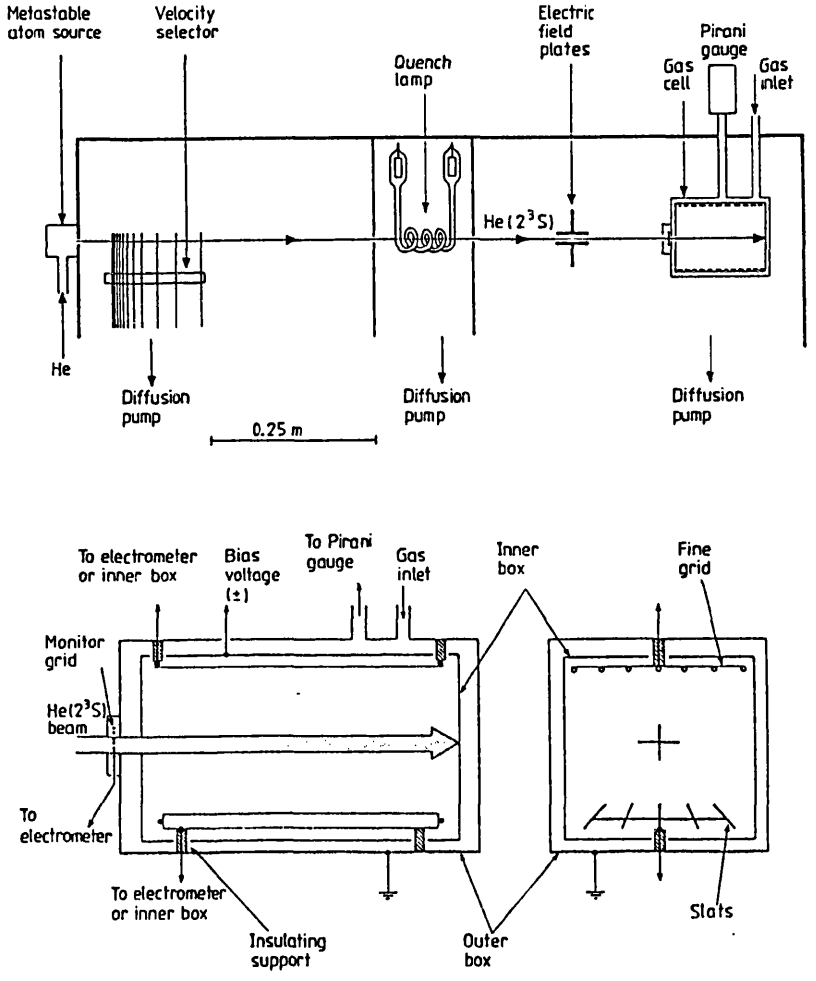

Figure 3.2 Gas cell apparatus of Jerram and Smith (1985)

To determine the absolute ionisation cross section the following relation is used

$$\ln\left(\frac{I_s^- + I_s^+ - 2I_g^+}{J}\right) = -n\sigma l + \ln(\gamma K) \qquad (3.3)$$

where I_s^- and I_s^+ are measured with the box and grid negative or positive respectively

relative to the slats. With the box and slats positive relative to the grid I_g^+ is measured. The secondary emission coefficient for metastable helium atoms on gold (all surfaces are coated with gold) is γ. The length of the gas cell is l, the number density of reagent gas atoms in the gas cell is n and K is a constant.

The derivation of Equation 3.3, is given by Jerram and Smith (1985) and will not be repeated here. It is clear that a plot of $\ln((I_s^- + I_s^+ - 2Ig^+)/J)$ against n will be a straight line with gradient $-\sigma l$, so that σ can be determined if currents and n and l are known. The number density n is deduced from an absolute measurement of the pressure of the gas in the cell.

The advantage of this method over other gas cell experiments such as Woodard et al (1978) is that it is not necessary to determine γ. Also the use of slats in place of the grid wires used by Dunning and Smith (1971) eliminates a problem identified by Jerram (1985) of extra ionisation caused by electrons orbiting the grid wires. The biggest problem with the experiment are the small current magnitudes and the necessity to determine the absolute number density of the reagent gas. Also the path length l may be larger than assumed due to elastic scattering, but this effect is likely to be small. Despite the difficulties of the measurements, fewer assumptions and uncertain calculations are necessary than in the afterglow experiments. Nevertheless the earlier flowing afterglow results are generally consistent with the results of Jerram and Smith (1985).

3.4.2 Simple crossed beam experiments

The most adaptable experimental arrangement is one in which the reagent gas is introduced to the metastable beam not in a cell but in the form of a beam. However the results are usually not absolute and have to be normalised, for example to the flowing afterglow rate constants or absolute cross sections as measured by Jerram and Smith (1985). The crossed beam technique was used for the work described in this thesis. The two beams cross at right angles and the ionisation products are separated in a mass spectrometer or detected in total. The remaining metastables may be detected as may those which have been elastically scattered. The electrons produced are also available for study.

The simplest system is that used by West et al (1975) (Figure 3.3) to measure the branching ratios of Penning and dissociative ionisation. No velocity selector is used and so

measurements can only be made over a distribution of collision velocity. This means that

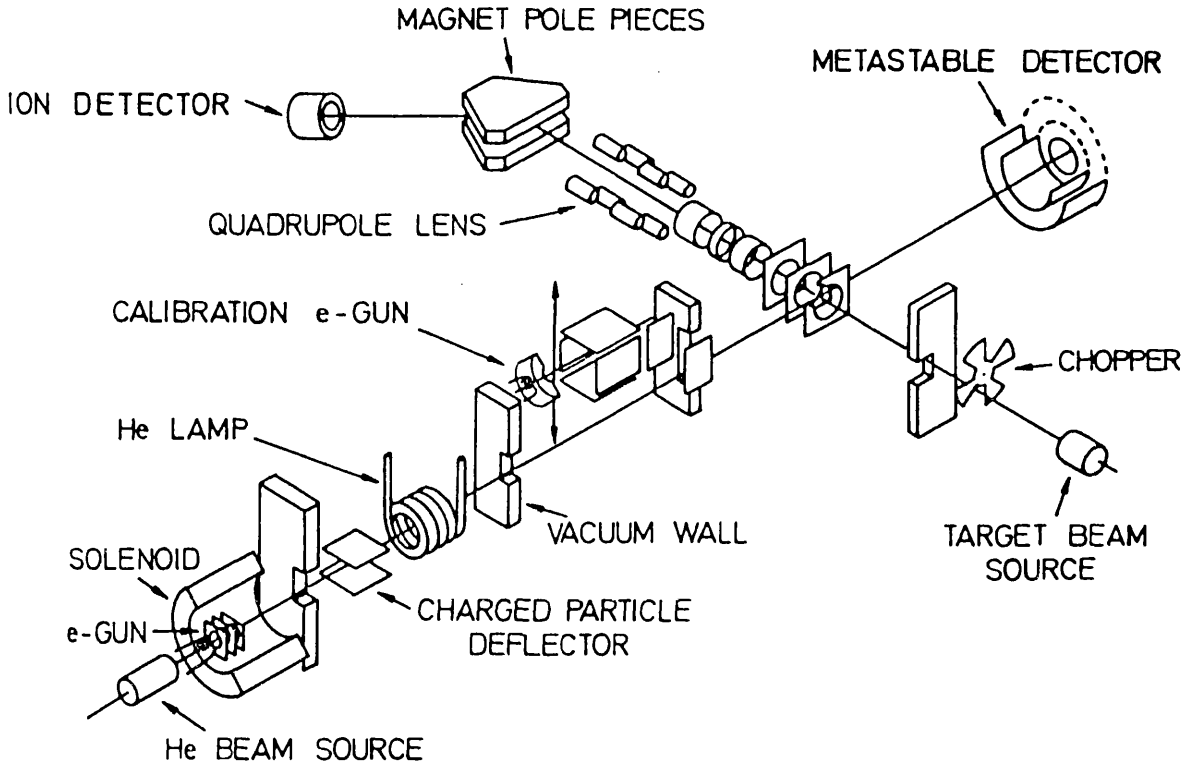

Figure 3.3 Crossed beam apparatus of West et al (1975)

the variation of cross section with velocity is not directly measurable. To make absolute measurements is complicated however by the need to know the absolute densities of both the metastable and reagent species in the interaction region. West et al used an ingenious method devised by Dunning, Smith and Stebbings (1971) by which the target beam is chopped, and the difference in the ejected electrons measured by the metastable detector is compared with the change in total ion count rate. From this can be deduced the secondary ejection efficiency γ of the metastable detector and thus the density of metastables. The density of reagent gas is found by replacing the metastable beam by an electron beam and measuring the current of ions produced at a collision energy 1 keV for which the ionisation cross section is well known. This method although original, is quite crude compared to the gas cell method, because it is dependent on small signal changes for the value of γ and an assumption of the overlap of the target and electron beams.

3.4.3 Crossed beam experiments incorporating time-of-flight

A much more sophisticated (but not absolute) time-of-flight technique has been developed

by experimenters such as Pesnelle et al (1975), Illenberger and Niehaus (1975), Parr et al (1980), Jerram (1985), and Kroon (1985). These experiments although not absolute can measure the velocity dependence of Penning ionisation cross sections. Figure 3.4 shows the apparatus of Pesnelle et al, in which the metastable beam is chopped by a slotted wheel and pulses of metastable atoms result. Because the beam produces a range of velocities (section 4.5.1), the pulse of metastables spreads out in the drift region and the atoms arrive at the detector at different times. At the moment a pulse of metastables is produced, a start pulse from the photo-diode is fed into a multi-channel analyser, which then begins to record either the detection of metastables or ions in the interaction region. The TOF distributions of ions and metastables are built up over many revolutions of the chopper wheel taking a number of hours. A relative ionisation cross section as a function of velocity is eventually calculated by converting the TOF spectra into velocity spectra and dividing the ion distribution by the metastable distribution. In order to make measurements with the singlet state, TOF spectra are recorded with the quench lamp on and off and a subtraction is made of the triplet distribution from the triplet plus singlet distribution. Thus four distributions must be recorded, each at a different time, in the Pesnelle et al experiment. Similarly if the partial cross sections of individual ion species are to be measured, the mass spectrometer must be used to build up a TOF distribution for each ion species individually.

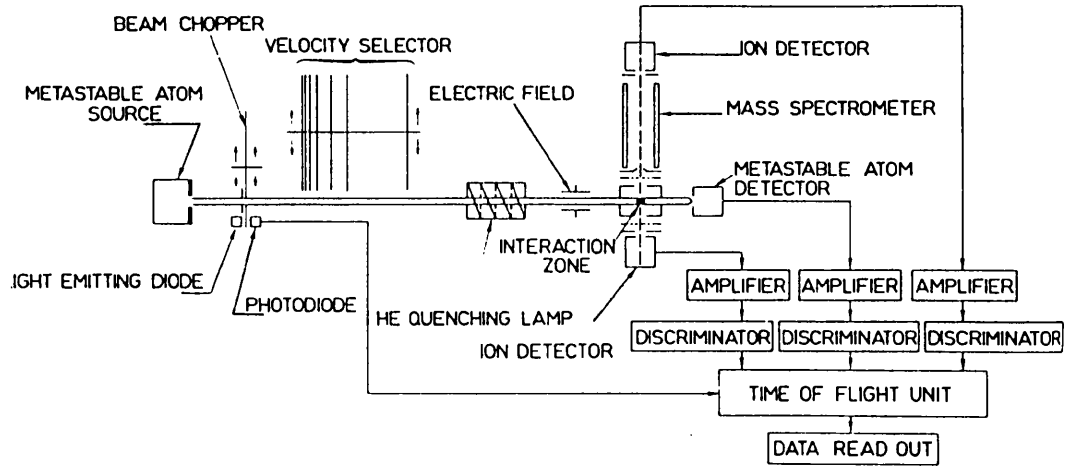

Figure 3.4 Crossed beam apparatus of Pesnelle et al (1975) incorporating the time-of-flight technique

The disadvantage of this is clearly that any change in the conditions of the experiment between the recording of distributions will result in a systematic error occurring in the results. For example this could be due to the gradual rise in background gas pressure with

time, quite common in crossed beam experiments, or due to gas freezing on a liquid nitrogen trap. This effect would be made worse in the Pesnelle et al experiment because there is no way of determining the origin of an ion detected by the total ion detector.

This latter problem has been overcome by Jerram (1985) by the substitution of the total ion detector by a TOF mass spectrometer. Now it is necessary for a coincidence to occur between the detection of a positive ion and an electron before a count is made, thereby ensuring that only ions produced in the interaction region are recorded (chapter 4.5.3).

Another improvement in the experimental set-up of Jerram is the replacement of the multi-channel analyser by a CAMAC interface unit and an LSI-11 microcomputer. This allows ten ion mass spectra to be recorded simultaneously, each at a different velocity. Similarly, for total cross sections, both the ion and metastable TOF distributions are recorded simultaneously. Because the computer is much slower at recording information than the multi-channel analyser, it is only possible to record one metastable and one ion in each chopper wheel cycle, making the acquisition of data rather slow in this experiment. No experiments were performed by Jerram using the singlet state but a development of his apparatus is used to do so in the work described in chapters 4 and 5 of this thesis.

3.4.4 Crossed beam differential scattering experiments

The apparatus for measuring differential elastic cross sections by Brutschy et al (1976) is shown in Figure 3.5. To provide a velocity-selected beam a supersonic nozzle source is used, as is generally the case in differential experiments. The supersonic nozzle source provides a narrow velocity range which can be varied over a small range by changing the helium gas temperature. The metastable states are induced after the nozzle by an axial electron beam. A fixed detector (not shown) is used with the TOF technique to determine the velocity distribution from the source. As usual a quench lamp is used to remove singlets when necessary, a second lamp has been added to provide adequate quenching at high velocity.

The target beam source is also of the supersonic nozzle type. Two more detectors which are not shown are used one out of the plane of Figure 3.5 at a fixed position to monitor changes in the experimental conditions with time, and the other, which can be moved, to measure the intensity of scattered metastable atoms as a function of angle. A stepping

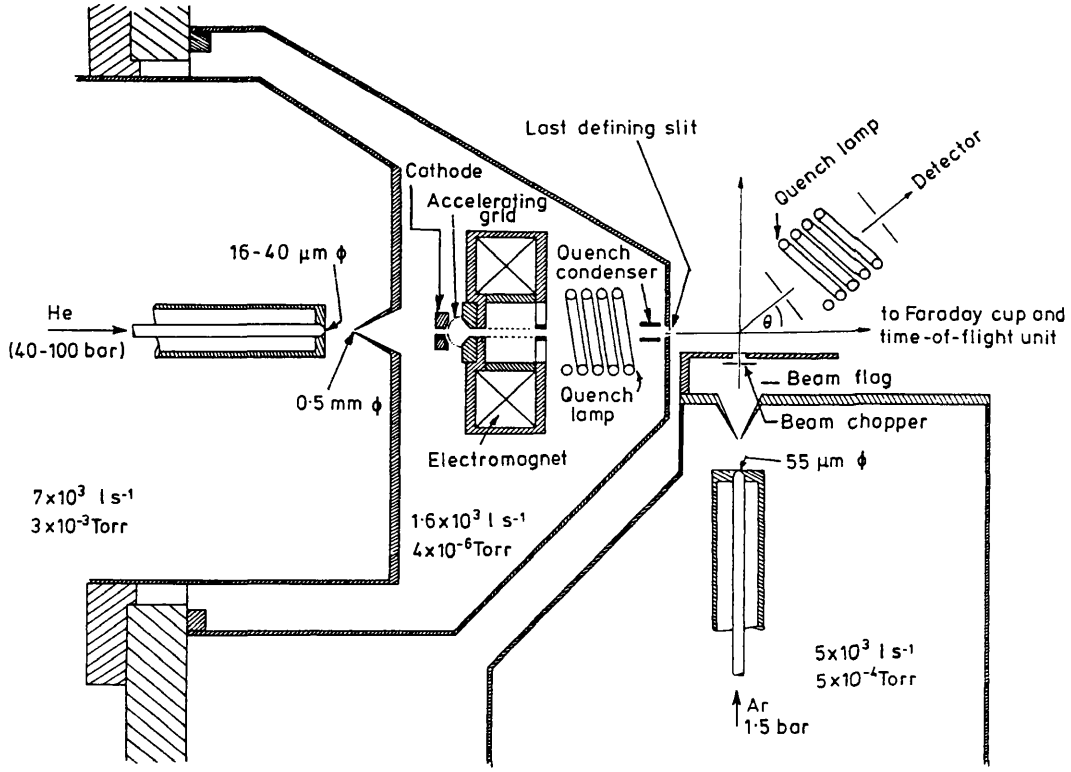

Figure 3.5 Crossed beam apparaatus of Brutschy et al (1976) for measuring elastic scattering cross sections

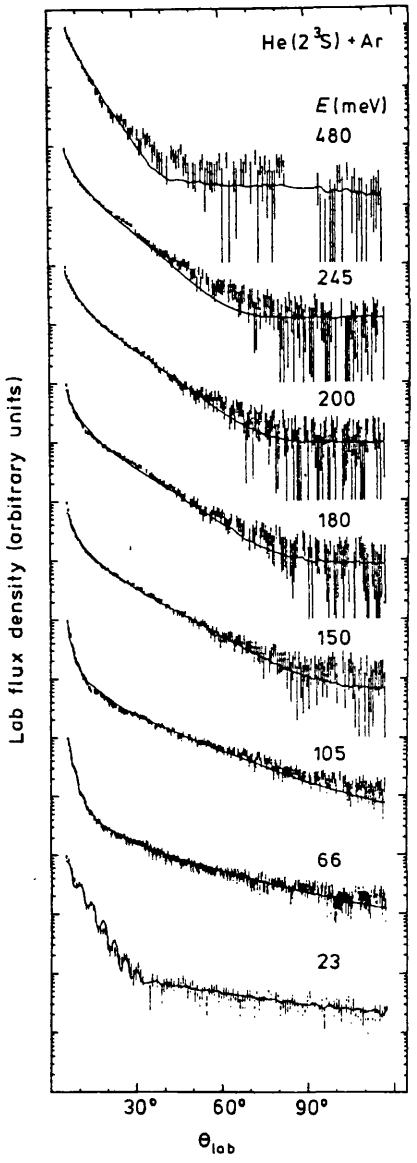

Figure 3.6 Differential elastic scattering cross sections for Ar + He(2^3S) at several energies

motor and a system of counters is used to record the elastic differential cross section. Figure 3.6 shows the results of a typical experiment using triplet helium and argon, the full curves are calculated from a proposed optical potential developed by the Freiburg group.

3.4.5 Crossed beam Penning-ionisation-electron-spectroscopy experiments

A typical apparatus for observing Penning ionisation electron spectra (PIES) is shown in Figure 3.7 taken from Yencha's review article (1984). The presence of the velocity selector means it is possible to observe the ejected electron energy distribution (EEED) from Penning ionisation as a function of metastable atom velocity. As usual, state selection is performed by a helical quench lamp and Rydberg atoms are removed by the electric field plates. A photon source can be substituted for the metastable beam in order to observe photoelectron peaks. Ejected electrons can pass from the ionisation chamber through a small aperture into an electrostatic energy analyser. Apparatuses of this type have been used successfully by Čermák (1966a,b,c), Hotop et al (1979) and Ohno et al (1983) among others.

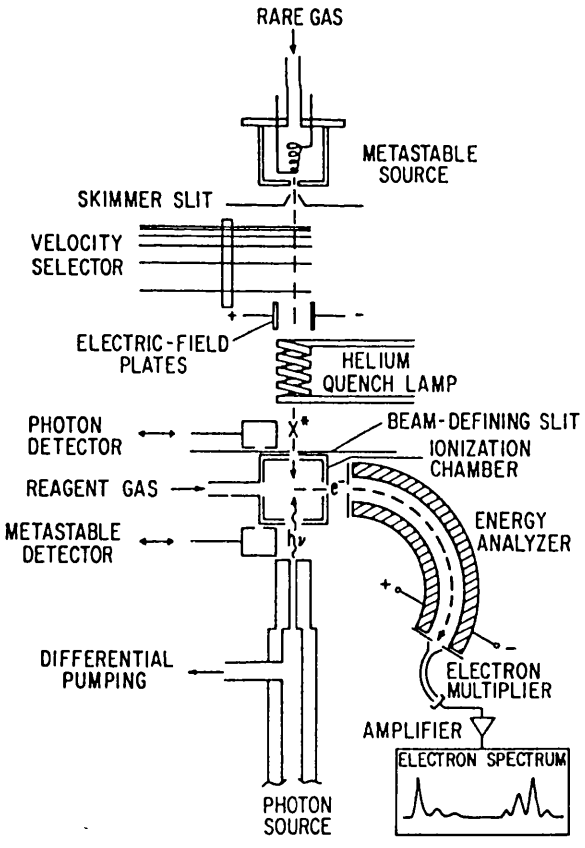

Figure 3.7 Apparatus for performing Penning ionisation electron spectroscopy

Figure 3.8 (Čermák 1976) shows a typical EEED curve for the $^2P_{3/2}$ and $^2P_{1/2}$ ionic fine structure states of argon by the two species of metastable helium and the resonance photons also produced by the source. The positions shown by arrows are those of the energy difference between the metastable energy and the ionisation potential of argon E_0. The peaks are displaced by ΔE the energy shift given by

$$E_e = E_0 + \Delta E \tag{3.4}$$

where E_e is the ejected electron energy and E_0 is the difference in the ionisation potential of the reagent gas and the metastable energy. Important information can be obtained simply from the width of the Penning ion peaks and the magnitude and direction of their shift. In the case of argon the peaks are narrow and slightly positively shifted. The implications of this is that the incoming potential curve V^* is largely repulsive with a well depth much less than the relative kinetic energy of the particles E_k. Figure 3.9 (Yencha 1984) shows how ionisation takes place largely at the repulsive wall, a region in which E_e varies only slowly with internuclear separation, and gives rise to narrow Penning peaks. The electron energy is positively shifted because, E_e is greater than E_0 at the repulsive wall. As described in chapter 2, associative ionisation is predicted by the possibility of E_e being greater than the sum E_0+E_k. With E_0 and E_k both known, the amount of associative ionisation can be deduced from the relative area under the EEED curve at energy greater than $E_0 + E_k$. This implies that the outgoing potential V^+ is not completely repulsive but has a small attractive well.

Other interaction potential systems can also be deduced from their EEED, for instance a strongly attractive incoming potential for which the well depth is much greater than the relative collision energy shown in figure 3.10 (Yencha (1984)). This situation applies in the case of water shown in Figure 3.11, (Čermák and Yencha (1976)) and is signified by a broad energy distribution, a consequence of the wide range of internuclear separations at which ionisation can occur. The peak will be negatively shifted as a result of the well depth.

Many rare gases have been studied in this way. The information gained about the interaction potentials can be compared with the information derived from total ionisation and differential cross section measurements. The advantage of PIES over other techniques is that the properties of the interaction potentials are more readily derived from the experimental results. However, it is also possible to obtain detailed information from the

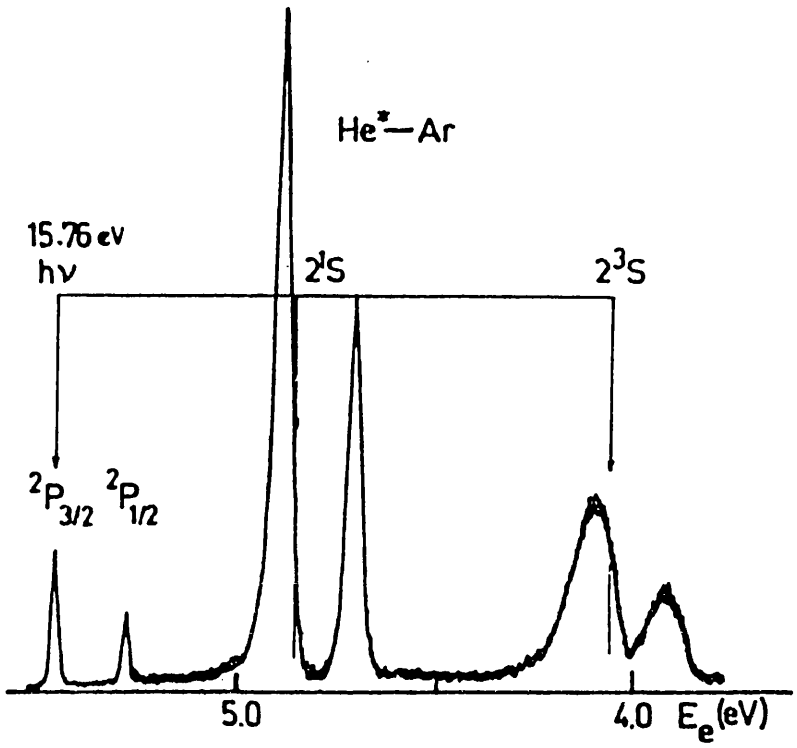

Figure 3.8 Ejected electron energy distribution for Ar + He^*
Čermáck (1976)

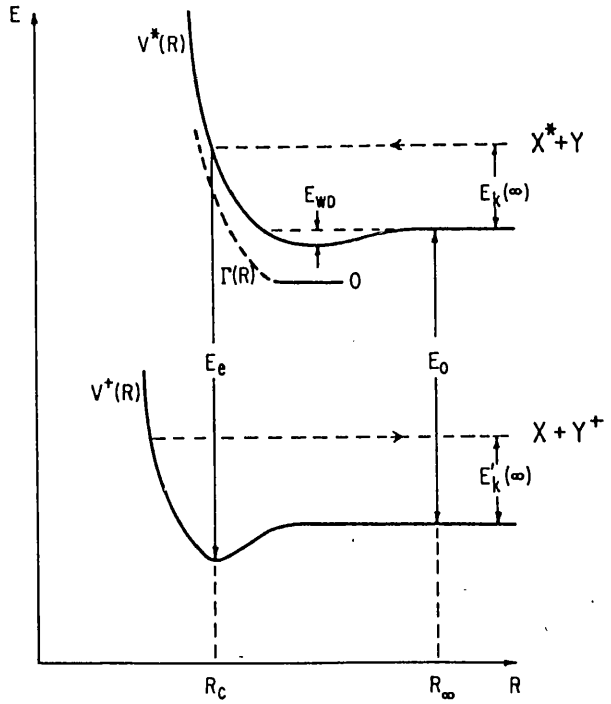

Figure 3.9 Potential model for Ar + He^* showing a repulsive wall in the incoming potential and a well depth E_{WD} much smaller than the relative kinetic energy $E_k(\infty)$ of the colliding particles (Yencha 1984)

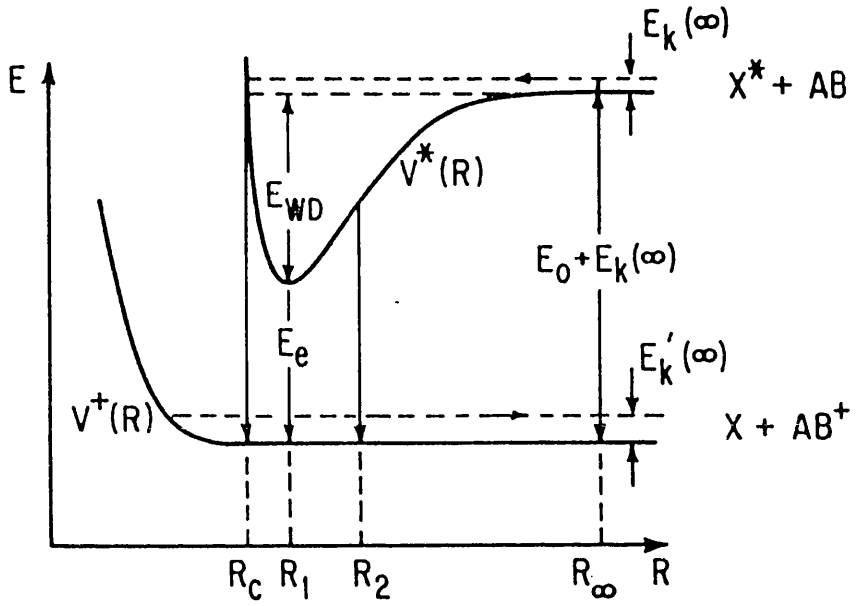

Figure 3.10 Potential model for H_2O + He^* showing an attractive potential with E_{WD} much greater than the relative kinetic energy $E_k(\infty)$ of the colliding particles (Yencha 1984)

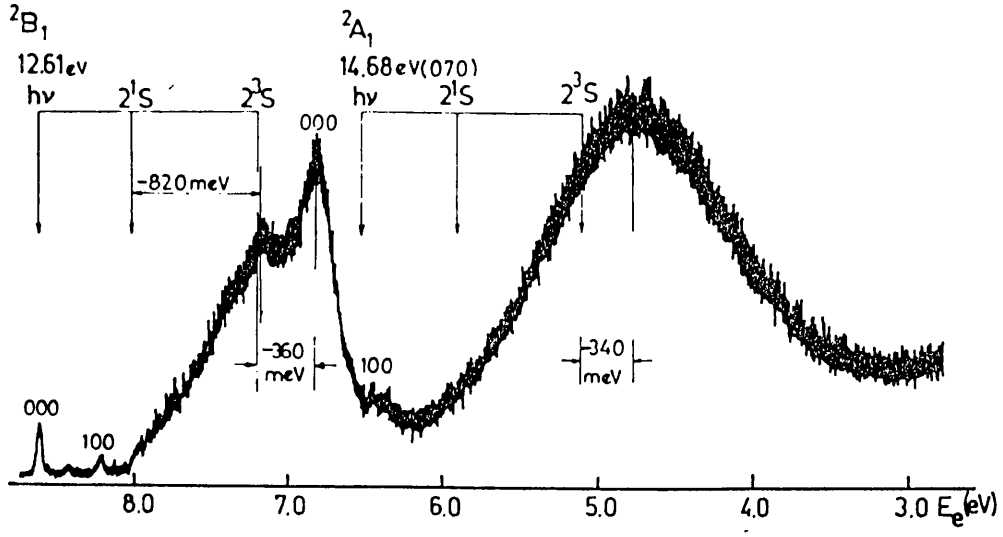

Figure 3.11 Ejected electron energy distribution for H_2O + He^* Čermáck and Yencha (1977)

variation of differential and total ionisation cross sections with collision velocity by the construction of theoretical interaction potentials.

This PIES technique continues to be used by workers such as Hotop et al (1979), Munakata et al (1979), and Ohno et al (1983), giving extensive information about the final vibrational and electronic states of the molecular ions formed. Also the technique of Penning ionisation electron-ion coincidence spectroscopy, (PIECOS) has been developed by Münzer (1978) from photo-ionisation work by Brehm and Von Puttkamer (1967) and has allowed the EEDC corresponding to individual dissociative branches to be studied. The technique, which is described in detail by Elland (1979), involves observing a coincidence between a specific positive ion (using a TOF mass spectrometer) and the ejected electron.

Chapter 4
Experimental Method and Apparatus

4.1 Introduction and general experimental arrangement

Figure 4.1 shows schematically the experimental arrangement used to measure both total ionisation cross sections and branching ratios. The basic crossed beam apparatus has been modified by several experimenters over a period of twenty five years.

The experimental setup is housed in four tanks, but only tanks T1, T2, T3 are shown because T4, which contains the target beam source, is located behind the experimental tank. Tank T1 has a hot cathode effusive gas source attached to one end and inside is a chopper wheel which pulses the metastable atom beam. A slotted switch situated below the chopper wheel provides start pulses for the time-of-flight system. In tanks T1, T2, T3 differential pumping is provided and the beam is collimated by the intervening apertures. Tank T2 houses the helical quench lamp used to eliminate He(2^1S) metastable atoms. The electrostatic pusher plates in tank T3 remove highly excited states from the beam. The metastable beam and target beam, which is perpendicular to the plane of Figure 4.1, cross in the interaction region. The positive ions and electrons produced are drawn out by an electric field and are detected by the electron and ion detectors situated below and above the interaction region respectively, and providing the start and stop pulses for a time-of-flight (TOF) mass spectrometer. The channel electron multiplier is used to detect the metastable atoms that pass through the target beam. The metastable atom velocity and identification of ion products are obtained by time-of-flight techniques.

Two separate experiments are performed with the apparatus described above. To determine the relative variation of ionisation cross section with velocity two sets of TOF distributions are recorded, one generated by stop pulses from the channeltron, produced by unscattered helium metastable atoms, and one generated by stop pulses from the interaction region, the result of ionising collisions with particles in the target beam. The two TOF distributions are converted into velocity distributions and a division of the latter by the former gives the relative variation of cross section as a function of collision velocity.

In the second experiment the information from the channeltron is discarded. Again a TOF distribution is recorded from stop pulses produced at the interaction region but this time the

Figure 4.1 Schematic diagram of the apparatus

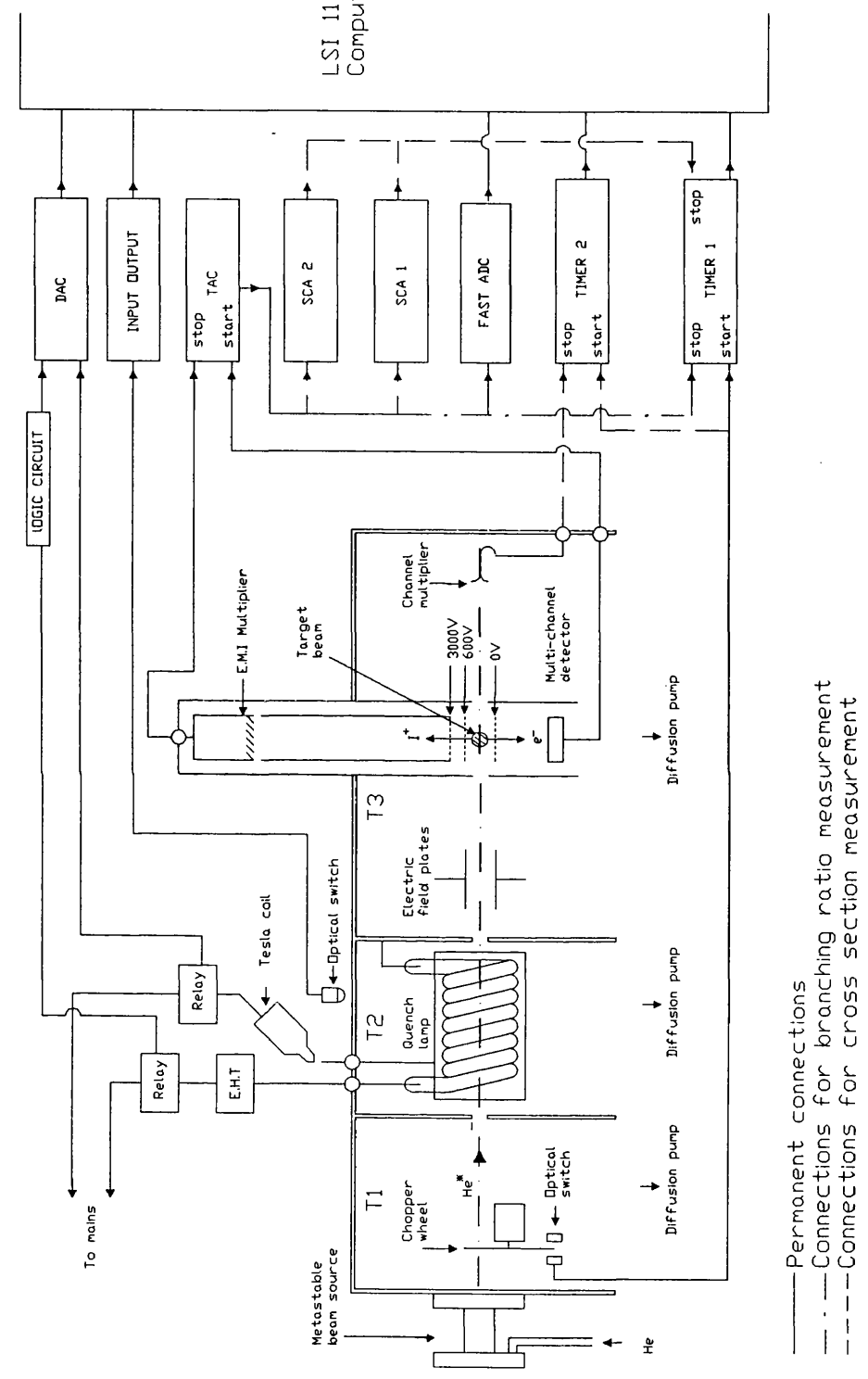

distribution is divided into ten time bins each representing ionisation occurring at a different collision velocity. The TOF mass spectrometer is used to record ten ion mass spectra, one for each time bin. In this way the variation of branching ratio for one or more product ions can be observed as a function of collision velocity.

For both experiments the quench lamp is rapidly turned on and off by the computer. This pulsing of the quench lamp is necessary to provide two sets of data simultaneously, one using only the $He(2^3S)$ content of the beam and one using both $He(2^3S)$ and $He(2^1S)$ metastables. By subtracting the former from the latter, data for collisions involving atoms in the $He(2^1S)$ state are obtained. This means that when measuring branching ratios not ten but twenty ion mass spectra must be recorded.

It is necessary to perform the two experiments separately because of the limited memory space and speed of the computer, which in the first experiment records four TOF distributions and in the second records one TOF distribution and twenty mass spectra. It also turns the quench lamp on and off and monitors its performance. A detailed account of the computer control system and individual pieces of apparatus is given in the rest of this chapter along with descriptions of the techniques used to analyse the data.

4.1.1 The vacuum system

The four vacuum tanks T1, T2, T3, and T4 are each pumped by an oil diffusion pump stack (Edwards type EO6, EO4 EO6 and EO4 respectively), those attached to tanks T1, T2, and T4 containing Apiezon C oil. Convalex 10 oil, because of its lower vapour pressure and back-streaming rate, is used in the pump on the experiment tank T3. To back the diffusion pumps a larger backing pump (Edwards ED660) has been installed, with a pumping speed (660 l/minute) double that used in previous experiments. This allows a greater amount of helium to be passed through the system than was previously possible.

4.2 The metastable atom beam and target beam

4.2.1 Construction of metastable atom beam source

The constricted arc hot cathode source was designed by Trujillo and is described in detail in his thesis. Figure 4.2a shows the source in cross section. It consists of a glass tube

36mm inside diameter and 40mm long held between copper front and back plates. The cathode filament, fixed to the back plate by two terminals, (one is insulated from the back plate, the other is in electrical contact with it) is made of folded nickel gauze with an overall area of 24 cm^2, and is coated with electron emissive material (see section 4.2.2). The disc-shaped filament shield, which is made of stainless steel, is also fixed to the back plate. The shield protects the cathode by masking it from the anode. Without it the cathode coating would quickly be lost due to localised discharges on the cathode surface. The cathode lifetime is 20 - 30 hours, after which the emissivity of the coating is reduced to such an extent that it is no longer possible to strike a discharge.

The anode and the intermediate electrode are parts of the front plate, as shown in Figure 4.2a. The rectangular aperture in the intermediate electrode is 0.5mm wide by 3mm long. The electrode is made from magnesium, which has a low sputtering yield, and it is insulated from the anode by a mica annulus. The anode, which is copper, contains the aperture through which the beam emerges. This is 3mm high and between 0.02mm and 0.08mm wide, (see section 4.2.5) depending on the required source output. The desired aperture width is achieved by separating two copper knife edges with strips of aluminium foil, above and below the desired aperture position. The intermediate electrode and the anode are separated by 0.25mm. The dimensions are designed to ensure a high current density in the region between these electrodes, giving rise to the characteristically wide metastable velocity distribution and high flux.

The current regulated supply was designed by and is described in detail by Trujillo (1975). It is capable of supplying 5 A with a voltage up to 90 V. The intermediate electrode is always at earth potential, and the cathode and anode are allowed to float during operation. However, a switch is provided to connect the intermediate electrode and anode when striking a discharge. A separate AC cathode heater supply allows up to 45A to be passed through the cathode filament at 3.5V. A glass U-tube manometer (see Figure 4.2b) containing diffusion pump oil is connected between the source and the adjoining vacuum tank to measure the source gas pressure, which during operation is between 0.5 and 1 torr. The manometer can be bypassed to pump the source directly through the vacuum tank, providing greater pumping speed during cathode outgassing.

Figure 4.2a Cross section through the metastable atom source designed and built by Trujillo (1975)

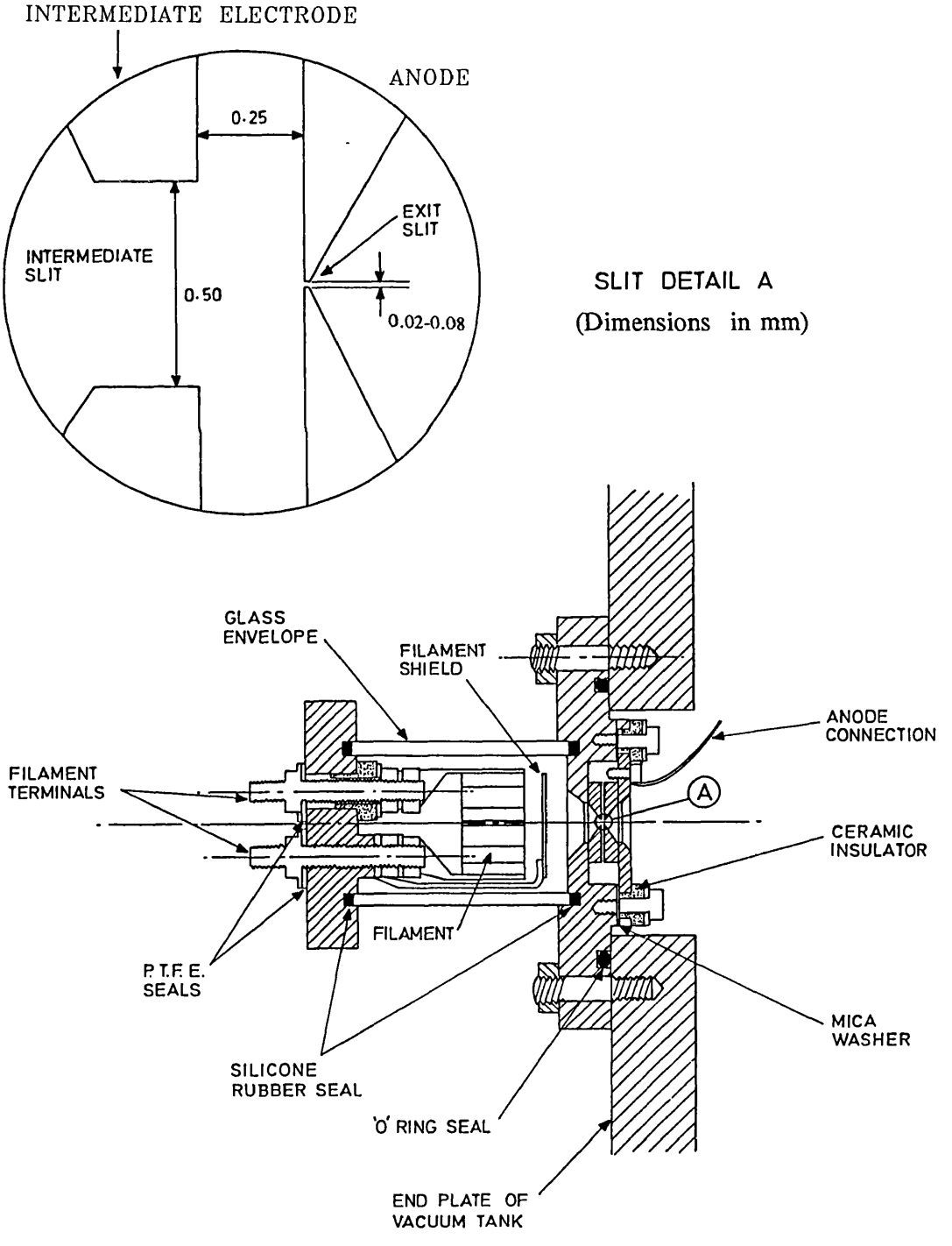

Figure 4.2b Photograph of the metastable atom source

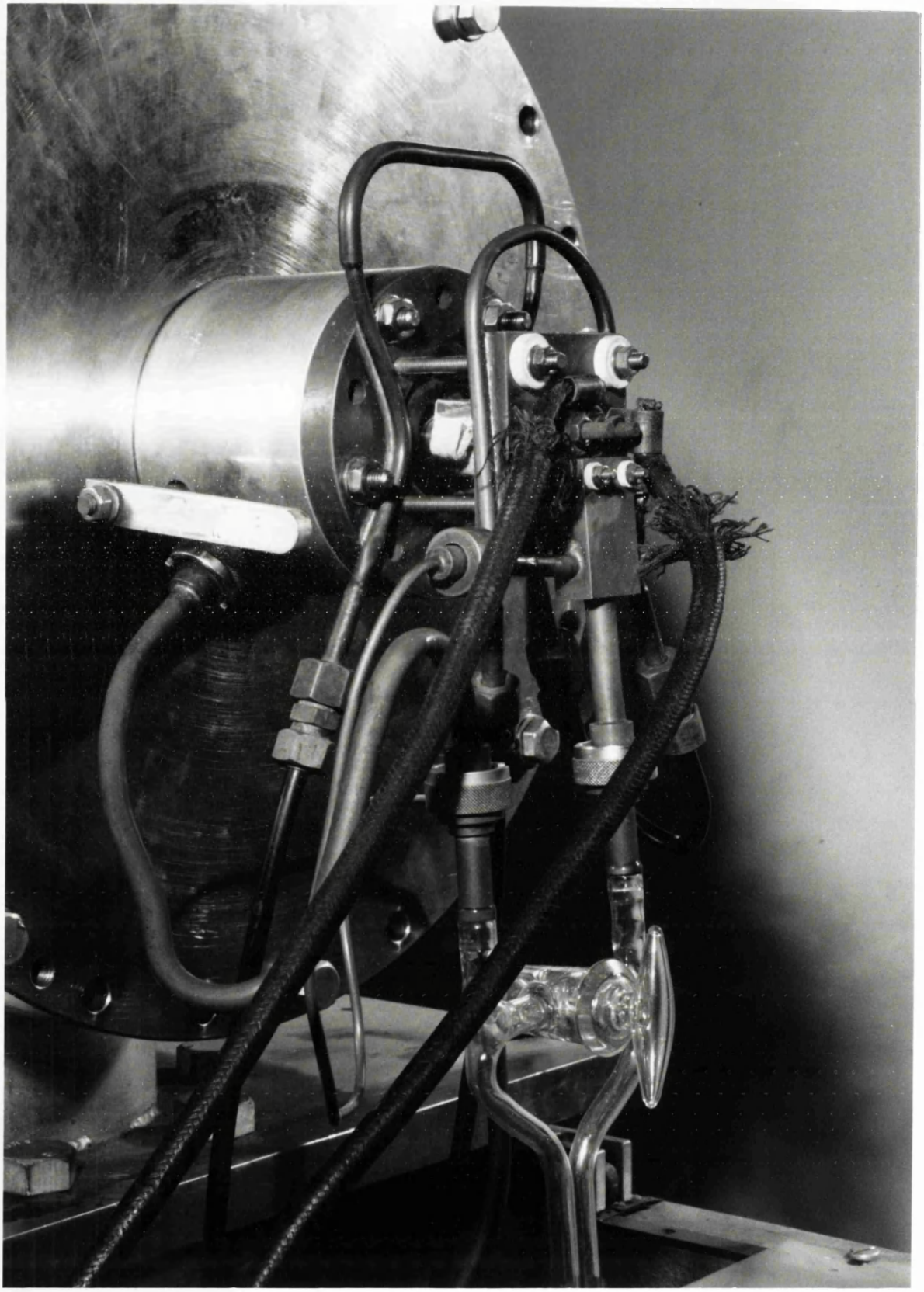

4.2.2 Cathode preparation

The cathode filament is made from a strip of nickel gauze 80mm long and 30mm wide, folded three times to make it 10mm wide and then spot-welded along the open edge. The strip is wound around a jig to give it a zig-zag shape and the ends are each spot welded to a stainless steel support. The cathode filament is cleaned ultrasonically in pure acetone, dried with a hot air gun and coated with a highly electron-emissive triple-carbonate mixture of barium, strontium and calcium, (Derby Luminescents, type EEM/36A). The cathode filament is heated to approximately 100° C to evaporate the butyl acetate solvent, and four more coats are carried out in a similar way until the gauze is completely filled and evenly covered. The cathode filament is once more thoroughly heated to remove as much solvent as possible and is then carefully fixed by its supports to the source back plate. The back plate is fitted to the glass tube and the assembly is secured in position on four studs protruding from the front plate (Figure 4.2b).

The source is pumped down by a backing pump to 10^{-3} torr and then through the source tank, via the manometer bypass, until the pressure stabilises below 10^{-6} torr. A small current is then passed through the cathode (1-5 A) and is gradually increased to 20 A at a rate which ensures that the tank pressure does not exceed 2×10^{-5} torr. A higher pressure ($5\text{-}10\times10^{-5}$ torr) indicates that the cathode coating is being shed and that the lifetime of the cathode filament will be significantly reduced. At 20 A the carbonates in the coating begin to dissociate to form oxides and a large amount of CO_2 is given off. The current is slowly increased to 30 A where it is maintained until the reaction is complete and the source tank pressure is below 10^{-6} torr.

4.2.3 Operation and characteristics of the source

With a cathode filament current of 30 A and the pressure in the vacuum tank less than 10^{-6} torr the source can be operated. The manometer bypass valve is then closed, and helium is slowly leaked into the source. When the pressure reaches 1.3 torr, (the manometer reads 20 mm of oil) a discharge may be struck. To strike the discharge, the anode and intermediate electrode are connected together and 100 V is applied between cathode and anode. When the discharge is bright and covering the intermediate electrode, the anode is disconnected from the intermediate electrode and the discharge strikes through the slit in the intermediate electrode and onto the anode. If the anode does not strike, the cathode

filament current is increased and the above procedure repeated until a discharge is achieved. The discharge current quickly increases from 0.2 to 0.5 A, along with an increase in discharge brightness and beam intensity. Initially the discharge colour is light blue, indicating the presence of impurities from the cathode filament, but over several hours the colour changes to a light pink. The change of colour is accompanied by a change in the velocity distribution of the metastable beam. Figure 4.3 shows two TOF distributions, 4.3a is produced by a new cathode and 4.3b by a cathode several hours old. Initially the presence of impurities in the source prevents the appearance of the characteristic high velocity peak visible in figure 4.3b. The high velocity peak which is present until near the end of the cathode life, has been explained by Trujillo (1975) as due to a region of high temperature (greater than 10^4K), which is not in thermal equilibrium. Such a high temperature does not seem feasible and a more likely source of the high velocity peak is the dissociative recombination of He_2^+. The low velocity or thermal distribution is however characteristic of a temperature in the source of 540K.

As the filament ages the coating is depleted due to sputtering. To strike a discharge, the cathode current must then be increased sometimes up to 40 A. However, eventually it is no longer possible to strike the discharge and the filament must be replaced.

4.2.4 Production of metastable He(2^1S)

The present source has been used in the work of Jerram (1985), Harper (1977) and Trujillo (1975), which were all concerned almost entirely with the He(2^3S) metastable state. Only Harper and Davies (1980) made preliminary measurements with He(2^1S) metastable atoms using a velocity selector. Trujillo found the percentage of He(2^1S) metastables in the beam to be 12 ± 1% at 1.59×10^3 ms^{-1} and 8 ± 4 % at 1.12×10^4 ms^{-1}, and these figures were considered by Harper (1977) and Jerram (1985) to be low enough to rule out experiments using He(2^1S). Present measurements of beam composition agree quite well with those of Trujillo (1975), indicating that He(2^1S) metastables make up no more than 15% of the beam content at any velocity.

A high total flux of metastable atoms is vital to the speed of data collection and reliability of an experiment using the He(2^1S) state. Table 4.1 shows a comparison between the Trujillo source and several others used in different beam experiments. An alternative design would have been considered if it could have given a good velocity range with an improved

Figure 4.3a Metastable TOF distribution from source with new cathode

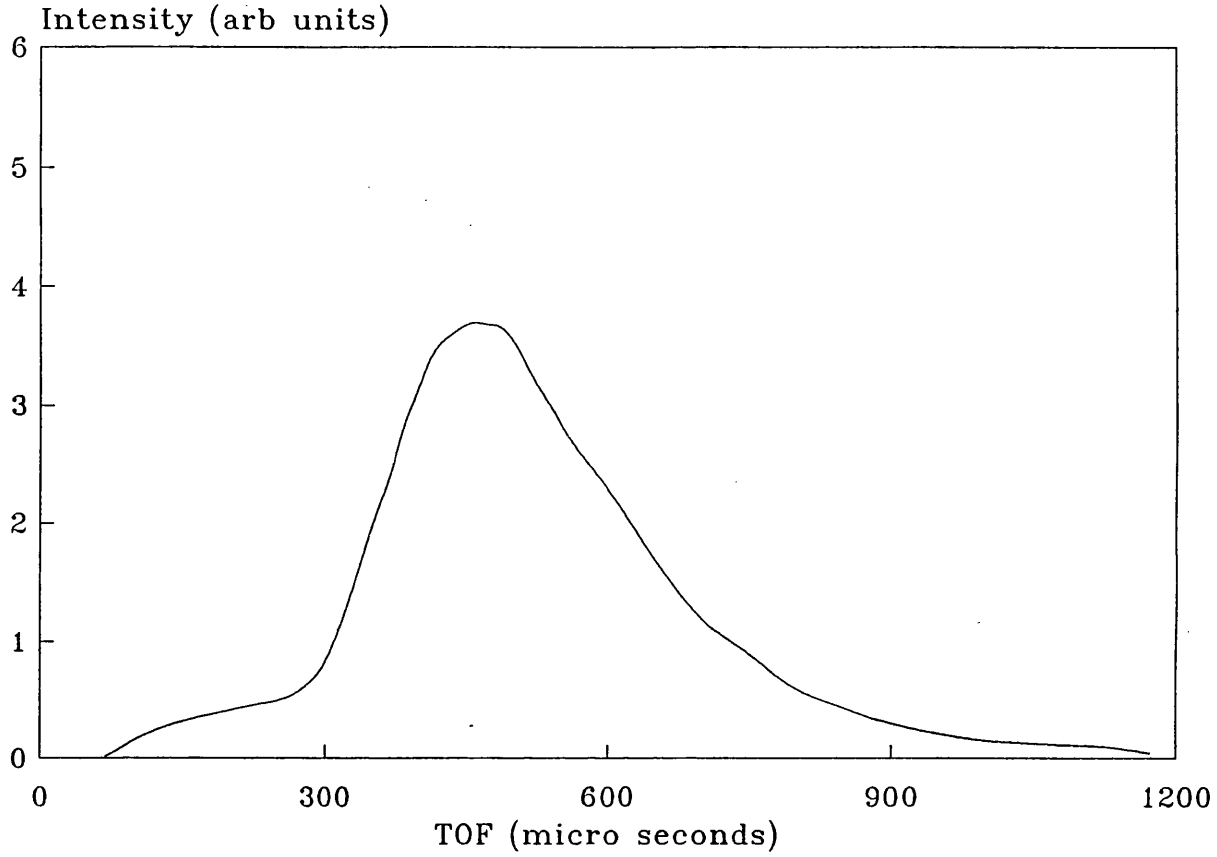

Figure 4.3b Metastable atom TOF distribution after several hours use

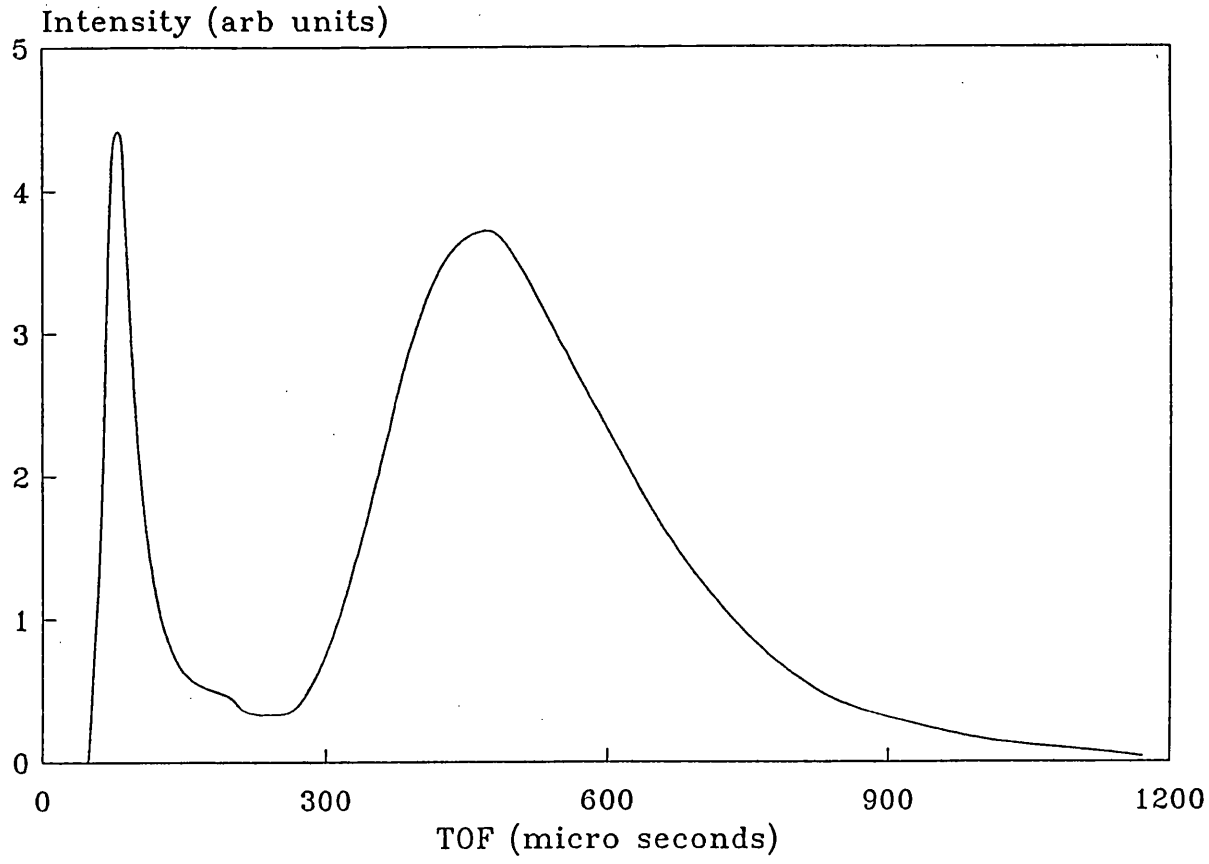

singlet flux. The velocity range produced by the Trujillo source (1-30 kms^{-1}) is superior to the other designs, although the Kroon (1985) source is quite good at 7-17kms^{-1}. However the percentage of He(2^1S) from the Kroon source is low at 5%, although the beam intensity is high. A big disadvantage of this source is that it uses a 1000 W power supply (Theuws et al 1982). The Fahey et al (1980) cold-cathode-arc supersonic-nozzle source produces a large He(2^1S) flux but with only a narrow velocity range of 1.3-2.3kms^{-1}. Brutschy et al (1976) give a figure of 85% for the He(2^1S) content of their beam with a good beam intensity, but again the velocity range is far too limited at 0.8-3 km^{-1}. Parr et al (1981), Illenberger and Niehaus (1975) and Pesnelle et al (1975) have used sources with moderately good velocity ranges (1-5kms^{-1}), but the percentages of He(2^1S) are small, and their beam intensities, although not reported, are probably similar to the Trujillo source as they are also hot cathode designs. The Trujillo source offers the best combination of velocity range and He(2^1S) flux required for the present purposes, provided it is operated near its maximum output, and has therefore been used throughout the experiments described in this thesis. The mode of operation has been thoroughly investigated to ensure that a good beam intensity is always achieved.

4.2.5 Maximising the metastable atom beam intensity

In his thesis Jerram (1985) indicates that the beam intensity obtained in his experiments was approximately 10^{12} $s^{-1}sr^{-1}$. An initial goal in the present work was to improve this figure to 10^{13} $s^{-1}sr^{-1}$. This would then allow experiments to be performed in a relatively shorter time and make He(2^1S) experiments feasible. The limited flux of He(2^1S) metastables in the beam as operated by Jerram implies that an experimental duration of up to 300 hours would be necessary to record a complete data set. This would be reduced to 30 hours if a factor of ten increase in beam intensity could be achieved. Maintaining such an increased output is initially dependent upon finding the optimum operating conditions. All of the design parameters which influence the beam intensity have been identified and where possible steps have been taken to improve the design and thus the source performance. Each of the parameters and the improvements made is described below.

a) Filament heater current: this has an effect on the density of free electrons in the plasma. It is set to the minimum level necessary to maintain a steady discharge and prolong the lifetime of the cathode. Increasing the current is found not to give a better metastable intensity, but does increase the photon flux.

Table 4.1

Comparison of metastable helium sources

Reference	Type of source	Intensity ($sr^{-1}s^{-1}$)	Percentage $He(2^1S)$	Velocity range kms^{-1}
Trujillo (Present) (1975)	Constricted arc	10^{12}	12	1-20
Fahey et al (1980)	Supersonic nozzle	3×10^{12}	5	1.3-2.3
Pesnelle et al (1975)	Hot cathode	------	33	1.2-4.5
Illenberger and Niehaus (1975)	Hot cathode	------	< 50	1-5
Kroon (1985)	Cold cathode	$1\text{-}2\times10^{14}$ *	5	7-17
Parr et al (1982)	Hot cathode	------	20-50	1-6
Brutschy et al (1976)	Supersonic nozzle	3×10^{14}	85	0.8-3

* Units of $sr^{-1}s^{-1}mm^{-2}$

b) Discharge current and voltage: these control the electron density and energy in the anode aperture region and therefore the amount of excitation and ionisation taking place. The constant current supply is normally set to 0.5 A and the voltage varies from 70-90 V. Higher current gives a minor improvement in the metastable intensity, but a much greater photon flux.

c) Pressure in the source and adjoining vacuum tank: elastic scattering of metastable atoms in the vacuum tank is a major limiting factor on the intensity of the metastable beam. Collisions which excite helium into its metastable states are thought to occur in the constricted arc region of the source, where the electron density and temperature are highest. Collisions between metastables in the beam and background helium which occurs in tank T1 just outside the exit aperture remove atoms from the beam by scattering. Figure 4.4a and 4.4b show the relationship between source and tank pressure and beam intensity. Increasing the source pressure leads to a corresponding increase in the tank pressure and a drop in the metastable atom signal. The source pressure is set at 0.5-1.3 torr for the best performance. Although the optimum pressure varies for each cathode, it has been found that the beam intensity is higher towards the lower end of the pressure range. Typically Jerram (1985) operated the source at pressures of over 1 torr resulting in a poor beam intensity. The vacuum tank pressure does not rise above 3×10^{-6} torr when the source is in use.

d) Anode slit width: This is the primary controlling factor for the beam intensity by setting the rate of effusion of helium into the vacuum tank. The width has been increased from 0.02mm to 0.08mm without causing the rapid increase in the vacuum tank pressure and a marked loss of beam signal as experienced by Trujillo (1975), probably because he did not compensate by lowering the source pressure. With the present combination of slit width and source pressure, beam intensities have been recorded of up to thirty times the level reported by Trujillo (1975) and Jerram (1985) and typically a factor of 10 is achieved.

e) Intermediate electrode slit width: This has some control on the electron density in the region of the anode slit. No adjustment to this width has been made; it remains 0.5mm.

f) Impurities: these cause collisional quenching of metastables within the source. The cathode coating is an important source of impurities, mainly CO_2, which continues to be produced by the cathode for some hours after a discharge has been struck. A black substance builds up on all of the surfaces inside the source, over the lifetime of each cathode, particularly on the intermediate electrode and filament shield. If this build up is not removed before a new cathode filament is fitted, the beam intensity is reduced drastically.

Figure 4.4a Metastable atom intensity verses source pressure

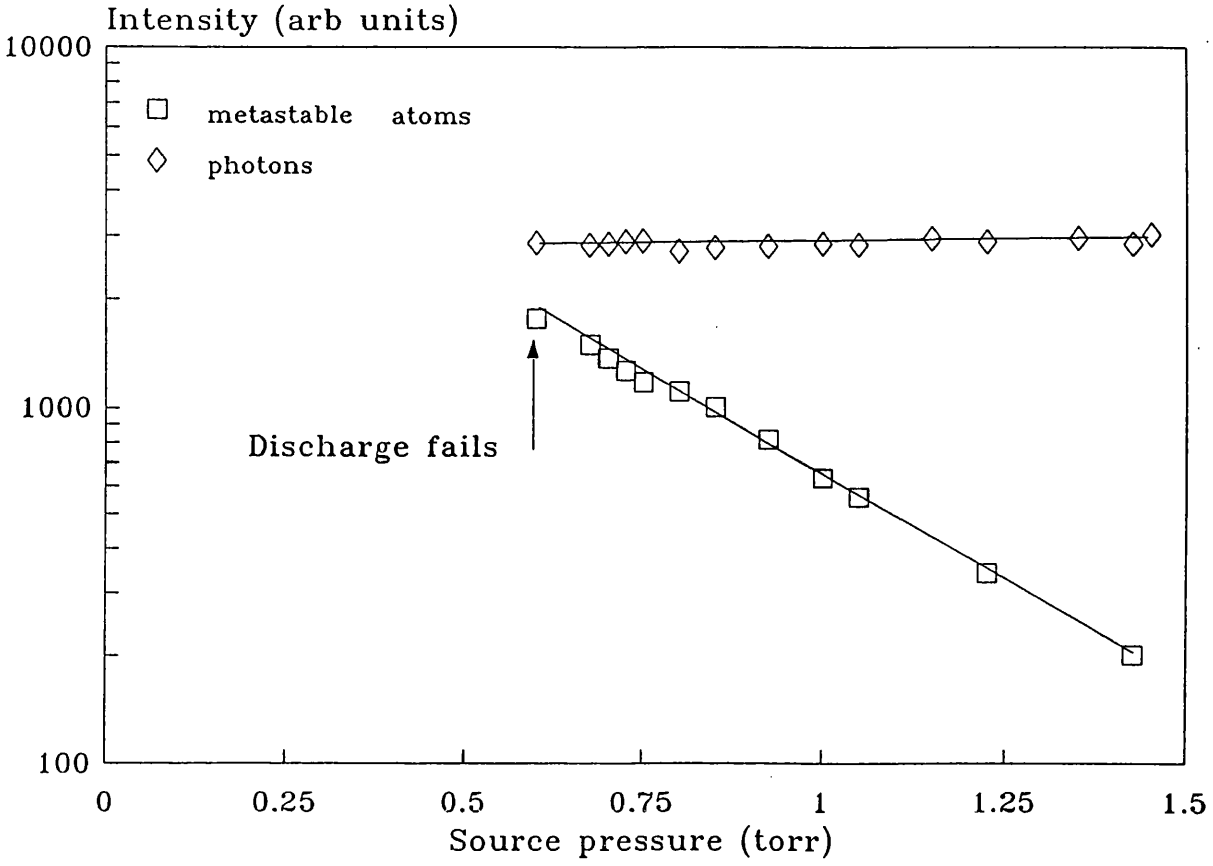

Figure 4.4b Pressure in source verses pressure in tank T1

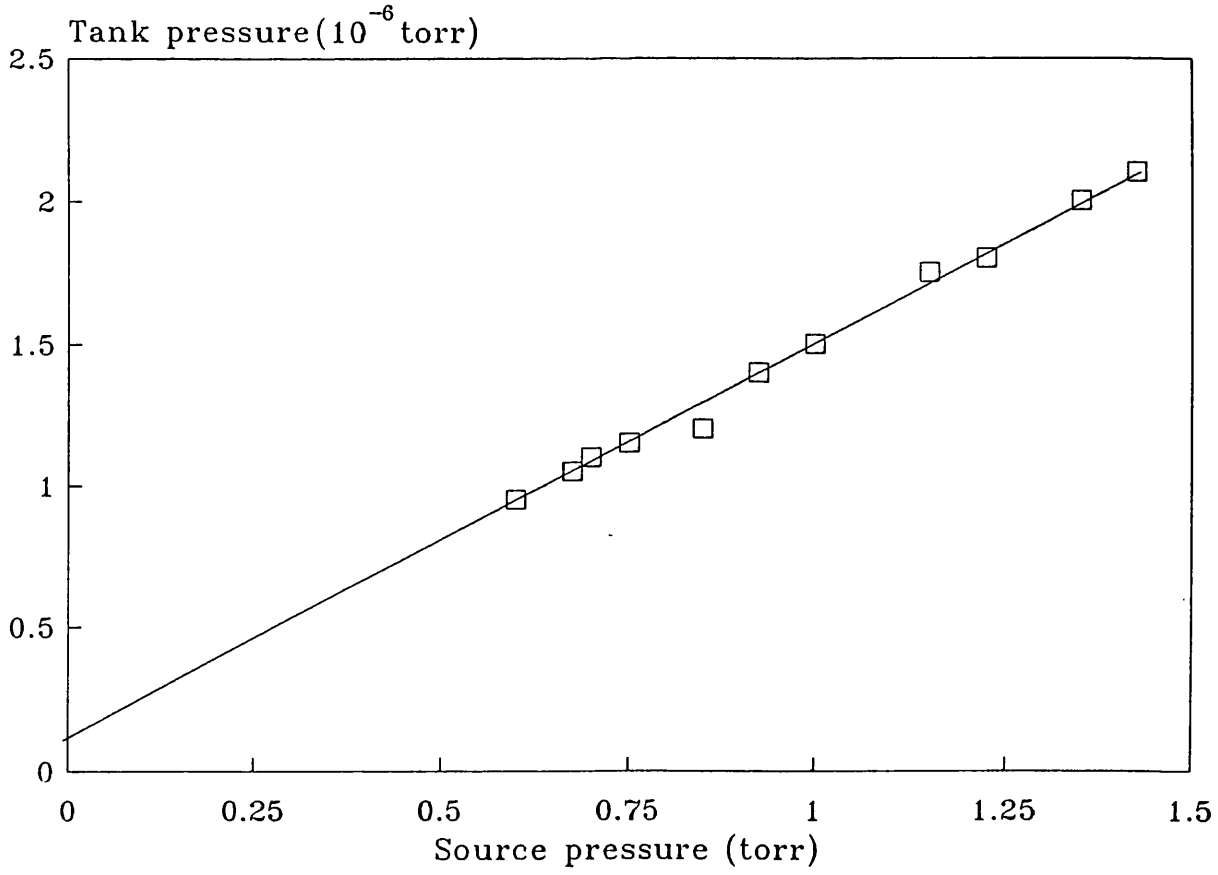

g) Cathode coating thickness: this affects the electron density in the source and also the amount of impurity in the discharge. The quantity of coating used is such as to maximise the lifetime of the cathode and the discharge current for a given heater current and to minimise impurities given off by the coating. The coating procedure described in section 4.2.2 was arrived at by trial and error and normally four to five coats are applied.

Figure 4.5 shows a plot of the intensity against beam velocity distribution before and after the changes were implemented. A very similar velocity distribution is apparent in the graphs, but with an increased intensity in the latter case. The improvements in the metastable beam intensity have also given rise to an increased photon flux. This is not a problem because the photon peak in the TOF spectrum arrives as a prompt pulse and is easily distinguished from the slower metastable flux.

No factor has been discovered which controls the ratio of the number of metastables in the high velocity distribution to the number in the thermal distribution and normally the peak of the high velocity part of the distribution is only about half that of the thermal part, although sometimes the two peaks are about equal. The amount of coating on the cathode may affect this ratio because each cathode appears to have a characteristic ratio associated with it.

4.2.6 The target beam

The target beam is formed in a tank adjacent to the experimental chamber. Gas is admitted through a needle valve and passes along a tube cooled by a cold trap before emerging through a multi-channel aperture array. The beam enters the interaction region through a small aperture placed 10mm from the multi-channel array, to provide collimation.

Cooling the gas reduces the thermal velocity of the cross beam. For gas in the form of a beam, the mean velocity is proportional to the square root of the gas temperature. Consequently when liquid nitrogen at 80K is used in the cold trap the gas temperature is reduced by a factor of approximately four and the mean velocity is approximately halved. Section 5.2 describes the corrections made to cross section measurements to compensate for the target beam velocity. Not all target gases can be cooled to such a low temperature because they condense in the multi-channel array. Only Ar and CH_4 can be cooled to liquid nitrogen temperature. N_2O is cooled to the freezing point of carbon dioxide (194K)

Figure 4.5 Comparison of new and old metastable atom intensity

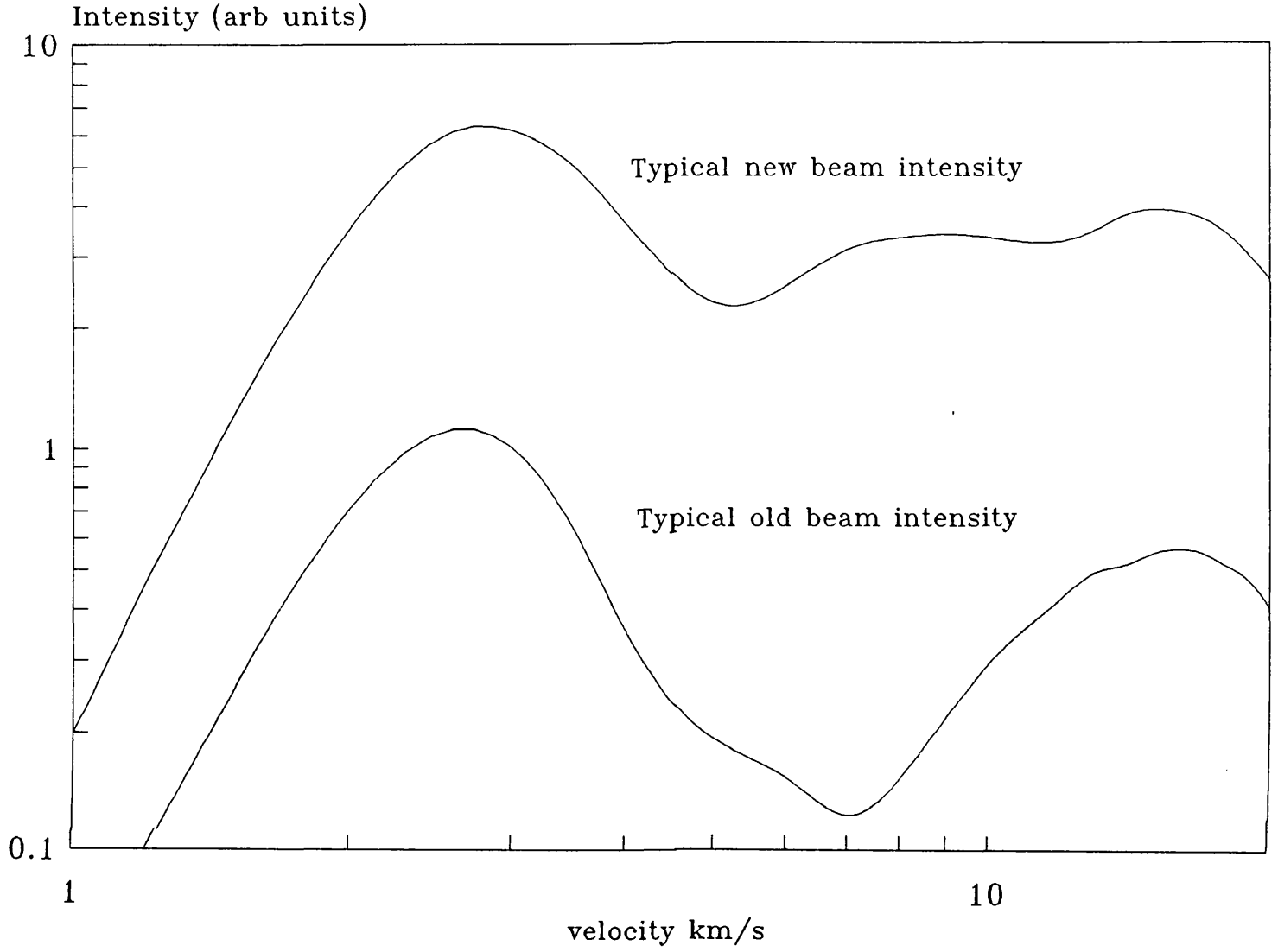

but the other target gases could only be used at room temperature.

The gas pressure is measured in the experimental tank T3 using an ionisation gauge. When a stable pressure of $1\text{-}2\times10^{-6}$ torr is reached, then data acquisition may begin. The ionisation gauge produces a background of ions so is switched off during data acquisition.

It is necessary to monitor the pressure in tank T3 between data runs because most of the gases freeze on the liquid nitrogen trap and then slowly evaporate as the liquid coolant level decreases. This is particularly true of N_2O, SF_6 and NH_3. In addition to this problem, NH_3 also tends to condense in the needle valve due to adiabatic expansion. The target beam intensity then decreases continuously and the needle valve must be frequently adjusted.

Gases used in the target beam were always of at least 99% purity and were supplied in lecture bottles (Cambrian Gases or Argo International). The purities are, Ar 99.995%; CH_4 99.995%; NH_3 99.96%; CO_2 99.99%; N_2O 99.5%; C_2H_2 99.5%; SF_6 99.9%.

4.3 The quench lamp

4.3.1 Introduction

To perform experiments using $He(2^3S)$ or $He(2^1S)$ it is necessary to separate atoms in the two states. A beam of nearly pure $He(2^3S)$ can be achieved by passing the beam through a region illuminated with radiation from a helium-filled discharge lamp. For earlier experiments using this apparatus a helical lamp of the type described by Hotop et al (1969) was developed by Allison (1978) and Harper (1977) in which the beam passes along the axis of the helix. In the previous experiments it was only necessary to remove most of the singlet metastable population, but in the present work where the difference in signal between the quench lamp on and off states is measured, it has been necessary to consider carefully how the quench lamp performance could be improved. The Harper lamp was used initially but a new lamp has also been built which is of superior performance.

4.3.2 The quenching process

Figure 4.6 shows the energy levels of helium and the transitions excited by the quenching radiation. 2058nm and other singlet radiation excites the $He(2^1S)$ metastable to the 2^1P or

Figure 4.6 The energy levels of helium

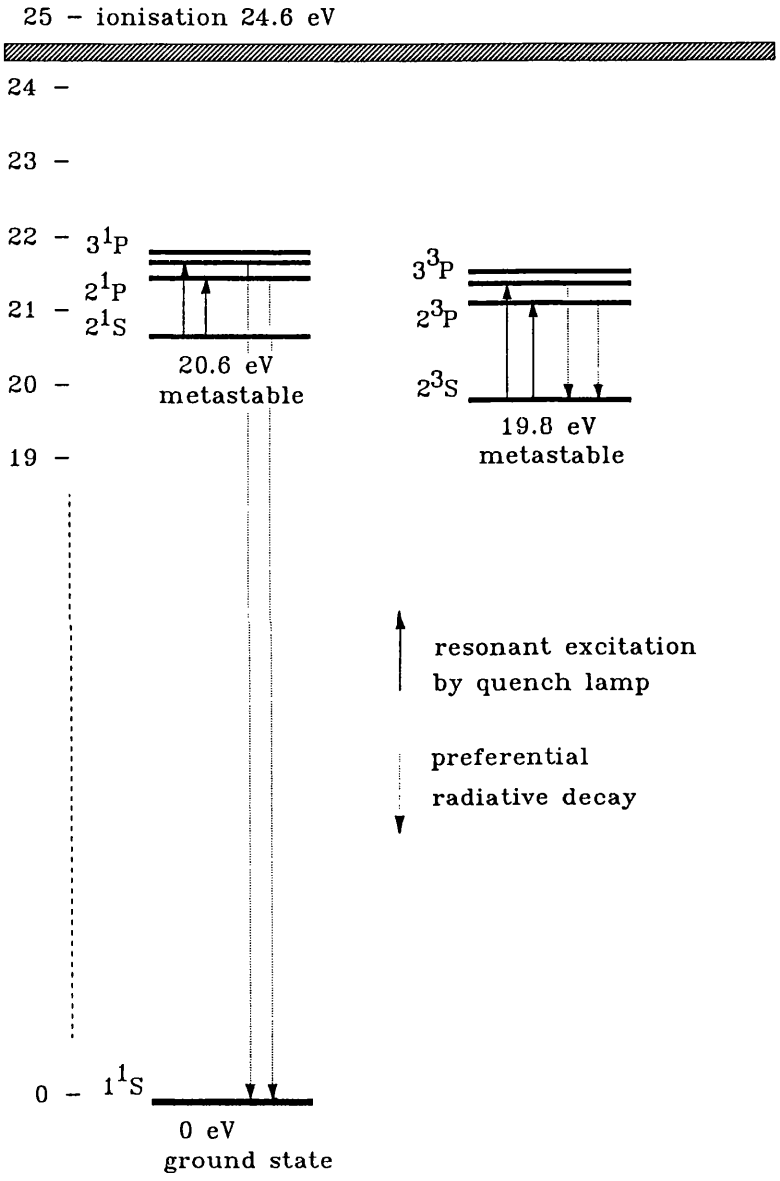

higher ^1P states. These preferentially decay to the 1^1S ground state with 98% probability. Ground state atoms cannot be excited to the He(2^1S) state by the 58.4 nm line because UV radiation of this wavelength does not pass through the glass quench lamp tube. He(2^3S) metastables are predominantly excited to the 2^3P state by the 1083 nm radiation, and other triplet radiation may excite higher ^3P states. These can only decay to the 2^3S state, leaving the He(2^3S) beam content intact.

4.3.3 Lamp performance

The performance of a quench lamp can be quantified in terms of the quenching efficiency, a measurement of the fraction of metastable atoms in the 2^1S state which is quenched by the lamp. It is desirable to have a quenching efficiency approaching 100% for metastables of all velocities, allowing the full He(2^1S) signal to be observed as the difference between signals with the lamp on and off.

The quench lamps used by Allison, Harper and Jerram were developed from the design described by Hotop in 1969. The lamps consist of six turns of a 6mm diameter Pyrex glass tube containing helium at a pressure of approximately 3 torr. Figure 4.7 shows the lamp built by Harper (1977) and used by Jerram (1985), and inherited by the present author. The performance of this lamp is estimated using three different expressions to calculate the quenching efficiency as a function of velocity. The first expression was devised by Parr et al in 1982 and recognises that the probability of a metastable absorbing a photon of quenching radiation is proportional to the amount of time spent in passing through the lamp. The expression given is

$$q(v) = 1 - e^{\left(-\frac{c}{v}\right)} \qquad (4.1)$$

where q is the quenching probability, c is a constant characteristic of the quench lamp, and v is the metastable velocity. Clearly a fast metastable is less likely to be quenched than a slow metastable because it spends less time passing through the lamp coils. Kroon (1985) has derived a more realistic expression as follows

$$q(v) = 1 - e^{\left(-\frac{BI}{v^2}\right)} \qquad (4.2)$$

Figure 4.7 The quench lamp used by Harper (1977)

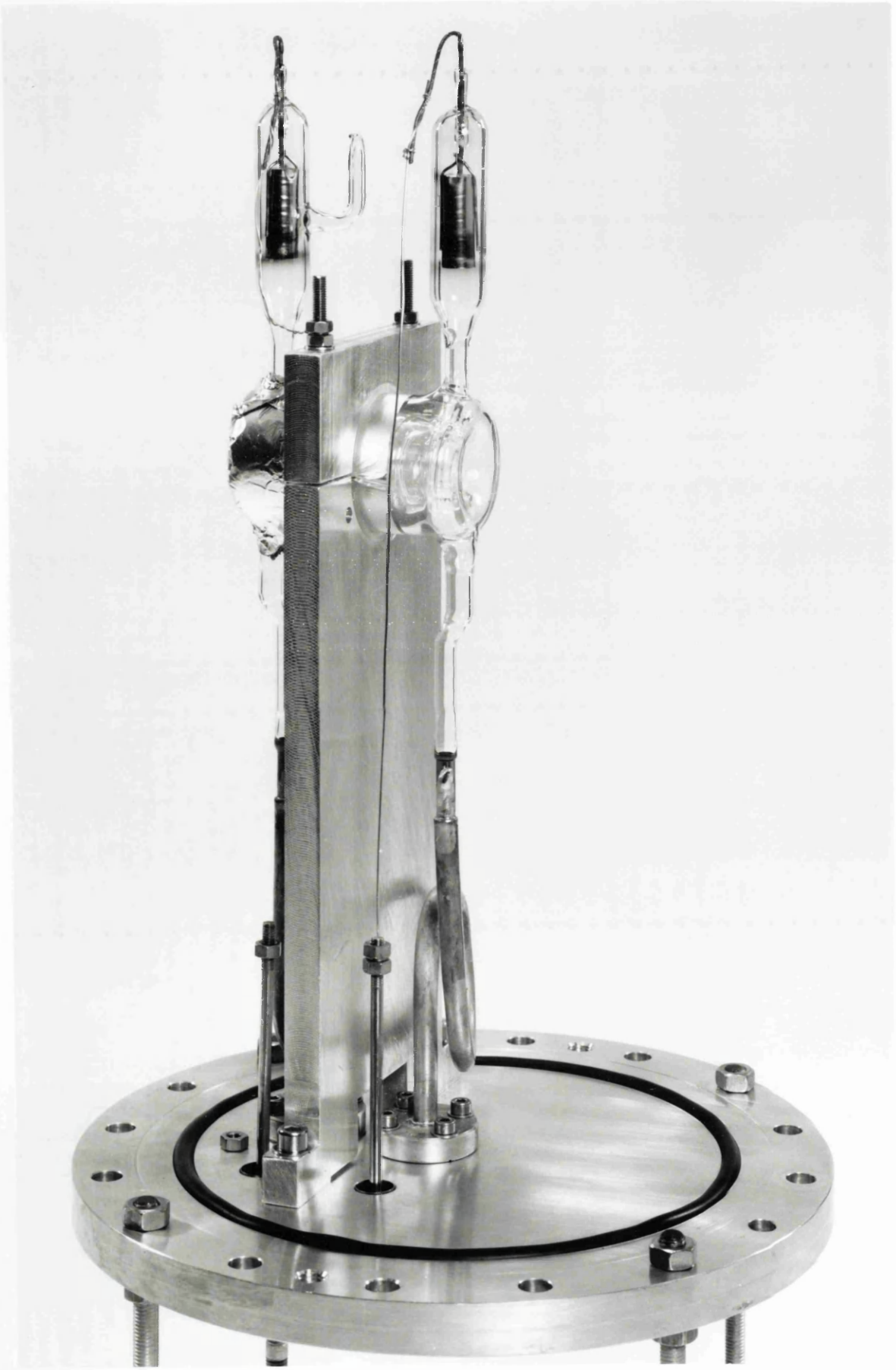

where B is a constant characteristic of the lamp and l is the length of the path followed by the beam through the lamp. The dependence on the square of velocity comes from consideration of the Doppler effect. A metastable atom passing through the lamp sees a shift in the frequency of the quenching radiation, due to its velocity component in the direction of the incident radiation. If the shift is greater than the width of the resonance line, the metastable atom does not absorb the radiation and quenching does not take place. The Doppler effect becomes significant above 10kms^{-1} reducing the quenching efficiency of the lamp. Jerram (1985) has derived a rigorous form of the quenching efficiency as a function of velocity

$$q(v) = 1 - \exp\left[-\left(\frac{D}{v}\right)\int_0^{\frac{\pi}{2}} e^{\left(-\left(\frac{M}{2KT}\right)v^2\sin^2\theta\right)}\, d\theta\right] \qquad (4.3)$$

where D is a constant characteristic of the quench lamp, m is the mass of the helium atom and k the Boltzmann constant. Jerram has shown that the Kroon expression is a good approximation to the rigorous formula. The three constants C,B,D from Equations 4.1, 4.2, and 4.3 are calculated by examining the variation of beam intensity, at a given velocity, as a function of quench lamp current. This can best be done by using a velocity selector to produce a beam of small velocity width. The flux from the lamp is assumed to be proportional to the discharge current.

Data recorded by Harper (1977) using a velocity selector is reanalysed in Appendix (1) using a more rigorous technique than used by either Harper or Jerram. Figure 4.8 shows a plot of quenching efficiency as a function of velocity for the Harper (1977) lamp with the efficiency calculated using expressions 4.1 and 4.2. It is clear that the Parr expression is inadequate at high velocities, because it does not consider the Doppler effect, and therefore greatly overestimates the quenching efficiency. The newly calculated figure of 47% quenching efficiency at 18 kms^{-1} using both the Kroon and Jerram expressions is lower than the figure of 55 % calculated by Jerram using the same formulae.

The quenching efficiency of the lamp (47%) was considered inadequate for a singlet experiment to be performed with good resolution at high velocity, because more than half of the He(2^1S) signal would be lost.

Figure 4.8 Variation of quenching efficiency with velocity

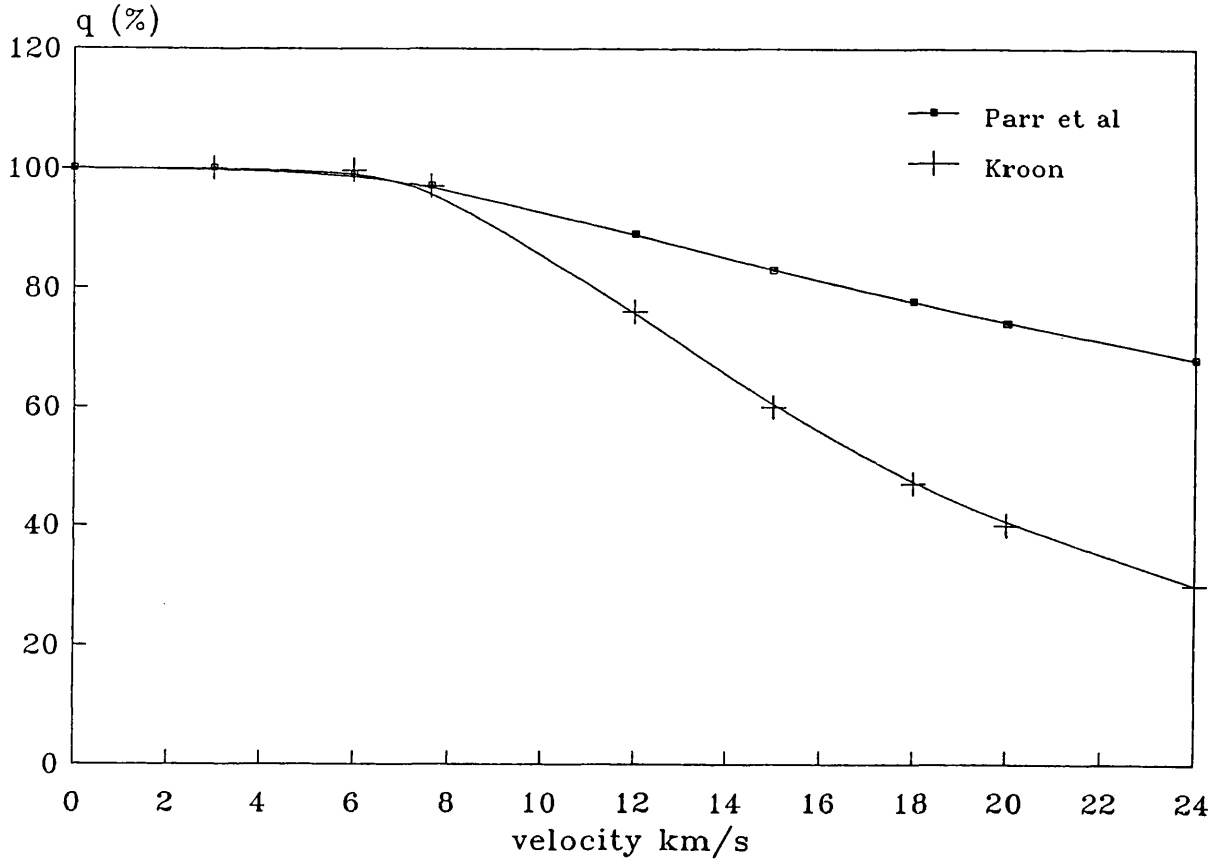

Figure 4.9 Variation of q(v) with quench lamp length

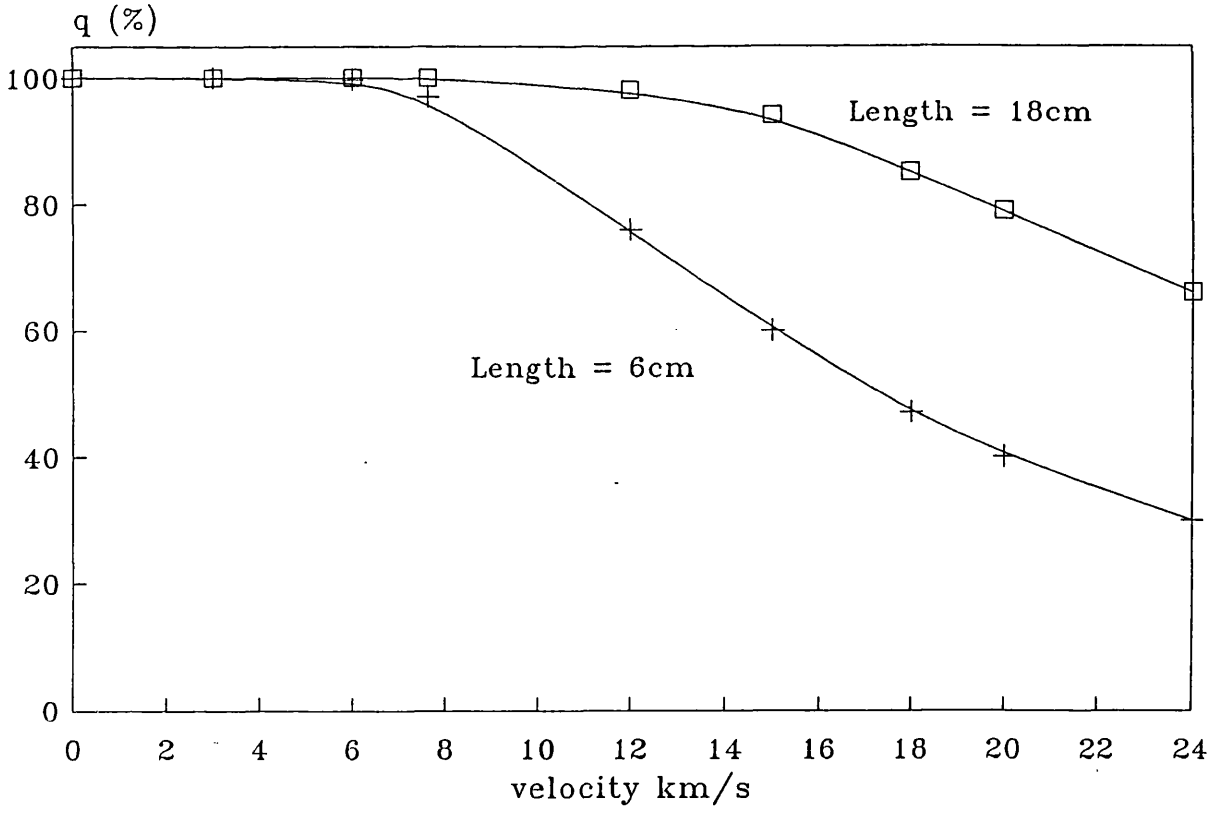

4.3.4 The new quench lamp

Figure 4.9 shows the theoretical quenching efficiency of a Hotop-type lamp but with eighteen turns compared to the six turns of the Harper (1977) lamp. This would give the lamp an emitting length superior by a factor of three. Such a lamp would have a quenching efficiency, calculated using expression 4.2, of 85% at 18 kms^{-1} compared to 47% calculated for the Harper (1977) lamp. This would give an improvement in the singlet metastable signal by a factor of nearly two.

A quench lamp with eighteen turns of Pyrex glass tube was constructed at UCL. Unfortunately, a discharge could not be struck with the supply which is available at UCL (5kV), unless the gas pressure in the lamp is less than 1 torr. This is comparable to the lamp used by Kroon (1985) which has ten turns of glass tube, with inner diameter 3mm. This lamp also operates at a pressure of 1 torr and has a performance similar to the Harper (1977) lamp. Taking this into account it is unlikely that the new lamp could supply a quenching power even double that of the Harper lamp and certainly not the desired factor of three improvement.

The requirement of a lower operating pressure can be overcome by increasing the tube diameter. Thus another lamp has been constructed using tubes of internal diameter 12mm, and 12 turns, shown in Figure 4.10 compared to the lamp used by Allison (1978).

The new lamp has an emitting length of 144mm (12mm $\times$ 12 turns) compared to 24mm (4mm $\times$ 6 turns) in the Allison and Harper lamps. A discharge can be struck at 5 kV and operated with a current of 56mA, double the current used by Jerram, in order to minimise the effect of the lower current density. This lamp has been used in the collection of all the data presented in this thesis, except for the total and partial cross sections of N_2O which were measured using the old lamp.

The lamp is enclosed in an air jacket for cooling, air circulation is provided by a diaphragm pump (Compton type D/1351VM). Circulating air is cooled by passing it through a cold trap containing solid CO_2 and solvent at -70° C. A trap containing activated alumina is included in the air circuit to remove water vapour. The large size of the lamp causes it to be prone to overheating; however the operation of the lamp in an "on/off" manner helps to prevent this.

Figure 4.10 The new lamp shown next to an old lamp for scale

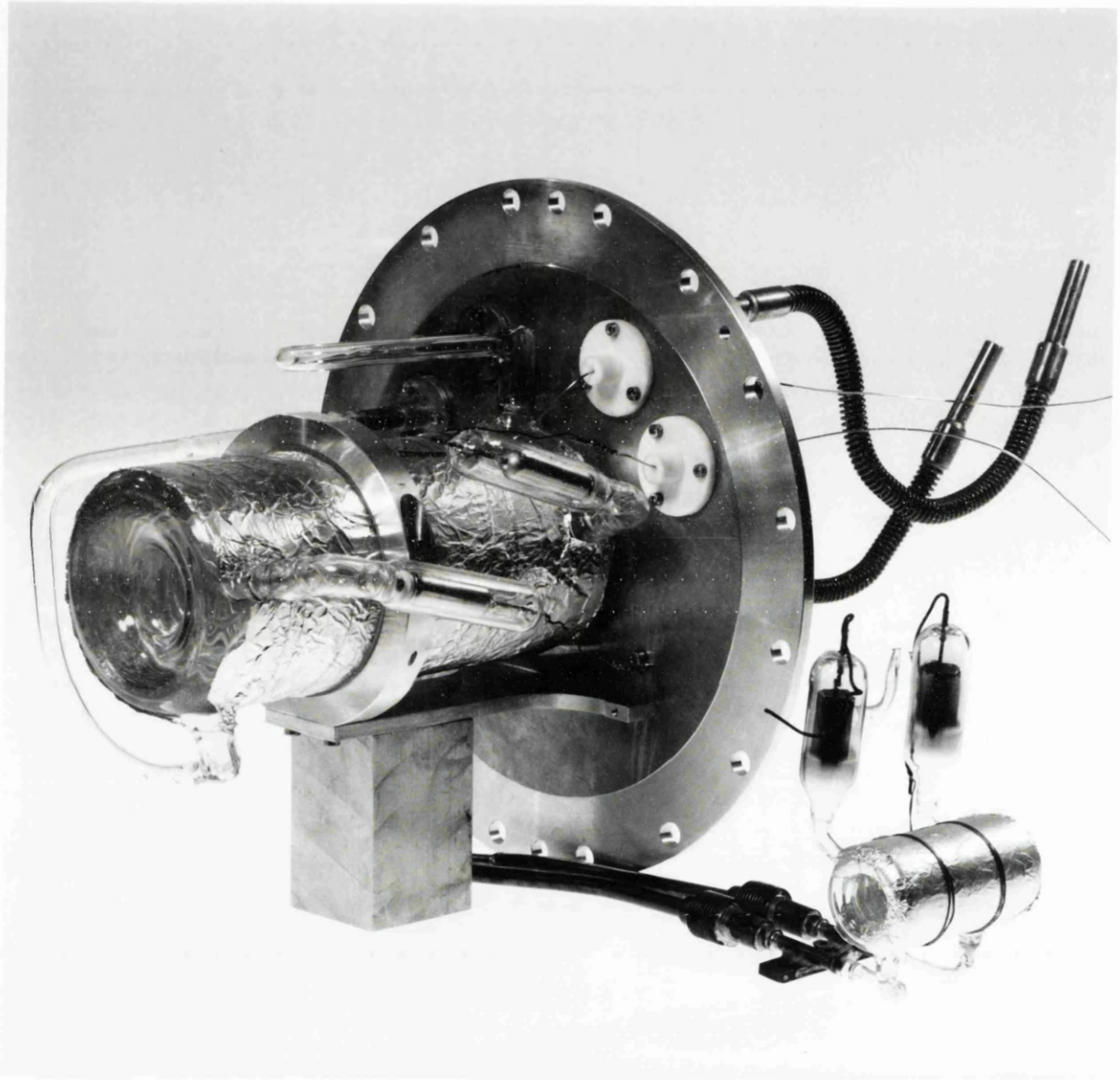

4.3.5 Comparison of new and old lamps

An assessment of the performance of the new lamp has been made by comparing the observed singlet to triplet intensity ratio with that for the old lamp. Figure 4.11a shows the singlet to triplet ratio measured using the old lamp during the recording of N_2O data. This is compared to the ratio using the new lamp measured during the recording of argon data. The percentage is always higher for the new than it is for the old lamp, but the ratio of the efficiencies of new to the old increases with velocity, as clearly shown in Figure 4.11b. The new lamp has a greater quenching efficiency than the old lamp at high velocity as desired, and is twice as efficient at 19km/s. The improvement is better than would be expected for a lamp three times the length of the old lamp shown by the solid line in Figure 4.11b.

The fact that the new lamp has a greater efficiency at low velocity (approximately a factor of 1.25), suggests that the old lamp is not as good as previously thought. However, it is possible that the metastable beam source now produces a larger fraction of singlet metastable atoms since the overall performance has been optimised.

The singlet to triplet ratio is not a smooth function of beam velocity, indicating that the velocity distribution of the singlet population is not the same as the triplet population. This is not surprising in the superthermal region where the metastable atoms are probably produced from the dissociative-recombination of He_2^+ (section 4.2.3). The different velocity distributions are the result of the dissociation of different ionic states of He_2^+. In the thermal velocity range it is likely to be due to regions of different temperature near the source aperture.

4.4 Utilising $He(2^1S)$ and $He(2^3S)$

To measure the total and partial ionisation cross sections for metastable $He(2^1S)$ with a reagent gas it is necessary to record TOF distributions with the quench lamp on ($He(2^3S)$ metastable atoms only) then with the lamp off ($He(2^3S)$ and $He(2^1S)$ metastable atoms). The singlet distributions are then derived from a subtraction of the first set from the second, as described by

$$f_{i,m}(v)[\text{singlet}] = f_{i,m}(v)[\text{quench off}] - f_{i,m}(v)[\text{quench on}] \qquad (4.4)$$

Figure 4.11a Singlet to triplet ratio for new and old lamp

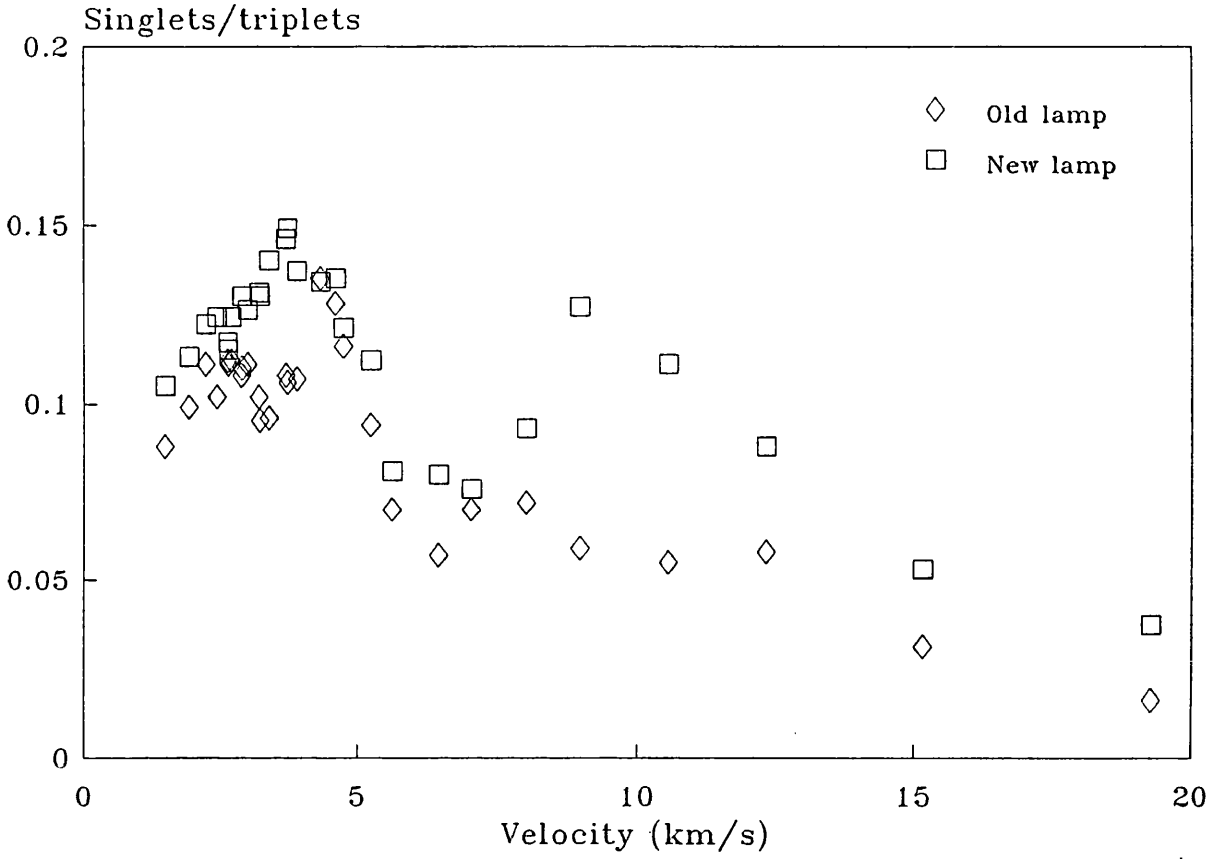

Figure 4.11b Improvement in quenching efficiency (q)

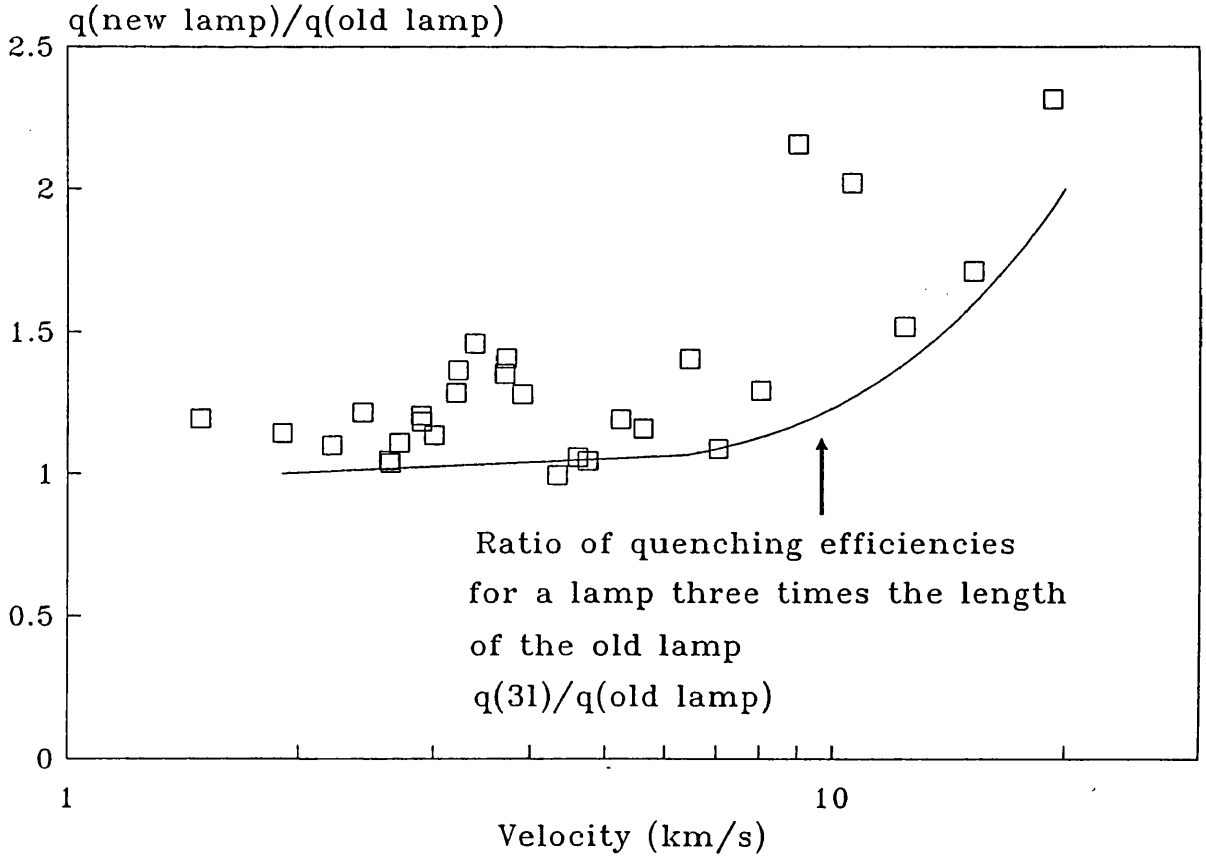

where $f_{i,m}(v)$ is an ion (i) or metastable (m) distribution as a function of velocity.

For this procedure to give a true singlet distribution it is essential that the experimental conditions do not change between the recording of the two distributions. The conditions which must remain constant between quench on and quench off distributions are the target beam intensity, the metastable beam intensity, the background pressure in the experimental tank and the detection efficiencies of metastable atom and ion detectors. All of these conditions change, but slowly over several hours and in the case of detection efficiency over several days. Only the metastable atom beam intensity varies at all significantly over a time scale of minutes, and, as described in section 4.2.3, the high velocity part of the beam output varies from zero to maximum intensity over a period of hours. The presence of an automatic pressure control such as used by Pesnelle et al (1975), would have helped to reduce this, but the short life of the cathodes used and the resulting drift in source output, would not be affected. With only a small fraction of singlets present in the beam (10-15%) it is very important that the signal is not swamped by small drifts in beam intensity between on and off periods. If the variation of beam intensity takes the form of brief fluctuations about a constant level, then it is possible to accumulate each distribution over a long period of time, in order to average these variations out. Pesnelle et al (1975) have used this technique, taking one hour to record each distribution and recording four distributions in turn. This technique would be useless in the present experiment, because of the drifting metastable atom intensity. Consequently a switching technique has been devised to record all distributions in rapid sequence. In the case of a total cross section experiment four distributions are recorded (ion and metastable distributions with lamp on and off), but for branching ratios twenty mass spectra must be obtained (10 mass spectra with the lamp on and off).

Figure 4.12 shows the data recording cycle in the form of a flow chart. The short data recording times ensure that no appreciable change in conditions takes place between the recording of quench on and off distributions. To test the effectiveness of this procedure the data recording cycle has been performed without operating the quench lamp so that the singlet distributions for metastables and ions should be empty. In fact the number of counts in the singlet distributions was less than 0.1 % of the number of counts in each parent distribution. With the singlet flux expected to be over 10% of the beam intensity this means that the singlet distribution would contain a background of less than 1%. This was judged to be very satisfactory.

Figure 4.12 Data recording cycle

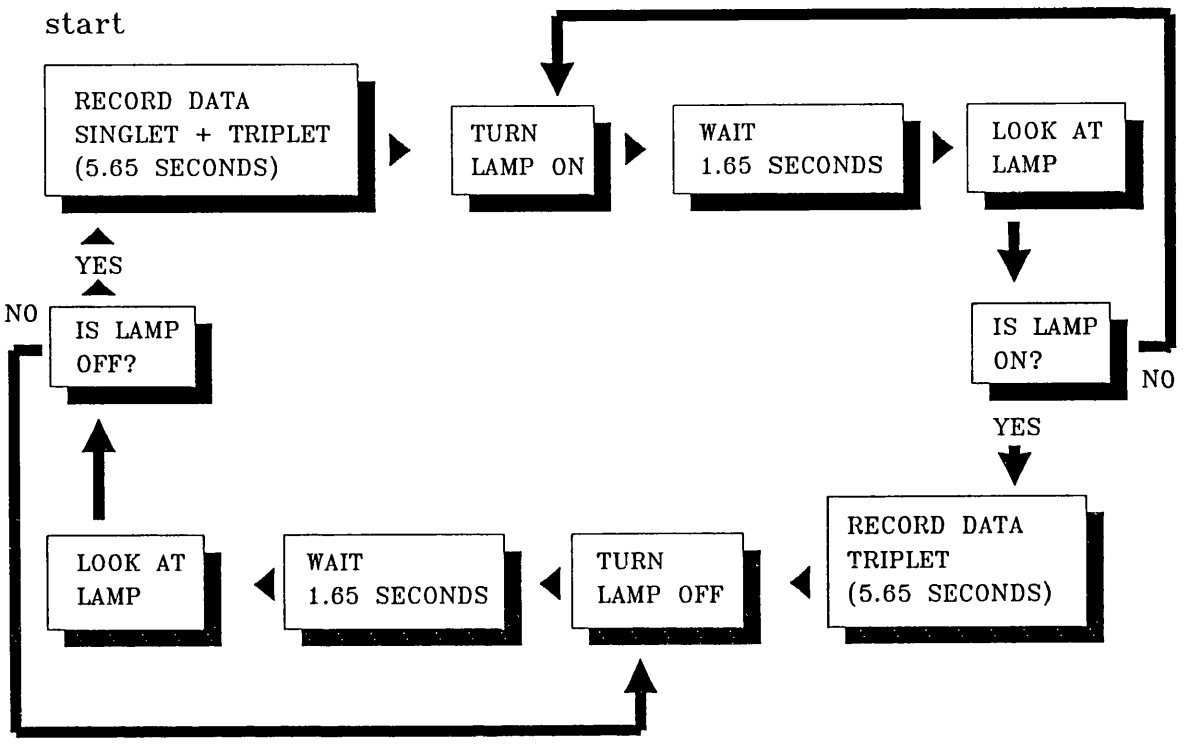

In the data recording cycle 77% of experimental time is spent recording data. A short time has to be allowed for the quench lamp to achieve equilibrium, either on or off. To ensure that the lamp strikes, an oscillating high voltage from a Tesla coil is applied to the foil wrapping of the quench lamp (Figure 4.10), for 0.2 seconds at the moment the lamp is switched on. Without such an impulse the lamp may fail to strike. The lamp and tesla coil are controlled by the computer through a CAMAC interface and a dual digital-to-analogue converter (DAC Hytec 620). This drives two relays; the first switches the Tesla coil and the second, through an intermediate logic circuit, the lamp supply. This intermediate step is necessary because the CAMAC crate is initialised immediately before data is collected and after the quench lamp is turned on or off, which means that all of the units interfaced with the CAMAC crate are reset. The constant quench lamp supply must be supplied by a unit which is not reset but which can be turned on or off by a signal from the DAC. This is achieved by a simple monostable circuit shown in Appendix 2. It is necessary to initialise the CAMAC crate before data is recorded because otherwise there is a tendency for spurious counts to be recorded in the TOF distributions, which can seriously distort the singlet distributions. The origin of these counts seems to be in the counting registers which

are affected by the Tesla coil. An optically activated switch (RS 305-434) is used to look at the lamp, communicating with the computer via an amplifier circuit (Appendix 3) connected to an input/output unit (Nuclear Enterprises type 9017), again interfaced through the Camac crate. If the lamp has not successfully been turned on or off a message appears on the monitor screen and the switching procedure is repeated.

4.5 Total ionisation cross section measurement

4.5.1 The TOF system and metastable atom detection

The chopper wheel, which has only one slit 5mm wide and 53mm from the centre of the shaft, rotates once every 4.5ms (222Hz) releasing a pulse of metastables and photons 6.5μslong. Figure 4.13 shows the photon peak profile, recorded over several hours, with its characteristic peak shape, a consequence of high count rate (section 4.5.5). The width is approximately 6.5μs indicating a stable chopper wheel speed. The chopper slit passes through a slotted switch (Schmidt type SW 304-560) 10°in angle before passing in front of the source aperture. The pulse from the switch is electronically delayed to compensate for the angular displacement and is applied as the start pulse for the timing system. Metastable flight times vary from 45μs to 1500μs giving a variation in resolution from 14% to 0.4%.

Metastables are detected with a channel electron multiplier (Mullard type B410 AL) which is separated from the chopper wheel by a TOF (time-of-flight) region of 1090mm. The channeltron is also sensitive to the ^1S - ^1P (584nm) radiation emitted by the source and so photons are recorded. The pulses are amplified by a fast preamplifier and then fed into a timing filter amplifier (Ortec 454). Background noise is eliminated by an integral discriminator (Nuclear Enterprises 4623). These pulses are used to provide stop signals for the counting system.

4.5.2 The photon masking circuit

A single shot time-of-flight system is used in both experiments, this means that for each start pulse only the first stop pulse contributes to a TOF distribution. As a consequence of the single-shot TOF system, metastables which arrive at the channeltron later than a photon (but in the same cycle) do not contribute to the metastable TOF distribution. As a

Figure 4.13 Start pulse

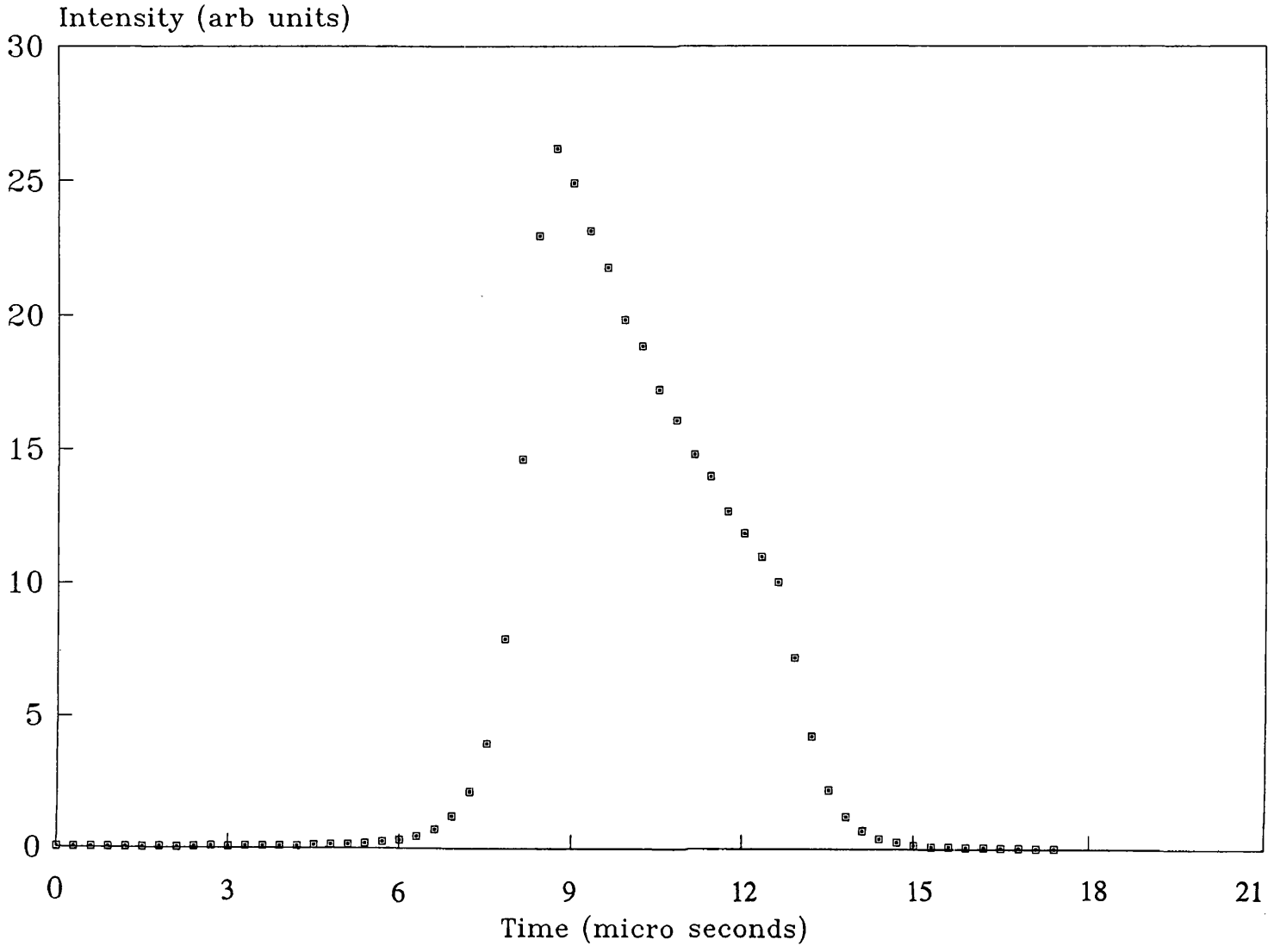

result of increasing the metastable count rate from 0.01 to 0.1 - 0.3 counts per cycle (section 4.2.5), the flux of photons has increased from 0.1 to 0.6 counts per cycle. The effect of this is thus that only 40% of the metastables which reach the detector contribute to the metastable TOF distribution. No distortion of the distribution results from this effect, but the statistical accuracy is reduced.

The high count rate experiment being performed makes it desirable to eliminate the recording of photons from the data collection process. This has been done by modifying the TOF logic circuit for the single-shot TOF system designed by Allison (1978) by adding a photon masking circuit (Appendix 4). This ensures that signals from the channeltron do not become stop pulses unless they occur more than 50μs after the delayed start pulse. The photon peak occurs approximately 36μs after the delayed start and the fastest metastables are detected a further 45μs later.

The photon masking circuitry is switched off to allow the photon peak to be observed, which is needed for determining the zero offset of the TOF distribution. The photons are usually recorded at the beginning and end of a data run in case there is any drift in the zero. The high flux of photons means that the peak channel can be determined accurately in a short time.

A photon masking circuit is not needed in the ion part of the TOF circuit because the photo-ionisation peak is not of sufficient magnitude to reduce the recorded ion signal. The photo-ionisation count rate is approximately 0.01 per cycle and so only one percent of the ions detected do not contribute to the ionisation TOF distribution.

4.5.3 The TOF mass spectrometer

Figure 4.14 shows a cross section through the interaction region and the ion drift tube, which constitute the TOF mass spectrometer. Allison (1978) designed the spectrometer and has described it in detail along with calculations of the resolution and the correct extraction voltages. Subsequent modifications were made by Harper (1977) who introduced grids of higher transparency. For the present work the only additional modification was that a multi-channel plate detector was substituted for one of the venetian blind electron multipliers previously used. The electrons from ionising collisions in the interaction region are accelerated through 600V by the electron extraction electrode C and are detected by a pair of multichannel plates (Mullard G25-20 ×50). The mounting shown in Figures 4.15a and

Figure 4.14 Cross section through the interaction region

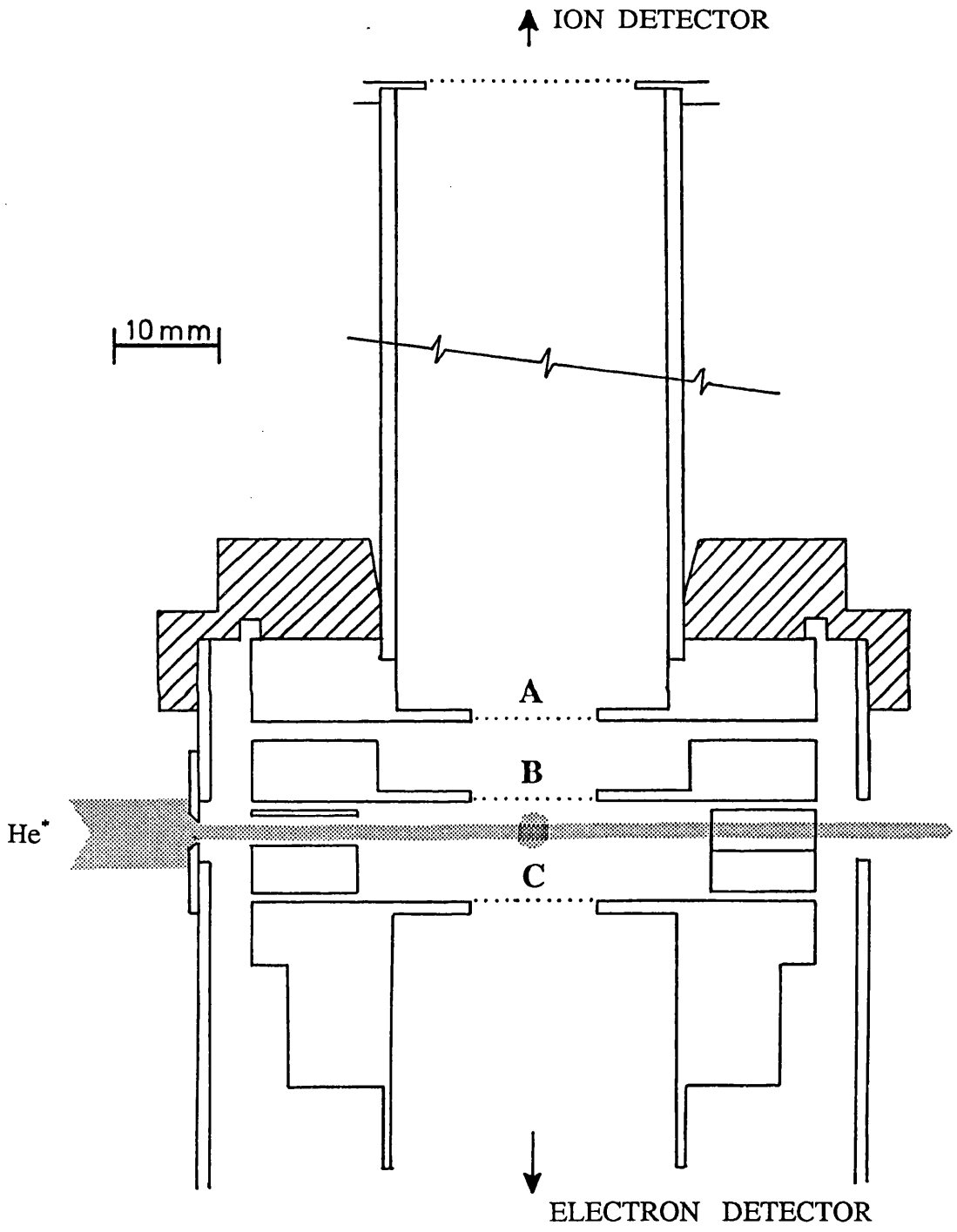

Figure 4.15a Cross section through the multi-channel plate mounting

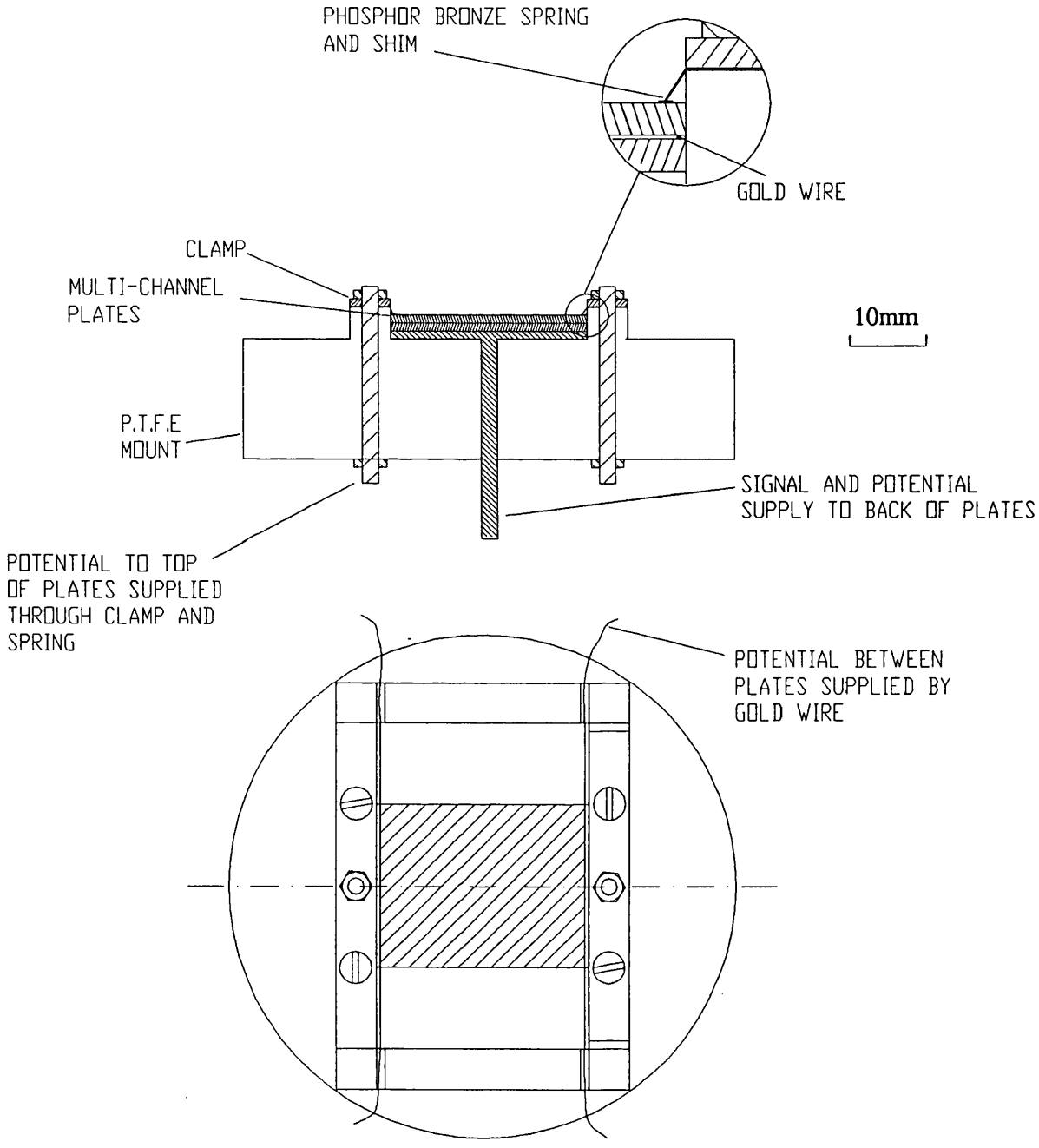

Figure 4.15b Photograph of the multi-channel plate mounting, also showing guard

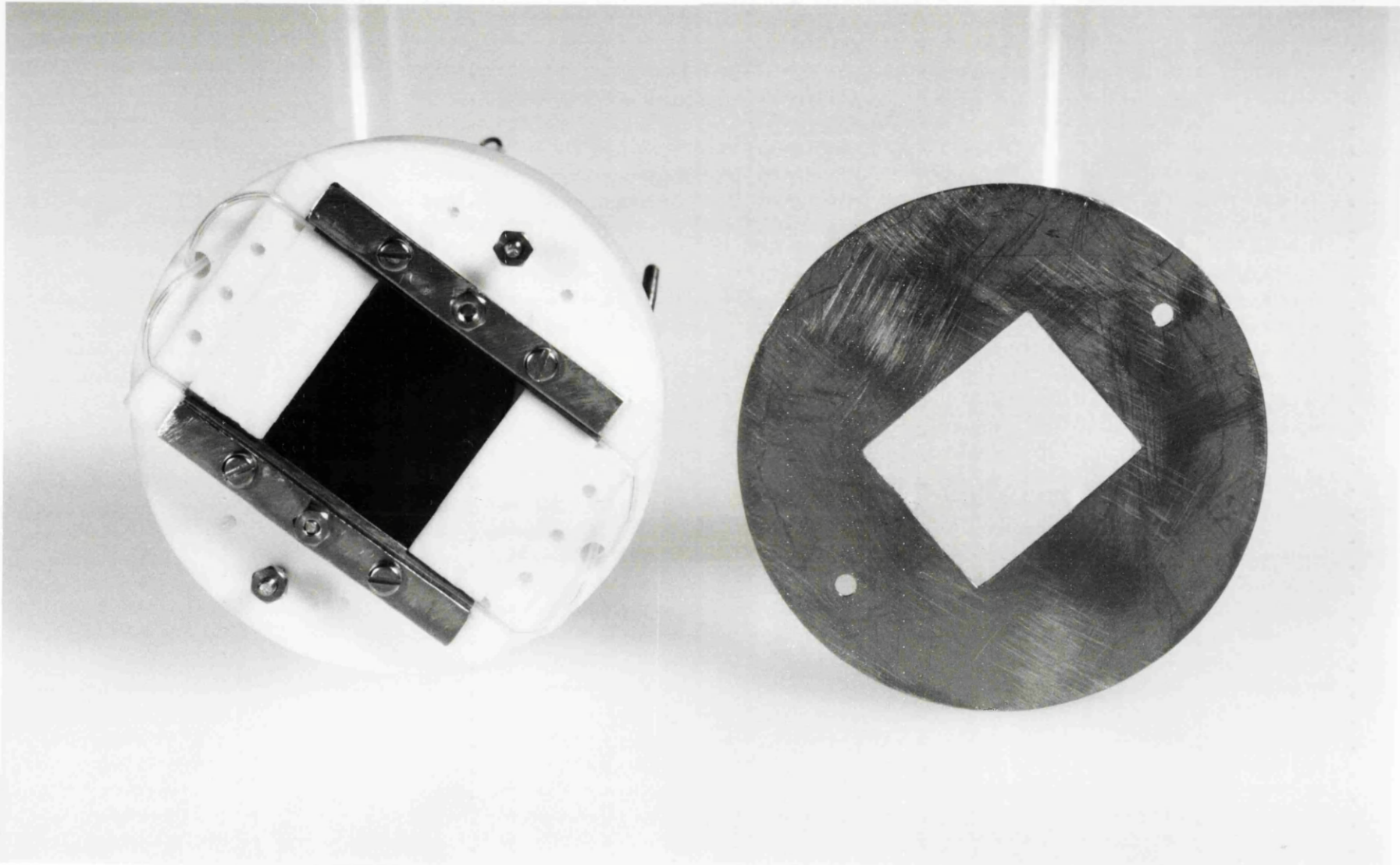

4.15b was designed to hold one of two old and damaged multi-channel plates, donated by the Mullard Space Science Laboratory of the author's department. The plate was cut in half and the two halves used as a sandwich, to give a detecting area 20×25mm. The mounting is designed to expose the maximum amount of channel plate area to incident electrons (greater than 90%). Good electrical contact is provided on the top face by means of two phosphor bronze springs (0.1mm thick) which run along the edge of the top plate. The springs press down on phosphor bronze shims (0.9mm wide) to increase the electrical contact with the top plate. The shims prevent the springs from damaging the channel plates by distributing the pressure from the springs evenly. Channel plates are very brittle; a figure of 1 g/mm^2 is quoted as the maximum pressure which should be applied to the surface. Gold wires (0.15mm diameter) are used to provide a potential to the middle of the sandwich, because of their high conductivity and small diameter. A stainless steel collector maintains the bottom of the back plate at ground potential and feeds pulses to a preamplifier. Each plate has a published gain of 10^3 at 1kV. The pair configuration is used with 1.5 kV across each plate (see Appendix 5a for circuit) and a gain ofapproximately 10^7 was achieved. No appreciable increase in electronic noise was observed after the installation of the channel plate detectors, indicating that the mounting design is satisfactory.

Positive ions from ionising collisions in the interaction region are extracted by the grid B in Figure 4.14 and are accelerated through grid A to 3000 eV. They then cross a 361mm drift region and are detected by an eighteen-stage venetian-blind electron multiplier (EMI 9642/2A), with copper-beryllium dynodes (see Appendix 5b for circuit). At manufacture the multiplier had a gain of 5×10^7 at the operating potential of 3kV.

The charge pulses from the electron and ion detectors are amplified by fast preamplifiers and then fed into amplifiers (Ortec type 454). Noise is eliminated by two constant fraction discriminators (Ortec type 463). The electron and ion signals are used to give start and stop pulses respectively for a time-to-amplitude converter (TAC) (Ortec 467), as shown in Figure 4.1. Mass information is derived from the amplitudes of the TAC pulses. Ions from background gas can in most cases be filtered out by passing the signal through a single-channel analyzer window (Ortec 406A), which allows pulses only of the desired height to pass through. This procedure is valid provided the background ions have a different mass to the target ions. Usually only one window is used to cover all the ionisation products because the gases used are of high purity and the residual background gas pressure of 2×10^{-8}

torr is less than 1% of the experimental running pressure of 2×10^{-6} torr. Finally the pulses from the TAC (irrespective of their amplitude) are used to provide stop signals for the flight of the metastables.

4.5.4 Data recording for total ionisation cross sections and high count rate corrections

A Quad Preset Counting Register (Hytec 351A), is used to measure the flight times of metastables. Counters 2 and 3 are used to count pulses from a clock pulse generator (Hytec type 95) set to 1 pulse per microsecond. The counters are interfaced via a CAMAC crate to an LSI-11/23 mini computer (DEC). A pulse from the metastable detector is used to stop counter 3. A pulse from the ion detector stops counter 2.

When determining total ionisation cross sections, information concerning the exact mass of individual ions is discarded. This is unfortunate but is necessary because the computer used to record the data is not able to do so quickly enough. Only 3ms is available to the computer to read information from the units in the Camac crate, and this is only sufficient to read two data registers.

If no metastable or ion is detected, counters 2 and 3 are stopped by an electronically generated end pulse which is automatically sent to the counters after 1600μs. The end pulse is also sent to counter 1 which acts as a flag to instruct the computer to record the contents of registers 2 and 3, irrespective of whether or not stop pulses have been received from the metastable or ion detectors.

Total cross section data is recorded by running a program called TOF3 (see Appendix 6). As described in section 4.4, four distributions are recorded simultaneously so that both singlet and triplet information is available. The data recording cycle is described below and is performed in an identical fashion for triplet and singlet distributions.

The computer reads the register of counter 1, if this is 0 then the register is read again. When the register reads 1, indicating the end of a cycle the computer reads the contents of registers 2 and 3. If a register contains a number greater than 1536 then the data is discarded, since 1536 μs is the flight time of the slowest metastable. Otherwise the data

is stored, and a new cycle begins.

The computer completes 1000 cycles and then sorts the data into 512 channels each of 3μs to make one TOF distribution. The data from the counting registers is divided by 3 to convert from microseconds to TOF distribution channel number. When the distribution has acquired data from 10^4 cycles it is plotted on the VDU (along with three other similarly recorded TOF distributions). After sixty to one hundred sets of 10^4 cycles the distributions are transferred to floppy disk.

Before data analysis is carried out, the TOF distributions are corrected for the effects of the high count rate. This is a consequence of the single-shot TOF system, which assumes that in every cycle not more than one metastable will reach the channeltron, and no more than one ionisation event will take place. If this condition is broken then the TOF distributions are distorted. This can be seen graphically in Figure 4.16, by a comparison of photon peak shapes observed, in high and low count rate experiments. The width of the peaks is a consequence of the time which the chopper slit takes to pass in front of the source slit. Photons arrive at the channeltron instantaneously. Figure 4.16a shows the flat trapezium shaped photon peak obtained from a weak source. In this experiment the chance of more than one photon being detected during the 6.5μs pulse width is very small because on average only one photon is detected for every ten chopper wheel cycles. By contrast the photon peak observed with the present high output source shown in Figure 4.16b is dominated by a sharp rise in counts and a more gradual fall. Several photons may be detected by the channeltron in the 6.5μs interval, but only the first to be detected can contribute to the TOF distribution. The photon peak shows this bias towards the photons detected first. The average number of photons detected per cycle is 0.5 in Figure 4.16b. The chance of more than one event occurring is determined by the Poisson distribution

$$P(r) = \frac{m^r \, e^{(-m)}}{r!} \qquad (4.5)$$

where r is the number of events in a cycle, P(r) is the probability of r events occurring in one cycle and m is the mean number of events per cycle. Table 4.2 shows the variation of P(r) with r, for various values of m and the last column shows the probability that more than one event occurs in a cycle and thus the fraction of events that will be missed by the counting system.

Table 4.2

Probability P(r) calculated using the Poisson distribution

m	P(r)				P(r) ≥2
	r=0	r=1	r=2	r=3	
0.01	0.990	0.009	0.00005	0.00005	
0.1	0.9048	0.09	0.0045	.00015	0.0047
0.2	0.8187	0.164	0.0164	0.0011	0.0176
0.4	0.6703	0.268	0.053	0.0071	0.0616
0.5	0.6065	0.3033	0.0758	0.0126	0.0902

The probability of more than one event occurring per cycle becomes significant when the mean number of events per cycle exceeds 0.2. This represents the upper limit of the count rate for both metastables and ions that could be expected in the current experiment. Clearly there will be some distortion of the kind shown on the photon peak for any distribution recorded from a high count rate. A cross section measurement, which is derived from the division of an ion distribution by a metastable distribution, will be affected if the two distributions are not identical (in which case they would be equally distorted). The cross section will be deformed at low velocity (high TOF times) where the counts per channel is more drastically reduced (see Figure 4.16). Some reduction of the deformation of the cross section can be achieved by making the ion and metastable atom count rates approximately equal. To compensate more fully for the effect of high count rate the data can be corrected retrospectively by using a program called HIGHCOUNT (Appendix 7). The number of cycles in which the data was recorded and the photon peak channel number are fed into the computer. The program then scans through the channels of a given TOF distribution from 1 to 512 and makes a running total of counts. Each count in channels 1 to i-1 represents a cycle in which channel i cannot record an event. The number of counts in channel i is corrected as follows

$$C_i' = \frac{C_i \, T}{T - \sum_{1}^{i-1} C_j} \qquad (4.6)$$

C_i' the new total in a channel i

C_i = the original total in channel i

T = the number of cycles over which the data was recorded

$\sum_{1}^{i-1} C_j$ = the running total of counts in channels 1 to i-1

The validity of this procedure can be shown by applying it to the sloping photon peak shown in Figure 4.16b. The saw tooth shape of Figure 4.16b is transformed to become the flat topped trapezium shaped peak of figure 4.16c. In Figure 4.17 a cross section in which the ion and metastable TOF distributions have both been corrected for a high count rate is shown, and compared with the uncorrected cross section. The difference is small, but not insignificant. In this case the count rates were both approximately 0.2 counts per cycle.

4.5.5 Data analysis

Data analysis is carried out using a computer program CROSCAL (Appendix 8). Firstly the four original TOF distributions are read into the computer and converted into velocity distributions. This is simply done by dividing the distance between the chopper wheel and metastable detector, or interaction region in the case of ionisation distributions, (1030mm and 860mm ± 0.1 % respectively) by the flight times. The photon peak channel number is subtracted from the TOF channel number and the result multiplied by three to give the time of flight in microseconds. The TOF distributions start a short time before the actual zero, which is given by the channel which contains the photon peak or the photo-ionisation peak. A zero offset occurs because of electronic delay and because the start pulse does not exactly coincide with the release of a pulse of metastables atoms from the source and chopper wheel. The ion distributions have a larger offset because of a delay caused by the ion flight time in the TOF mass spectrometer.

First the triplet cross section is determined. The metastable atom and ion velocity distributions are divided into 30 velocity bins and the weighted mean velocity of each bin is calculated. The bins are chosen to maximise velocity resolution while making sure that each bin contains enough information to ensure that the data is statistically meaningful. Some of the bins overlap in order to make the variation of cross section with velocity as continuous as possible.

Figure 4.16 Comparison of photon peak shapes

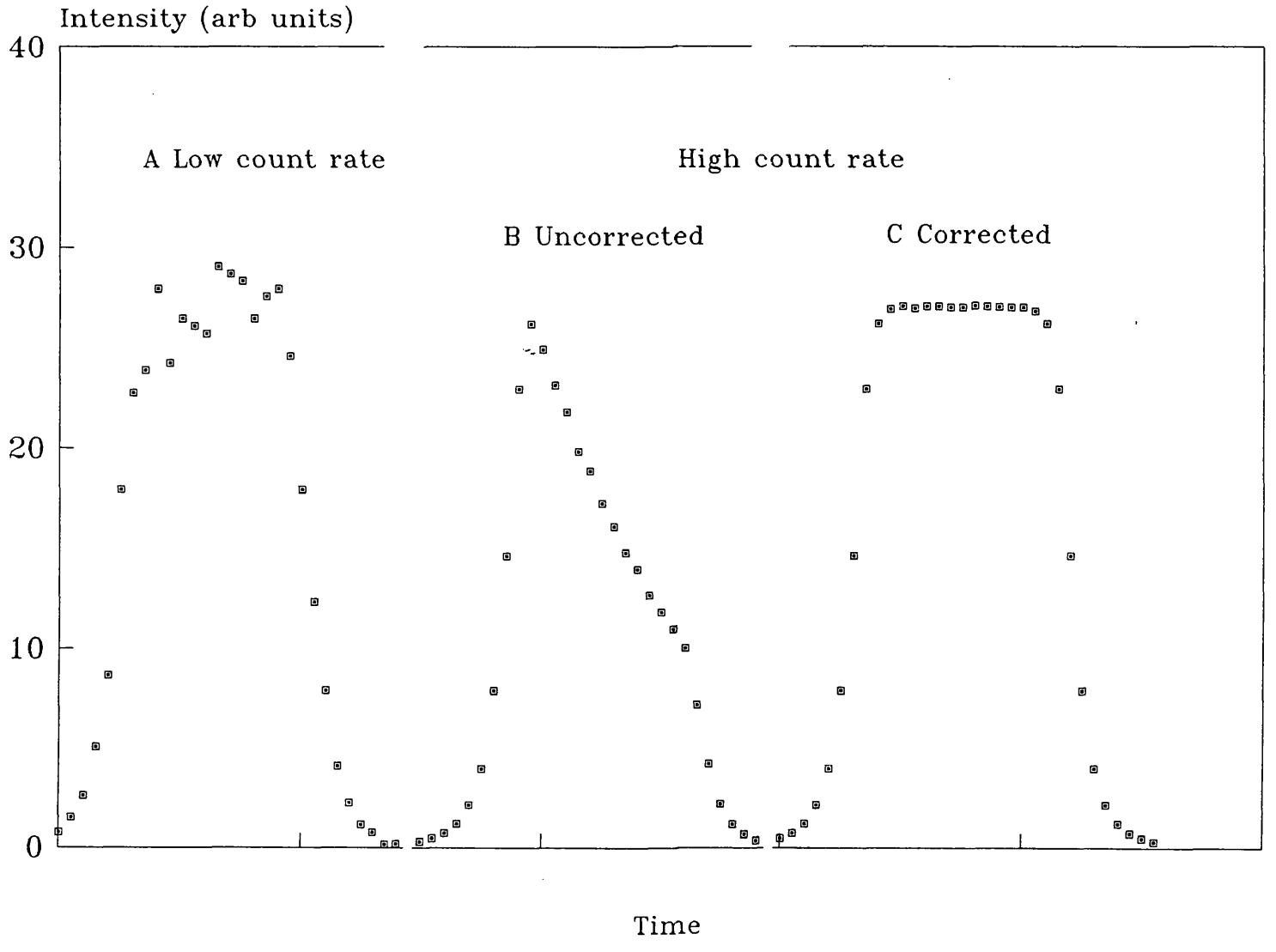

Figure 4.17 The effect of a high count rate

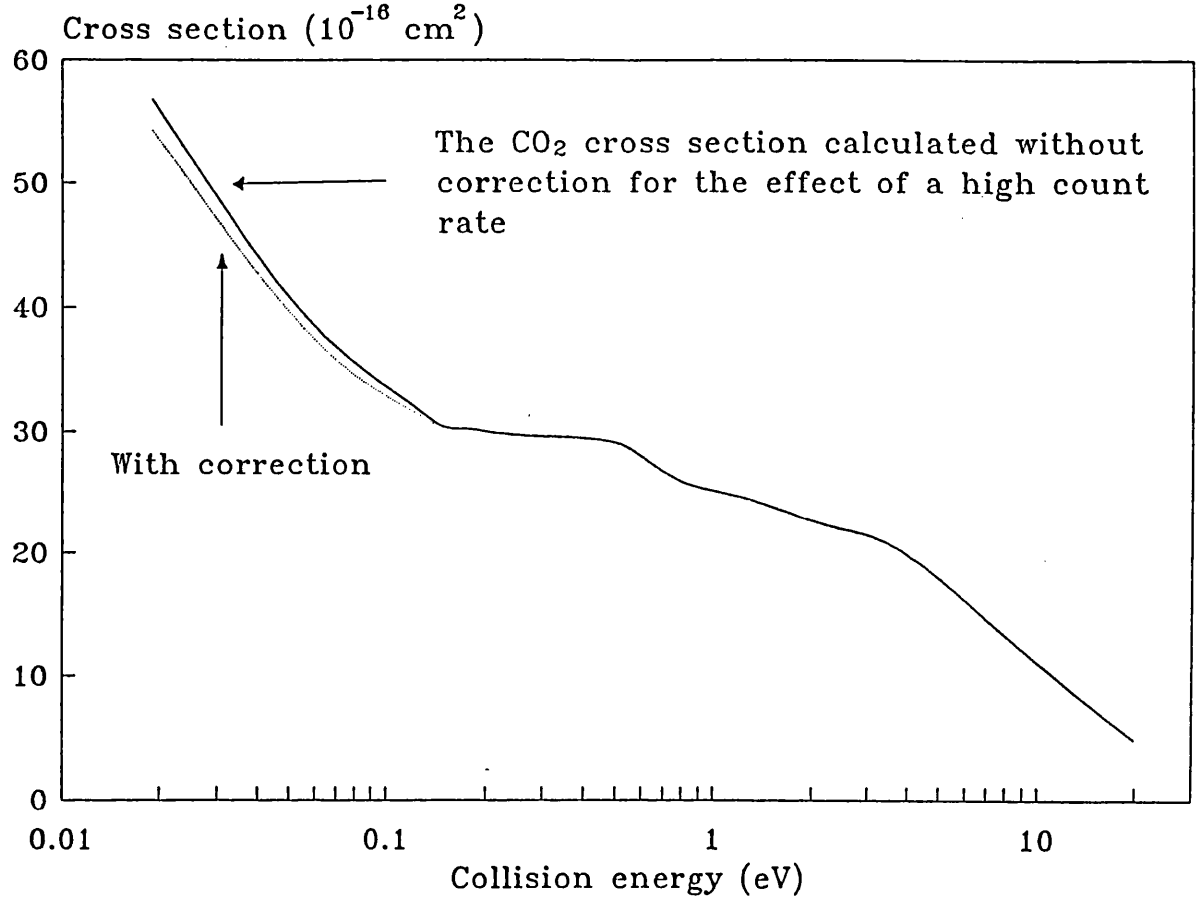

The effective cross section $\sigma_{eff}(v)$ can be calculated as follows

$$\sigma_{eff}(v) = \frac{\sum_{i}^{i+di} n(i) - di\ b_n}{\sum_{j}^{j+dj} m(j) - dj\ c_m} \qquad (4.7a)$$

where v is the average of the weighted mean velocities calculated for the ion and metastable atom velocity bins, n(i) and m(j) are the number of counts in channels i and j respectively, b_n and c_m are the mean number of the background counts in each channel, and i and di are related to j and dj by $j = i \times l_m/i_n$ and $dj = di \times l_m/l_n$ in which l_n and l_m are the distances from the chopper wheel to the interaction region and the channeltron respectively.

The error on each sum is given by the square root of the sum and the fractional error on the effective cross section is given by summing in quadrature the fractional errors on the two sums. To calculate the singlet cross section a subtraction procedure is used as follows

$$\sigma_{eff}(v) = \frac{\left[\sum_{i}^{i+di} k(i) - di\ b_n\right] q_{(off)} - \left[\sum_{i}^{i+di} n(i) - di\ b_n\right] q_{(on)}}{\left[\sum_{j}^{j+dj} l(j) - dj\ c_m\right] q_{(off)} - \left[\sum_{i}^{i+di} m(j) - dj\ c_m\right] q_{(on)}} \quad (4.7b)$$

where k(i) and l(j) are the number of counts in channels i and j respectively and $q_{(off)}$ and $q_{(on)}$ signify the state of the quench lamp. CROSCAL calculates the error on the numerator and denominator of Equation 4.7b from the addition in quadrature of the errors on the sums. The fractional error on the effective cross section is calculated by adding together in quadrature the fractional errors on the numerator and denominator. This means that the errors on singlet cross sections are much larger than they are on the triplet cross sections.

The velocity calculated by CROSCAL in this case is simply the average of the four weighted mean velocities, and is not sufficiently precise. In order to calculate the precise velocity a simple program which subtracts the distributions recorded with the quench lamp on from those recorded with the quench lamp off is used. The resulting singlet distributions are used to determine accurately the velocity dependence of the singlet ionisation cross section. This is done using CROSCAL but reading the two singlet distributions into the computer in the position that is normally occupied by the triplet distributions. Thus Equation 4.7a is used to calculate the singlet total ionisation cross section; the errors calculated are incorrect and are discarded, but the velocity calculated is more precise because the weighted mean velocity is calculated after the subtraction procedure has been carried out.

The resulting effective total ionisation cross sections as a function of collision velocity are in some cases rather incomplete, with information lacking particularly at low velocity. To give a more continuous picture of the velocity dependence of the ionisation cross section a second analysis computer program CROSS2 (Appendix 9) is used. This program is similar to CROSCAL except that the ionisation cross section is calculated at a velocity decided by the program user, with the velocity bin size and position entered by hand. In this way the total ionisation cross section can be calculated at velocities between those determined using CROSCAL. CROSS2 is also used to extend the velocity range of the experiment in cases where sufficient raw information exists at very low or very high velocity.

Both the effective cross section and beam velocity calculated above must be corrected for

the relative velocity of the target beam to obtain a true cross section at the collision velocity. The technique used to perform these corrections is described later in section 4.7.

4.6 Branching ratios

4.6.1 Data collection and analysis

With the present apparatus the variation of the branching ratio with velocity can be measured for each ion product of chemi-ionisation. The TOF mass spectrometer shown in Figure 4.11 is used to distinguish between ion products of different mass in the way described in section 4.5.3. In this experiment no channeltron pulses are recorded and so no information is available about the metastable beam intensity distribution and thus the cross section cannot be determined. Only the relative production of the various ion products at the same collision velocity is revealed. However when this information is coupled with the previously measured total cross sections, the partial cross sections can be obtained. As with the total cross section experiments, the TAC output is used to provide a stop pulse to the timing system, but now the TAC pulses are also fed into a fast analogue-to-digital converter (Nuclear Enterprises NE 9060) which is interfaced to the LSI-11 minicomputer via the CAMAC crate.

To produce an ion mass spectrum as a function of collision velocity, the metastable TOF distribution determined from the ion production in the interaction (ie the 'ion TOF distribution' region is split up into ten time bins. To do this it is important to know the zero offset of the distribution before the experiment begins, simply done by recording the TOF distribution of ionisation. The photo-ionisation peak is observed and incorporated in the branching ratio program TOF1M (Appendix 10). TOF1M records the mass spectra due to ionisation occurring with the quench lamp on and off, in the same way that TOF3 records total cross section data, by using the data recording cycle described in section 4.4 and shown in Figure 4.12. The computer reads the contents of counting register 1; if this is 0 then the register is read again. When the register contains a 1 the computer reads the contents of counting register 2 (ionisation time) and the ADC register (mass information). Data is rejected if it does not fall within the correct range of the ADC register (1-512). TOF1M builds up a two-dimensional array in which the channel number is determined by the ion mass and the bin number is determined by the time of ionisation. The result is a set of ten mass spectra, each recorded at a different velocity. Periodically an overall mass

spectrum is displayed on the VDU.

Before the singlet data can be examined a simple program is used to subtract the ten mass spectra recorded with the quench lamp on from the ten spectra recorded with the quench lamp off. This gives ten ion mass spectra due to ionisation by singlet metastable atoms.

Analysis of a set of ten mass spectra is carried out using the programs BRCAL (Appendix 11). Firstly a simple plotting program is used to look at the mass spectra and determine the range of channels occupied by each mass peak. The mass spectrometer is calibrated before the experiment by examining the mass peaks produced by background gases in the tank and observing their channel numbers. Then ANYJS is used to examine each mass spectrum in turn, adding up the number of events in each mass range and the total number of counts in the spectrum. The fraction of an ion product is then found by dividing the number of counts in the mass range which it occupies by the total number of counts in the mass spectrum. The beam velocity which corresponds to each spectrum is determined as follows. An ion TOF distribution is recorded before and after the data run, so as to average any fluctuation in the source. These are added together and a modified form of CROSCAL is then used to divide the distribution up into ten TOF bins corresponding to those used by TOF1M. The weighted mean velocity of each bin is then determined. The percentage of each ion species is thus calculated, as a function of beam velocity. To convert from beam velocity to collision velocity the procedure described later in section 4.7 is used.

The accuracy of branching ratios decreases with velocity, especially if the fraction of a particular ion is low. Therefore measurements of branching ratios are made for velocities only as high as 14 kms^{-1}, considerably lower than for total cross sections measurements.

To convert branching ratios into partial cross sections they are simply multiplied by the total ionisation cross sections, calculated by the method described in section 4.5.4. This is done after the velocity corrections have been carried out. As with branching ratios the partial cross sections cover a much more limited velocity range than the total cross sections.

Each mass spectrum is 256 channels long and the channel number of a given ion product is roughly proportional to the square root of its mass (the precise relationship is given by Allison 1978). A variable mass range is achieved in cases where the ion mass produces a channel number between 256 and 512. A channel offset is read into the computer at the

beginning of a TOF1M run and the offset is subtracted from the ion channel number, in order to fit the ion peak into the mass spectrum. Thus the mass resolution of a 512 channel spectrum is achieved and the limited capacity of the computer memory is not exceeded.

The ion peak width is approximately four channels at half maximum and the resolution of light ions is good, for example ten channels separate the peaks of NH_3^+ and NH_2^+ (masses 17 and 16). The mass resolution declines with increasing mass, but no heavy rare gases have been used so the problem of separating close mass peaks has not arisen. SF_6 (mass 146), which is heavier even than xenon, has been examined, but it produces ion fragments which differ by nineteen mass units (SF_5^+ 127 and SF_4^+ 108) and so are easily separated.

In the case of argon, the tail of the Ar^+ peak overlaps the much smaller $ArHe^+$ peak and thus the latter is significantly increased by the additional counts. To correct this, the lower-mass tail of the Ar^+ peak is measured and assuming the peak is symmetrical, the contribution to the $ArHe^+$ channels due to the higher-mass tail is subtracted.

Since the background mass spectrum is very small (section 4.2.6), no background subtractions have been necessary. The amount of background is easily monitored by observing the size of the H_2O^+ mass peak, which is always visible, because its position is different from any of the peaks produced in the experiment.

4.6.2 Detection efficiencies

The detection efficiencies of both the electron and ion detectors have been determined as a function of target atom mass. In order to make corrections to the branching ratio measurements such corrections are necessary if detection efficiencies vary significantly with target mass. The same procedure as was used by both Allison (1978) and Jerram (1985) has been applied.

The detection efficiencies are determined by recording the ion counts N_1, the electron counts N_2 and the number of coincidences N_3 in a given time. The counts are related to the ion detection efficiency (A_1), and the electron detection efficiency (A_2) as follows

$$N_1 = A_1 N \tag{4.8}$$

$$N_2 = A_2 N \tag{4.9}$$

$$N_3 = A_1 A_2 N \tag{4.10}$$

where N is the total number of ionisation events occurring. The detection efficiencies are thus

$$A_1 = N_3/N_2 \quad (4.11)$$

$$A_2 = N_3/N_1 \quad (4.12)$$

The values of A_1 and A_2 determined in this way are shown in table 4.3 and plotted in Figure 4.18a and their product plotted in Figure 4.18b giving the combined detection efficiency of the two detectors.

Table 4.3

Detection efficiencies for positive ions and electrons

		Detection efficiencies %	
Ion species	Mass	Electron	Ion
CH_4	16	49.9 ± 0.4	12.26 ±0.17
NH_3	17	52.17 ± 0.66	11.43 ± 0.32
N_2	28	50.17 ± 0.42	11.14 ± 0.09
Ar	40	46.4 ± 0.66	11.7 ± 0.25
CO_2	44	49.39 ± 0.44	11.43 ± 0.51
Kr	83.8	49.9 ± 1	7 ± 0.3
SF_6	146	50 ± 0.6	7.98 ± 0.14

The detection efficiencies are determined by the area of the detectors, the secondary emission coefficients, the transparency of the extraction grids, and the sensitivity of the electronic counting system.

As would be expected the electron detection efficiency does not vary with mass. The ion

Figure 4.18a Detection efficiency for positive and negative ions and electrons

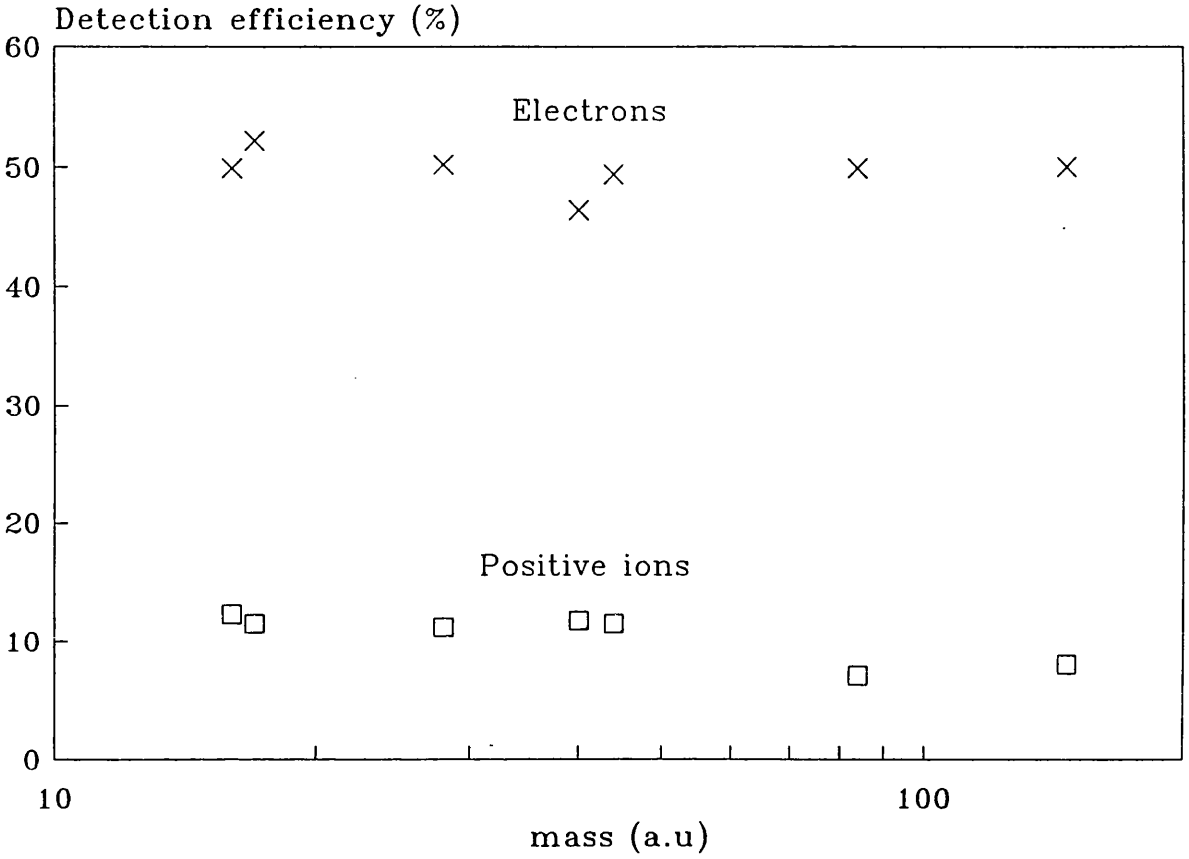

Figure 4.18b Combined detection efficiency of ion and electron detectors (A_1xA_2)

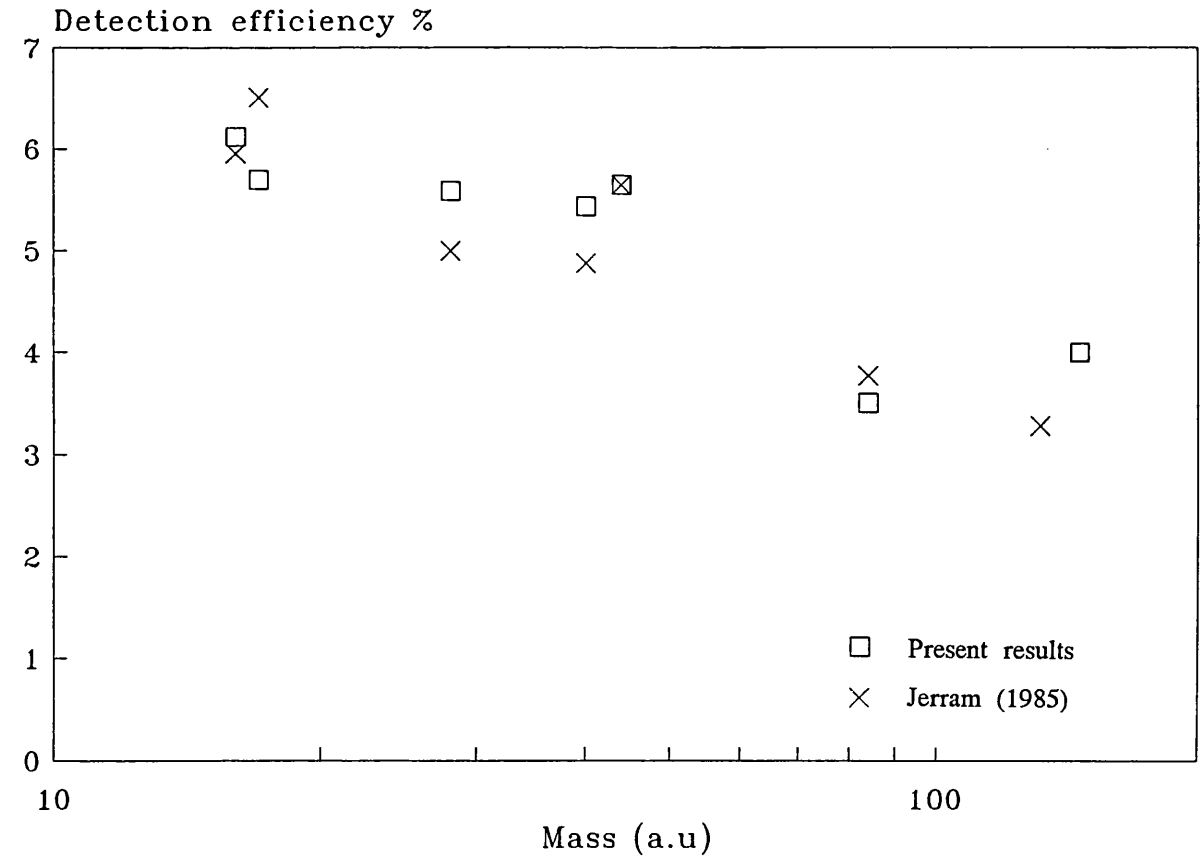

detection efficiency is also virtually constant in the range 16 - 44 mass units, in agreement with the results of Allison (1978). No corrections are therefore made to the branching ratios of CO_2 or N_2O which produce ion fragments spanning this range. In most hydrocarbon cases the masses of ion fragments lie in a small range, for example, CH_4^+ and CH_3^+, and so these are left uncorrected. Above 44 mass units there is a clear decline in the ion detector efficiency with increasing mass. This is seen more clearly in a plot of combined detection efficiency $A_1 \times A_2$ in Figure 4.18b. The present results are shown compared to those measured by Jerram (normalised to the present efficiency for mass 44). Thus there may be significant differences in detection fragments of the branches of SF_6, because of the large differences in their masses, and their large mass numbers (108-146). The variation in detection efficiency for these target masses could not been measured and so no corrections can be made to their branching ratios.

4.7 Correction for the thermal motion of target atoms

The effective cross sections described in section 4.5.6 must be corrected to take into account motion of the target particle. Because of this the relative collision velocity of a target atom and metastable helium atom is greater than the calculated metastable beam velocity.

The most probable velocity in the target beam is given by

$$\alpha = \sqrt{\frac{3kT}{m}} \qquad (4.13)$$

where k is the Boltzmann constant, T is the gas temperature in the source and m is the mass of a target gas atom.

A slow metastable atom has a greater probability of undergoing a collision with a target atom than a fast metastable atom, because it spends a longer time in the beam. This effect is dependent on the ratio of the metastable atom velocity to the most probable atom velocity in the target beam. The desired final result is a true cross section $\sigma(g)$ at a mean relative velocity g between the target atom and a metastable helium atom.

The corrections for a beam and for a gas cell target have been calculated by several authors notably Pauli (1960), Berkling et al (1962) and Lang et al (1971). The Berkling et al

corrections give a cross section $\sigma_{ion}(v_i)$,

$$\sigma_{ion}(v_i) = \frac{\sigma_{eff}(v)}{F_{b0}(s,x)} \tag{4.14}$$

where v_i is the beam velocity and $\sigma_{eff}(v_i)$ is the effective cross section measured in section 4.5.5, $F_{b0}(s,x)$ is a correction tabulated by Berkling et al, and defined in Massey and Burhop (1971) as follows

$$F_{b0}(s,x) = 4\pi^{\frac{1}{2}} x^{-2\beta} \int (x^2+z^2)^{\beta} z^2 e^{-z^2}\, dz \tag{4.15}$$

$$\beta = \frac{(s-3)}{2(s-1)} \tag{4.16}$$

where s derives from the form of interaction potential chosen

$$V \propto r^{-s} \tag{4.17}$$

x is the ratio of the metastable atom beam velocity v_i to the target beam velocity α

$$x = \frac{v_i}{\alpha} \tag{4.18}$$

A similar function $F_{a0}(s,x)$ for a gas cell is also tabulated. The advantage of this method is that only the cross section must be adjusted, the collision velocity becomes the beam velocity. The disadvantage is that the cross section corrections can be large, and they depend strongly on the assumed form of the interaction potential, which may introduce large errors.

The correcting method described by Lang et al (1971) also depend on the same assumed interaction potentials, but the cross section $\sigma_{ion}(g)$ is given at the mean collision velocity of the two beams g, not the beam velocity v_i. The corrected cross section $\sigma_{ion}(g)$ is given by:

$$\sigma_{ion}(g) = \frac{\sigma_{eff}(v_i)}{f(s,x)\, w(x)} \tag{4.19}$$

$$w(x) = \frac{g}{v_i} \tag{4.20}$$

w(x) is equivalent to $F_{b0}(\infty,x)$ the Berkling et al correction for a hard sphere interaction

potential. The function f(s,x) is not tabulated by Lang et al but a conversion from the function $F_{b0}(s,x)$ of Berkling et al (1962) is given by

$$f(s,x) = F_{bo}(s,x)\,[F_{bo}(\infty,x)]^{\frac{(3-s)}{(s-1)}} \qquad (4.21)$$

In the case where $s=\infty$, the function $f(\infty,x)=1$; in the case where $s=6$, over the range of the present experiments, $f(6,x)=1$ to within 1%.

The cross section corrections of Lang et al (1971) are more reliable than those of Berkling et al because they are much less dependent on s. Also a more physical solution is achieved, because the cross sections are determined at the relative collision velocity and so the true energy range of the experiment is apparent. Thus the correction procedure of Lang et al has been chosen to calculate the values of $\sigma_{ion}(v_i)$ in chapter 5. It has been assumed that f(s,x) is always 1. The corrections are most necessary for light targets and are greatest at low collision velocity. For collisions at $1 kms^{-1}$ w varies from 1.2 for collisions with ammonia to 1.03 for collisions with sulphur hexafluoride.

Chapter 5
Results and discussion

5.1 Introduction

In this chapter the ionisation cross sections and branching ratios of Ar, CO_2, N_2O, CH_4, C_2H_2, NH_3 and SF_6 are presented. The data, which has been corrected as described in chapter 4 for the effects of relative collision velocity and high count rate, is tabulated in Tables 5.2 to 5.14 and is presented graphically in Figures 5.2 to 5.33.

The relative data has in every case been normalised to absolute measurements. Table 5.1 indicates to which absolute data the present results have been normalised together with the normalisation error and a key to Figures 5.2 to 5.33.

The triplet data for Ar, CH_4 NH_3 are normalised to the gas cell measurements of Jerram (1985) carried out on the present apparatus and measured as a function of collision energy. This is important because it makes the normalisation procedure simple.

Other cross sections are normalised to the flowing afterglow results of Schmeltekopf and Fehsenfeld (1970) for SF_6, N_2O, CO_2 or the pulsed radiolysis results of Ueno et al (1980) in the case of C_2H_2. These results are presented as an absolute rate constant k at a particular temperature. To derive the normalisation factor a rate constant is calculated from the relative cross section measurements using the following relationship:

$$k' = \int_0^\infty f(v)\sigma'(v)v\, dv \qquad (5.1)$$

where σ' and k' are the measured cross section and calculated rate constant respectively and f(v) is the Maxwellian velocity distribution function. The normalisation constant is simply given by $k=Nk'$, where N is the normalisation constant and k is the reported rate constant. The normalised cross section can now be found from $\sigma(v) = N\sigma'(v)$.

The absolute afterglow cross sections shown in Figures 5.2 to 5.32 have been calculated by the authors of the papers from their absolute rate constant k by assuming that the cross

section σ is independent of velocity. k is measured at a given temperature which is converted to a mean collision energy. To do this the average collision velocity is first calculated using Equation 5.2, where m is the mass of the target particle, k_B is the Boltzmann constant and T is the given temperature:

$$\bar{v} = \left(\frac{8k_BT}{\pi m}\right)^{\frac{1}{2}} \tag{5.2}$$

In the present work the singlet cross sections are normalised using the same factor as for the corresponding triplet cross sections. The assumption implicit in this is that the detection efficiency of the channeltron is equal for the two metastable species. Evidence for the validity of this assumption is given in section 5.2.

The total ionisation cross sections are shown in figures 5.2 to 5.32 as discrete points, along with partial cross sections shown as smooth curves drawn through the data points. In the case of argon the partial cross sections have not been shown because of the large amount of information given on these graphs. Error bars are shown on the total cross sections and the branching ratios. Error bars are shown at three points only on the partial cross sections. These are calculated by adding the errors from the branching ratio and total cross section in quadrature.

No error bars are shown on the triplet cross sections because the errors are so small. The errors for the singlet cross sections are larger and in general the amount of data taken is enough to ensure that the error bars are less than ten percent in the mid energy range (0.04 eV - 0.3 eV) where the population of $He(2^1S)$ is at its highest. This criterion means that data acquisition can be completed for one target species in roughly one week, though more in the case of argon. At high energy, where the singlet fraction is low, the error bars are much larger because of the subtraction procedure described in section 4.5.5. It would be necessary to record ten times as much data, to reduce the errors in these regions to one third of their present level which was impractical.

For the same reasons the error bars shown on the singlet branching ratios are very large at high and low energy. However, again the errors on the triplet data are very small and no error bars are shown.

The total ionisation cross sections for argon with both metastable species are compared with the plentiful relative measurements of other experimenters. The variation of branching ratios for argon have been compared with the data of Jerram (1985) and Pesnelle (1975) in the triplet case; in the singlet case only the data of Pesnelle (1975) is available for comparison.

The triplet ionisation cross sections and branching ratios of CO_2, CH_4, C_2H_2, and NH_3 are compared with the only relative data available, that of Jerram (1985). No relative data is available to compare with the present singlet cross sections and branching ratios of these molecules, nor with the singlet and triplet data of N_2O and SF_6.

Figure 5.1 Energy resolution of experiment

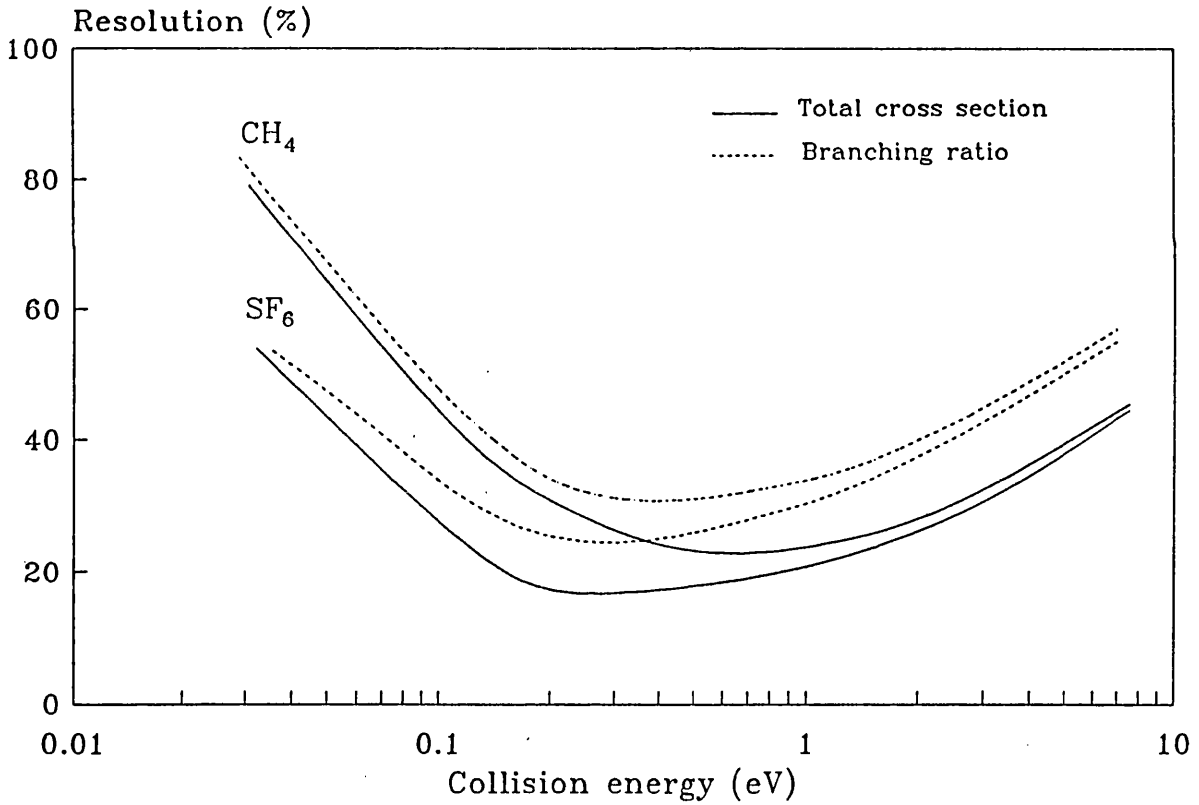

The energy resolution as a function of energy is shown graphically in Figure 5.1, calculated for the molecules at two extremes of mass, methane and sulphur hexafluoride. The major energy broadening is due to the width of the TOF bins. The resolution is poorer for branching ratio results than for total ionisation cross section results because the TOF bins used are wider for these measurements. The effects of the finite width of the start pulse

and the spread in thermal motion of the target beam are also important. An expression for the latter is given by Chantry (1971) as follows

$$W_{\frac{1}{2}} = (11.1 y k_B T E_0)^{\frac{1}{2}} , \quad y = \frac{m}{(m+M)} \tag{5.3}$$

where $W_{1/2}$ is the width at half maximum, k_B is the Boltzmann constant, T is the temperature of the beam and E_0 is the mean beam energy. M and m are the masses of the projectile and target particles respectively. The total energy resolution is the quadrature sum of these three factors.

5.2 Ar + He(2^3S)

In Figure 5.2 the present data is compared with the relative data of Kroon (1985), Jerram (1985), Pesnelle et al (1975), Woodard et al (1978) and Parr et al (1982) whose data is identical to the data of Illenberger and Niehaus (1975) which is not shown. The data of Parr et al (1982) is shown only where it diverges from the data of Jerram (1985) to which it is also identical below 0.2 eV.

Figure 5.2 shows a good agreement with the magnitude and variation of the relative data of Jerram (1985). Below 0.04 eV the present measurement is higher than the data of Jerram. This effect could be due to differential scattering of metastable atoms in the experimental chamber by a high background gas pressure, but this is not thought to be the case. The low energy data agrees well with the absolute measurement of Schmeltekopf and Fehsenfeld (1970), better than does the relative data of Jerram. The cross section rises smoothly from 0.04 eV to a maximum at 0.5 eV, and agrees well with Jerram (1985) and Parr et al (1982). However, agreement is poor with the data of Woodard et al (1978). This has been accounted for by Jerram (1985) as a result of the design of their gas cell.

The small dip at 0.7 eV shown in the present data is better defined than in the relative data of Jerram (1985). Above 2eV there is possibly some oscillatory structure, superimposed on to a slowly declining cross section.

Associative ionisation is at its maximum of 20% at the lowest collision energy of 0.02 eV and decreases rapidly to below 0.2% at 1 eV. This is in good agreement with the measurements of Jerram (1985) and Pesnelle et al (1975), although, as figure 5.3 shows,

the present measurements show slightly more associative ionisation. This is most likely to be due to the overlap of the two mass peaks. The single energy measurements (Table 5.15) of Herce et al, (1968a) Hotop et al (1969) and West et al (1975) show considerably less associative ionisation than the present results, whereas the data of Allison (1978) using the present mass spectrometer is in good agreement. The most likely explanation is that the collision energies reported in the other work are lower than the actual values, because as Figure 5.3 shows, the fraction of $ArHe^+$ decreases rapidly with energy. The single-energy experiments do not employ the TOF technique and so the reported energies are less reliable than the energy dependent measurements.

5.3 Ar + He(2^1S)

The relative total ionisation cross section for argon with He(2^1S) has been normalised using the same factor as for the triplet data, assuming that the detection efficiency of the channeltron used is equal for the two metastable species. This assumption is supported by the agreement between the present data and the relative data of Burdenski et al (1981), Sidiqui et al (1984) and Parr et al (1982). Good agreement is also found with the absolute measurements of Schmeltekopf and Fehsenfeld (1970) and Riola et al (1974).

A much steeper rise in cross section is apparent in Figure 5.4 at lower energy than in the triplet case, following the data of Parr et al closely at the lowest energy and showing no signs of a minimum in the cross section (Burdenski et al 1981). The small magnitude of the cross section at low energy eliminates the possibility of differential scattering in the experimental tank, which would have boosted the observed cross section. The cross section reaches a maximum between 0.1 and 0.2 eV where it lies between the diverging data of Parr et al and Burdenski et al. The data of Kroon shows a similar shape to the present data but with much lower magnitude. Kroon (1985) has made the same assumption as has been made in the present work, that the detection efficiency of his metastable detector is equal for both metastable species. Kroon's triplet data, normalised to the theoretical cross section of Siska (1979), is in good agreement with the present results. Kroon has multiplied the singlet cross section by the same normalisation factor as for the triplet cross section.

The implication, therefore, from the discrepancy between the cross section measured by Kroon and the cross section measured by the other experimenters including the present author, is that the detection efficiency of his metastable detector is in fact higher for

$He(2^3S)$ than it is for $He(2^1S)$. This could be due to the indirect method of detection used involving an electron multiplier detecting electrons ejected from a stainless steel surface. Dunning and Smith (1971) and Dunning et al (1971) have considered the detection efficiency for metastable helium by several targets. Although the detection efficiency determined is the same for the two metastable species with a target of chemically cleaned stainless steal, the detector used by Kroon is untreated and so it is reasonable that the detection efficiencies be different.

Above 0.3 eV there is no data with which to compare the present results, and between 0.3 and 0.9 eV the statistical accuracy of the results is quite low. Above 0.9 eV the cross section declines slowly in a similar fashion to the triplet cross section and with a similar magnitude to it as Figure 5.6 shows.

The fraction of associative ionisation at low energy is almost double that in the triplet case (43% at 0.031 eV). The fraction decreases more rapidly however, and is in good agreement with the data of Pesnelle et al (1975), though slightly larger (Figure 5.5). The other single energy measurements (Table 5.16) all show much less associative ionisation than either the present data or that of Pesnelle et al, (Figure 5.5) indicating that the collision energies reported in Table 5.16 are lower than the actual values.

5.3 CO_2+ $He(2^3S)$

The cross section for ionisation of carbon dioxide by $He(2^3S)$ shows a continuous decline in magnitude with increasing energy (Figure 5.7), indicating that the interaction potential is weakly attractive. This is in agreement with the PIES results of Hotop et al (1979). The present results show a good agreement with the data of Jerram (1985), continuing the trend of his data into both low and high energy regions (the present results extend the energy range of measurements by a factor of two).

No associative ionisation occurs and Penning ionisation accounts for more than sixty percent of the ionisation products (Figure 5.8), with dissociative ionisation providing the rest. The amounts of each branch detected agree well with the data of Jerram, with better accuracy in the case of the smallest branch, CO^+. The single energy measurements (Table 5.15) are in good agreement with the present results excepting those of Hotop et al (1969) which

gives a low percentage of O^+.

5.4 CO_2 + He(2^1S)

The total ionisation cross section of carbon dioxide by He(2^1S) shows a good agreement with the absolute measurements of Riola et al (1974) and is within the errors of Schmeltekopf and Fehsenfeld (1970). Figure 5.9 shows the cross section declining with energy below 0.2 eV with only small fluctuations. This is expected from the PIES data of Tuffin et al (1981), which indicates the presence of a slightly more attractive potential than in the triplet case. At 0.2 eV the singlet and triplet cross sections are equal, and at higher energy the cross section oscillates about the level of the triplet cross section (Figure 5.11). This may be due to a genuine structure in the cross section, but fluctuations due to the lower statistical accuracy at high energy cannot be ruled out.

The branching ratios of Figure 5.10 show more CO_2^+ Penning ionisation than in the triplet case and less O^+. There is a cross over in the magnitude of CO^+ and O^+ above 0.6 eV. The single energy measurements in Table 5.16 show good agreement with the present results except for the O^+ percentages, which are roughly double. Again no associative ionisation occurs.

5.5 N_2O + He(2^3S)

The total ionisation cross section of nitrous oxide by He(2^3S) shown in Figure 5.12 has the smallest variation with energy of any measured. The cross section rises slightly with energy below 0.05 eV, but the trend over the remaining energy range is downwards, suggesting, as in the case of carbon dioxide, a weak attractive potential in agreement with the PIES results of Hotop et al (1979).

The branching ratios (Figure 5.13) are more interesting than the total ionisation cross section. Penning ionisation accounts for only half of the ionisation products at low energies and is overtaken by the NO^+ branch above 0.7 eV, which increases over the energy range as do the other three dissociative branches.

West et al (1975) do not record any N_2^+ or N^+ (Table 5.15), as have been detected in

present measurements. This may be due to inadequate resolution of the mass spectrometer used by West et al. The mass peaks of NO^+ and N_2^+ are very close (30 and 28 atomic mass units respectively) and could easily appear as one peak. The percentage of NO^+ recorded by West et al is similar to the combined percentage of NO^+ and N_2^+ recorded in the present experiment, which suggests that the explanation is reasonable. In addition the data of Hotop et al (1979) gives a percentage of N_2^+ and O_2^+ in agreement with the present data and they also report some N^+.

West et al (1975) report detection of HeO^+ (1%) but none has been detected in the present experiment or by Hotop et al (1979). This is almost certainly a spurious detection, due to dissociation of N_2O molecules in the drift space between the interaction region and the analysing magnet, the possibility of which is admitted in their paper.

5.6 N_2O + He(2^1S)

The total ionisation cross section for nitrous oxide by He(2^1S) shows a much more pronounced energy dependence than in the triplet case (Figure 5.14) indicating a more attractive interaction potential. There is a smooth fall in cross section up to 0.15 eV where a small hump appears; the decline continues to 0.5 eV where the singlet and triplet cross sections are equal. Above 0.5 eV the cross section oscillates about the level of the triplet cross section (Figure 5.16). As in the case of carbon dioxide this oscillation may be due to statistical fluctuation, but the spiked structure at 0.8 eV is more than twice the length of its error bar from the value of the triplet cross section, and is therefore likely to be real physical structure.

The branching ratios shown in Figure 5.5 show a lower fraction of Penning ionisation than in the triplet case (30% compared with 50%). Once again the data of West et al disagrees with the present results in the case of NO^+, N_2^+ and N^+ but the percentages of N_2O^+ and O^+ are in good agreement. Hotop et al (1979) report a much greater fraction of N^+; the ratio of N^+ to N_2O^+ agrees with the present results.

5.7 CH_4 + He(2^3S)

The cross section for ionisation of methane by He(2^3S) increases with energy in a similar fashion to that of argon, indicating that the interaction potential is repulsive in an argon-

like way. The present data shows good agreement with the results of Jerram (1985) up to 0.3 eV, but above this energy there is significant disagreement (Figure 5.17). A dip is observed between 0.3 and 2 eV, where the data of Jerram is at a maximum. This is the only case of such a divergence in the two sets of data. An explanation for this difference may be found in the comparison of triplet and singlet cross sections shown in Figure 5.21. The total ionisation cross section of methane by $He(2^1S)$ shows a pronounced maximum in the same energy region as the peak detected by Jerram. The quench lamp used by Jerram (Chapter 4.3.4) was not as effective at high energy as the one used in the present experiment, and so the cross section measured by Jerram at high energy may contain a contribution from the singlet cross section.

Figure 5.18 shows that the dissociative channel of ionisation is predominant; Penning ionisation declines over the energy range and is overtaken by the CH_3^+ dissociative branch above 0.04eV. This is in good agreement with the results of Jerram (1985) and the single energy measurements in Table 5.15. No associative ionisation has been observed.

5.8 CH_4 + $He(2^1S)$

The total cross section for ionisation of methane by $He(2^1S)$ shows evidence of an argon-like repulsive interaction potential as for the triplet case. There is evidence of a minimum in the cross section at 0.033eV. As with argon the cross section reaches its maximum at a lower energy than for the triplet case (Figure 5.19) where it is in good agreement with the data of Schmeltekopf and Fehsenfeld (1970) and Lindinger (1974). Unusually a second sharper and higher maximum is visible at 1 eV which may be due to structure in the repulsive wall of the interaction potential such as the small attractive region suggested by Brutschy et al (1982) for the Ar + $He(2^1S)$ system (Chapter 6.1).

Figure 5.20 shows that the fraction of Penning ionisation is lower for the singlet than for the triplet interaction, as in the cases of nitrous oxide and carbon dioxide. The fraction of CH_2^+ is higher at low energy than it is for the triplet case, and is in good agreement with the single energy measurements of Table 5.16.

5.9 C_2H_2 + $He(2^3S)$

The total cross section for ionisation of acetylene by $He(2^3S)$ shows a gradient similar to

that recorded by Jerram (1985) in the mid-energy region, but with a slightly higher gradient at low energy (Figure 5.22). The present cross section is normalised, as is that of Jerram (1985), to the absolute measurement of Ueno et al (1980), which is at low energy. This means that the present cross section is generally lower than that of Jerram. The shape of the cross section indicates a weakly attractive system, in agreement with the PIES data of Ohno et al (1983). Above 4.5eV there is a small rise in the cross section (Figure 5.22) which may be due to a repulsive wall at small interatomic separation.

Penning ionisation is the predominant branch of ionisation (Figure 5.23) but declines with energy and is equalled by the increasing dissociative channel C_2H^+ at 4 eV. The measurements of Jerram show a cross over in the branches at 2.5 eV; this is probably due to lower statistical accuracy in his measurements. There is good agreement with the measurements of Hotop et al (1969) shown in Table 5.15. No associative ionisation has been observed.

5.10 C_2H_2 + He(2^1S)

The total ionisation cross section of acetylene by He(2^1S) shows a more rapid decline with increasing energy than the triplet case (Figure 5.24), as for nitrous oxide and carbon dioxide, and again indicates a more attractive potential than in the triplet case. A small hump is apparent at 0.16 eV and a second larger hump at 0.35 eV. Above 0.4eV the cross section is similar to the triplet cross section (Figure 5.26) without any appreciable structure.

Figure 5.25 shows the fraction of Penning ionisation to be lower than in the triplet case as in all other cases. The data of Hotop et al (1969) also shows a lower percentage of Penning ionisation (Table 5.16), but not as pronounced as in the present results. Penning ionisation remains predominant over the entire range of energy, with the dissociative channel highest at mid energies (0.35-1.3 eV) and no associative ionisation observed.

5.11 NH_3 + He(2^3S)

The total cross section for ionisation of ammonia by He(2^3S) shows a rapidly declining cross section with energy (Figure 5.27). The present data is in good agreement with that of Jerram (1985), with the trends shown by Jerram continued at low energy. This rapid decline would be expected from the PIES data of Ohno et al (1983) which shows that the

NH_3 + He(2^3S) system is strongly attractive. At high energy (above 9eV) the cross section is constant, and may have reached a minimum because collisions are penetrating to a repulsive wall in the interaction potential. At higher energies still, the cross section may be expected to increase as the imaginary part of the potential rises.

Penning ionisation provides the major branch in Figure 5.28, but declines with energy and is overtaken by the NH_2^+ branch above 1 eV, as compared to 2eV in the work of Jerram (1985). The variation of the NH^+ branch is better defined than by Jerram, because of the superior statistical accuracy of the present data. No associative ionisation has been observed.

5.12 NH_3 + He(2^1S)

The total cross section at 0.03 eV is the largest cross section of any recorded in this work. Figure 5.29 shows good agreement with the absolute measurement of Schmeltekopf and Fehsenfeld (1970). The cross section declines in a similar fashion to the triplet cross section (Figure 5.31), with the exception of a maximum at 0.3 eV. The hump appears in only the Penning ionisation cross section. As would be expected, the singlet interaction potential is even more strongly attractive than is the triplet potential.

Penning ionisation provides the major branch in Figure 5.30, with the predominant dissociative channel NH_2^+ unusually declining with energy. There is not enough NH^+ data at high and low energy to make reasonable measurements in these regions. The error bars are very large over most of the energy range, but the measurements vary smoothly.

5.13 SF_6 + He(2^3S)

The total ionisation cross section for sulphur hexafluoride with He(2^3S) shown in Figure 5.32 behaves in a very similar way to that of argon. The cross section rises smoothly with energy, before reaching a maximum at 0.28 eV. This suggests that the interaction potential is repulsive as in the case of argon. A gentle argon-like decline is interrupted by a peak at 0.83eV, suggesting there is some structure, either in the repulsive wall of the interaction potential, or in the imaginary part of the interaction potential. Penning ionisation is the major branch of ionisation as in the case of argon, although no associative ionisation has been detected (Figure 5.33).

Table 5.1

Normalisation errors for total and partial cross sections given in tables 5.2 to 5.14 and key to figures 5.2 to 5.33

Target species	Normalised to	Normalisation error (%)	Key
	Present data		□◇△○⧖
Ar	Jerram (1985)	6	■
CO_2	Schmeltekopf and Fehsenfeld (1970)	30	o
N_2O	Schmeltekopf and Fehsenfeld (1970)	30	
CH_4	Jerram (1985)	8	
C_2H_2	Ueno et al (1980)	15	□
NH_3	Jerram (1985)	6	
SF_6	Schmeltekopf and Fehsenfeld (1970)	30	
	Other absolute measurements		
	Lindinger et al (1974)		▲
	Bolden et al (1970)		△
	Riola et al (1974)		⧗

Table 5.2 Relative cross sections and branching ratios for Ar + He(2^3S)

Total cross section

g kms^{-1}	σ(g) $10^{-16}cm^2$	E meV	g kms^{-1}	σ(g) $10^{-16}cm^2$	E meV
0.97	4.27 ± 0.05	0.018	2.88	14.9 ± 0.1	0.157
1.00	4.32 ± 0.05	0.019	2.89	15.0 ± 0.1	0.159
1.12	4.48 ± 0.12	0.023	3.03	15.1 ± 0.1	0.174
1.12	4.47 ± 0.05	0.024	3.21	16.6 ± 0.1	0.196
1.19	4.59 ± 0.06	0.027	3.25	16.6 ± 0.1	0.200
1.29	4.75 ± 0.06	0.029	3.69	18.5 ± 0.2	0.259
1.35	5.25 ± 0.05	0.035	4.33	19.4 ± 0.2	0.359
1.42	5.47 ± 0.05	0.038	5.22	19.7 ± 0.3	0.517
1.51	5.96 ± 0.06	0.043	5.69	19.1 ± 0.4	0.616
1.60	6.54 ± 0.07	0.049	6.38	18.5 ± 0.4	0.772
1.68	7.05 ± 0.06	0.054	7.07	19.3 ± 0.3	0.950
1.85	8.04 ± 0.07	0.065	8.00	19.4 ± 0.3	1.22
1.92	8.72 ± 0.06	0.070	9.21	19.6 ± 0.3	1.61
2.22	10.93 ± 0.09	0.093	10.6	18.0 ± 0.3	2.15
2.43	12.4 ± 0.1	0.111	12.8	18.4 ± 0.2	3.12
2.62	13.5 ± 0.1	0.130	15.7	15.9 ± 0.2	4.69
2.63	13.5 ± 0.1	0.132	19.7	16.6 ± 0.1	7.39
2.73	14.1 ± 0.1	0.142			

Branching ratios (%) Partial cross sections ($10^{-16}cm^2$)

g kms^{-1}	E meV	Ar+	$ArHe^+$	$\sigma(Ar^+)$	$\sigma(ArHe^+)$
1.13	0.031	76.2 ± 2.5	23.8 ± 1.5	3.6	1.1
1.62	0.050	77.6 ± 0.8	22.8 ± 0.4	5.1	1.46
2.11	0.084	81.3 ± 0.5	18.7 ± 0.3	7.6	1.75
2.5	0.118	87.4 ± 0.5	12.6 ± 0.2	11.2	1.60
3.0	0.170	93.4 ± 0.6	6.6 ± 0.2	14.0	1.01
3.5	0.230	96.9 ± 0.8	3.1 ± 0.1	17.0	0.54
4.6	0.400	99.1 ± 1.4	0.9 ± 0.1	19.3	0.16
6.0	0.680	99.8 ± 1.7	0.2 ± 0.06	18.9	0.03
8.5	1.37	100 ± 1.6		19.4	

Figure 5.2 Ar + He(2^3S)

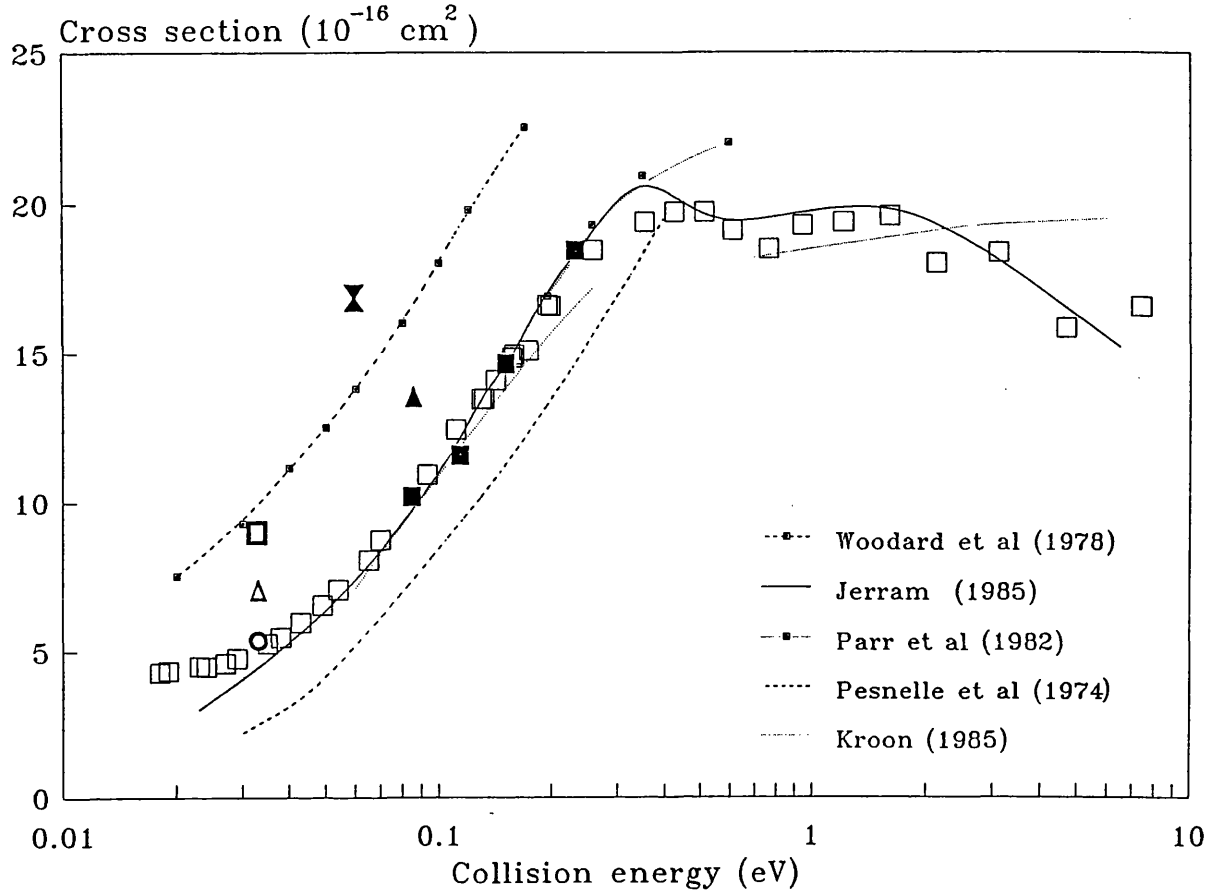

Figure 5.3

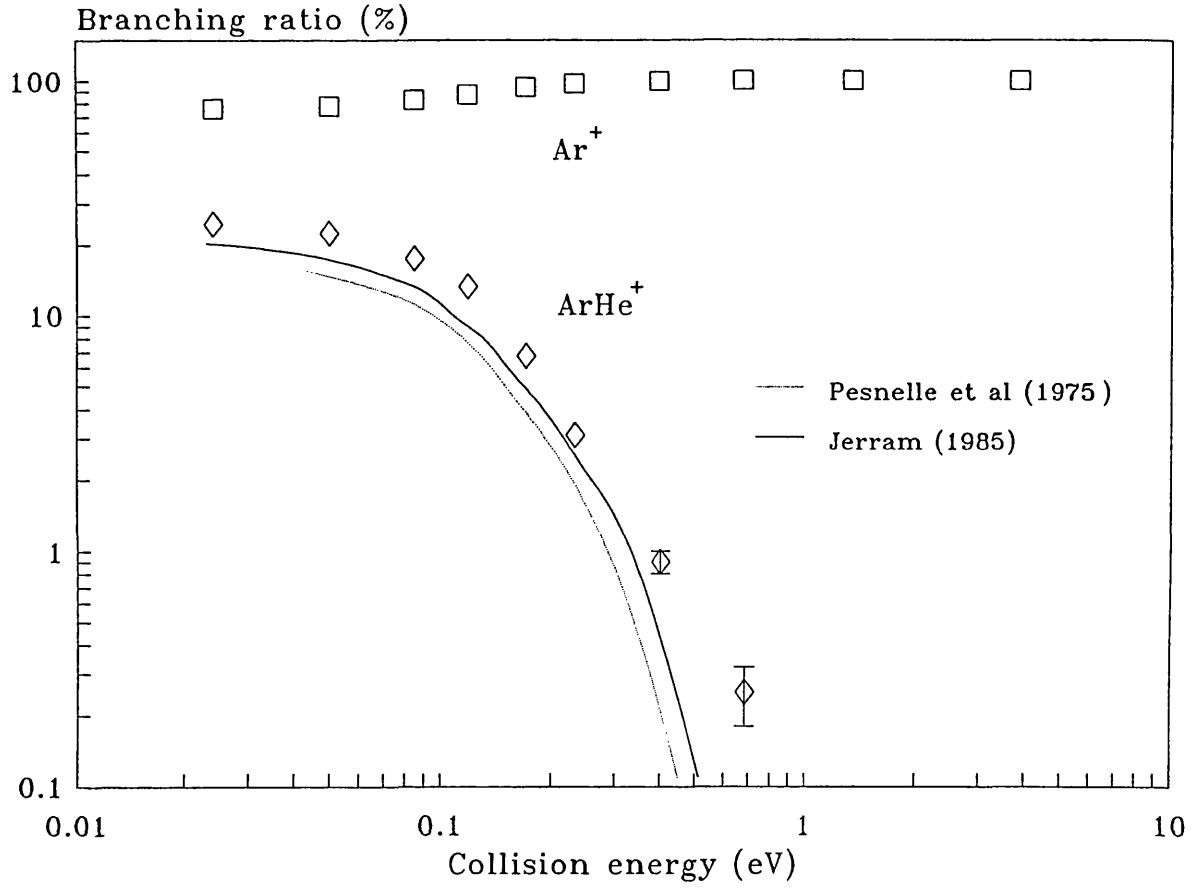

Table 5.3 Relative cross sections and branching ratios for Ar + He(2^1S)

Total cross section

g kms^{-1}	σ(g) $10^{-16}cm^2$	E meV	g kms^{-1}	σ(g) $10^{-16}cm^2$	E meV
1.04	4.1 ± 1.5	0.021	3.20	26.4 ± 1.2	0.173
1.09	5.8 ± 1.4	0.023	3.16	27.4 ± 1.4	0.196
1.16	7.4 ± 1.4	0.025	3.22	27.2 ± 1.4	0.199
1.22	9.8 ± 1.4	0.028	3.41	24.0 ± 1.4	0.221
1.26	11.4 ± 1.3	0.030	3.69	24.2 ± 1.6	0.258
1.31	12.0 ± 1.4	0.033	3.70	25.1 ± 1.5	0.260
1.38	14.3 ± 1.4	0.036	3.99	24.6 ± 2.0	0.290
1.44	15.2 ± 1.0	0.039	4.32	28.0 ± 2.8	0.354
1.52	19.1 ± 0.8	0.044	4.03	21.5 ± 2.7	0.407
1.61	20.4 ± 0.9	0.049	4.68	26.5 ± 2.7	0.416
1.69	21.4 ± 0.8	0.054	5.21	21.0 ± 4.2	0.515
1.85	23.2 ± 0.8	0.065	5.62	29.5 ± 6.8	0.600
1.93	23.9 ± 0.8	0.070	6.41	23.0 ± 5.4	0.783
2.22	25.0 ± 0.8	0.093	7.00	25.2 ± 5.7	0.933
2.42	26.0 ± 1.2	0.111	8.06	20.4 ± 4.4	1.23
2.62	28.7 ± 1.3	0.130	9.26	17.4 ± 2.9	1.63
2.63	29.1 ± 1.4	0.131	10.5	17.2 ± 3.0	2.09
2.73	26.5 ± 1.1	0.142	12.8	20.5 ± 3.6	3.13
2.87	26.0 ± 1.2	0.157	15.0	21.6 ± 4.3	4.28
2.89	25.9 ± 1.1	0.158	19.2	16.3 ± 5.1	6.70

Branching ratios (%)

g kms^{-1}	E meV	Ar^+	$ArHe^+$
1.13	0.031	57.4 ± 13	42.6 ± 7.1
1.62	0.050	71.9 ± 2.7	28.1 ± 1.4
2.11	0.084	92.7 ± 2.7	7.3 ± 1.0
2.5	0.118	97.6 ± 2.5	2.4 ± 0.7
3.0	0.170	98.9 ± 3.0	0.1 ± 0.05
3.5	0.230	100 ± 1.5	

Partial cross sections ($10^{-16}cm^2$)

$\sigma(Ar^+)$	$\sigma(ArHe^+)$
11.8	8.8
17.7	6.9
28.5	2.2
32.4	0.8
36.1	0.04
36.9	

Figure 5.4 Ar + He(2^1S)

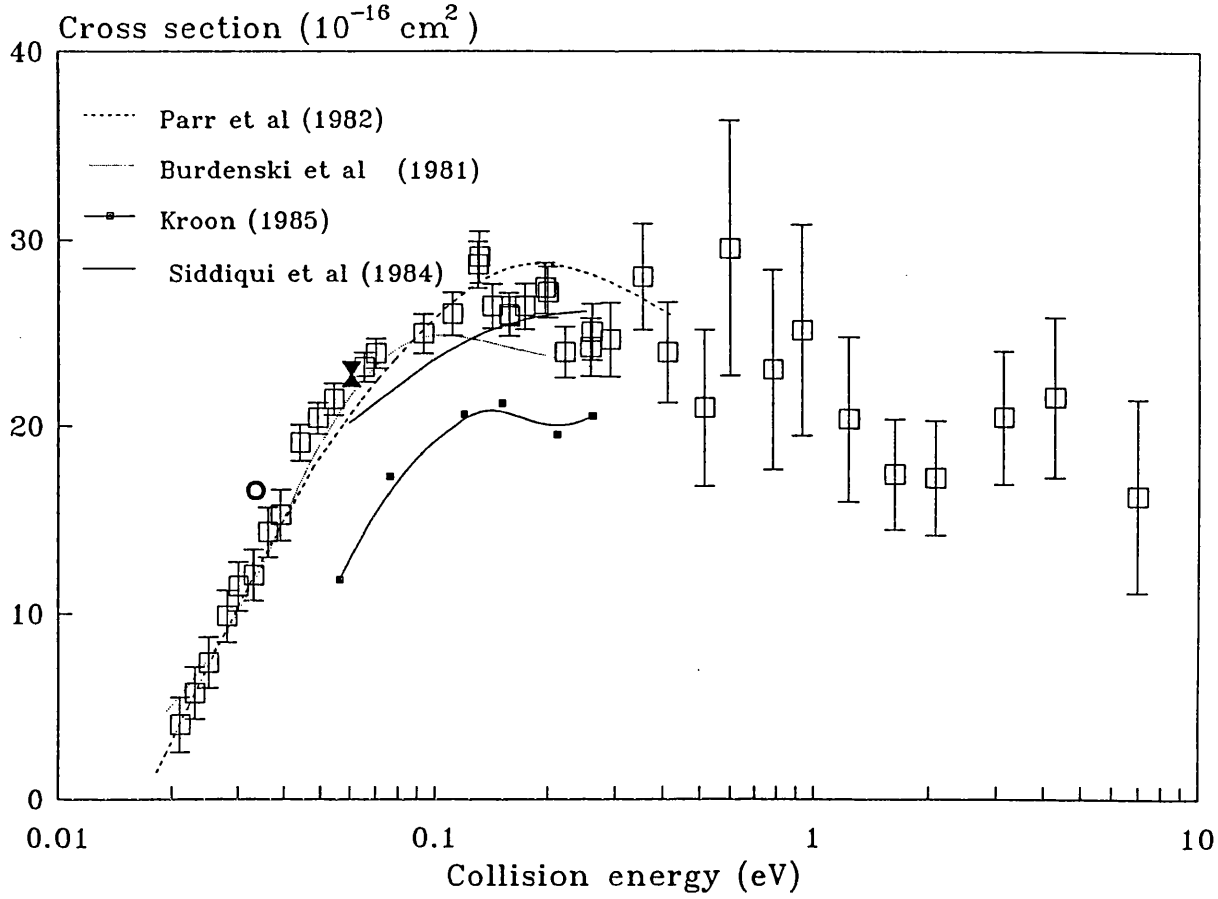

Figure 5.5

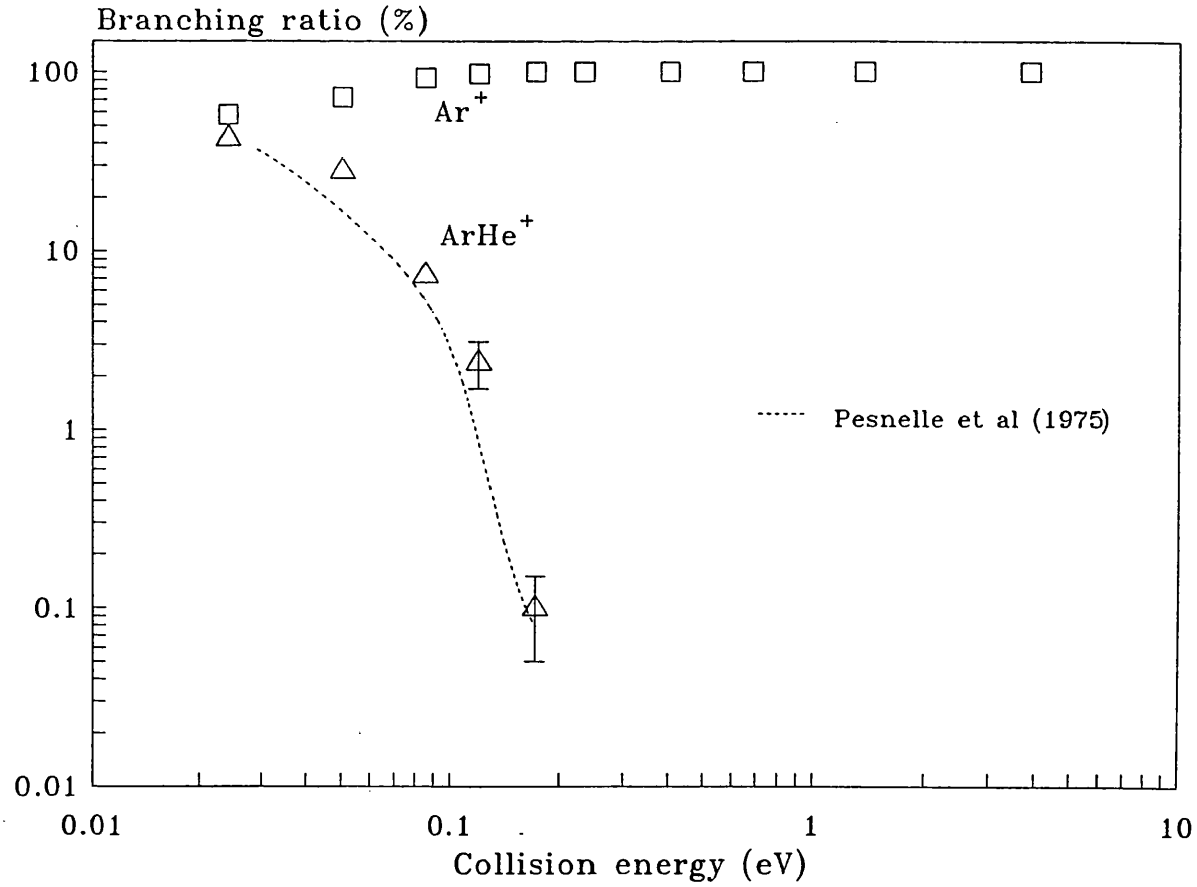

Figure 5.6

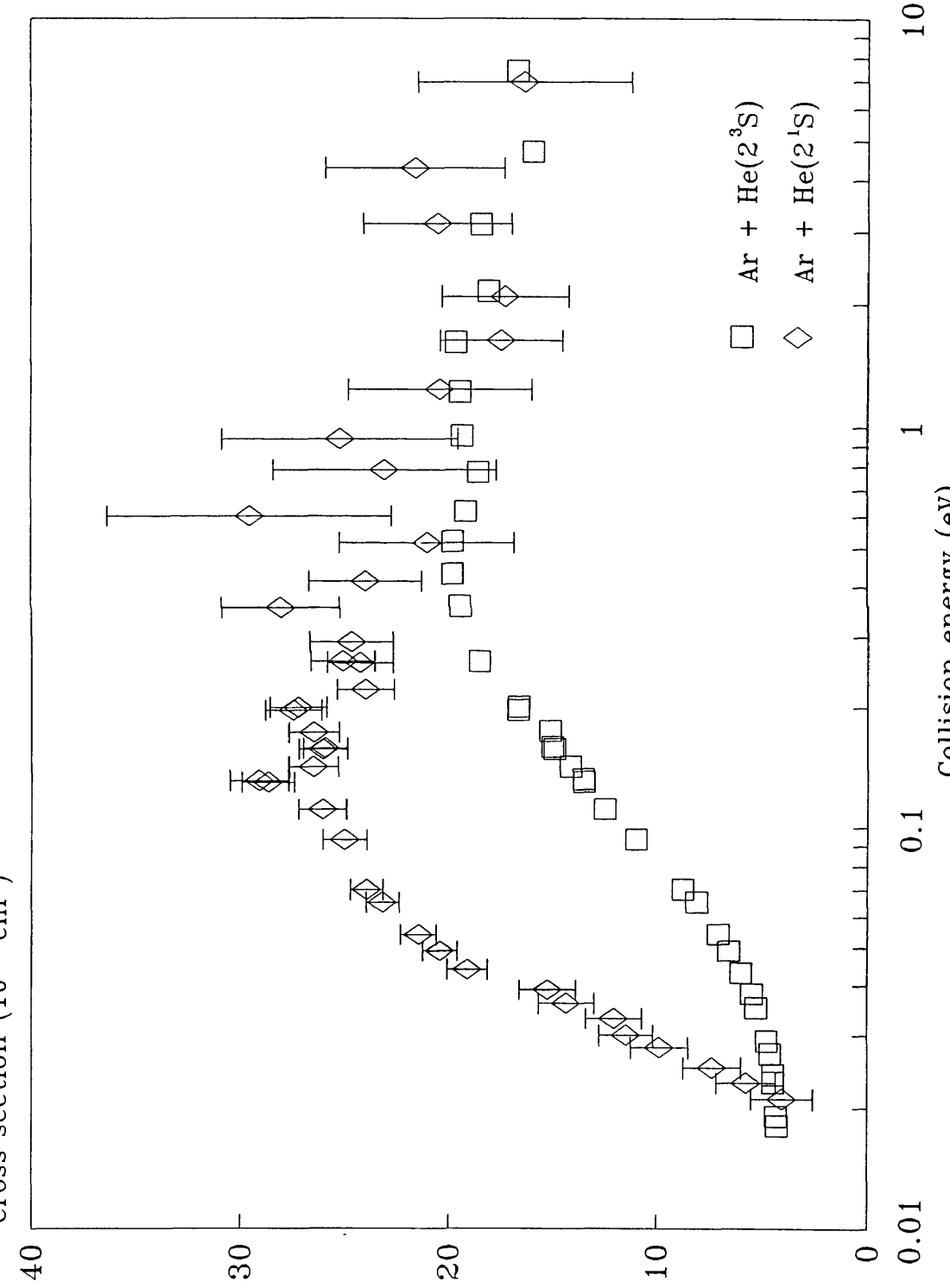
Cross section (10^{-16} cm^2)
40
30
20
10
0
0.01
0.1
1
10
Collision energy (eV)
Ar + He(2^3S)
Ar + He(2^1S)

Table 5.4 Relative cross sections and branching ratios for CO_2 + He(2^3S)

Total cross section

g kms^{-1}	σ(g) $10^{-16}cm^2$	E meV	g kms^{-1}	σ(g) $10^{-16}cm^2$	E meV
0.97	53.9 ± 0.4	0.019	2.91	30.1 ± 0.2	0.161
1.05	52.6 ± 0.4	0.021	3.21	30.5 ± 0.2	0.197
1.14	49.1 ± 0.4	0.025	3.24	30.0 ± 0.2	0.201
1.19	47.2 ± 0.3	0.027	3.69	29.1 ± 0.3	0.261
1.25	45.3 ± 0.2	0.030	3.70	29.8 ± 0.3	0.262
1.31	43.9 ± 0.2	0.033	4.33	29.2 ± 0.3	0.358
1.37	42.6 ± 0.2	0.036	4.74	29.3 ± 0.3	0.430
1.43	41.3 ± 0.3	0.039	5.21	28.9 ± 0.4	0.520
1.51	40.4 ± 0.6	0.044	5.69	27.6 ± 0.6	0.620
1.6	38.7 ± 0.4	0.049	6.37	25.3 ± 0.6	0.777
1.7	37.5 ± 0.3	0.055	7.07	25.0 ± 0.5	0.956
1.86	35.4 ± 0.2	0.066	8.00	24.6 ± 0.5	1.22
1.93	35.1 ± 0.2	0.071	9.13	23.3 ± 0.5	1.59
2.07	33.7 ± 0.2	0.082	10.5	21.9 ± 0.5	2.10
2.16	33.2 ± 0.2	0.089	12.6	21.5 ± 0.4	3.05
2.24	32.8 ± 0.2	0.096	15.2	19.1 ± 0.5	4.41
2.48	31.9 ± 0.2	0.118	18.8	13.7 ± 0.3	6.78
2.62	30.5 ± 0.2	0.131	19.8	15.1 ± 0.5	7.46
2.66	30.5 ± 0.2	0.135	23.9	10.4 ± 0.5	10.9
2.73	29.9 ± 0.5	0.143	32.2	4.88 ± 0.5	19.8
2.89	30.1 ± 0.2	0.160			

Branching ratios (%) Partial cross sections ($10^{-16}cm^2$)

g kms^{-1}	E meV	CO_2^+	CO^+	O^+	σ(CO_2^+)	σ(CO^+)	σ(O^+)
1.33	0.034	65.4 ±1.0	5.0 ±0.3	29.6 ±0.7	28.8	2.2	13.0
1.49	0.042	67.8 ±0.4	5.0 ±0.1	27.2 ±0.3	27.1	2.0	10.9
2.06	0.081	69.1 ±0.3	4.9 ±0.1	26.0 ±0.2	22.2	1.6	8.6
2.45	0.115	70.3 ±0.4	4.9 ±0.1	24.8 ±0.2	22.4	1.6	7.9
2.94	0.166	71.5 ±0.4	4.8 ±0.1	23.7 ±0.2	21.5	1.4	7.1
3.54	0.24	71.9 ±0.5	4.7 ±0.1	23.4 ±0.3	21.2	1.4	6.9
4.4	0.371	73.0 ±0.9	4.9 ±0.2	22.1 ±0.5	21.3	1.4	6.5
5.7	0.622	74.2 ±1.2	5.4 ±0.3	20.4 ±0.6	20.0	1.5	5.6
8.1	1.26	74.3 ±1.2	6.8 ±0.3	18.9 ±0.6	18.3	1.7	4.6
13.0	3.23	73.0 ±0.8	9.1 ±0.3	17.3 ±0.4	15.5	1.9	3.6

Figure 5.7 CO_2+ He(2^3S)

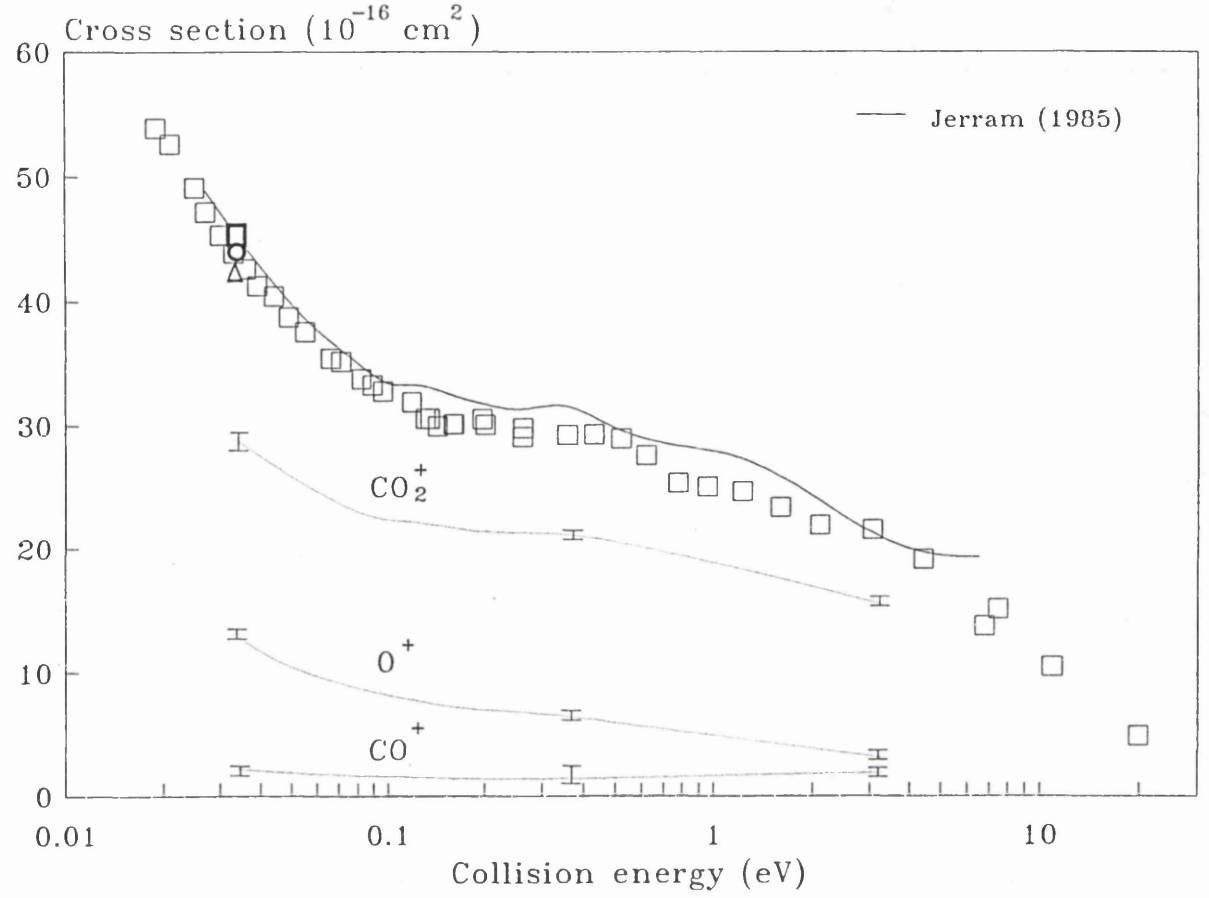

Figure 5.8

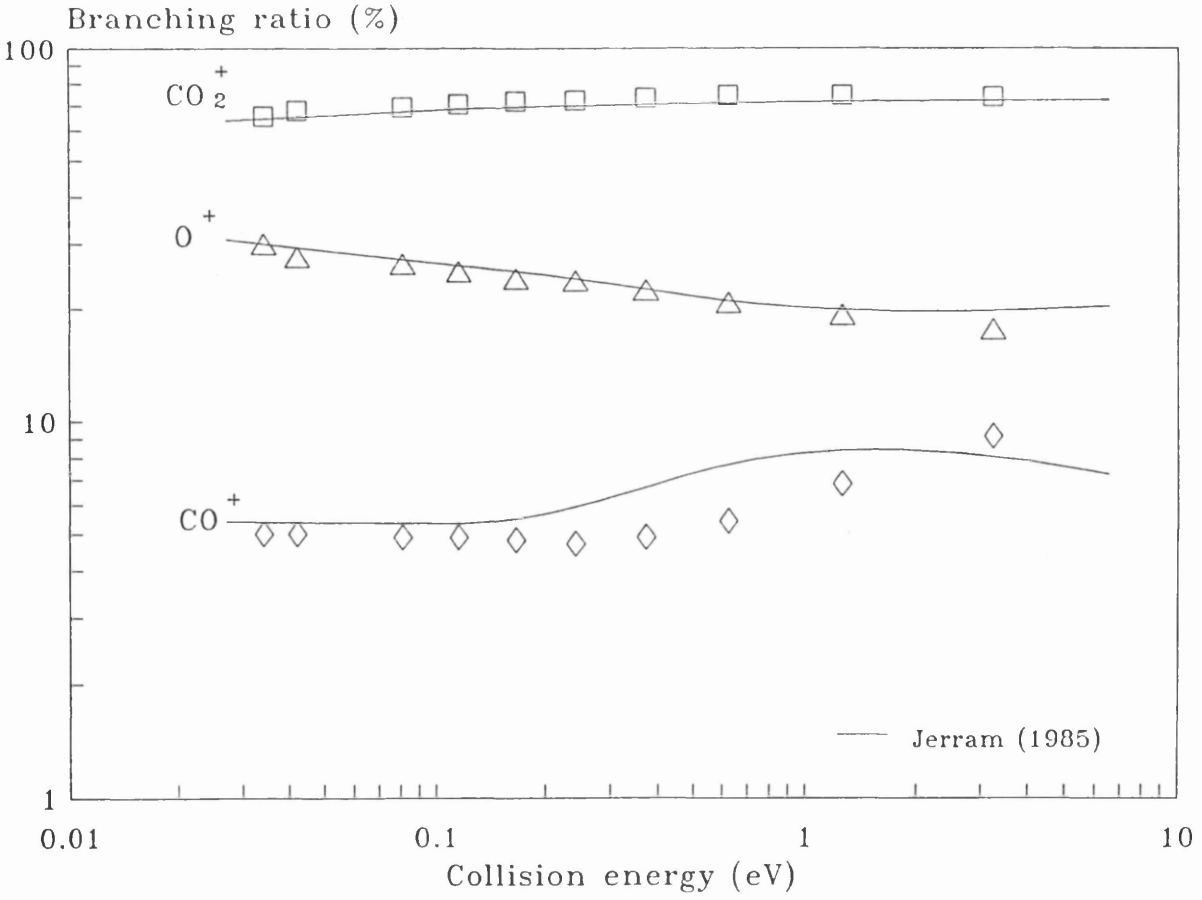

Table 5.5 Relative cross sections and branching ratios for carbon CO_2 + He(2^1S)

Total cross section

g kms^{-1}	σ(g) $10^{-16}cm^2$	E meV	g kms^{-1}	σ(g) $10^{-16}cm^2$	E meV
1.14	77.5 ± 12	0.025	3.02	36.8 ± 2.3	0.174
1.21	78.4 ± 8.5	0.028	3.21	35.1 ± 1.6	0.198
1.27	71.8 ± 5.1	0.031	3.25	35.3 ± 2.4	0.202
1.31	63.3 ± 5.2	0.033	3.41	33.4 ± 2.4	0.222
1.38	61.6 ± 4.8	0.036	3.69	36.2 ± 3.1	0.26
1.44	60.0 ± 4.6	0.039	3.70	35.9 ± 2.0	0.267
1.52	61.5 ± 4.4	0.044	3.92	30.7 ± 3.0	0.294
1.50	63.2 ± 4.0	0.049	4.31	25.7 ± 3.6	0.355
1.69	60.0 ± 3.7	0.054	4.64	18.3 ± 4.8	0.411
1.86	57.1 ± 2.6	0.066	4.65	24.1 ± 4.2	0.418
1.94	54.2 ± 2.7	0.072	5.22	16.1 ± 6.1	0.521
2.07	46.5 ± 2.7	0.082	5.68	23.1 ± 7.0	0.617
2.16	46.2 ± 2.9	0.089	6.37	40.0 ± 11	0.776
2.25	47.5 ± 2.9	0.097	7.08	39.2 ± 9.8	0.959
2.45	40.7 ± 2.5	0.115	7.93	20.6 ± 6.1	1.20
2.64	44.4 ± 2.8	0.133	9.27	15.2 ± 4.3	1.64
2.66	44.7 ± 3.0	0.135	10.4	23.3 ± 6.1	2.05
2.75	46.5 ± 3.1	0.145	12.3	38.6 ± 18	2.88
2.91	42.0 ± 2.8	0.161	14.4	14.0 ± 11	3.99
2.92	41.5 ± 2.6	0.163	20.7	12.0 ± 11	8.18

Branching ratios (%) Partial cross sections ($10^{-16}cm^2$)

g (kms^{-1})	E (meV)	CO_2^+	CO^+	O^+	$\sigma(CO_2^+)$	$\sigma(CO^+)$	$\sigma(O^+)$
1.33	0.034	75.3 ±3.0	12.9 ±1.2	11.8 ±1.2	50.5	8.6	7.9
1.49	0.042	66.8 ±1.0	9.8 ±0.4	23.4 ±0.6	41.4	6.1	14.5
2.06	0.81	71.2 ±0.9	11.2 ±0.4	17.6 ±0.4	33.1	5.2	8.2
2.45	0.115	68.0 ±0.9	10.6 ±0.3	21.4 ±0.5	27.7	4.3	8.7
2.94	0.166	66.6 ±1.2	10.9 ±0.4	22.5 ±0.5	27.6	4.5	9.3
3.54	0.241	67.2 ±2.2	10.9 ±0.5	21.9 ±0.7	23.5	6.6	7.7
4.4	0.371	62.3 ±3.8	12.8 ±1.0	24.9 ±1.4	14.7	3.0	5.9
5.7	0.622	75.0 ±3.8	13.5 ±1.6	11.5 ±1.5	17.3	3.1	2.7
8.1	1.25	77.3 ±3.8	13.5 ±1.6	9.2 ±1.3	14.7	7.6	1.7
13.0	3.23	69.5 ±2.9	20.7 ±1.6	9.8 ±1.1	21.0	6.3	3.0

Figure 5.9 CO_2 + He(2^1S)

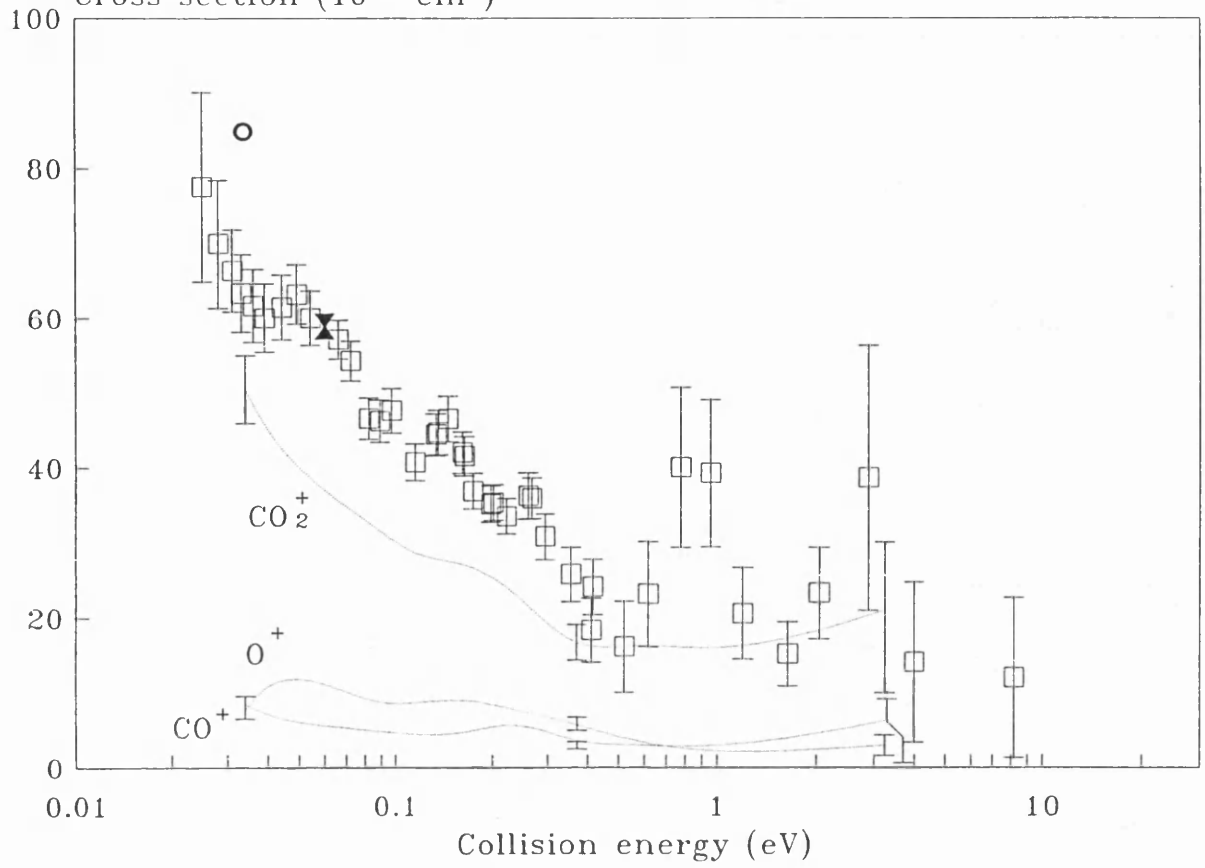

Figure 5.10

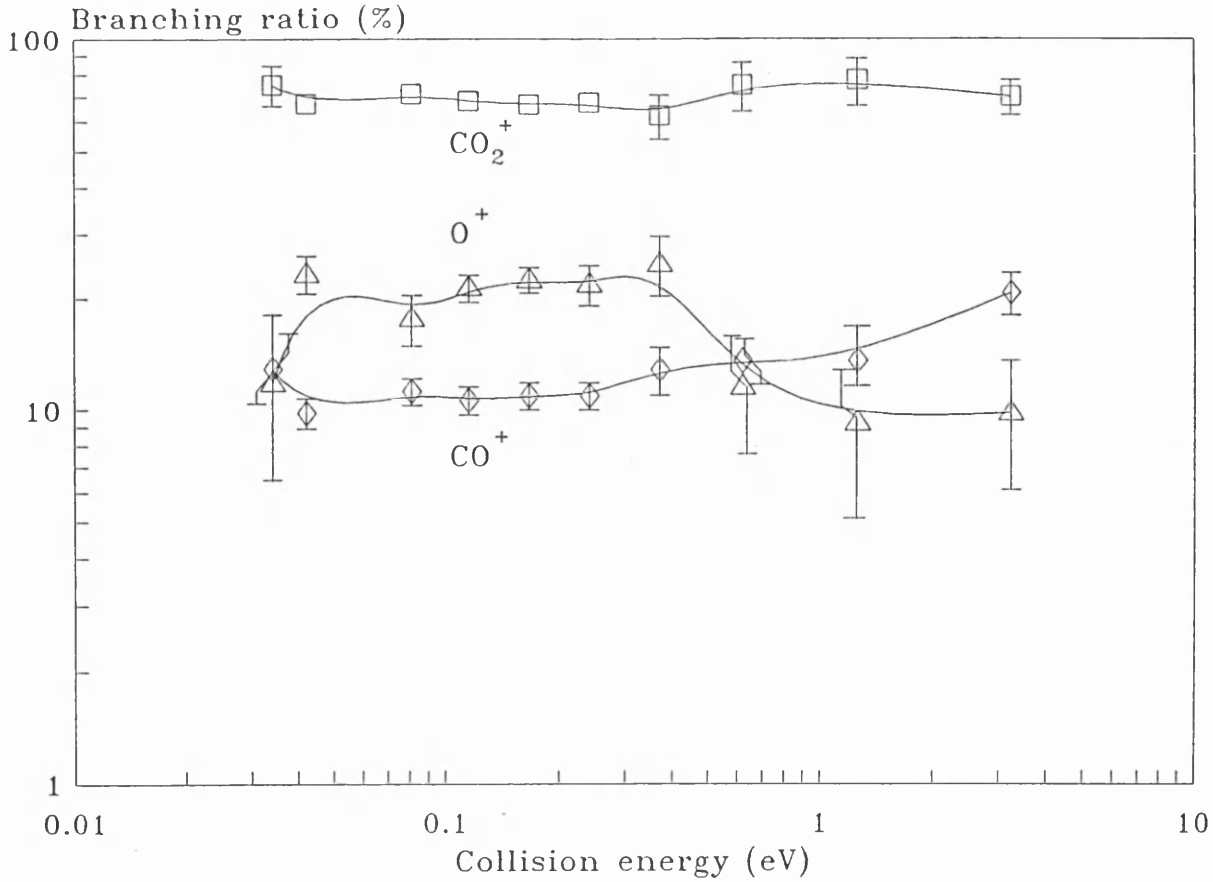

Figure 5.11

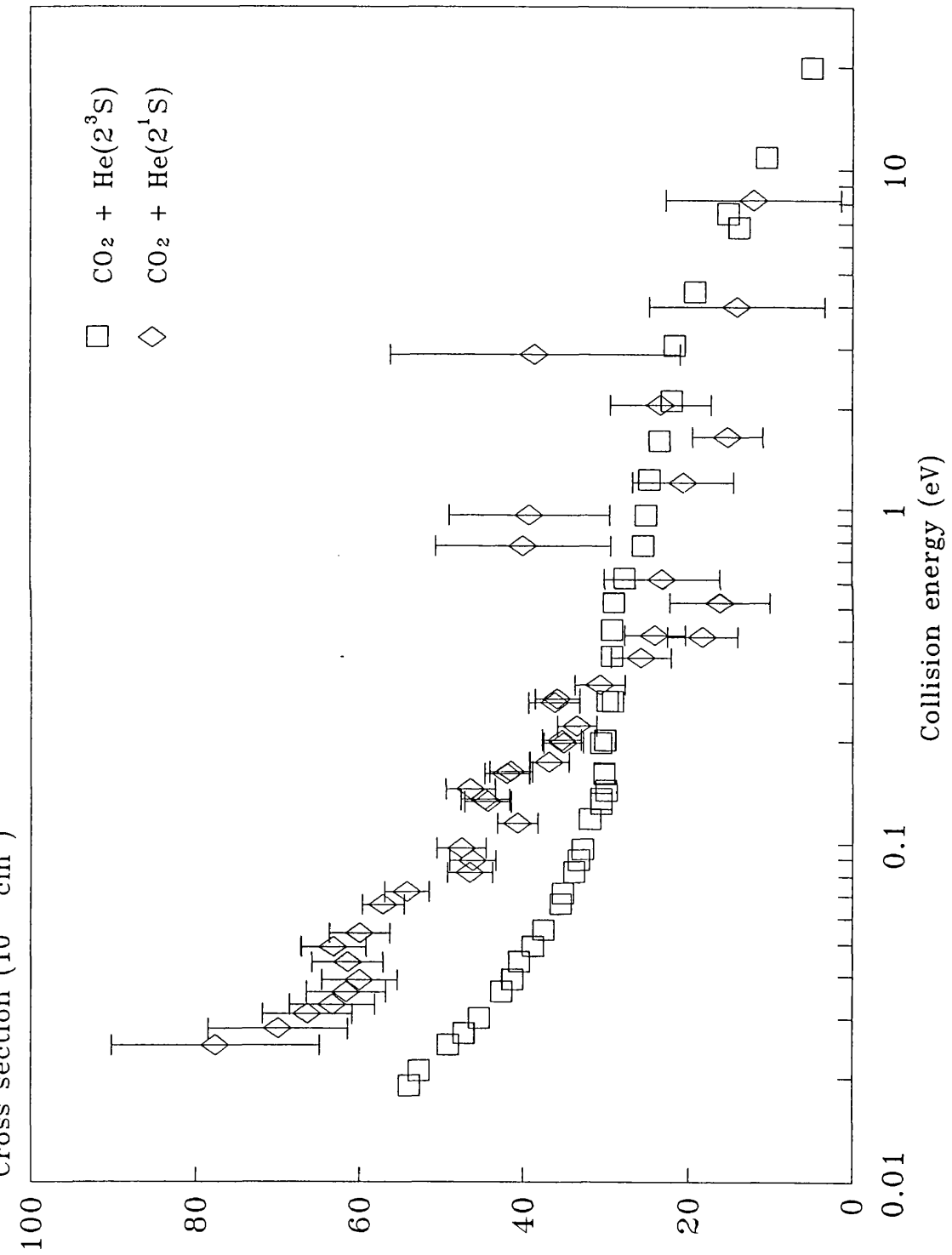
Cross section (10^{-16} cm^2)
100
80
60
40
20
0
0.01
0.1
1
10
Collision energy (eV)
CO_2 + He(2^3S)
CO_2 + He(2^1S)

Table 5.6 Relative cross sections and branching ratios for N_2O + $He(2^3S)$

Total cross section

g kms^{-1}	σ(g) $10^{-16}cm^2$	E meV	g kms^{-1}	σ(g) $10^{-16}cm^2$	E meV
1.0	28.8 ± 0.6	0.019	3.24	32.3 ± 0.2	0.201
1.05	30.9 ± 0.5	0.021	3.27	32.1 ± 0.2	0.205
1.14	31.2 ± 0.4	0.025	3.49	30.9 ± 0.2	0.223
1.24	32.7 ± 0.2	0.03	3.69	32.3 ± 0.3	0.261
1.32	33.3 ± 0.2	0.033	3.92	30.6 ± 0.2	0.293
1.44	33.4 ± 0.3	0.039	4.66	30.0 ± 0.3	0.415
1.45	32.8 ± 0.2	0.040	5.20	30.1 ± 0.6	0.520
1.50	32.1 ± 0.1	0.043	5.69	30.2 ± 0.4	0.621
1.61	32.7 ± 0.2	0.050	6.37	28.0 ± 0.5	0.778
1.86	32.0 ± 0.1	0.066	7.08	29.3 ± 0.6	0.959
1.94	32.1 ± 0.1	0.072	8.04	29.0 ± 0.5	1.24
2.08	31.2 ± 0.1	0.083	9.20	29.1 ± 0.4	1.62
2.11	31.8 ± 0.2	0.090	10.6	27.9 ± 0.4	2.14
2.25	31.7 ± 0.2	0.097	12.7	28.7 ± 0.4	3.10
2.45	31.9 ± 0.2	0.115	15.5	24.7 ± 0.3	4.59
2.65	32.1 ± 0.2	0.134	19.6	21.6 ± 0.2	7.36
2.66	32.1 ± 0.2	0.136	20.4	22.9 ± 0.2	7.96
2.76	31.9 ± 0.2	0.146	23.3	21.1 ± 0.3	10.3
2.85	32.3 ± 0.2	0.155	26.0	21.2 ± 0.3	12.9
2.96	32.4 ± 0.2	0.162	28.8	20.7 ± 0.3	13.9
3.05	31.5 ± 0.2	0.178	31.9	20.3 ± 0.4	19.5

Branching ratios (%) Partial cross sections ($10^{-16}cm^2$)

g (kms^{-1})	E (meV)	N_2O^+	NO^+	N_2^+	O^+	N^+	$\sigma(N_2O^+)$	$\sigma(NO^+)$	$\sigma(N_2^+)$	$\sigma(O^+)$	$\sigma(N^+)$
1.24	0.029	49.9 ± 0.9	39.3 ± 0.8	8.2 ± 0.4	2.4 ± 0.2	0.1 ± 0.01	13.3	12.8	2.7	0.64	0.03
1.64	0.051	50.5 ± 0.4	38.6 ± 0.3	8.5 ± 0.2	2.3 ± 0.1	0.2 ± 0.01	16.5	12.6	2.8	0.75	0.06
2.24	0.096	48.6 ± 0.3	39.8 ± 0.3	8.9 ± 0.1	2.4 ± 0.1	0.2 ± 0.01	15.4	12.6	2.8	0.76	0.06
2.64	0.133	46.7 ± 0.3	40.8 ± 0.3	9.5 ± 0.2	2.7 ± 0.1	0.2 ± 0.01	15.0	13.1	3.1	0.86	0.06
3.14	0.188	50.0 ± 0.4	37.7 ± 0.3	9.2 ± 0.2	2.8 ± 0.1	0.3 ± 0.05	15.9	12.0	2.9	0.89.	0.10
3.74	0.267	44.1 ± 0.5	42.3 ± 0.4	10.2 ± 0.2	3.2 ± 0.1	0.3 ± 0.1	14.1	13.5	3.3	1.02	0.10
4.6	0.411	42.4 ± 0.7	42.6 ± 0.7	11.1 ± 0.4	3.4 ± 0.2	0.5 ± 0.1	12.7	12.8	3.5	1.02	0.15
5.9	0.674	42.4 ± 0.9	42.4 ± 0.9	11.0 ± 0.4	3.9 ± 0.2	0.4 ± 0.1	12.5	12.8	3.2	1.1	0.12
8.3	1.33	37.7 ± 0.7	44.8 ± 0.8	12.6 ± 0.4	4.4 ± 0.2	0.5 ± 0.1	10.9	13.0	3.7	1.4	0.15
13.2	3.35	35.1 ± 0.4	45.9 ± 0.5	13.2 ± 0.2	4.3 ± 0.1	1.2 ± 0.1	9.8	12.9	3.7	1.2	0.3

Figure 5.12 N_2O + $He(2^3S)$

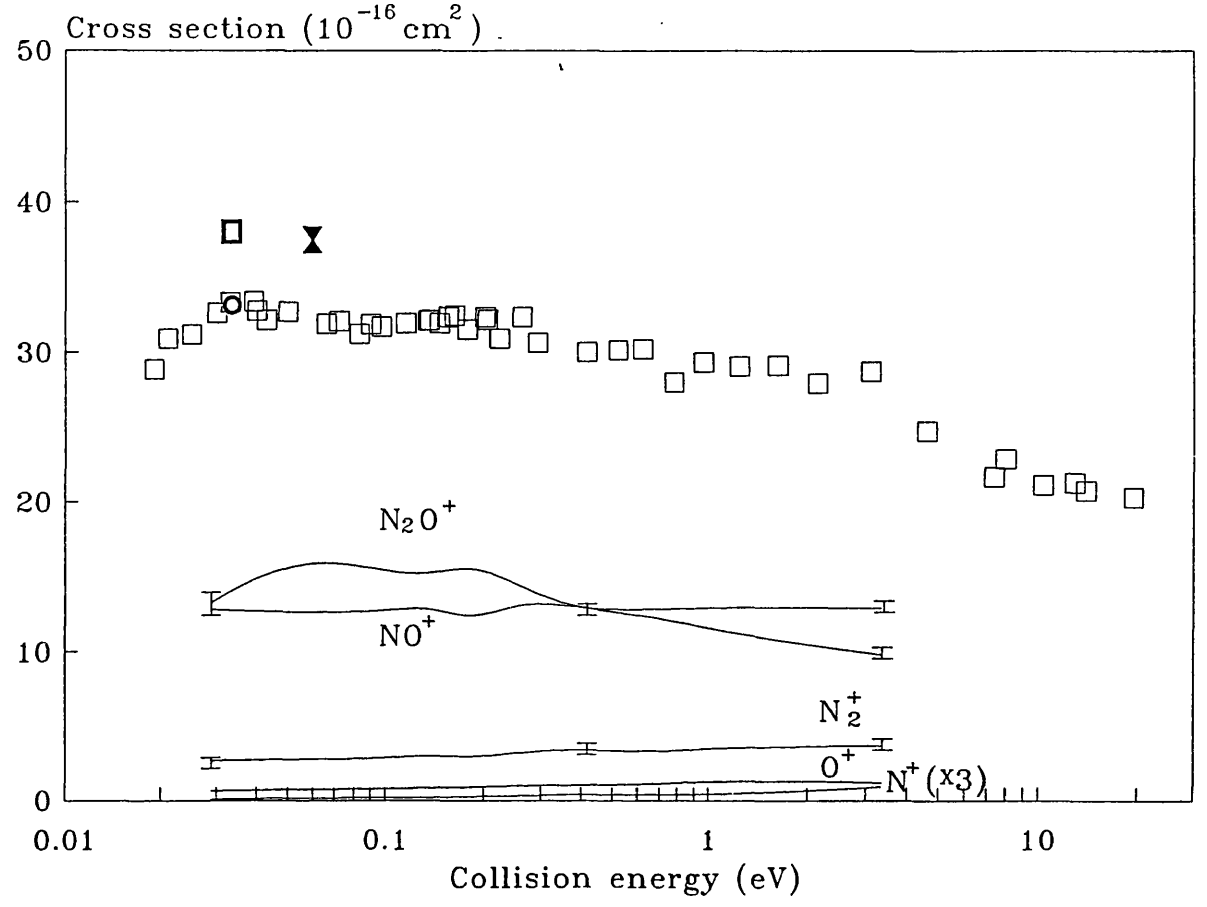

Figure 5.13

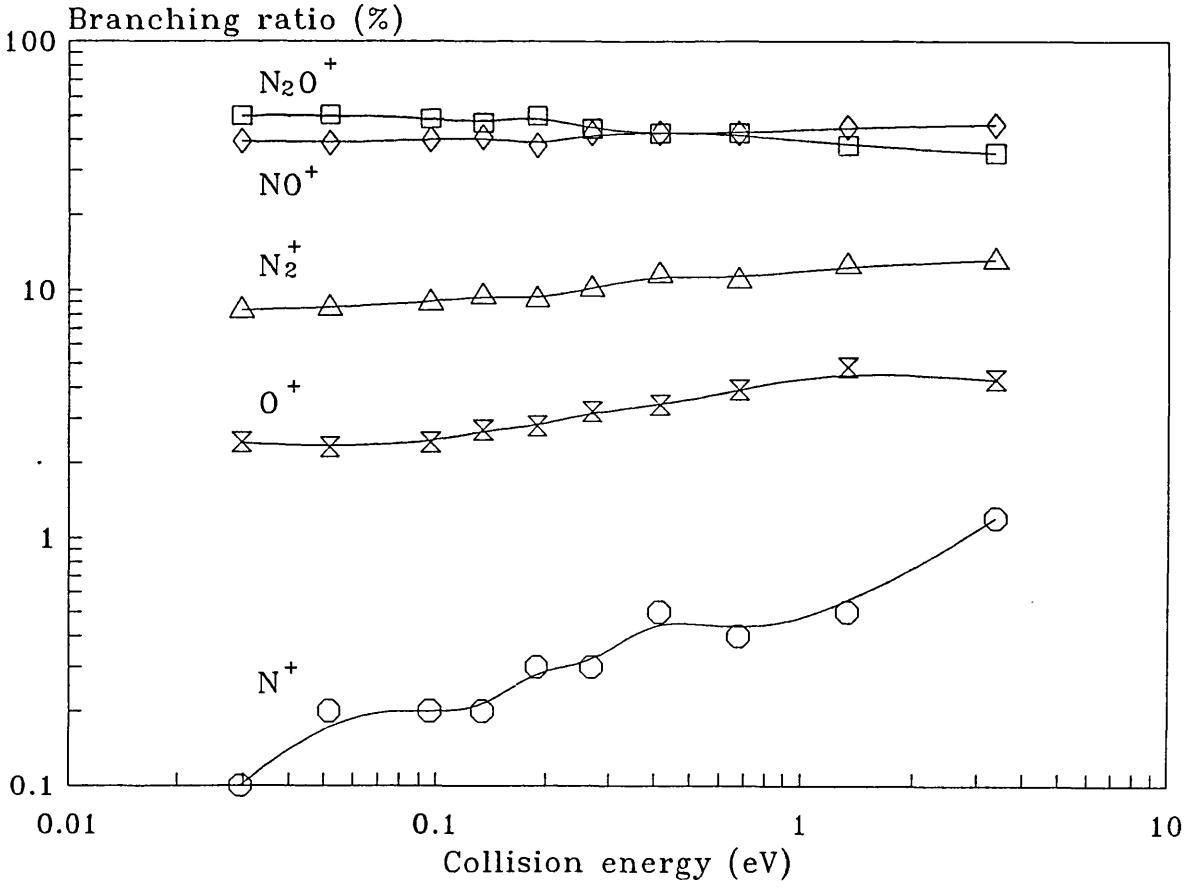

Table 5.7 Relative cross sections and branching ratios for N_2O + $He(2^1S)$

Total cross section

g kms^{-1}	σ(g) $10^{-16}cm^2$	E meV	g kms^{-1}	σ(g) $10^{-16}cm^2$	E meV
1.39	94.2 ± 3.2	0.035	3.41	49.1 ± 3.7	0.223
1.40	88.7 ± 3.7	0.038	3.70	50.7 ± 4.3	0.262
1.45	90.2 ± 4.3	0.040	3.72	50.8 ± 3.7	0.264
1.54	79.6 ± 5.3	0.045	3.91	44.1 ± 4.3	0.292
1.62	78.1 ± 3.2	0.050	4.33	36.2 ± 4.8	0.359
1.70	74.6 ± 3.2	0.055	4.63	43.7 ± 5.6	0.411
1.87	68.9 ± 3.2	0.067	4.69	35.8 ± 4.8	0.421
1.94	65.8 ± 3.2	0.072	5.23	33.3 ± 9.1	0.523
2.08	61.5 ± 3.0	0.083	5.69	43.8 ± 12	0.620
2.17	57.0 ± 3.2	0.090	6.34	70.4 ± 6.9	0.768
2.25	63.8 ± 3.3	0.097	7.13	39.6 ± 11	0.971
2.45	53.4 ± 3.2	0.115	7.99	20.9 ± 5.9	1.22
2.66	52.1 ± 3.2	0.135	9.11	18.4 ± 7.5	1.59
2.66	53.6 ± 3.2	0.135	10.6	13.4 ± 6.9	2.17
2.76	49.3 ± 2.7	0.146	12.8	22.0 ± 6.4	3.14
2.90	48.9 ± 2.6	0.161	15.1	42.3 ± 12	4.34
2.91	49.3 ± 2.7	0.162	18.3	42.3 ± 20	6.40
3.06	50.0 ± 3.2	0.179	20.6	24.5 ± 11	8.10
3.23	54.4 ± 3.7	0.200	23.7	22.5 ± 11	10.7
3.26	53.3 ± 3.7	0.204			

Branching ratios (%) Partial cross sections ($10^{-16}cm^2$)

g (kms^{-1})	E (meV)	N_2O^+	NO^+	N_2^+	O^+	N^+	$\sigma(N_2O^+)$	$\sigma(NO^+)$	$\sigma(N_2^+)$	$\sigma(O^+)$	$\sigma(N^+)$
1.24	0.029	28.3 ± 7.3	53.0 ± 5.2	12.4 ± 2.6	3.2 ± 1.3	3.1 ± 0.5	26.7	49.9	11.6	3.0	2.9
1.64	0.051	31.0 ± 2.4	51.5 ± 2.3	10.8 ± 1.3	4.0 ± 1.4	2.7 ± 0.2	24.7	40.2	8.4	3.1	2.1
2.24	0.096	32.3 ± 2.3	47.1 ± 1.0	11.8 ± 0.7	5.8 ± 2.0	3.0 ± 0.2	16.8	24.5	6.1	3.0	1.6
2.64	0.133	33.6 ± 2.2	44.9 ± 1.0	12.7 ± 1.0	5.5 ± 0.5	3.3 ± 0.2	16.2	24.4	6.3	3.6	1.5
3.14	0.188	31.2 ± 2.8	46.8 ± 2.4	12.1 ± 1.2	7.0 ± 0.6	2.9 ± 0.2	14.3	24.3	5.5	6.1	1.7
3.74	0.267	30.0 ± 4.2	43.8 ± 4.1	16.0 ± 1.6	7.5 ± 0.9	2.7 ± 0.3	15.2	22.2	8.1	3.8	1.4
4.6	0.411	27.5 ± 8.9	46.8 ± 8.9	10.6 ± 4.7	11.8 ± 2.5	3.3 ± 0.6	12.0	20.5	4.6	5.2	1.4
5.9	0.674	28.0 ± 11	41.6 ± 11	21.0 ± 5.5	5.9 ± 3.3	3.4 ± 0.7	12.3	18.2	9.2	2.6	1.5
8.3	1.33	38.8 ± 9.5	40.5 ± 10	13.1 ± 5.5	3.8 ± 3.2	3.8 ± 0.7	7.8	8.2	2.6	0.8	0.8

Figure 5.14 N_2O + He(2^1S)

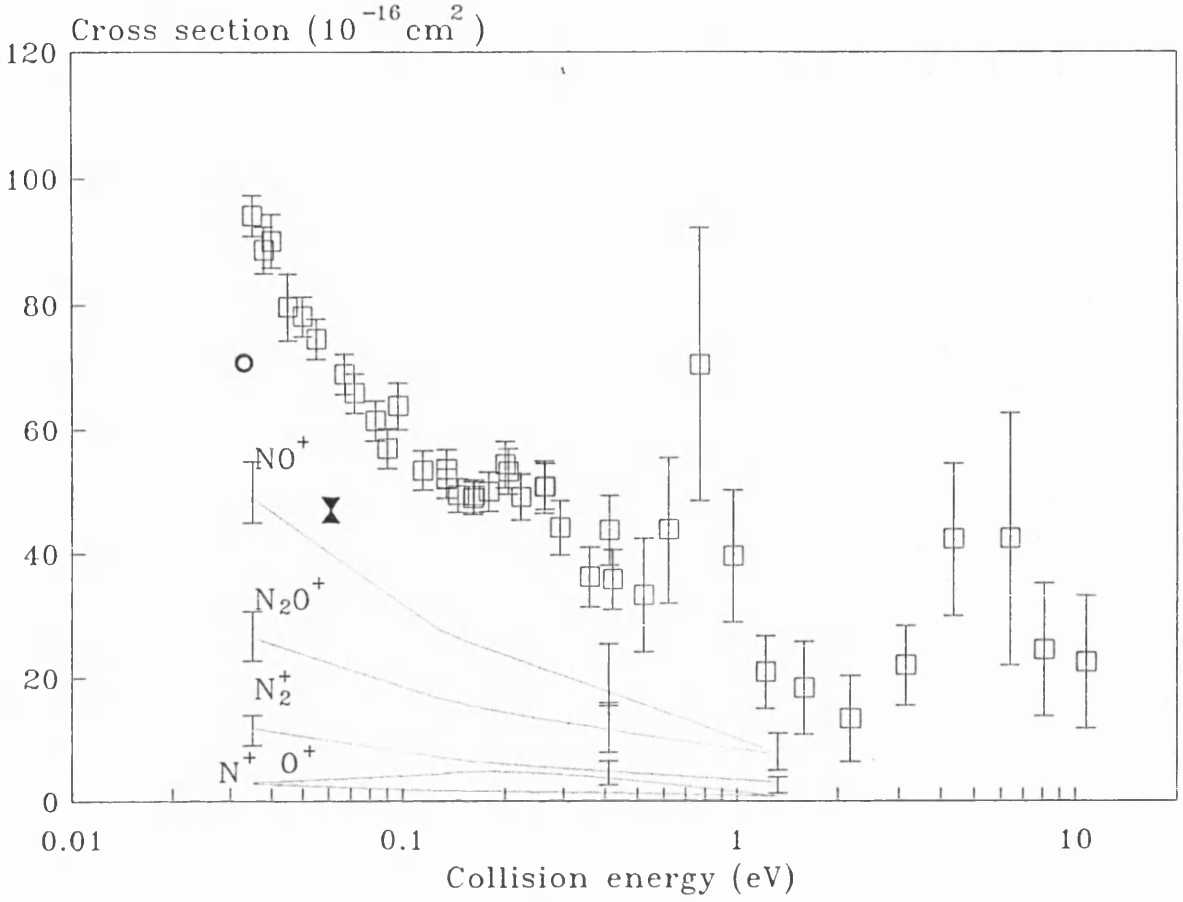

Figure 5.15

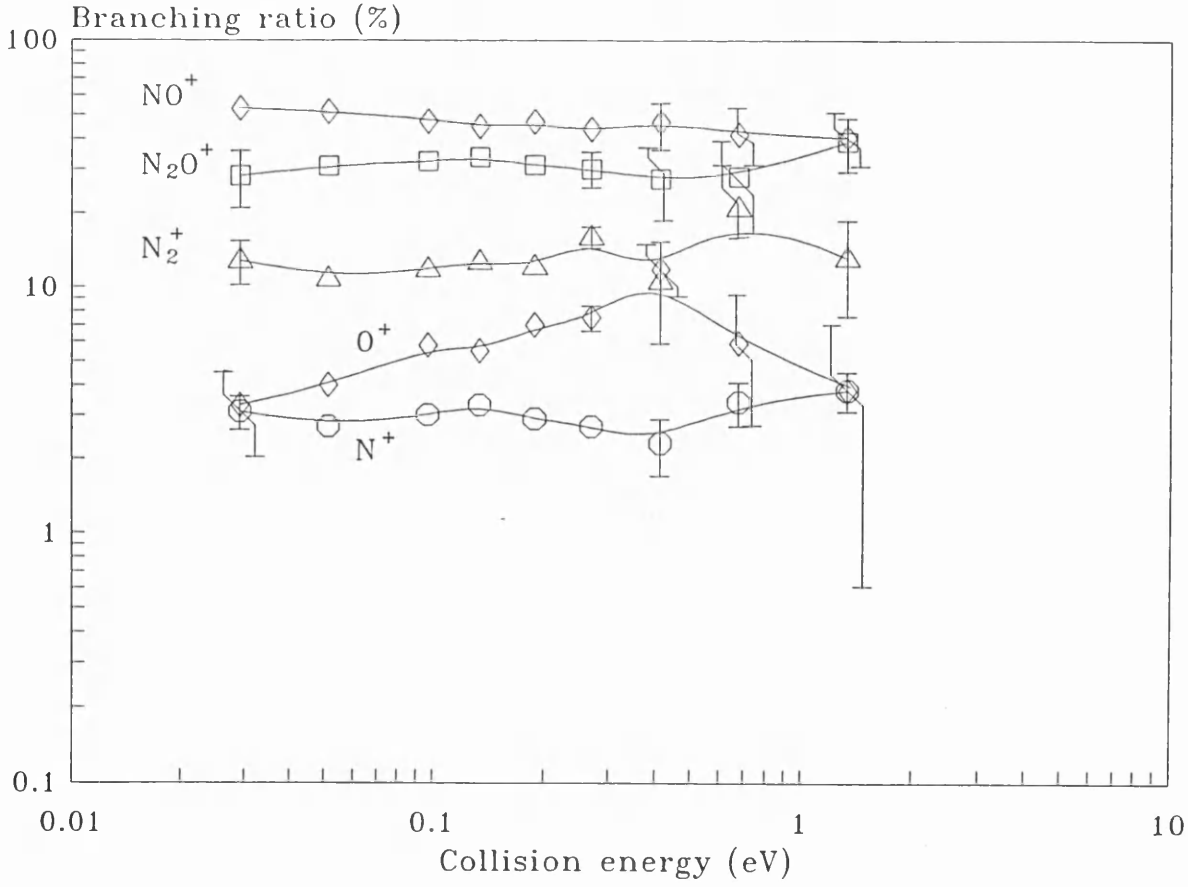

Figure 5.16

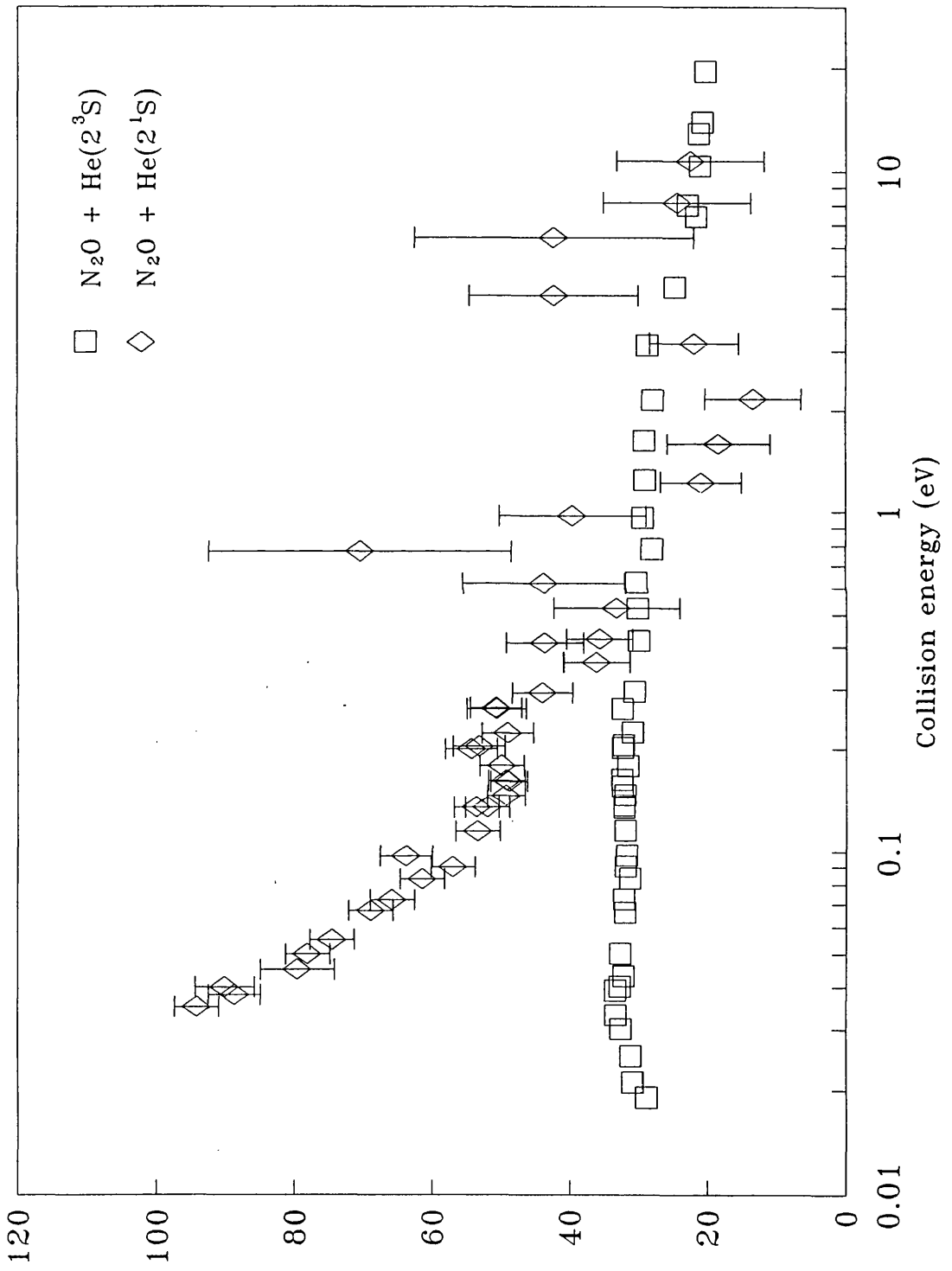
Cross section (10^{-16} cm^2)
120
100
80
60
40
20
0
0.01
0.1
1
10
Collision energy (eV)
N_2O + He(2^3S)
N_2O + He(2^1S)

Table 5.8 Relative cross sections and branching ratios for CH_4 + He(2^3S)

Total cross section

g kms^{-1}	σ(g) $10^{-16}cm^2$	E meV	g kms^{-1}	σ(g) $10^{-16}cm^2$	E meV
0.916	6.7 ± 0.3	0.014	2.92	23.0 ± 0.1	0.142
1.04	7.8 ± 0.3	0.018	3.05	22.8 ± 0.5	0.155
1.1	8.2 ± 0.2	0.02	3.24	24.1 ± 0.2	0.175
1.12	8.7 ± 0.2	0.021	3.27	23.9 ± 0.2	0.178
1.15	9.0 ± 0.1	0.022	3.69	25.6 ± 0.3	0.227
1.34	10.4 ± 0.2	0.03	3.70	26.0 ± 0.2	0.228
1.41	11.0 ± 0.2	0.033	4.32	26.9 ± 0.4	0.311
1.45	11.4 ± 0.2	0.035	4.74	26.9 ± 0.4	0.375
1.55	12.5 ± 0.1	0.04	5.21	25.6 ± 0.5	0.453
1.62	13.3 ± 0.2	0.044	5.68	24.6 ± 0.5	0.538
1.57	15.7 ± 0.2	0.049	6.37	23.6 ± 0.5	0.677
1.86	15.5 ± 0.2	0.058	7.06	23.8 ± 0.5	0.831
1.47	16.3 ± 0.1	0.063	8.01	23.3 ± 0.5	1.07
2.09	17.4 ± 0.2	0.073	9.17	24.9 ± 0.5	1.40
2.18	18.2 ± 0.1	0.079	10.5	24.9 ± 0.5	1.85
2.26	19.1 ± 0.1	0.085	12.8	25.8 ± 0.3	2.71
2.46	20.6 ± 0.2	0.101	15.7	21.2 ± 0.2	4.10
2.66	21.5 ± 0.1	0.118	20.0	16.7 ± 0.3	6.65
2.67	21.6 ± 0.2	0.119	21.8	16.4 ± 0.3	7.92
2.76	22.0 ± 0.3	0.127	25.3	16.3 ± 0.3	10.7
2.91	23.04 ± 0.2	0.141			

Branching ratios (%) Partial cross sections ($10^{-16}cm^2$)

g (kms^{-1})	E (meV)	CH_4^+	CH_3^+	CH_2^+	$\sigma(CH_4^+)$	$\sigma(CH_3^+)$	$\sigma(CH_2^+)$
1.18	0.02	51.8 ±1.6	44.4 ±1.4	3.8 ±0.4	5.2	4.44	0.38
1.66	0.046	47.7 ±0.5	48.2 ±0.5	4.1 ±0.2	6.3	6.4	0.54
2.14	0.076	46.0 ±0.4	49.7 ±0.4	4.3 ±0.1	8.2	8.8	0.77
2.54	0.108	45.3 ±0.4	47.9 ±0.4	4.8 ±0.1	9.5	10.5	1.0
3.03	0.153	44.9 ±0.4	50.1 ±0.5	4.9 ±0.1	10.2	11.4	1.1
3.52	0.204	45.0 ±0.6	50.4 ±0.6	4.7 ±0.2	11.1	12.4	1.2
4.4	0.323	44.7 ±1.1	50.1 ±1.5	5.2 ±0.4	12.0	13.5	1.4
6.0	0.600	44.8 ±1.4	50.5 ±1.5	4.7 ±0.5	10.7	12.2	1.2
8.5	1.21	40.9 ±1.4	53.7 ±1.6	5.4 ±0.5	9.5	12.5	1.3
14.7	3.60	36.0 ±1.3	55.2 ±1.6	8.8 ±0.7	8.5	13.0	2.1

Figure 5.17 CH_4+ He(2^3S)

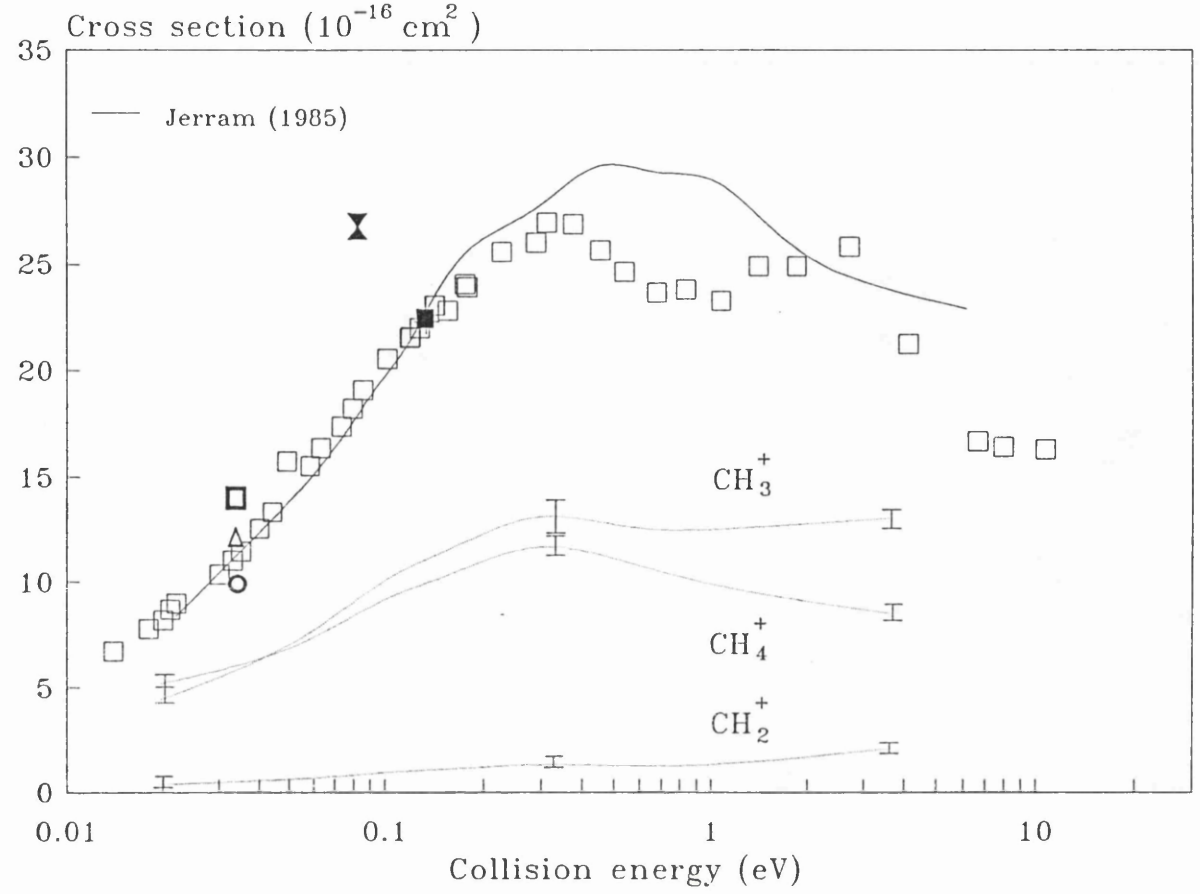

Figure 5.18

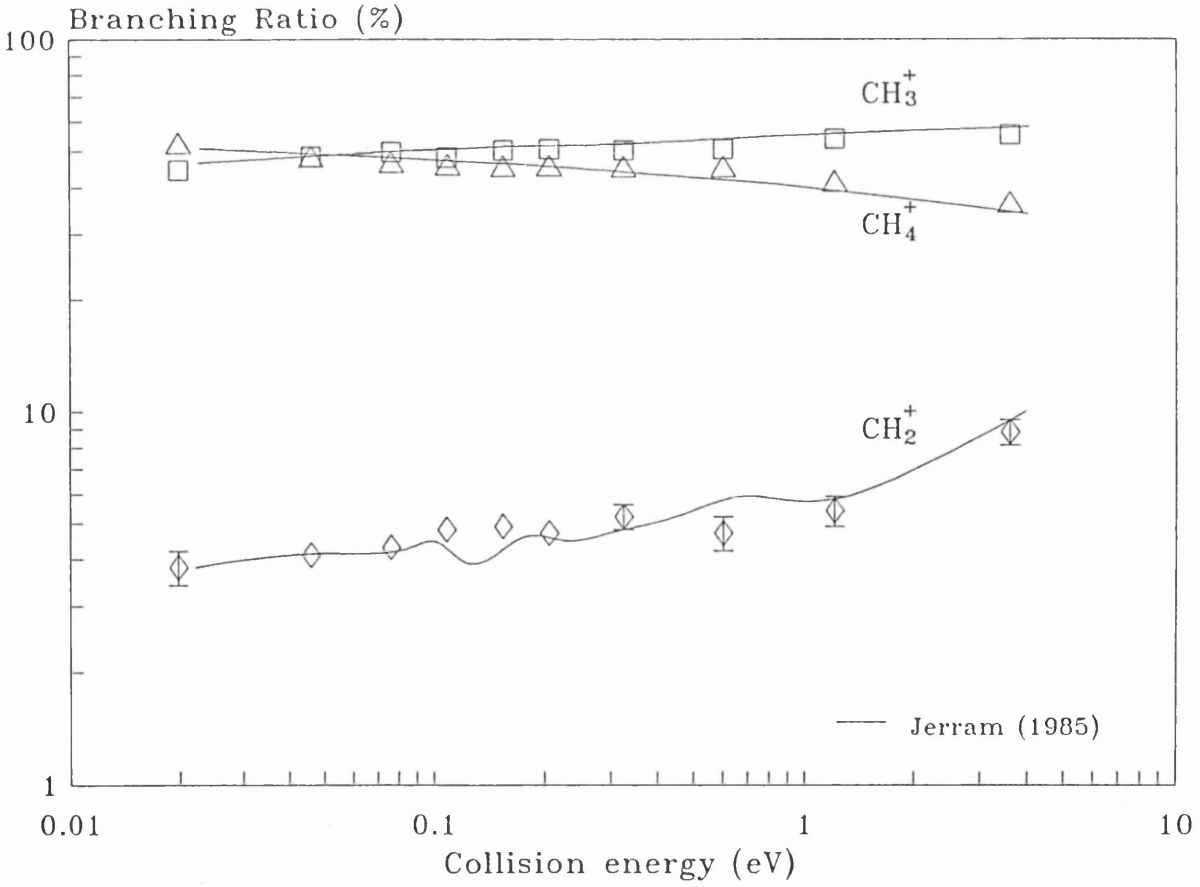

Table 5.9 Relative cross sections and branching ratios for CH_4 + He(2^1S)

Total cross section

g kms^{-1}	σ(g) $10^{-16}cm^2$	E meV	g kms^{-1}	σ(g) $10^{-16}cm^2$	E meV
1.04	30.6 ± 3.9	0.018	3.23	37.8 ± 2.3	0.175
1.17	30.1 ± 4.0	0.023	3.27	36.9 ± 2.4	0.178
1.34	30.6 ± 2.3	0.030	3.45	31.6 ± 5.3	0.196
1.40	29.2 ± 1.9	0.033	3.70	30.0 ± 2.8	0.228
1.45	29.6 ± 1.9	0.035	3.71	30.4 ± 2.6	0.229
1.54	32.0 ± 1.9	0.040	3.90	27.6 ± 3.0	0.252
1.63	32.4 ± 1.4	0.044	4.32	25.8 ± 3.7	0.313
1.70	32.2 ± 1.7	0.048	4.62	25.1 ± 3.7	0.357
1.87	34.3 ± 1.4	0.058	4.63	25.8 ± 4.6	0.358
1.94	36.1 ± 1.5	0.063	5.16	24.4 ± 6.9	0.444
2.09	34.3 ± 1.4	0.073	5.72	27.9 ± 7.2	0.546
2.25	38.0 ± 1.4	0.079	6.33	34.2 ± 9.2	0.664
2.18	35.4 ± 2.0	0.084	7.11	41.0 ± 10	0.846
2.46	35.5 ± 2.0	0.101	8.12	47.7 ± 12	1.10
2.65	36.9 ± 3.4	0.117	9.19	30.2 ± 6.9	1.41
2.66	37.0 ± 2.3	0.118	10.4	26.4 ± 2.0	1.81
2.76	37.8 ± 2.3	0.127	12.3	21.4 ± 1.7	2.50
2.93	36.0 ± 2.0	0.143	15.1	11.9 ± 5.5	3.79
2.93	35.7 ± 2.2	0.143	18.5	18.6 ± 4.7	5.68
3.05	35.6 ± 1.8	0.155			

Branching ratios (%) Partial cross sections ($10^{-16}cm^2$)

g (kms^{-1})	E (meV)	CH_4^+	CH_3^+	CH_2^+	$\sigma(CH_4^+)$	$\sigma(CH_3^+)$	$\sigma(CH_2^+)$
1.18	0.020	24.2 ±6.0	67.5 ±5.7	8.3 ±1.0	7.4	20.7	2.7
1.66	0.046	32.0 ±2.3	60.3 ±2.2	7.2 ±0.4	10.6	19.5	2.5
2.14	0.076	30.4 ±1.9	61.2 ±1.9	8.4 ±0.3	10.5	21.2	2.9
2.54	0.108	30.1 ±2.3	62.2 ±2.4	7.2 ±0.3	10.8	22.5	2.6
3.03	0.153	27.4 ±2.8	62.6 ±2.4	8.0 ±0.4	9.7	22.1	2.8
3.52	0.204	27.9 ±2.4	62.4 ±3.0	9.9 ±0.6	8.8	19.6	3.0
4.4	0.323	26.2 ±7.8	67.0 ±3.6	6.8 ±1.6	6.9	17.6	1.8
6.0	0.600	19.3 ±10	68.4 ±8.3	12.3 ±2.1	6.0	21.2	3.8
8.5	1.20	26.3 ±8.0	64.7 ±11	9.2 ±1.5	11.0	26.9	3.8
14.7	3.60	15.4 ±11	68.0 ±13	6.6 ±1.9	2.3	11.4	0.96

Figure 5.19 CH_4 + $He(2^1S)$

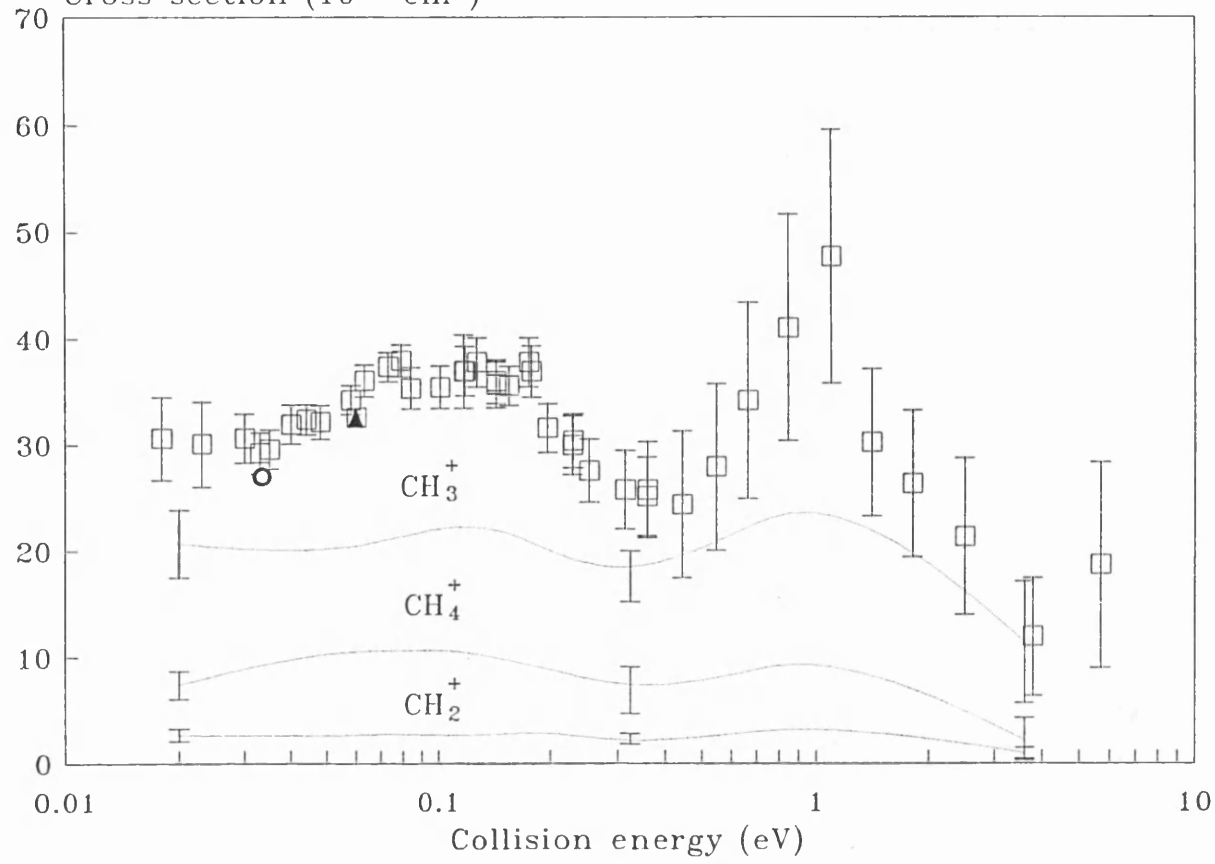

Figure 5.20

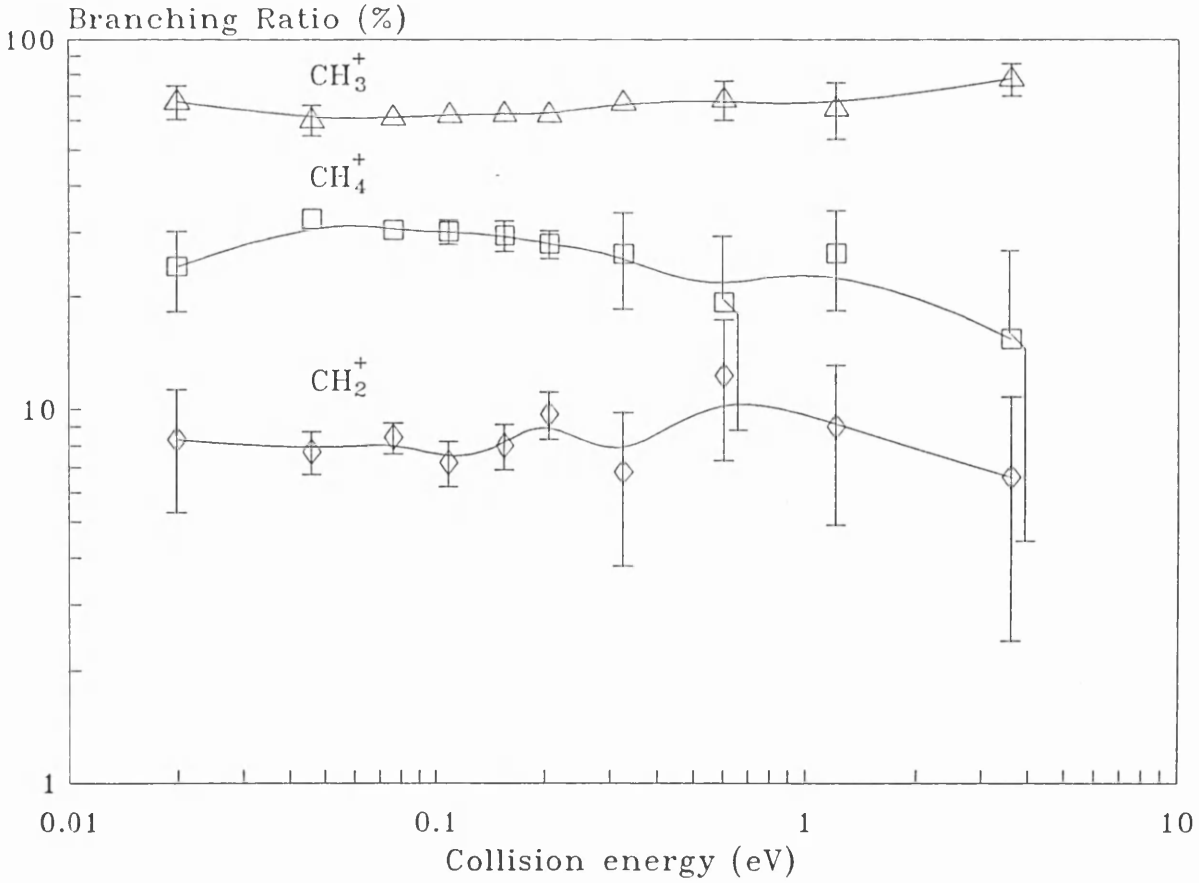

Figure 5.21

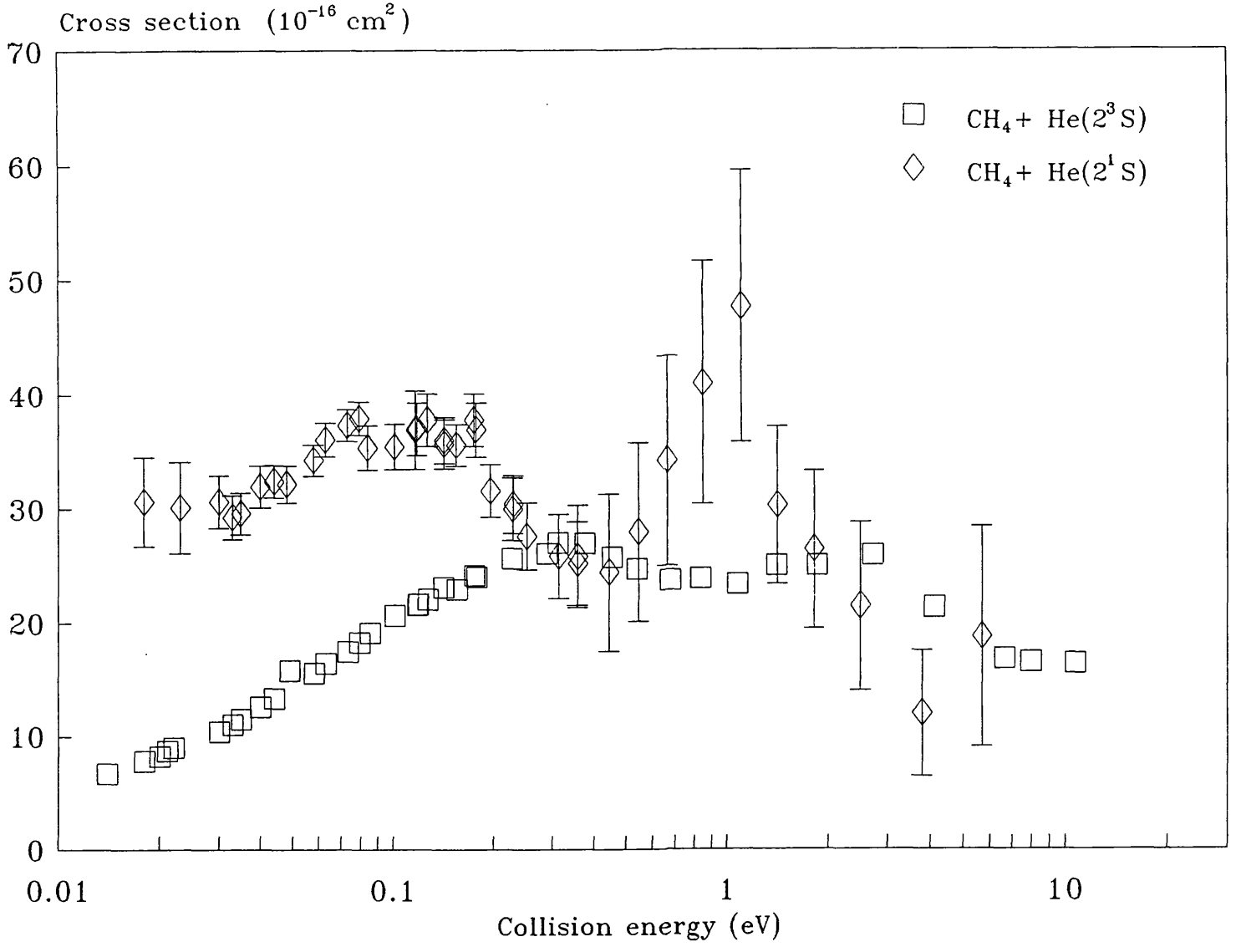
Cross section (10^{-16} cm^2)
70
60
50
40
30
20
10
0
0.01
0.1
1
10
Collision energy (eV)
CH_4 + He(2^3S)
CH_4 + He(2^1S)

Table 5.10 Relative cross sections and branching ratios for C_2H_2 + He(2^3S)

Total cross section

g kms^{-1}	σ(g) $10^{-16}cm^2$	E meV	g kms^{-1}	σ(g) $10^{-16}cm^2$	E meV
1.10	48.6 ± 2.1	0.022	3.75	33.8 ± 0.4	0.257
1.13	48.9 ± 1.6	0.023	4.37	32.4 ± 0.7	0.348
1.26	46.8 ± 0.8	0.029	4.88	32.8 ± 0.6	0.420
1.40	43.0 ± 0.8	0.035	5.63	30.9 ± 0.9	0.578
1.50	40.4 ± 0.3	0.042	5.70	32.3 ± 0.9	0.594
1.62	39.3 ± 0.3	0.049	6.39	30.5 ± 0.7	0.744
1.97	35.9 ± 0.2	0.071	7.10	31.8 ± 0.7	0.918
2.31	33.8 ± 0.3	0.097	8.03	31.0 ± 0.7	1.18
2.50	32.8 ± 0.3	0.114	9.24	31.7 ± 0.6	1.56
2.70	33.1 ± 0.3	0.133	10.6	29.1 ± 0.5	2.06
2.71	32.8 ± 0.3	0.134	12.9	31.5 ± 0.5	3.03
2.81	32.4 ± 0.3	0.149	15.8	26.6 ± 0.3	4.54
2.95	32.4 ± 0.4	0.151	20.1	24.8 ± 0.2	7.88
2.96	32.1 ± 0.3	0.160	21.8	26.6 ± 0.3	8.70
3.09	31.2 ± 0.3	0.174	22.8	25.5 ± 0.3	9.46
3.28	32.4 ± 0.3	0.196	25.4	27.9 ± 0.4	11.8
3.30	32.4 ± 0.3	0.199			

Branching ratios (%)

g kms^{-1}	E meV	$C_2H_2^+$	C_2H^+
1.27	0.029	73.7 ±1.0	26.3 ±0.6
1.73	0.054	71.9 ±0.4	28.1 ±0.5
2.20	0.088	69.6 ±0.4	30.4 ±0.2
2.58	0.120	67.7 ±0.4	32.3 ±0.3
3.67	0.170	66.2 ±0.5	33.9 ±0.4
3.72	0.250	64.4 ±0.7	35.6 ±0.5
4.4	0.350	62.8 ±1.2	37.2 ±1.0
6.0	0.625	57.2 ±1.4	42.8 ±1.2
8.5	1.31	55.3 ±1.2	44.7 ±1.1
14.7	3.92	49.7 ±0.4	50.3 ±0.6

Partial cross sections ($10^{-16}cm^2$)

$\sigma(C_2H_2^+)$	$\sigma(C_2H^+)$
34.5	12.3
33.7	13.1
24.1	10.5
21.9	10.6
21.8	11.2
21.9	12.0
20.3	12.0
18.0	13.4
17.2	14.0
14.0	14.2

Figure 5.22 C_2H_2+ He(2^3S)

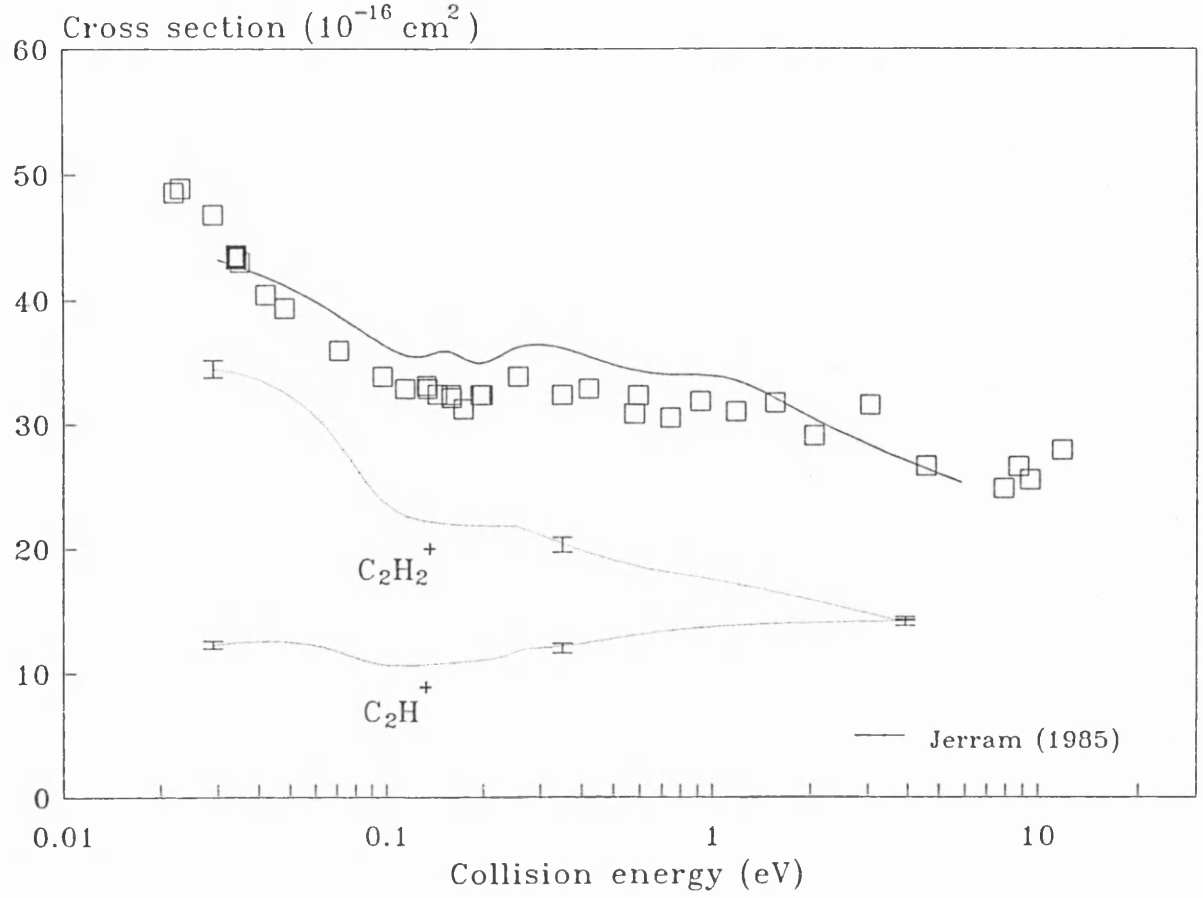

Figure 5.23

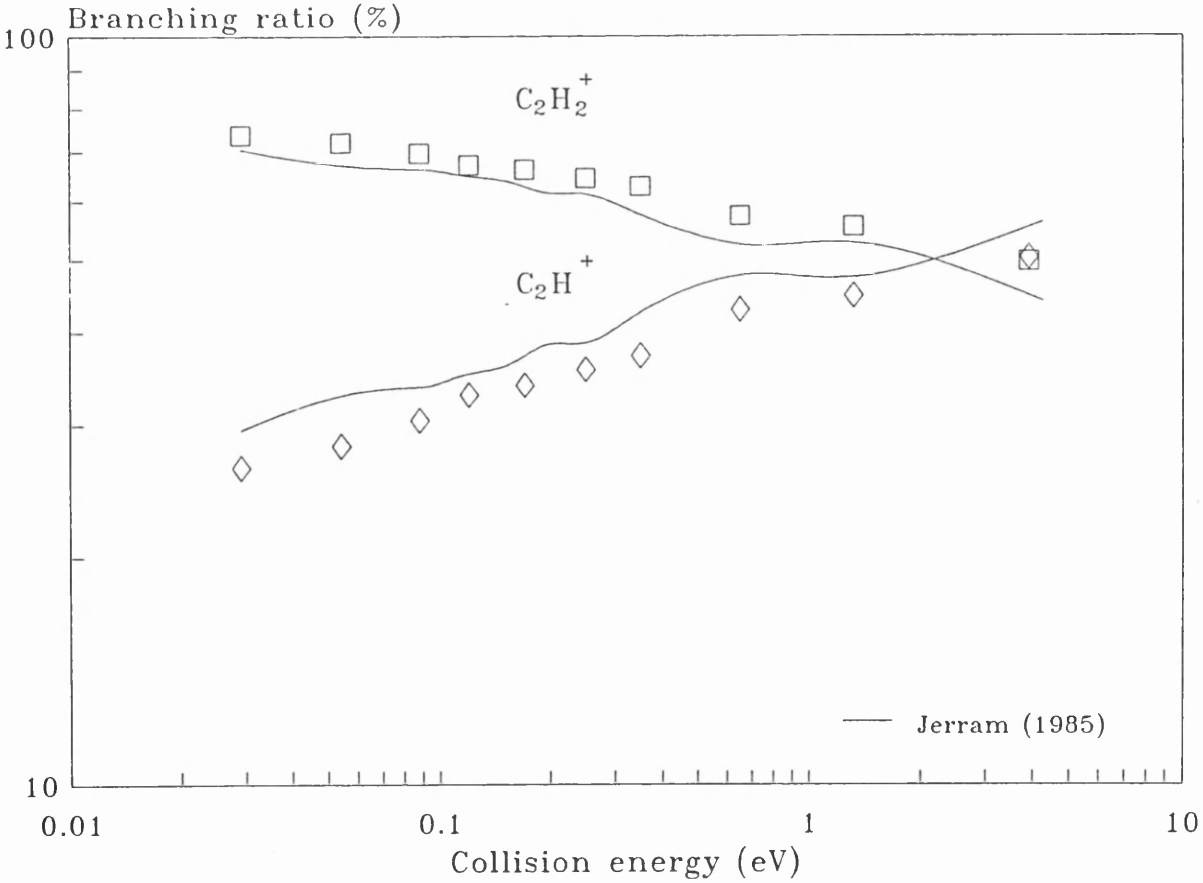

Table 5.11 Relative cross sections and branching ratios for C_2H_2 + He(2^1S)

Total cross section

g kms^{-1}	σ(g) $10^{-16}cm^2$	E meV	g kms^{-1}	σ(g) $10^{-16}cm^2$	E meV
1.26	84.4 ± 21	0.029	3.76	31.1 ± 3.7	0.258
1.42	66.5 ± 11	0.037	3.96	28.7 ± 4.4	0.286
1.43	69.4 ± 11	0.037	3.98	34.2 ± 3.7	0.288
1.46	68.7 ± 3.3	0.039	4.05	34.0 ± 6.3	0.299
1.48	61.7 ± 5.2	0.040	4.18	38.8 ± 6.3	0.319
1.60	61.2 ± 5.8	0.047	4.26	45.1 ± 6.3	0.331
2.01	59.9 ± 3.7	0.074	4.40	47.2 ± 8.4	0.353
2.31	54.7 ± 4.6	0.098	4.67	40.9 ± 9.6	0.398
2.50	49.2 ± 4.0	0.114	4.78	42.3 ± 6.3	0.416
2.70	45.6 ± 4.0	0.133	5.20	29.0 ± 8.9	0.512
2.71	47.3 ± 4.2	0.134	5.75	27.4 ± 9.3	0.565
2.80	45.1 ± 3.8	0.144	6.38	31.2 ± 12	0.745
2.95	50.9 ± 4.2	0.159	7.05	41.0 ± 14	0.907
2.96	51.9 ± 4.2	0.160	8.21	31.0 ± 9.5	1.23
3.10	47.9 ± 3.8	0.175	9.09	24.2 ± 7.9	1.51
3.23	44.5 ± 4.0	0.196	10.7	30.6 ± 11	2.07
3.30	42.1 ± 3.7	0.198	12.5	25.5 ± 10	2.85
3.43	38.0 ± 3.7	0.215	15.9	22.9 ± 8.7	4.58
3.48	37.0 ± 3.6	0.221	17.8	21.1 ± 16	5.81
3.75	29.8 ± 3.1	0.256			

Branching ratios (%)

g (kms^{-1})	E (meV)	$C_2H_2^+$	C_2H^+
1.27	0.029	59.6 ±13	40.4 ±7.6
1.73	0.054	63.2 ±3.4	36.8 ±2.1
2.20	0.088	67.1 ±2.5	32.9 ±1.6
2.58	0.120	69.4 ±2.8	31.6 ±1.9
3.67	0.170	61.4 ±3.3	38.6 ±2.1
3.72	0.250	66.5 ±3.5	33.6 ±2.8
4.4	0.350	54.5 ±8.5	45.5 ±5.3
6.0	0.625	54.9 ±16	45.1 ±14
8.5	1.31	54.2 ±12	45.8 ±11
14.7	3.92	64.3 ±10	35.7 ±5.9

Partial cross sections ($10^{-16}cm^2$)

$\sigma(C_2H_2^+)$	$\sigma(C_2H^+)$
50.2	34.1
38.5	22.4
37.8	18.5
32.9	14.9
28.1	12.3
20.4	10.3
41.2	21.5
15.7	13.1
11.9	10.0
15.3	8.5

Figure 5.24 C_2H_2+ He(2^1S)

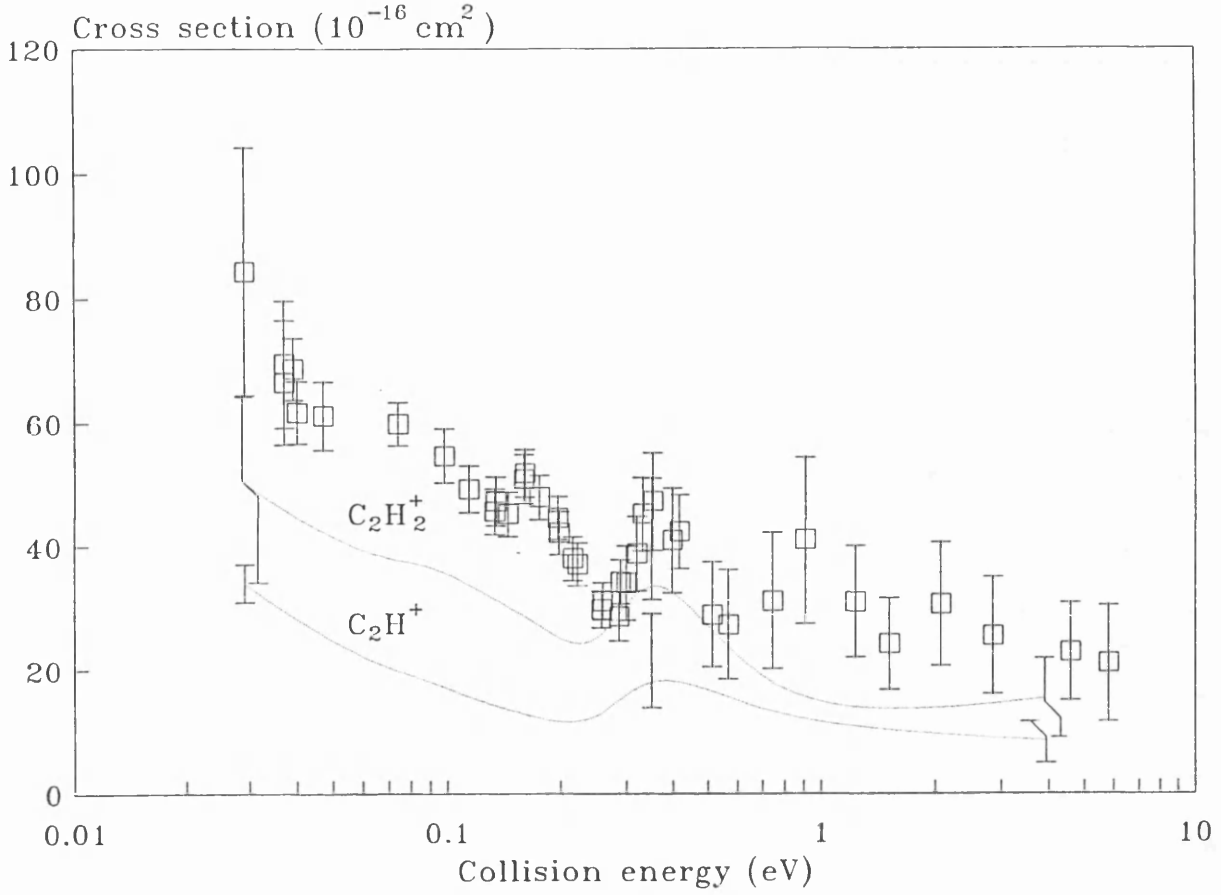

Figure 5.25

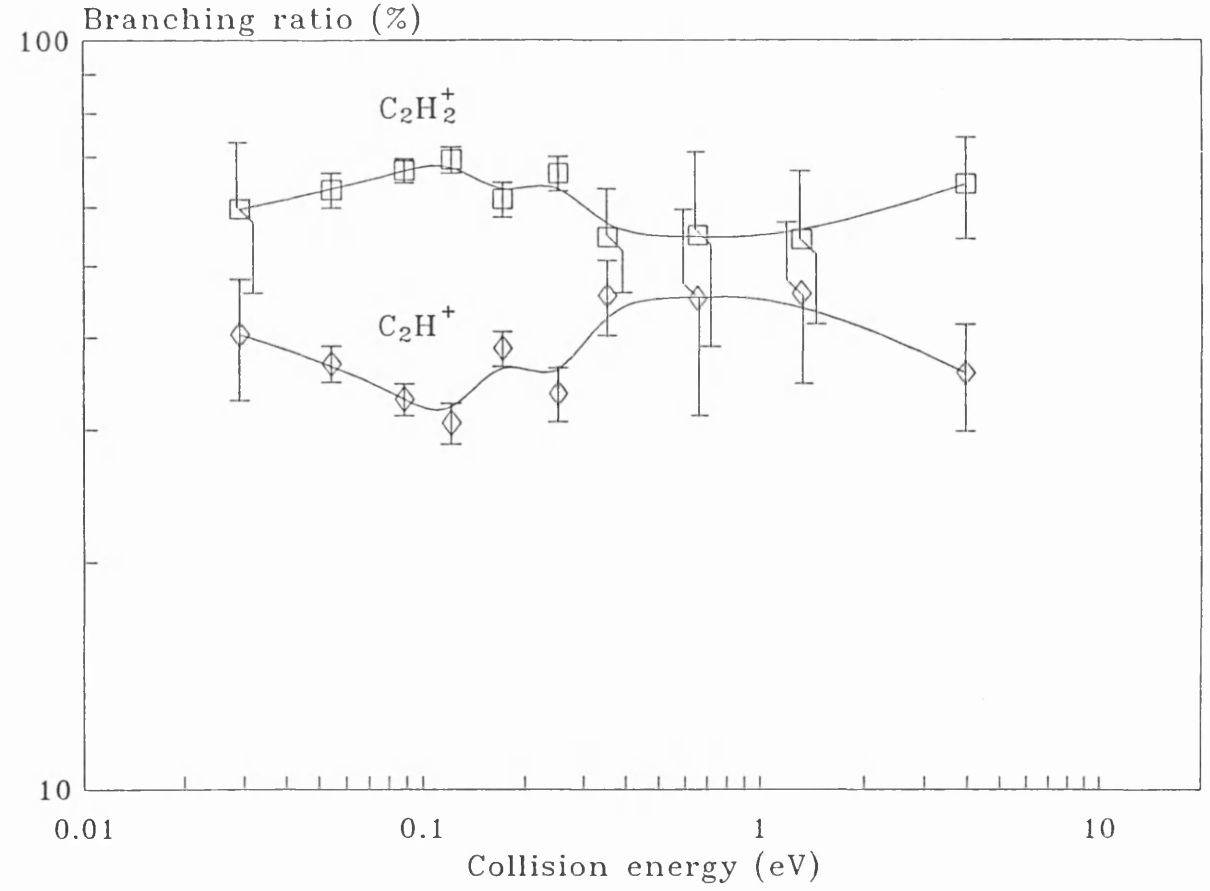

Figure 5.26

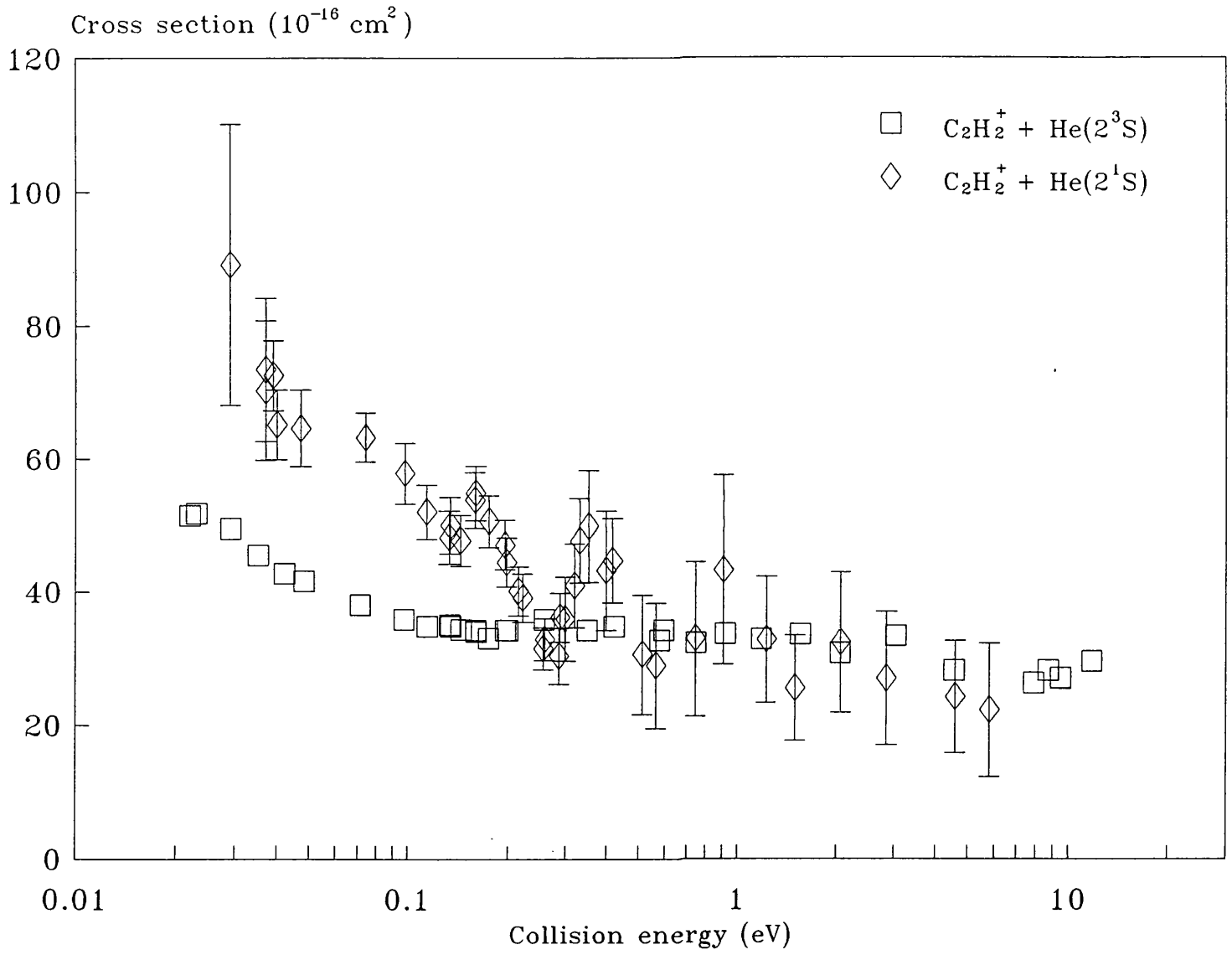
Cross section (10^{-16} cm^2)
120
100
80
60
40
20
0
0.01
0.1
1
10
Collision energy (eV)
$C_2H_2^+$ + He(2^3S)
$C_2H_2^+$ + He(2^1S)

Table 5.12 Relative cross sections and branching ratios for NH_3 + $He(2^3S)$

Total cross section

g	σ(g)	E	g	σ(g)	E
kms^{-1}	$10^{-16}cm^2$	meV	kms^{-1}	$10^{-16}cm^2$	meV
1.22	87.9 ± 2.7	0.025	3.31	44.8 ± 0.4	0.185
1.25	58.1 ± 2.0	0.027	3.34	44.4 ± 0.4	0.189
1.29	80.7 ± 1.5	0.028	3.50	40.7 ± 0.4	0.207
1.34	79.1 ± 1.1	0.030	3.77	41.2 ± 0.5	0.204
1.41	75.0 ± 0.7	0.033	3.80	41.9 ± 0.4	0.245
1.43	74.7 ± 0.9	0.035	3.99	35.3 ± 0.5	0.269
1.49	72.4 ± 0.6	0.037	4.39	36.2 ± 0.7	0.362
1.55	69.7 ± 0.5	0.041	4.72	33.6 ± 0.7	0.377
1.68	67.1 ± 0.1	0.048	4.78	35.1 ± 0.6	0.387
1.75	64.3 ± 0.4	0.052	5.28	33.5 ± 0.9	0.471
1.87	61.3 ± 0.3	0.059	5.75	31.3 ± 0.9	0.559
1.96	58.4 ± 0.3	0.067	6.43	28.5 ± 0.7	0.699
2.06	57.8 ± 0.3	0.072	7.08	27.9 ± 0.6	0.848
2.20	55.1 ± 0.4	0.081	8.03	26.0 ± 0.6	1.09
2.28	54.2 ± 0.4	0.088	9.25	27.1 ± 0.6	1.45
2.35	53.0 ± 0.1	0.093	10.7	24.8 ± 0.5	1.92
2.55	50.3 ± 0.4	0.110	12.9	24.8 ± 0.5	2.80
2.74	49.1 ± 0.3	0.127	15.8	19.5 ± 0.2	4.22
2.75	45.0 ± 0.5	0.128	20.0	16.7 ± 0.2	6.73
2.85	47.2 ± 0.3	0.137	20.1	16.6 ± 0.2	6.83
2.94	46.1 ± 0.3	0.151	23.2	15.0 ± 0.2	9.09
3.00	48.3 ± 0.3	0.152	26.1	15.0 ± 0.2	11.5
3.13	43.9 ± 0.3	0.166	30.5	15.2 ± 0.3	15.8

Branching ratios (%) Partial cross sections ($10^{-16}cm^2$)

g (kms^{-1})	E (meV)	NH_3^+	NH_2^+	NH^+	$\sigma(N_3^+)$	$\sigma(NH_2^+)$	$\sigma(NH^+)$
1.36	0.031	64.6 ±0.9	38.8 ±0.6	0.6 ±0.1	51.1	27.1	0.47
1.79	0.054	64.5 ±0.4	34.9 ±0.3	0.6 ±0.1	40.5	21.9	0.37
2.25	0.085	64.1 ±0.4	35.7 ±0.3	0.6 ±0.1	34.7	19.1	0.32
2.62	0.116	63.2 ±0.4	36.2 ±0.3	0.6 ±0.1	31.2	18.2	0.30
3.11	0.163	62.8 ±0.5	36.5 ±0.4	0.7 ±0.1	27.8	16.1	0.31
3.59	0.218	61.1 ±0.7	38.3 ±0.6	0.6 ±0.1	24.0	15.7	0.24
4.7	0.371	56.5 ±1.4	43.0 ±1.2	0.5 ±0.1	16.6	14.9	0.17
6.0	0.600	55.1 ±1.7	44.0 ±1.6	0.9 ±0.2	16.8	13.4	0.27
8.3	1.16	48.0 ±1.7	51.0 ±1.8	1.0 ±0.2	12.6	13.4	0.24
13.9	3.26	42.7 ±1.5	56.3 ±1.6	1.0 ±0.2	9.9	13.0	0.23

Figure 5.27 NH_3+ $He(2^3S)$

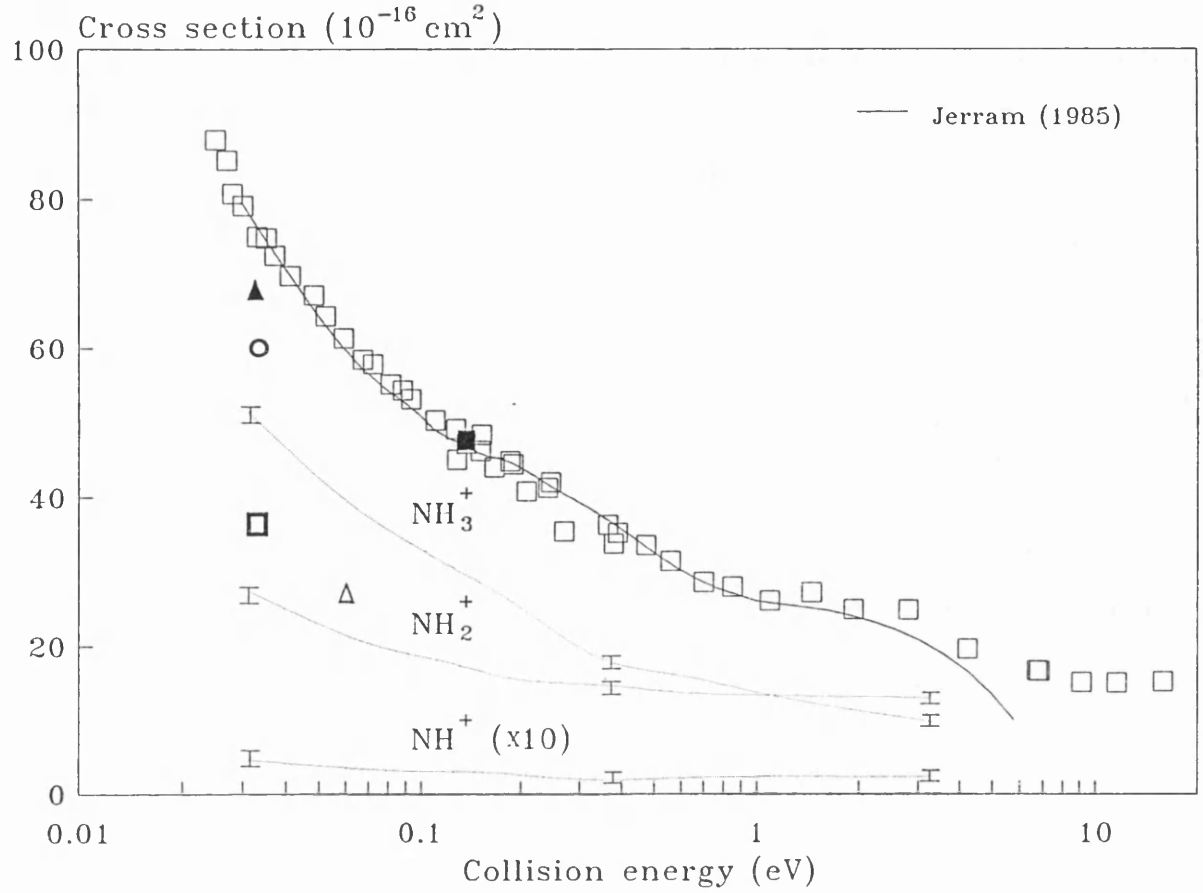

Figure 5.28

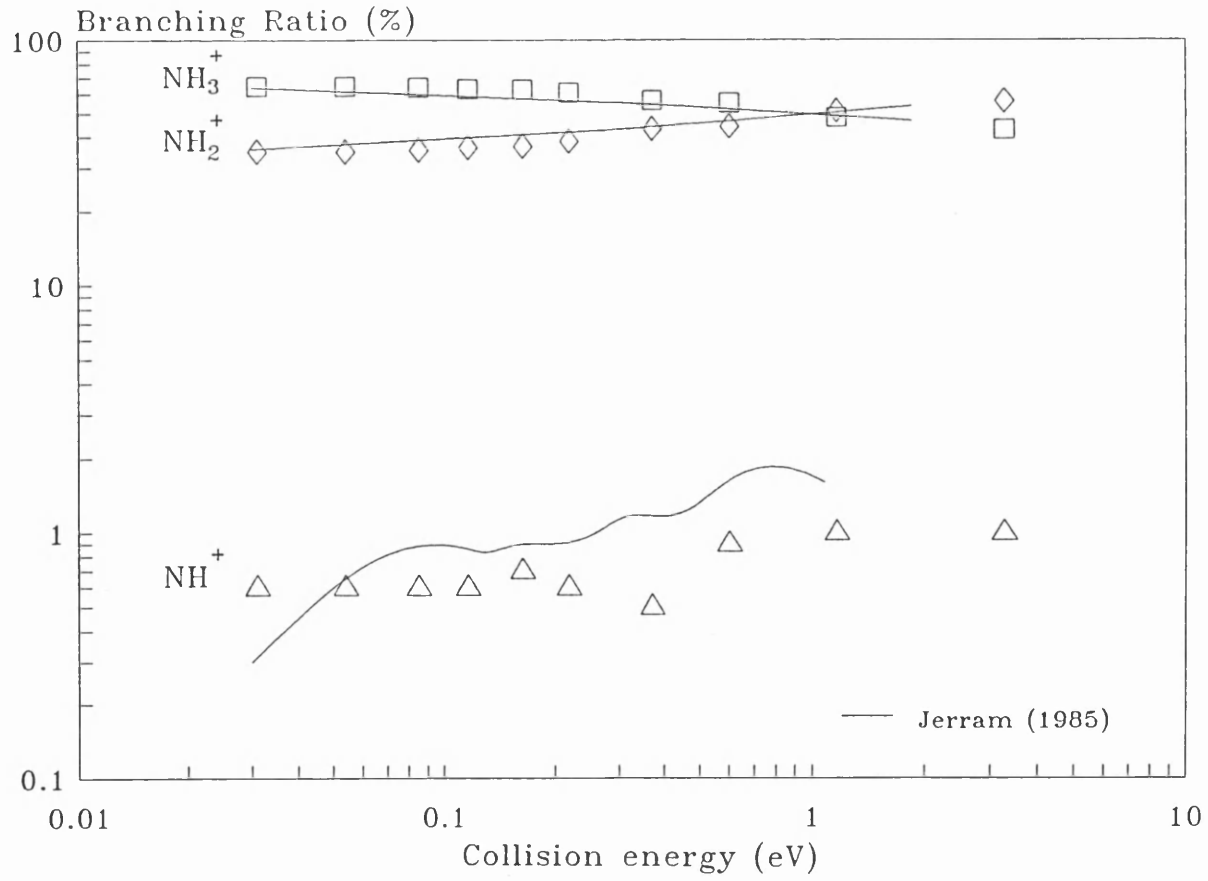

Table 5.13 Relative cross sections and branching ratios for NH_3 + $He(2^1S)$

Total cross section

g kms^{-1}	σ(g) $10^{-16}cm^2$	E meV	g kms^{-1}	σ(g) $10^{-16}cm^2$	E meV
1.34	141 ± 35.0	0.03	3.50	57.8 ± 4.9	0.207
1.45	117 ± 13.2	0.036	3.77	68.4 ± 7.5	0.240
1.22	100 ± 8.8	0.042	3.80	66.7 ± 6.7	0.249
1.75	92 ± 8.8	0.052	3.99	67.0 ± 9.3	0.264
1.83	89.4 ± 8.8	0.057	4.39	62.4 ± 10	0.362
1.90	86.3 ± 8.8	0.061	4.73	51.1 ± 9.3	0.381
1.97	91.7 ± 7.0	0.065	4.79	61.6 ± 9.3	0.387
2.06	80.2 ± 4.0	0.072	5.22	52.3 ± 12	0.461
2.20	75.0 ± 6.7	0.081	5.75	53.3 ± 11	0.554
2.28	73.3 ± 5.7	0.088	6.38	45.4 ± 13	0.688
2.35	79.8 ± 5.3	0.093	7.05	36.4 ± 11	0.840
2.55	76.1 ± 4.0	0.110	8.15	34.3 ± 8.4	1.12
2.74	59.5 ± 4.0	0.127	9.25	26.9 ± 5.8	1.45
2.76	58.5 ± 4.0	0.128	10.3	17.2 ± 5.3	1.80
2.85	63.5 ± 4.0	0.137	12.9	21.5 ± 6.7	2.87
2.98	64.8 ± 4.0	0.151	15.2	29.0 ± 6.6	3.90
2.99	64.8 ± 3.6	0.152	18.2	22.9 ± 8.4	5.62
3.13	57.4 ± 4.9	0.165	19.5	27.5 ± 7.9	6.43
3.32	62.5 ± 4.5	0.186	24.1	19.3 ± 7.8	9.82
3.34	60.6 ± 4.9	0.189	26.5	17.9 ± 8.0	11.9

Branching ratios (%) — Partial cross sections ($10^{-16}cm^2$)

g (kms^{-1})	E (meV)	NH_3^+	NH_2^+	NH^+	$\sigma(N_3^+)$	$\sigma(NH_2^+)$	$\sigma(NH^+)$
1.36	0.031	74.3 ±13.0	25.7 ±9.4		105	36.2	
1.79	0.054	66.2 ±4.4	32.9 ±3.2	0.9 ±0.5	60.5	30.0	0.8
2.25	0.085	67.2 ±3.5	31.9 ±2.5	0.9 ±0.4	39.6	28.3	0.7
2.62	0.116	62.7 ±3.6	29.6 ±2.6	0.7 ±0.4	24.6	20.9	0.5
3.11	0.163	65.2 ±4.2	34.2 ±3.2	0.6 ±0.4	37.4	19.6	0.3
3.59	0.218	70.0 ±5.8	29.4 ±6.2	0.6 ±0.6	42.9	18.0	0.3
4.7	0.371	83.9 ±13	15.9 ±13	0.2 ±1.0	47.8	9.1	0.1
6.0	0.600	77.5 ±27	22 ±14	0.6 ±3.0	39.2	11.1	0.3
8.3	1.16	76.5 ±31	24 ±15		25.6	7.9	
13.9	3.26	88.4 ±24	11.6 ±16		21.5	2.8	

Figure 5.29 NH_3+ He(2^1S)

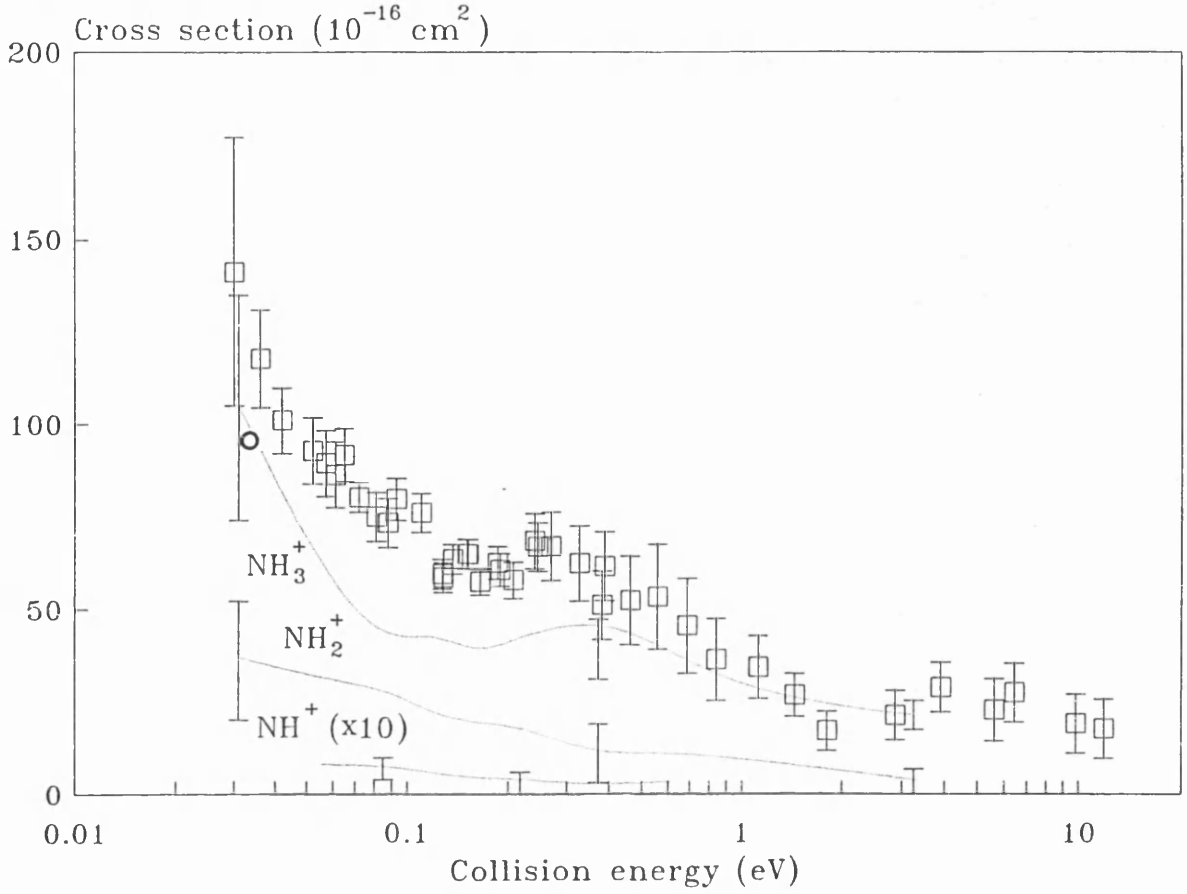

Figure 5.30

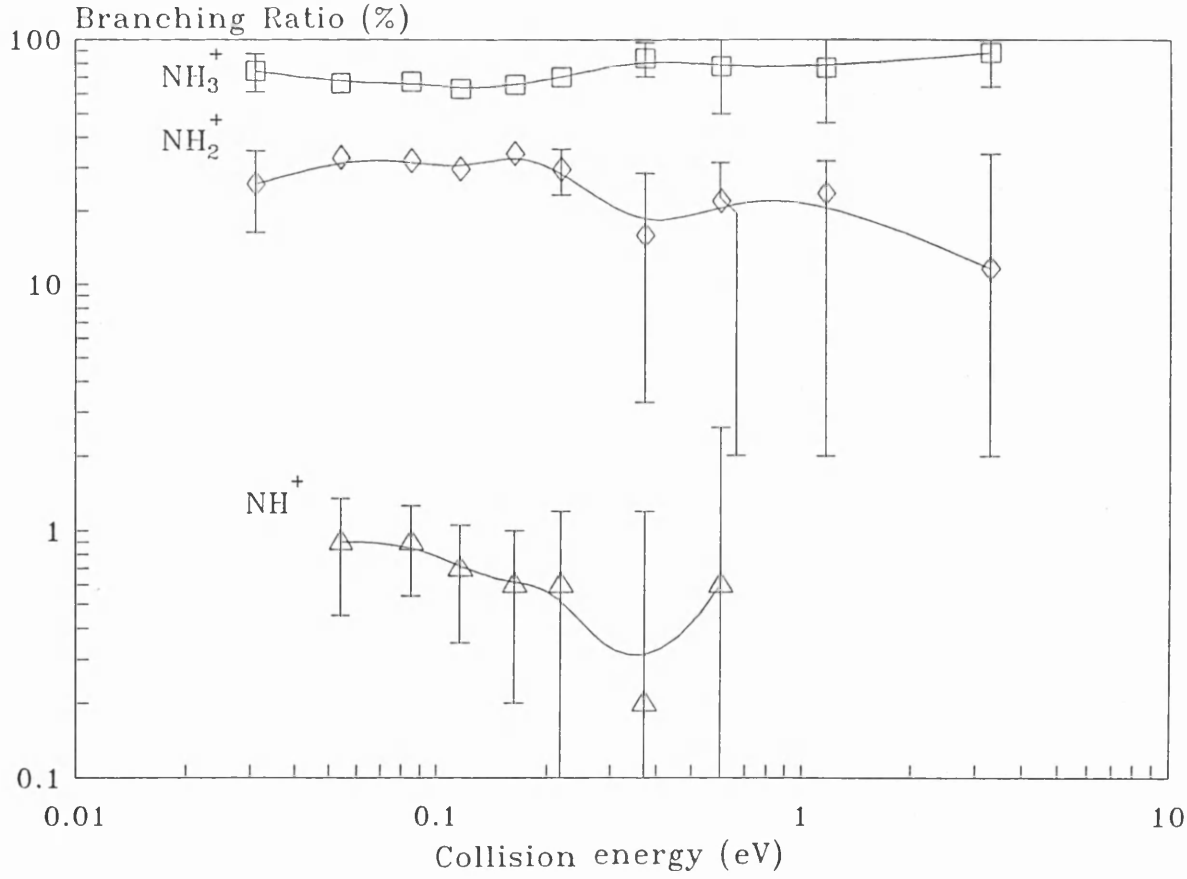

Figure 5.31

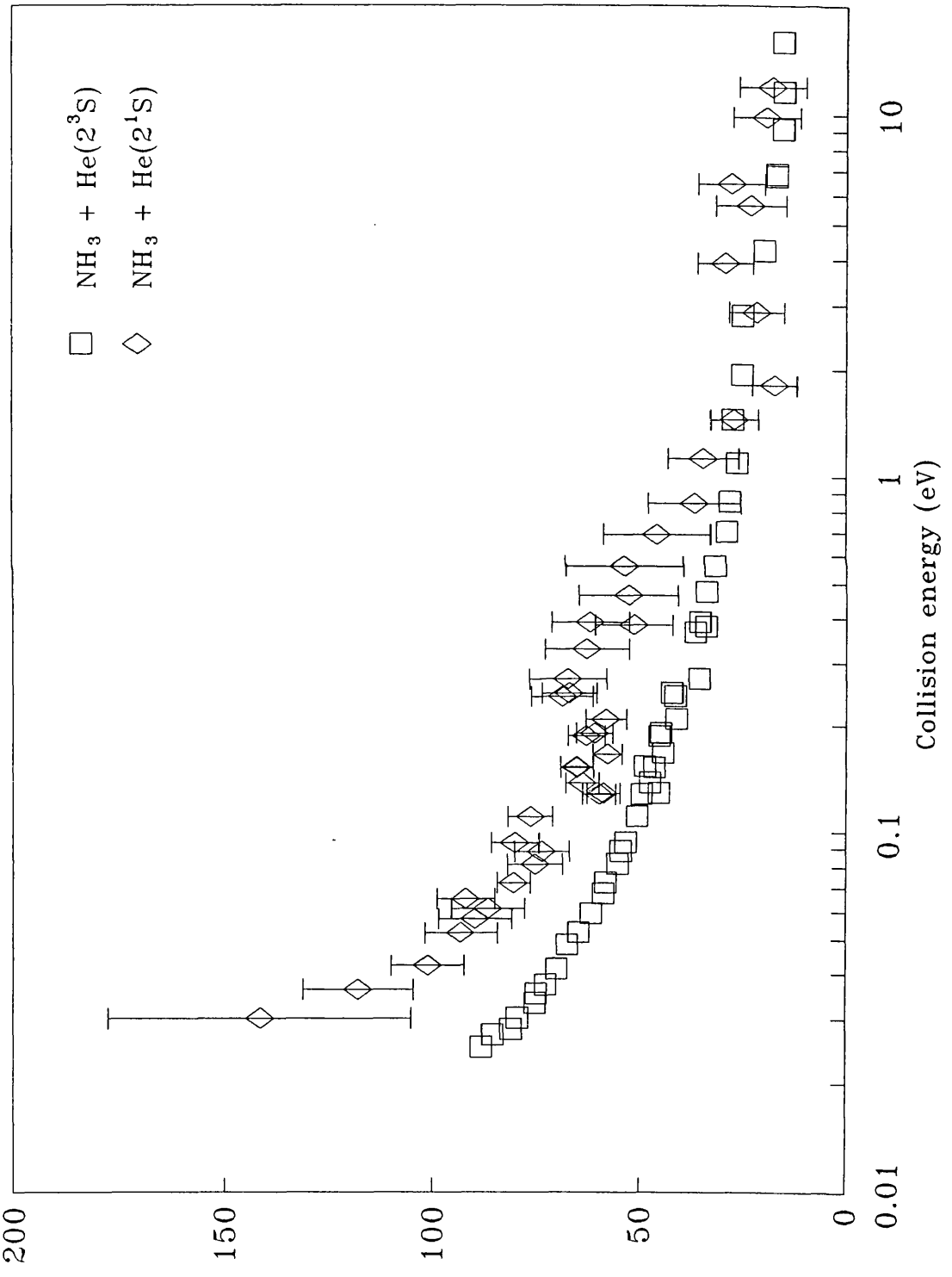
Cross section (10^{-16} cm^2)
200
150
100
50
0
0.01
0.1
1
10
Collision energy (eV)
NH_3 + He(2^3S)
NH_3 + He(2^1S)

Table 5.14 Relative cross sections and branching ratios for SF_6 + $He(2^3S)$

Total cross section

g kms^{-1}	σ(g) $10^{-16}cm^2$	E meV	g kms^{-1}	σ(g) $10^{-16}cm^2$	E meV
0.974	14.8 ± 0.6	0.019	2.88	32.0 ± 0.9	0.169
1.02	15.3 ± 2.0	0.021	2.89	32.8 ± 1.2	0.170
1.06	16.3 ± 1.5	0.023	3.02	31.2 ± 0.9	0.185
1.11	16.5 ± 1.0	0.025	3.21	31.7 ± 0.9	0.209
1.20	16.7 ± 0.5	0.029	3.24	31.8 ± 1.0	0.214
1.24	17.5 ± 0.5	0.031	3.68	33.6 ± 1.4	0.276
1.30	18.0 ± 0.8	0.034	3.91	32.2 ± 2.4	0.311
1.37	18.4 ± 0.8	0.038	4.32	33.4 ± 2.1	0.379
1.42	19.1 ± 0.7	0.041	4.72	33.0 ± 2.0	0.453
1.51	20.9 ± 0.6	0.046	5.20	32.9 ± 3.2	0.550
1.59	21.8 ± 0.8	0.052	5.70	33.4 ± 3.3	0.660
1.67	23.2 ± 0.5	0.057	6.39	38.9 ± 3.4	0.832
1.72	23.7 ± 0.5	0.060	7.11	36.2 ± 2.2	1.03
1.84	24.8 ± 0.5	0.069	8.07	29.6 ± 2.8	1.32
1.92	26.0 ± 0.5	0.075	9.25	31.9 ± 2.2	1.74
2.23	28.5 ± 0.7	0.101	10.7	27.9 ± 1.8	2.32
2.24	29.0 ± 0.7	0.119	12.9	31.3 ± 1.5	3.39
2.62	29.4 ± 0.8	0.140	15.8	31.1 ± 1.0	5.09
2.63	30.3 ± 0.8	0.141	19.9	30.9 ± 0.9	8.03
2.73	30.6 ± 0.8	0.151			

Branching ratios (%) Partial cross sections ($10^{-16}cm^2$)

g (kms^{-1})	E (meV)	SF_6^+	SF_5^+	SF_4^+	$\sigma(SF_6^+)$	$\sigma(SF_5^+)$	$\sigma(SF_4^+)$
1.1	0.024	85.8 ±2.3	9.4 ±0.8	4.9 ±0.6	14.1	1.6	0.8
1.6	0.051	84.4 ±0.7	9.8 ±0.2	5.8 ±0.2	18.4	2.2	1.3
2.1	0.088	83.6 ±0.5	10.0 ±0.2	6.4 ±0.1	22.2	2.6	1.7
2.5	0.125	83.8 ±0.6	9.9 ±0.2	6.3 ±0.2	24.5	2.9	1.8
3.0	0.180	83.1 ±0.6	10.4 ±0.2	6.5 ±0.2	26.2	3.3	2.0
3.5	0.245	82.9 ±0.8	10.3 ±0.3	6.8 ±0.2	26.4	3.3	2.0
4.4	0.387	82.1 ±1.6	10.9 ±0.7	7.0 ±0.5	27.4	3.6	2.1
6.0	0.720	83.5 ±2.5	10.2 ±0.7	6.3 ±0.5	29.5	3.6	2.3
8.5	1.45	82.0 ±1.8	9.7 ±0.6	8.3 ±0.6	27.7	3.2	2.8
14.6	4.26	78.4 ±1.4	10.7 ±0.4	10.9 ±0.4	24.4	3.3	3.4

Figure 5.32 SF_6 + $He(2^3S)$

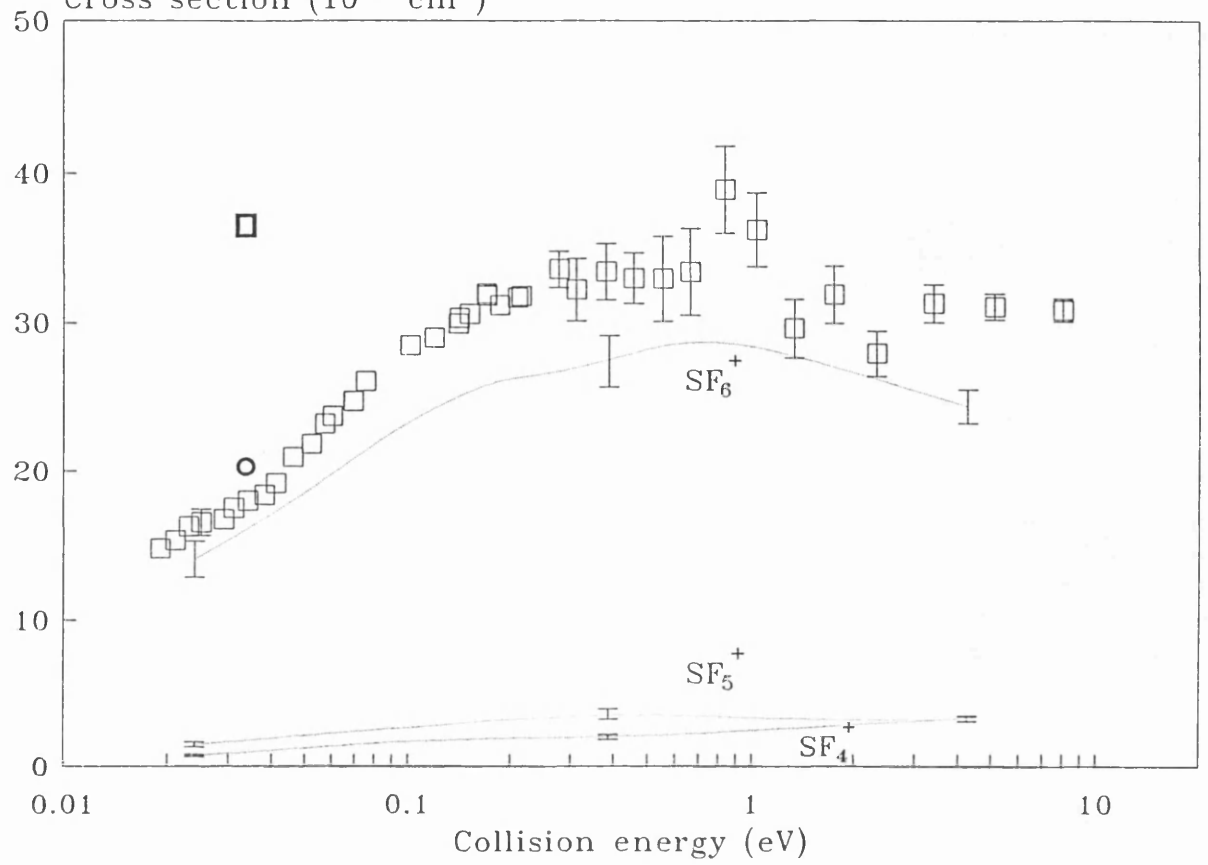

Figure 5.33

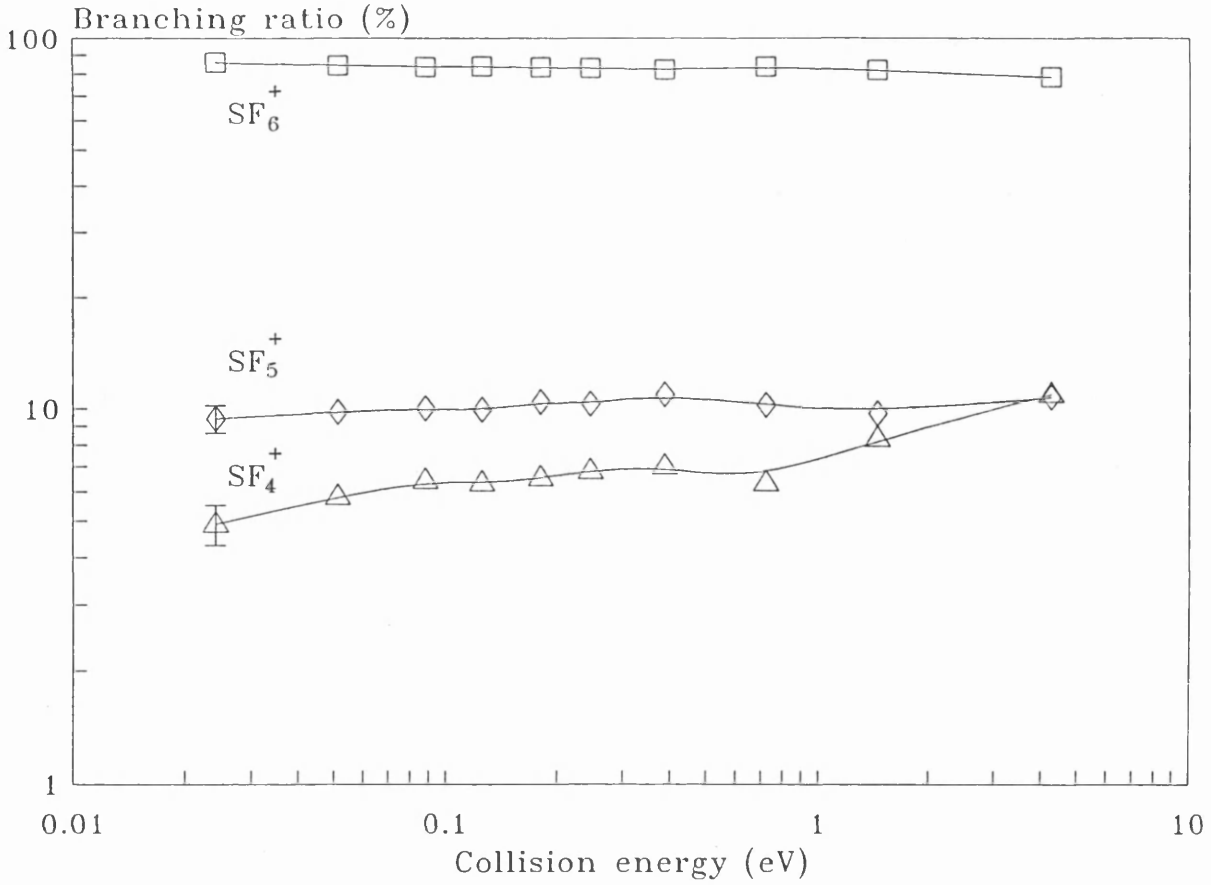

Table 5.15

Comparison of present branching ratios with other data

Collisions with $He(2^3S)$

Ion branch	Present work	Jerram (1985)	Allison (1978)	West et al (1975)	Hotop et al (1969)	Hotop et al (1979)	Herce et al (1968a/b)
			0.06eV	0.066eV	0.035eV	0.173eV	0.046eV
	0.031eV	0.023					
Ar^+	76.2	79.7	77	88	86.6		87_a
ArHe+	23.8	20.3	23	12	13.4		13_a
	0.036eV	0.027eV					
CO_2^+	65.4	63.7	69.5	69	70		
CO^+	5.0	5.4	5.2	4.5	11		
O^+	29.6	30.8	25.3	27	19		
	0.051eV						
N_2O^+	50.5			47		58.8	
NO^+	38.6			51		31.8	
N_2^+	8.5			0		6.8	
N^+	0.2			0		0.1	
O^+	2.3			2.4		2.5	
HeO^+	0			0.4		0	
	0.02eV	0.027eV					
CH_4^+	51.8	50.5	41		49		46.7_b
CH_3^+	44.4	45.3	53		47		49.1_b
CH_2^+	3.8	3.8	6		5		42_b
	0.021eV	0.029eV					
$C_2H_2^+$	73.7	67.9			72		
C_2H^+	26.3	32.1			28		

Table 5.16

Comparison of present branching ratios with other data

Collisions with $He(2^1S)$

Ion branch	Present work	Allison (1978)	West et al (1975)	Hotop et al (1969)	Herce et al (1968a/b)
		0.06eV	0.066eV	0.035eV	0.046eV
	0.024eV				
Ar^+	57.4	97	96	83	91_a
ArHe+	42.6	3	4	17	9_a
	0.034eV				
CO_2^+	73.3	63.6	68	70	
CO^+	12.9	12.2	9	11	
O^+	11.8	24.3	23	19	
	0.051eV				
N_2O^+	31.0		31		
NO^+	51.5		61		
N_2^+	10.8		0		
N^+	2.7		0		
O^+	4.0		7		
HeO^+	0		1		
	0.02eV				
CH_4^+	24.2	30		34	37.9_b
CH_3^+	67.5	59		58	56.7_b
CH_2^+	8.3	11		7	5.4_b
	0.029eV				
$C_2H_2^+$	73.7			68	
C_2H^+	26.3			32	

Chapter 6

Comparison of theoretical and experimental results for collisions of $He(2^3S)$ and $He(2^1S)$ with Ar

6.1 Introduction

In this section experimental measurements of the total ionisation cross sections for Ar by $He(2^3S)$ and $He(2^1S)$, are compared with theoretical results calculated from model interaction potentials.

The first potential developed to describe the interaction of He^* and Ar was devised by Olsen (1972). It is a simple interaction potential, the real part of which (Figure 6.1) is defined at all separations R by a single expression (Appendix 12), which is a modified form of the $Ar + He^+$ potential of Smith et al (1967). The simple form of the Olsen potential makes it relatively easy to convert into a computer subroutine which is also readily adaptable between the singlet and triplet cases. The Olsen potential has been employed by several experimenters and is used here to make a comparison with the later more sophisticated potentials.

The imaginary part of the potential is given by Olsen as a simple exponential.

$$\Gamma(R) = e^{-BR} \tag{6.1}$$

However, a more adaptable exponential form given by

$$\Gamma(R) = Ae^{-BR} \tag{6.2}$$

has been used by Illenberger and Niehaus (1975), Pesnelle et al (1974), Woodard et al (1978) and Jerram (1985) to fit experimental results more closely. In Equation 6.1 and Equation 6.2 A and B are constants chosen to give the best fit to the experimental results and Γ is the imaginary part or coupling width of the optical potential. Olsen's form of coupling width was chosen with the minimum number of parameters which would give a theoretical cross section that fitted the limited experimental results available at the time.

Equation 6.2 has been used in this work.

The Freiburg group (Brutschy et al 1976 (triplets) and Haberland and Schmidt al 1977 (singlets)) have performed high resolution differential cross section experiments on argon with both singlet and triplet helium metastable species (Figures 6.1 and 6.5). They have devised several interaction potentials which deserve analysis. As with Olsen the short range repulsion is represented by a shielded Coulomb potential. However, the potential is not defined by a single expression but by several expressions each in a different region, that is to say it varies in a piece-wise continuous fashion (Appendices 13 and 14). The Coulomb potential is interpolated by means of an exponential spline function to a Morse potential in the case of the triplet interaction (Brutschy et al 1976), and by a double Morse potential in the case of the singlet potential (Haberland and Schmidt 1977). This is in turn interpolated to a Van der Waals potential by a cubic spline function. The potentials are considerably different from the Olsen potential at small separations. Again, Equation 6.2 is used to describe the coupling widths.

The Pittsburg group (Siska 1979 (triplets) and Martin et al 1978 (singlets)) have performed differential cross section measurements on both singlet and triplet metastable states and have devised their own interaction potentials (Appendices 15 and 16). They use a third method to describe the functional form of the interaction potential, which they refer to as Ion-Atom-Morse-Morse-Spline-Van der Waals (IAMMSV). Two piece-wise functions describe the interaction, one at small separations and the other at large separations. The transition between the two functions is provided by a switching function which allows a smooth change to take place. Once again Equation 6.2 is used to represent the coupling width.

The work of the Pittsburg group took place after the work of the Freiburg group. In both singlet and triplet cases a better velocity resolution for their differential cross section measurements is claimed and the work shows smaller experimental errors. There is close agreement between the triplet potentials of Siska (Pittsburg group 1979) and Brutschy et al (Freiburg group 1976) (Figure 6.1), but less good agreement between the singlet potentials (Figure 6.5). Martin et al (1978) have used a local gradient maximum in the real part of their potential (Figure 6.5) in order to produce the so-called rainbow effect in their differential cross sections. Haberland and Schmidt (Freiburg 1977) have introduced a minimum in the real part of their potential in order to produce the same effect (Figure 6.5).

Where possible all three potentials are used to calculate the theoretical cross sections described in section 6.3.

6.2 Fitting Procedure

Equation 2.17 is used as the basis of the calculations made in this chapter. However, there is a problem in the expression derived by Miller (1970) because the integral is defined as being from R_0 to infinity. R_0 is defined as the point at which $V_0 = 0$ and therefore the integral is infinite for all l. This gives the meaningless result that all $P_l = 1$. In order to resolve this, a substitution is made which makes $R = R_0 \sec(\theta)$ to give

$$P_l(R) = P_l(\theta) = 1 - \exp\left[-2\int_0^{\frac{\pi}{2}} \frac{\Gamma(\theta)}{\hbar v_l(\theta)} R_0 \sec(\theta)\tan(\theta)\, d\theta\right] \qquad (6.3)$$

in which as R tends to R_0 θ tends to 0 and so the tendency of v_0 to go to 0 is countered by the $\sec(\theta)\tan(\theta)$ term in the numerator (Equation 6.3), which also tends to zero. As a result the equation no longer tends to infinity and can be used for calculation. The theoretical ionisation cross section has been calculated for nine velocities (from 1 - 20 km/s) and the value of χ^2 calculated from

$$X^2 = \frac{1}{N-n}\sum_N \left| \frac{\sigma_{calc} - \sigma_{exp}}{\Delta\sigma_{exp}} \right|^2 \qquad (6.4)$$

In the cases where one or more parameters have been varied to find the best fit, i.e. the lowest value of χ^2, the method of Marquand (Bevington 1969) has been used. The computer programs used to perform the analysis were written in Fortran 77 and run on a Dell PC AT computer. They are described in Appendices 17 and 18.

6.3 Comparison of theoretical and experimental results for $He(2^3S)$ + Ar

To examine the fit of the Olsen curve to the present data over the whole velocity range it is reasonable to adjust the parameters A and B in Equation 6.2, as has been described above. Olsen chose the value of B (using Equation 6.1) which best fitted his theoretical cross section calculations to the limited total ionisation cross section data which was

Figure 6.1 Interaction potentials for Ar + He(2^3S)

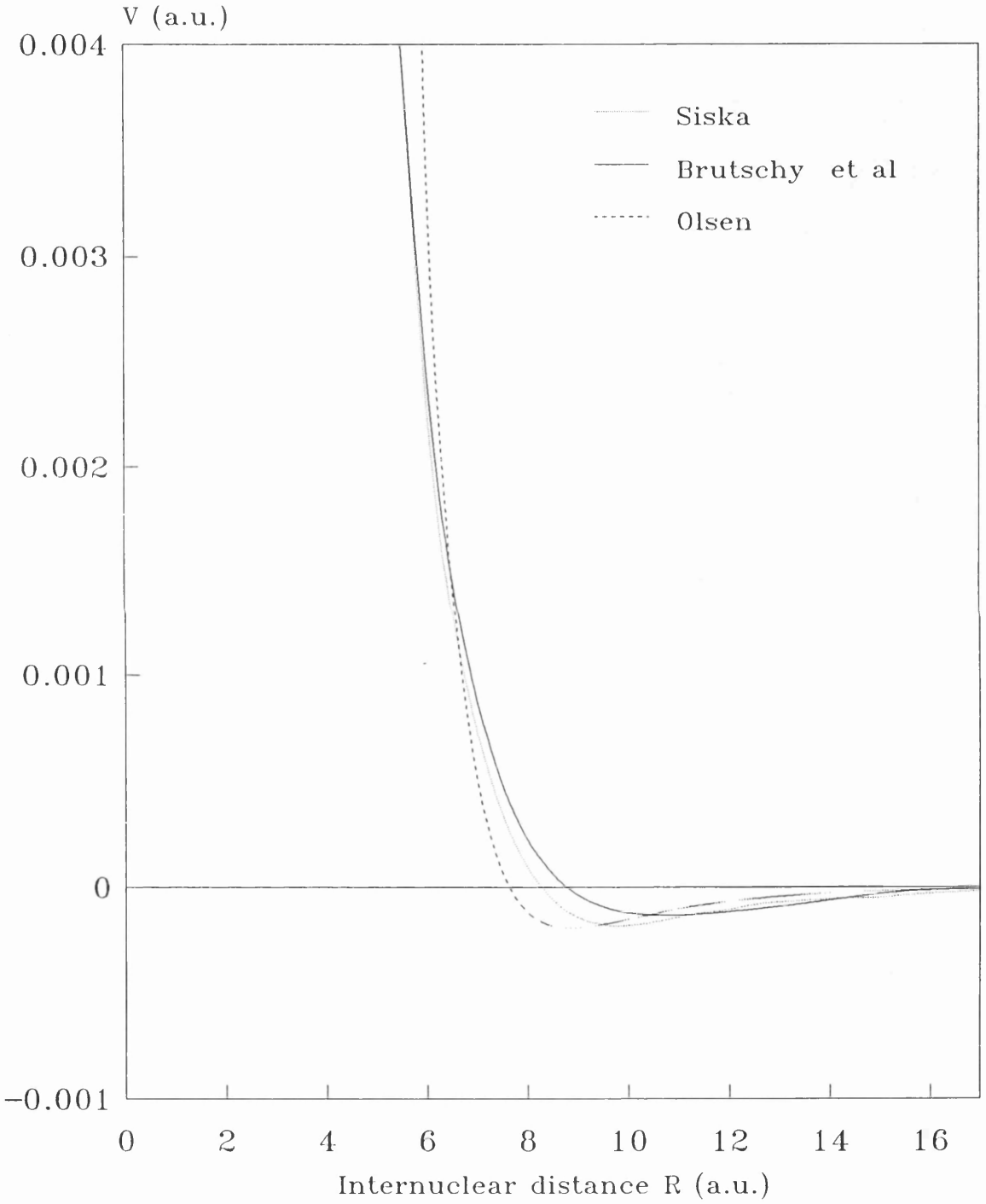

Figure 6.2 Coupling width Γ for Ar + He(2^3S)

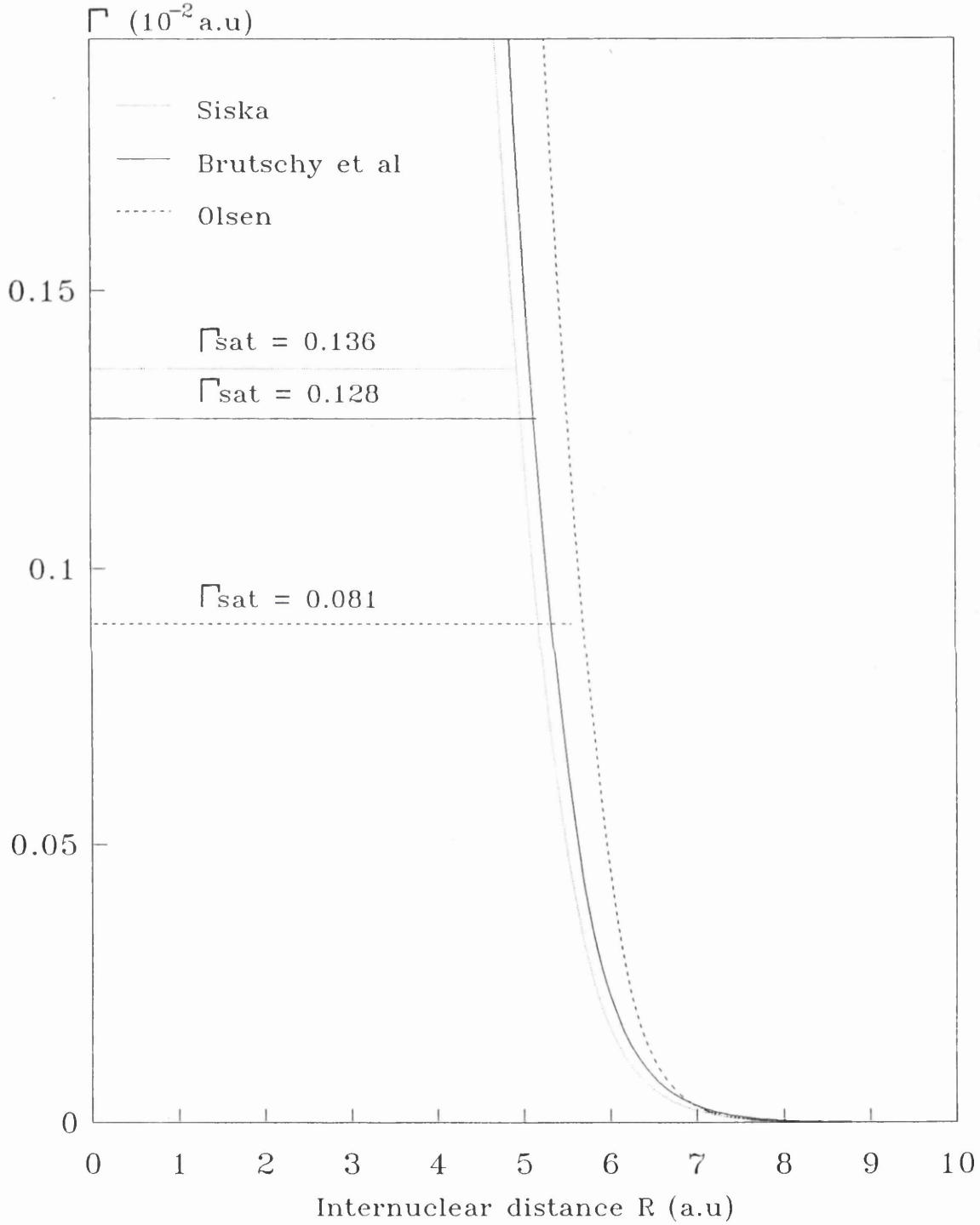

available at the time; i.e. at low energy to the absolute measurements of Schmeltekopf and Fehsenfeld (1970) at 0.03 eV, and at high energy to the data of Mosely et al (1972) from 100 - 1000 eV. However, the data of Mosely et al is now thought to be outside the range of validity of the theoretical treatment used in the present work. The best values of A and B were calculated using the program CRS (Appendix 17) to fit the data over the whole velocity range using nine data points. However, the fit was very poor with a value of χ^2 over 100. The procedure was repeated but for only the low velocity data below 4Km/s. The best values of A and B were determined and Γ is plotted in Figure 6.2. The fit is now good with χ^2 equal to 3.7 over the fitted range. The calculated cross section is plotted in Figure 6.3 over the complete velocity range. Clearly the Olsen potential (the combination of real and imaginary parts) represents the low velocity interactions well. These interactions are at relatively large internuclear separation ($R > 4$ a.u.).

The Siska and Brutschy et al potentials (Figure 6.1 and 6.2) are more closely defined than that of the Olsen potential because they have been designed to fit differential cross section measurements. This does not allow any variation of A and B without causing a distortion of the theoretical differential cross sections to take place. The aim of this analysis has therefore been to calculate the ionisation cross sections from the theoretical potentials of these two groups as given by them in their papers. Unfortunately the value of A given by Brutschy et al does not reproduce the theoretical ionisation cross section shown in their paper. The value of A has therefore been varied to find the best fit to this theoretical cross section. An exact fit has been achieved indicating that the value of A calculated here is in fact the one used by Brutschy and the value quoted in their paper is incorrect.

Figure 6.3 shows the calculated cross sections using both the Brutschy et al and Siska potentials. Clearly both potentials give a better fit to the present experimental results at low velocity than at high velocity, as with the Olsen potential, but the Siska potential gives the better agreement of the two. Once again the cross sections are too large at high velocity, though not to the same extent as the cross section calculated from the Olsen potential. In order to obtain a better fit to the experimental data a modification to Γ has been used which was proposed first by Nakamura (1975). The modification consists of a saturation of Γ at small separation, given by

$$\Gamma(R) = Aexp(-BR) \quad for\ R > Rsat$$

$$\Gamma(R) = Aexp(-BRsat) \quad for\ R \leq Rsat \qquad (6.5)$$

Figure 6.3 Theoretical cross sections calculated using interaction potentials for the Ar+He(2^3S) system and compared with the present experimental results

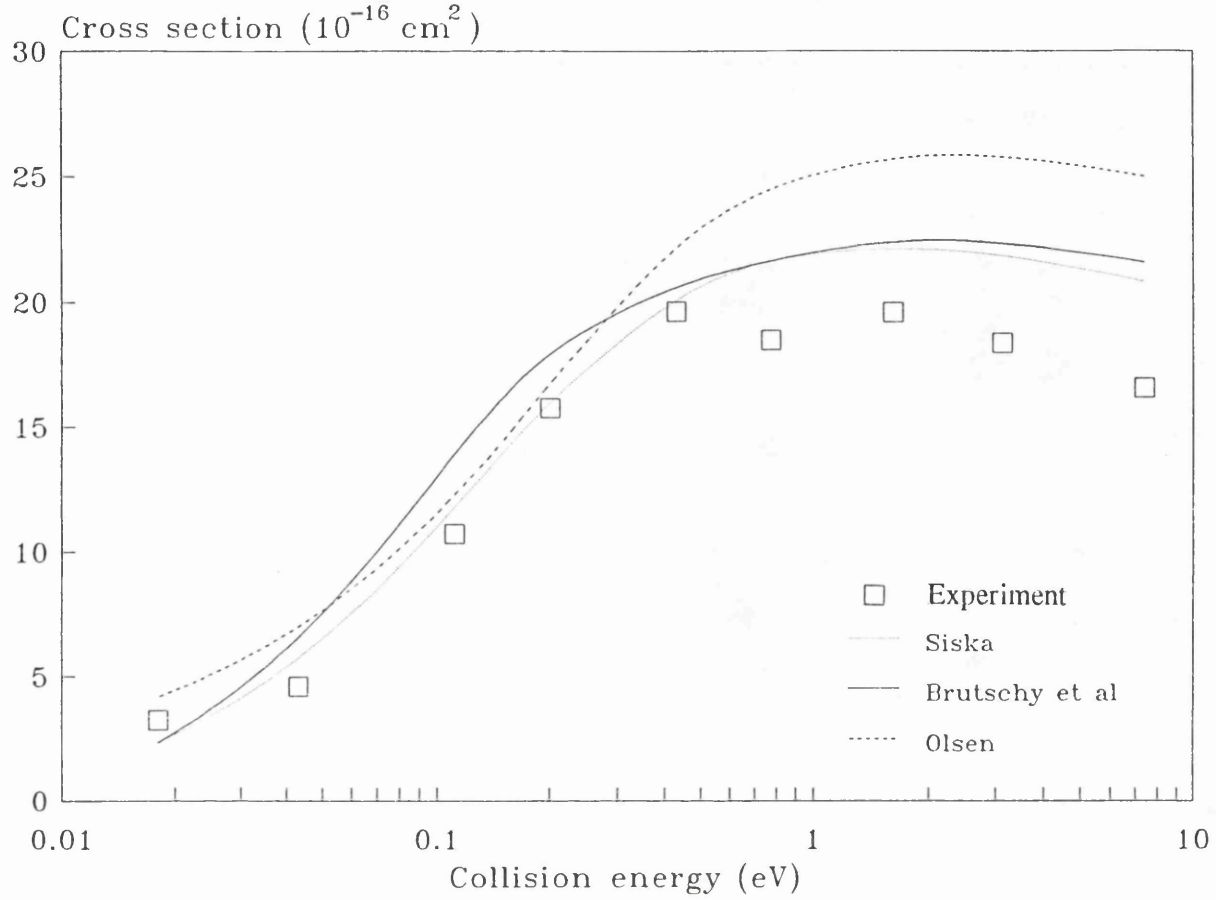

Figure 6.4 Theoretical cross sections calculated with a saturating form of Γ the imaginary part of the Ar+He(2^3S) interaction potential

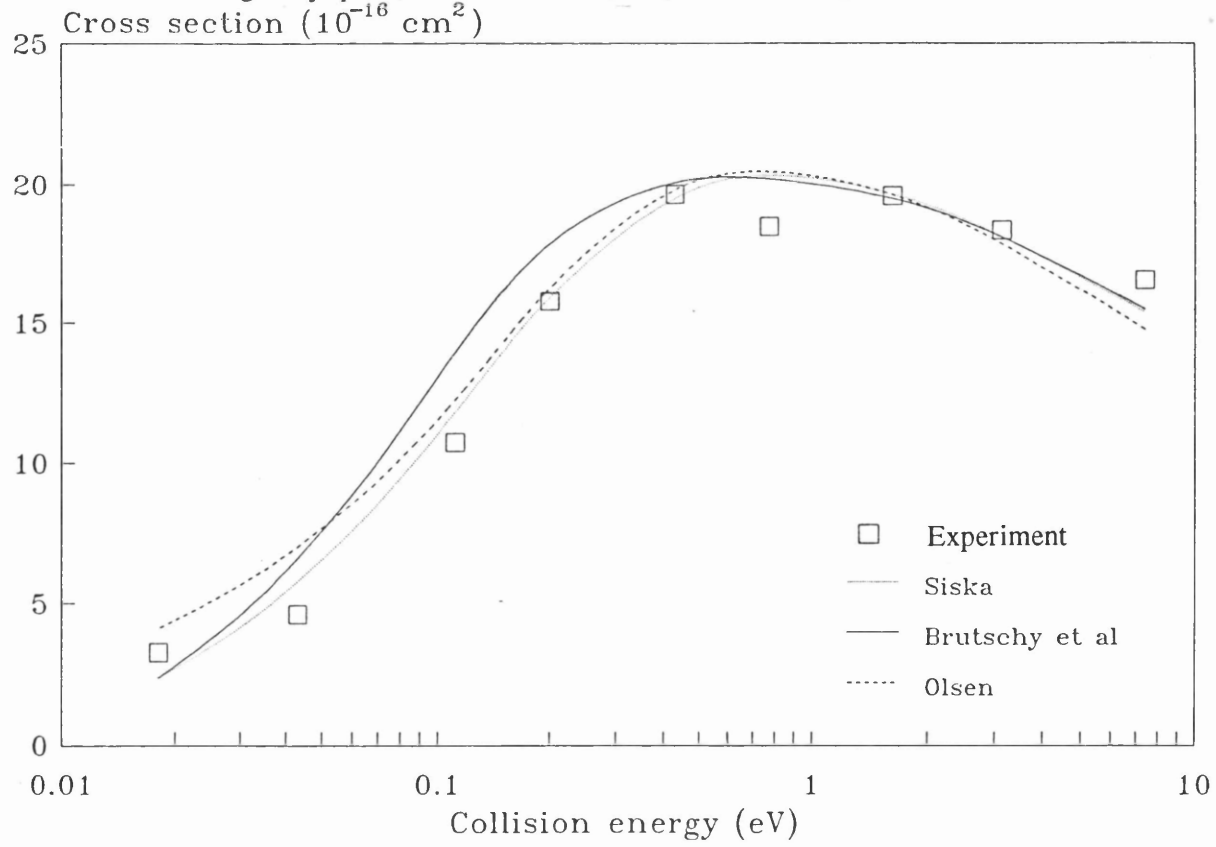

and supported by the calculations of Miller et al (1972) and Bieniek (1978) which show a maximum in Γ at internuclear separation between R=2 a.u. and R=8 a.u. for the He(2^3S) + H reaction. This saturation in Γ has been used by Kroon (1985) and Jerram (1985) to explain the high velocity decline in their triplet cross sections. The form of Γ suggested is given in equation 6.3. Kroon (1985) has also introduced a form in which Γ decreases for small R, but this has not been used here as it is considered over-elaborate.

The new form of Γ has been used to calculate the total ionisation cross section using the Olsen potential with the values of A and B calculated above. The fitting procedure has been used to find the best value of Rsat (5.62 a.u.). The resulting cross section is shown in figure 6.4 along with the cross sections calculated in the same way for the Siska and Brutschy potentials, using the A and B values given in their work. It is clear from figure 6.4 that a much better fit is now possible for all the potentials. The Brutschy et al potential gives a cross section in the middle velocities somewhat higher than the other two and the Olsen potential is high at the lowest velocities. Only the Siska potential is in very close agreement over the complete velocity range (although even this potential cannot produce the slight dip in the cross section at 0.8 eV). The value of Rsat determined for the Siska potential is the lowest for the three potentials Rsat = 4.9 a.u. (Γsat = 1.36×10^{-3} a.u.) compared to Rsat=5.06 a.u. for Brutschy et al (Γsat = 1.28×10^{-3} a.u.) and Rsat = 5.62 a.u. for Olsen (Γsat = 0.87×10^{-3} a.u.). This is very important because collisions which penetrate to small R result in large-angle differential scattering. The high-energy large-angle differential cross section calculations made using the Siska and Brutschy et al potentials will be distorted if Rsat is too large. Such measurements have been made by Brutschy et al at energies as high as 0.48 meV and 0.245 meV, for which collisions may approach R = 4.5 a.u. and R = 4.9 a.u. respectively, using a classical calculation and the interaction potential of Brutschy et al. The theoretical differential cross sections calculated at large angle for these energies are boosted by the reduction in Γ(R) to the extent that they lie above the experimental data and do not fall within the error bars. This means that none of the potentials can satisfactorily represent both differential and ionisation cross sections at the higher energies. What may be stated is that the saturation needed to make the Siska potential fit the experimental results is slightly less distorting to differential cross section calculations than that for the Brutschy et al potential. The Olsen potential is known to give a poor fit to differential cross section data even without a saturating Γ.

Figure 6.5 Interaction potentials for Ar + He(2^1S)

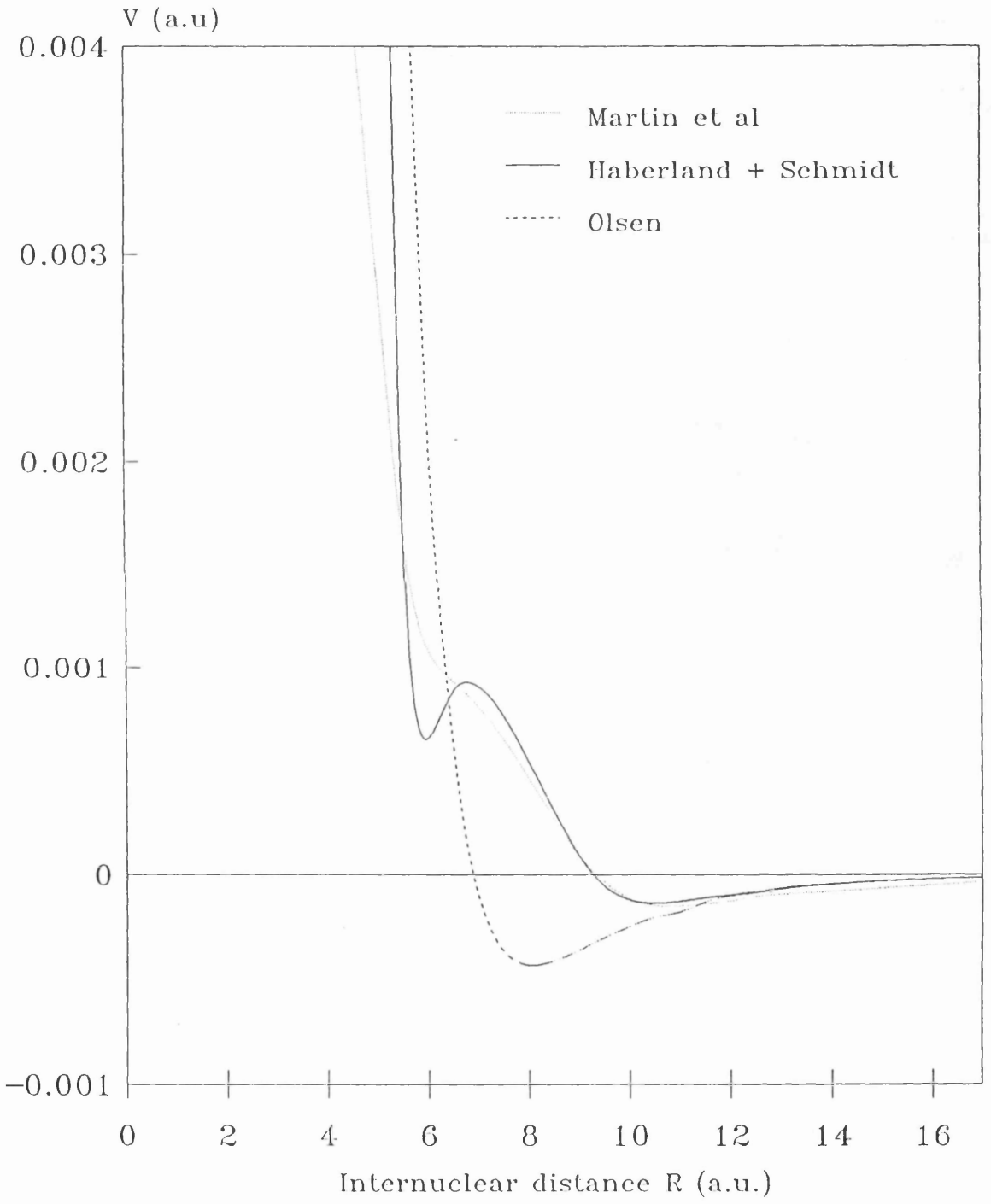

Figure 6.6 Coupling width Γ for Ar + He(2^1S)

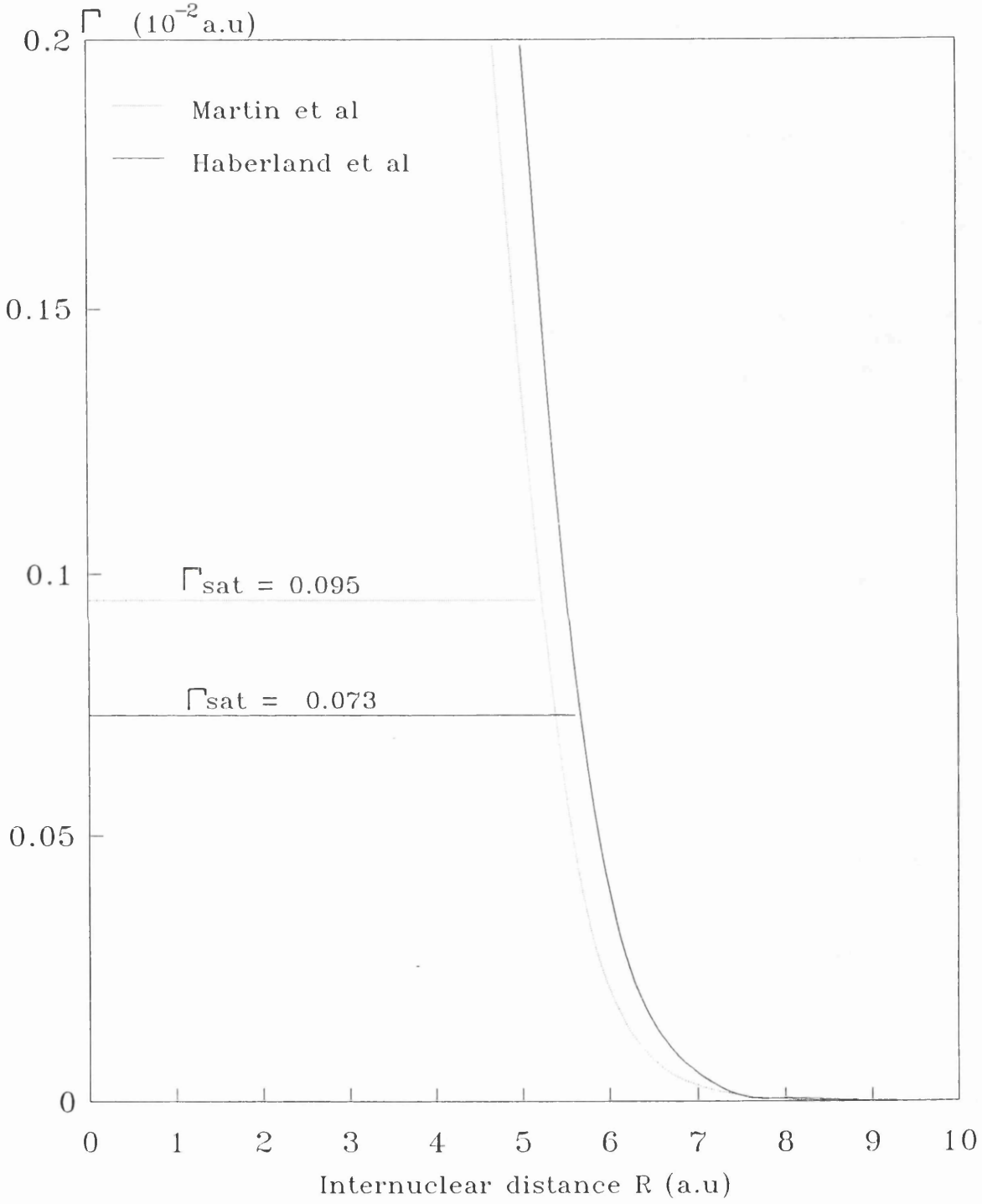

6.4 Comparison of theoretical and experimental results for $He(2^1S)$ + Ar

An attempt has been made to find the best values of the parameters A and B in the imaginary part of the Olsen potential to fit the experimental results at low velocity, as was done successfully with the triplet potential. However in this case it is not possible to get a good fit. The real part of the potential will only allow a gently sloping rise in the ionisation cross section (Figure 6.7) similar to that found in the triplet case. Because of this no theoretical cross sections calculated from the Olsen potential are shown in Figure 6.8.

Figure 6.7 shows the ionisation cross sections calculated using the potentials as given by Martin et al (1978), Olsen (1972) and Haberland and Schmidt (1977). The real and imaginary potentials of Martin et al are used in their given form so that the differential calculations for which they were derived are not altered (Figure 6.5). For the Haberland and Schmidt potential only the real part is used in this work. The imaginary part of the potential Γ has been modified by Haberland and Schmidt, introducing a gradient minimum at R=5.75 a.u. by means of a second exponential term. In a later publication by Brutschy et al (1982) they have used a nearly identical real potential but have reverted to the simple form of Γ, as used in the present calculations (Figure 6.6). Because the potentials are so similar, it is reasonable to use the exact form of Γ given by Brutschy et al (1982).

Unfortunately it has not been possible to use this later real potential devised by Brutschy et al (1982) for any calculations because the potential, which includes two switching functions, cannot be constructed correctly from the information given in the Brutschy et al paper. The only difference between the two potentials of the Freiburg group is the depth of the intermediate minimum. In the Brutschy et al (1982) paper the minimum introduced by Haberland and Schmidt (1977) has been reduced in depth by a factor of two for better agreement with differential cross section data.

As in the case of the triplet interaction, the calculated singlet cross section does not decrease at high velocity in the same way that the experimental cross section does. Once again a saturating form of Γ has been used to fit the high end of the velocity range. The saturation gives a good agreement between experiment and theory at high velocity (Figure 6.8) with Γ saturating at Rsat = 5.16 a.u. for the Martin et al potential (Γsat = 0.95×10^{-3} a.u.) and Rsat = 5.6 a.u for the Haberland and Schmidt potential (Γsat = 0.73×10^{-3} a.u.).

Figure 6.7 Theoretical cross sections calculated using interaction potentials for the Ar+He(2^1S) system and compared with the present experimental results

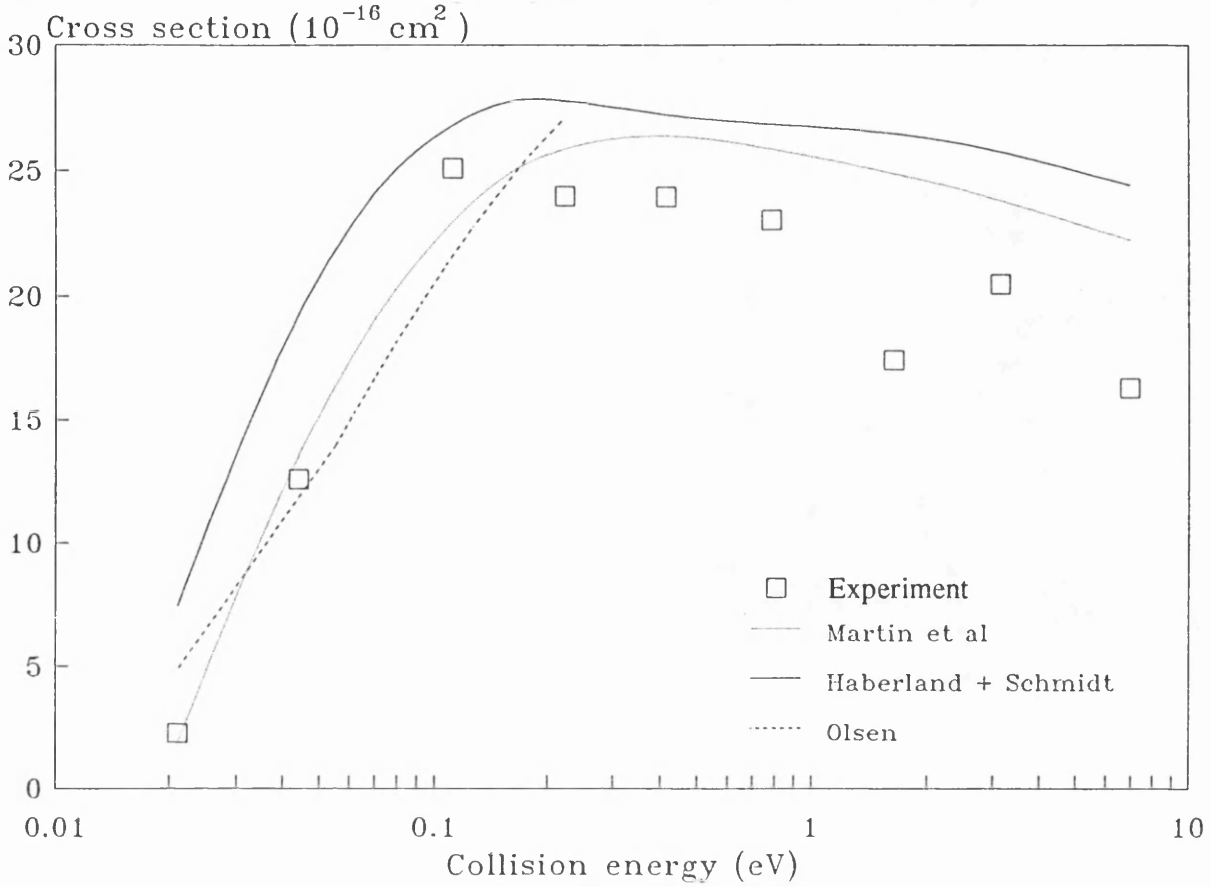

Figure 6.8 Theoretical cross sections calculated with a saturating form of Γ the imaginary part of the Ar+He(2^1S) interaction potential

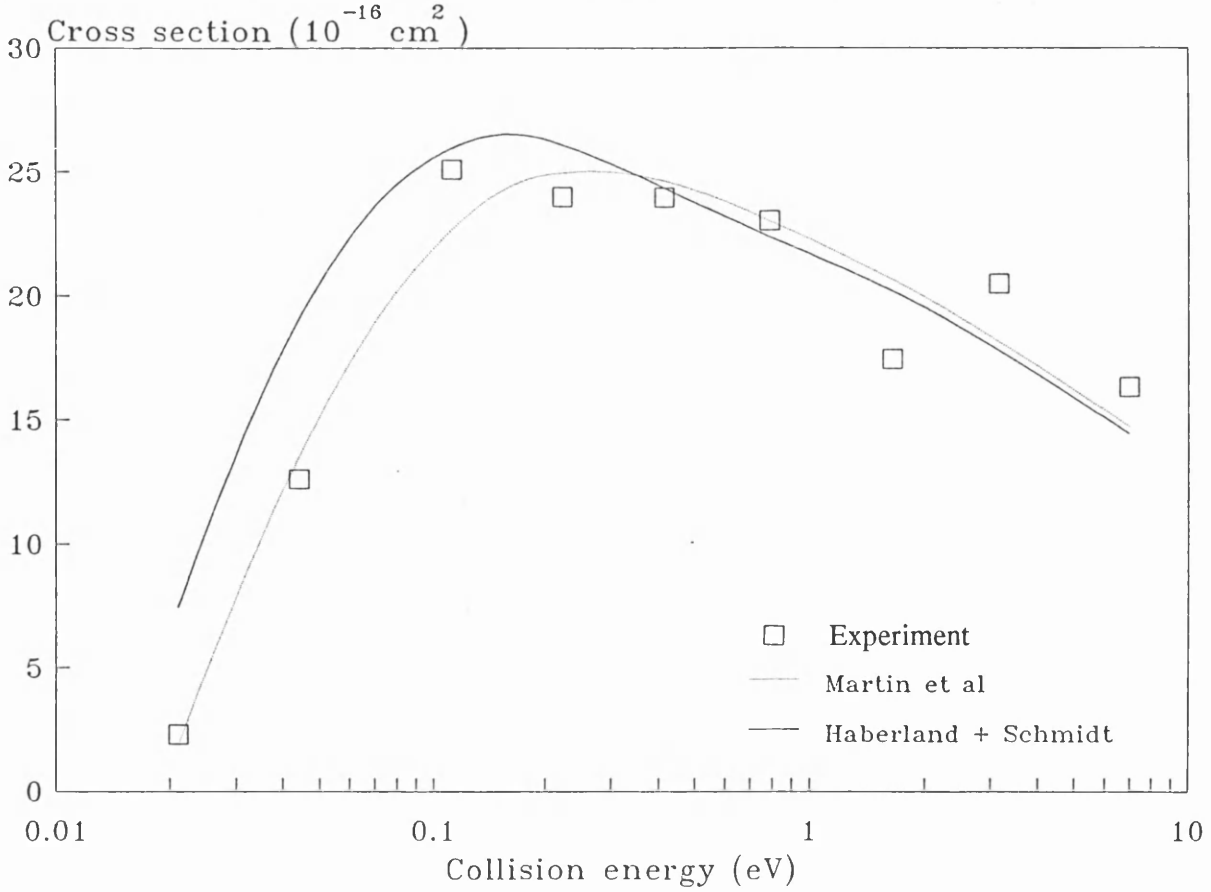

As Figure 6.8 shows, the cross section calculated using the potential of Martin et al fits the experimental data better than the cross section calculated from the work of Haberland and Schmidt, because the latter lies above the experimental measurements at low velocities. Neither cross section shows a maximum at 0.11 eV as does the experiment; the Martin et al potential gives a maximum at 0.2 eV and the Haberland and Schmidt potential shows a better agreement with a maximum at approximately 0.15 eV.

Burdenski et al (1981) have made measurements of the total ionisation cross section for He(2^1S) + Ar up to a velocity of 3km/s and have calculated theoretical cross sections using the potentials of the Freiberg group. By adopting the same saturating form of Γ as used here the value of Rsat was found to be 5.93 a.u., which is a higher value than calculated in this work (Rsat = 5.6 a.u.). This may be due to the more pronounced decline in their measured cross section over their much shorter velocity range. The value of Rsat determined by Burdenski et al is large enough to affect the differential cross section calculations of the Freiberg group down to 100 meV, boosting the large-angle cross sections to the extent that they fall outside the experimental errors of the work. The value of Rsat determined here for the Martin et al potential, Rsat = 5.16 a.u., is in much better agreement with the differential measurements of the Freiburg and Pittsburg groups. Only

Figure 6.9 Variation of turning point with angular momentum

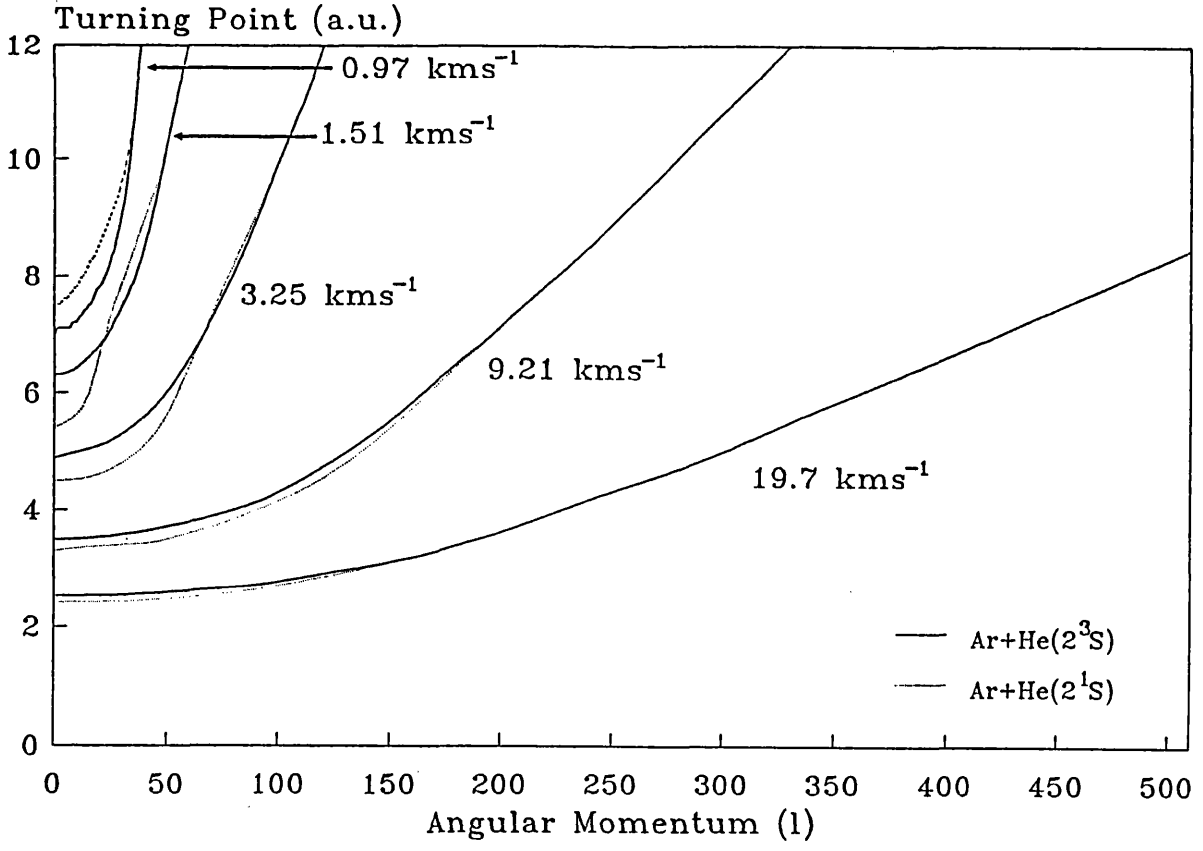

Figure 6.10 Variation of cross section with angular moment

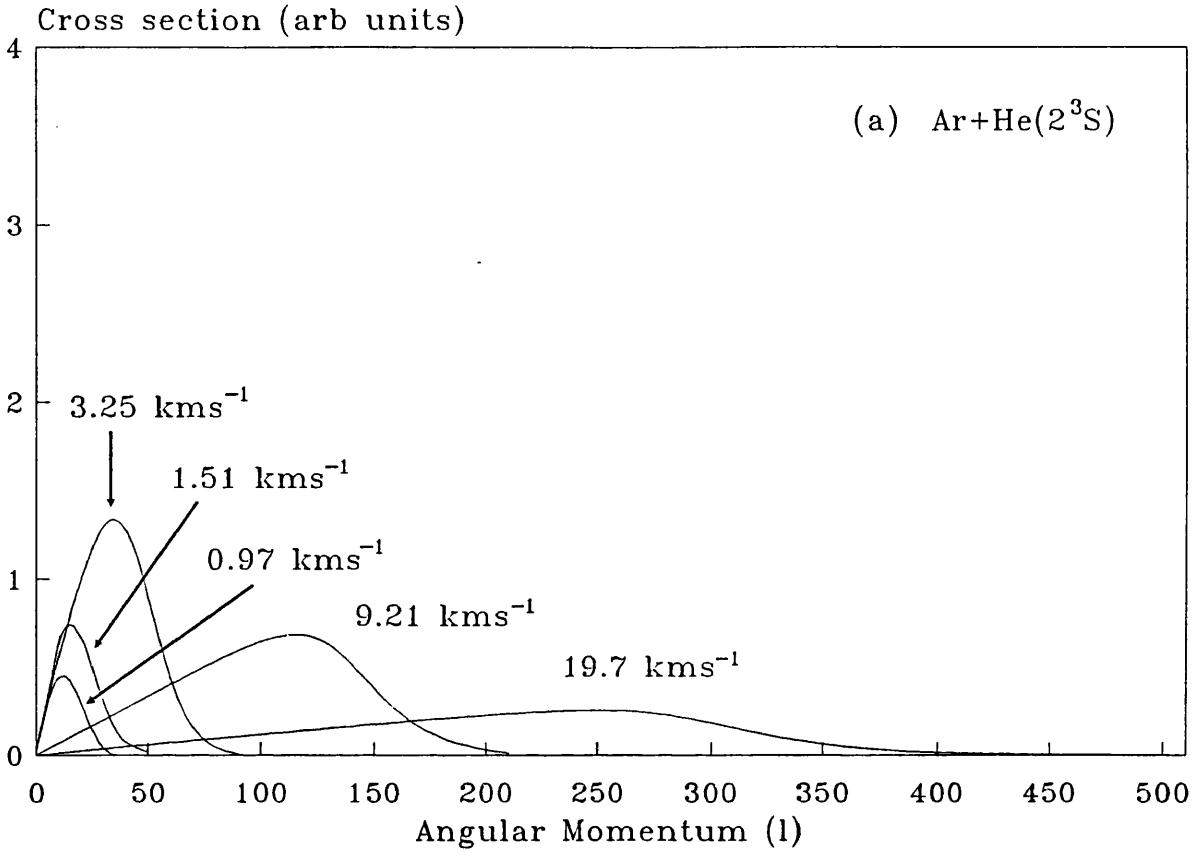

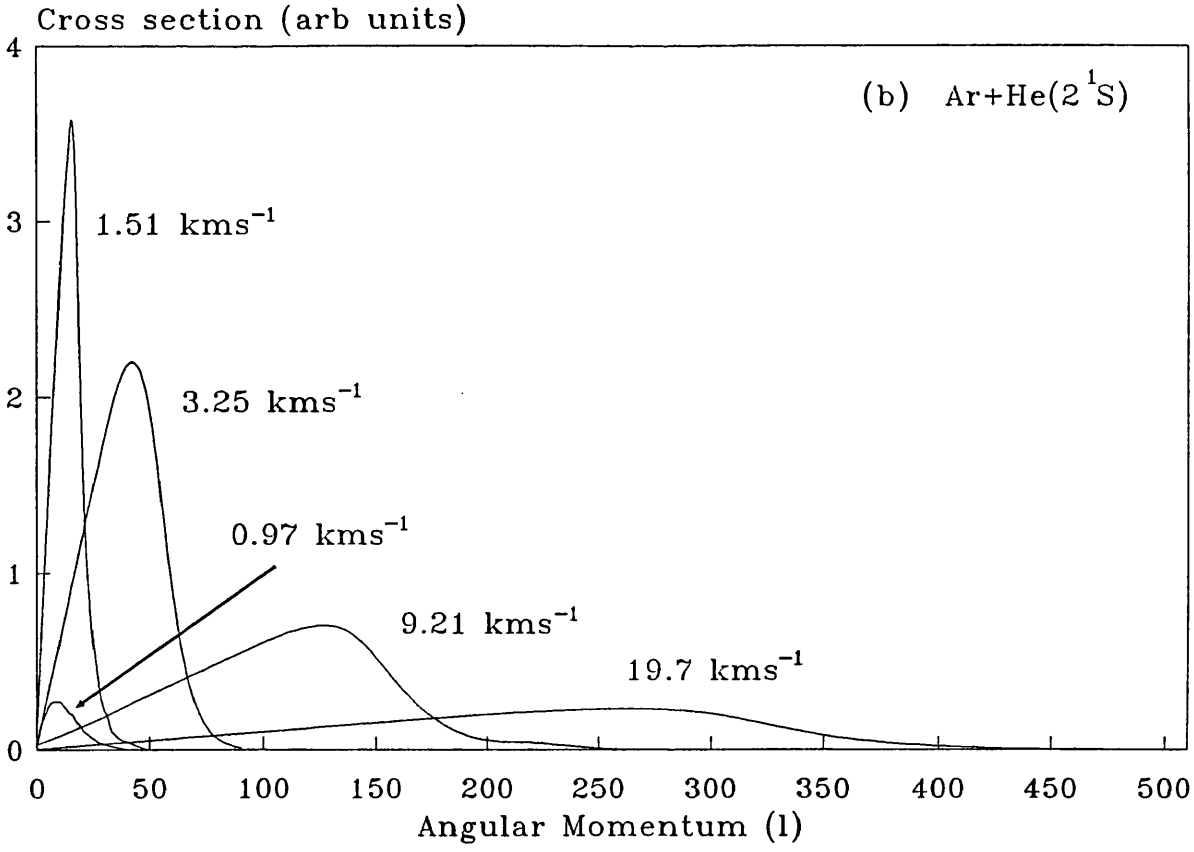

differential cross sections at 180 meV are affected by the saturation at 5.16 a.u. The classical turning point for 180 meV interactions with low values of angular momentum ($L<40$) can penetrate to R = 5.03 a.u., the region in which Γ is saturated. Interactions of less than 180 meV cannot penetrate to the saturated region, and so the calculated differential cross sections at these energies remain the same.

Figures 6.9 shows how the turning points at zero angular momentum and collision velocities between 1.15 kms^{-1} and 3.25 kms^{-1} (48 meV - 200 meV) begin to reach the region in which Γ is saturating (4.5 a.u. - 5.5 a.u.). Also shown graphically is the fact that colliding particles which have large angular momentum may have lower turning points than particles with low velocity and with low angular momentum. As a consequence of this (Figure 6.10a and b) collisions with large angular momentum remain important at high collision velocity.

In conclusion there is still a discrepancy between the ionisation and differential cross sections, but at higher energy than reported by Burdensky et al. Burdenski et al have suggested that an extra channel for de-excitation of the 2^1S state may be important at higher energies, and put forward radiative de-excitation as the most likely explanation for this discrepancy.

6.5 Approximate cross sections

The expression for the approximate cross section derived by Illenberger and Niehaus (Equation 2.27) suggests that for a range of energies between 20 meV and 100 meV a log-log plot of cross section versus energy will result in a straight line. The gradient of this line M is approximately given by

$$M \sim \frac{D}{B} - \frac{1}{2} \qquad (6.6)$$

where D and B are given by equation 2.26. Oddly, the target which fulfils this condition least in Figures 6.11 and 6.12 is argon. The triplet interaction can be represented by a straight line, but clearly not the singlet interaction, where the simplification is valid at a lower range of collision energy (0.02 - 0.06). For the other molecules studied, quite good agreement is obtained, confirming the validity of the simplification adopted by Illenberger and Niehaus.

Figure 6.11 Log–Log plot of cross section against energy for collisions with $He(2^3S)$

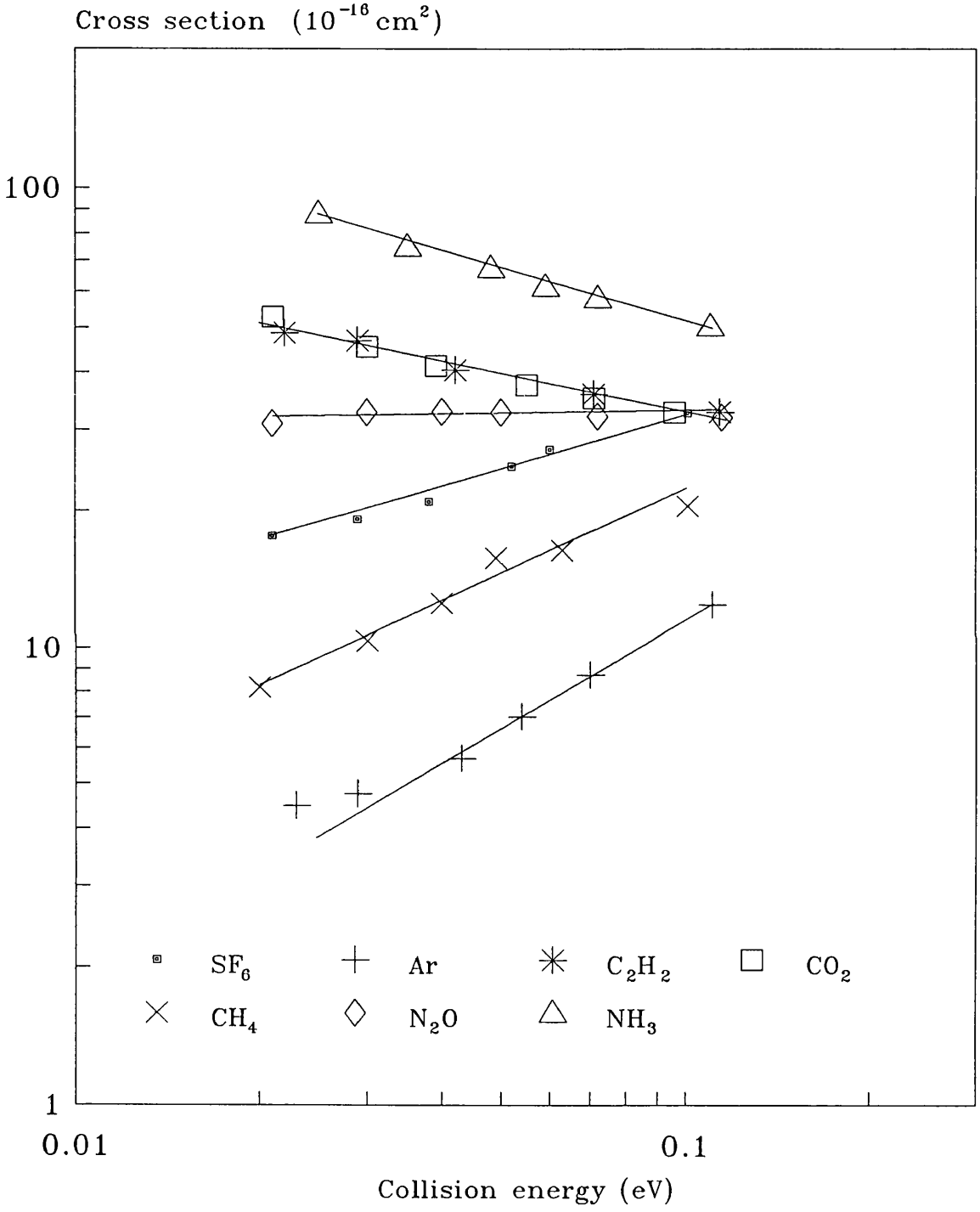

Figure 6.1.2 Log–Log plot of cross section against energy for collisions with $He(2^1S)$

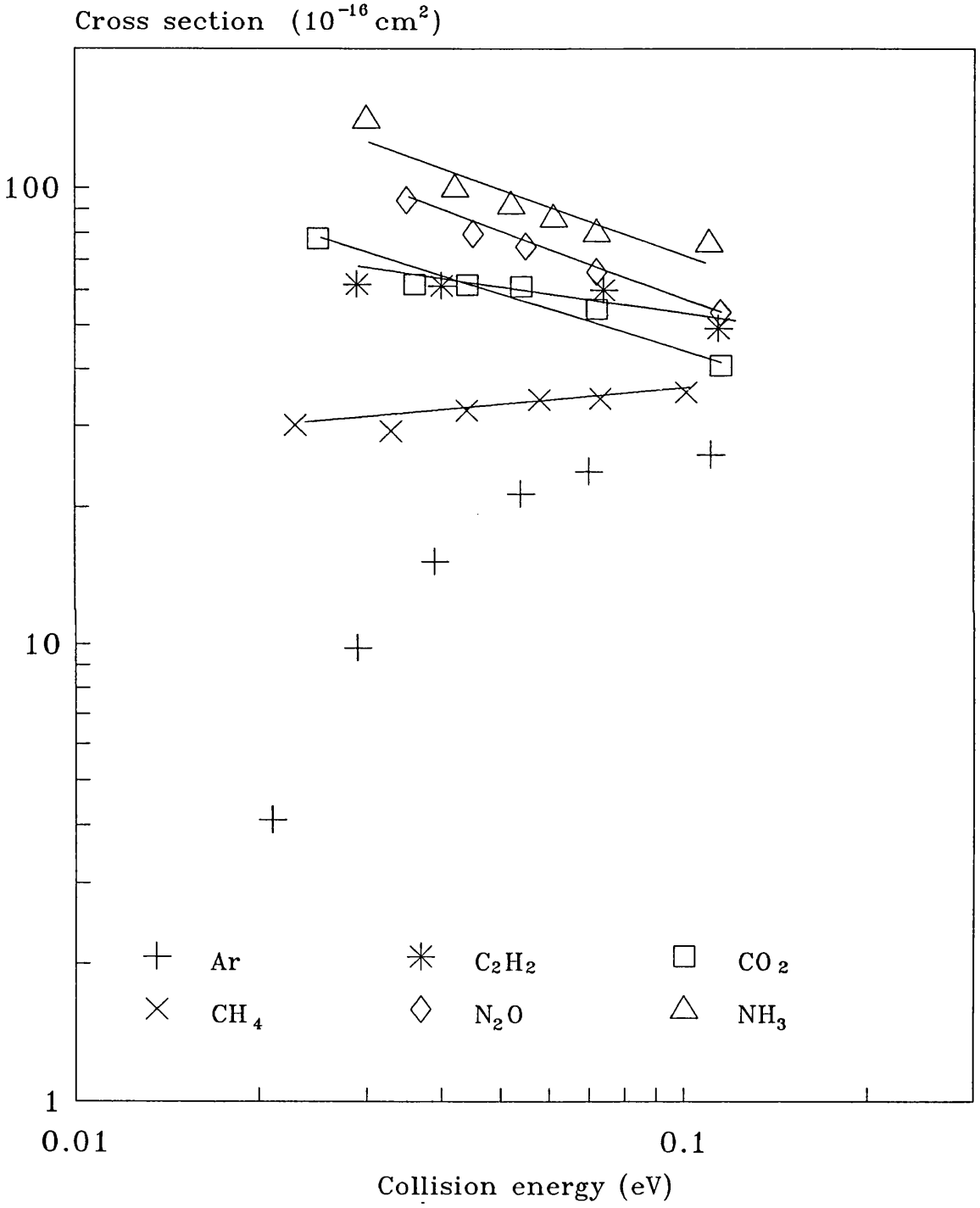

Chapter 7

Conclusions and suggestions for further work

7.1 Conclusions

Total and partial cross sections for collisions of Ar, CO_2, N_2O, CH_4, C_2H_2, NH_3 with helium atoms both in the $He(2^3S)$ and $He(2^1S)$ metastable states of helium have been made and also for SF_6 with the triplet state only. The total ionisation cross section for $He(2^1S)+Ar$ is in good agreement with other available data at low collision velocity (below $5kms^{-1}$), and there is no reason to believe that the results at high velocity (5-20 kms^{-1}) are not equally reliable, although the error bars are larger. In every other case the variation of total ionisation cross section for collisions with $He(2^1S)$ are the first to be measured.

The procedure of normalising the singlet cross section with the same normalisation constant as for the corresponding triplet cross section has been tested in the case of argon and is found to be very satisfactory. This technique has allowed comparisons to be made between absolute measurements of total ionisation cross sections and both present triplet and singlet results, where several absolute measurements exist. The other available absolute results are at single energies, and normally fall within the error bars of the present cross sections.

The triplet measurements agree well with the previous results of Jerram (1985) and in most cases extend his measurements into higher and lower energy regions. The only significant disagreement is in the case of methane, which is likely to be the result of much better performance of the present quench lamp than that used by Jerram.

The branching ratios are the first energy-dependent ratios measured in the case of collisions with the singlet metastable state, as are the cases of N_2O and SF_6 for the triplet metastable state. Where comparisons are possible in the singlet case, agreement with other single energy measurements is within the error bars, which are large at energies above 0.2 eV. For the triplet case, the agreement with the energy-dependent measurements of Jerram is good, and the present results increase the accuracy by an order of magnitude. In most cases the fraction of Penning ionisation decreases with energy and associative ionisation is only apparent for argon.

The present total ionisation cross sections for both metastable species with argon have been compared with theoretically generated cross sections. In the triplet case it is possible to obtain a good agreement between experiment and cross sections calculated using any of the model potentials, provided a saturating form of imaginary potential is used. The potential which gives the best agreement is that of Siska (1979).

In the singlet case, the potential devised by Olsen (1972) is not satisfactory, as it does not reproduce the steeply rising cross section at low energy. The interaction potential derived by the Pittsburg group (Martin et al 1978) is superior to that of the Freiburg group (Haberland and Schmidt 1977), again using the saturating form of imaginary potential.

In both singlet and triplet cases, the necessary saturation in the imaginary part of the interaction potential reduces the ability of these potentials to produce theoretical high energy differential elastic cross sections which fit experimental data. To reproduce the present experimental results, the saturation in the imaginary part of the interaction potential was introduced at lower internuclear separation than in the work of Burdenski et al (1981). The present work allows the theoretical interaction potentials to describe both elastic and inelastic processes satisfactorily to higher interaction energies than any previous experiments.

7.2 Possible improvements and suggestions for further work

It is almost certainly possible to improve the detection efficiency of the present ion detector. This would be done by replacing the electron multiplier with the available multi-channel plates of larger detecting area (1000 mm^2 compared with 314 mm^2). A mounting identical to that described in chapter 4 could be used.

The quench lamp used in the present experiment has proved to be more than three times as effective as the previous lamp introduced by Harper (1977). However it is not ideal, tending to overheat. This leads to unwanted outgassing in the lamp and makes refilling and baking the lamp frequent necessities. This might be overcome if the present air cooling system were replaced by a water cooling system. Alternatively the 2058 nm resonant radiation could be produced by means of a 1064 nm YAG laser pumping a tunable dye laser. This would be expensive but is the most likely way to achieve full quenching at velocities up to and above 20 kms^{-1}

As stated in chapter 5, in order to reduce by a factor of three the magnitude of the error bars in the present experiment, it would be necessary to increase the amount of data recorded by a factor of ten. This would best be achieved by increasing the count rate of the experiment but to do this it would be necessary to change from a single-shot to a multi-shot TOF system. This would require a change to a faster computer, fast enough to accept counts a few microseconds apart, and to operate in the multi-channel-analyser mode. The TOF mass spectrometer would need to be replaced in favour of a quadropole mass spectrometer because the time delay between the detection of electron and ion in the TOF type would lead to multiple start pulses in a very high count rate experiment.

With a redesigned interaction region it would be possible to observe the ejected electron energy distributions for different molecules. This could be done by using the multi-channel plate detector to its full capacity as a position sensitive device. Electrons would be collimated as in the Hotop et al (1977) system and then spread out according to energy by passing them through an electric field perpendicular to their trajectory. The multi-channel plates could be inclined with respect to this trajectory to increase sensitivity. A one-dimensional position sensitive anode would be used (or a combination of a phosphor strip and charge-coupled device). The present TOF system would be useful for recording ejected electron energy distributions (EEED) as a function of collision energy, which has been rarely done.

By further collimation of the metastable atom beam and the introduction of a second channeltron detector displaced from the present one by several degrees, it would be possible to perform differential elastic scattering experiments, in a similar manner to that of Kroon (1985), with the cross section measured as a function of energy at a fixed angle. This would help, as it already has in the case of argon, in the formulation of theoretical potential surfaces for the interaction of the systems described in this thesis.

Appendix 1

Analysis of efficiency of the quench lamp built by Harper (1977)

The quenching efficiency as a function of current is given by equation A1:

$$q(I) = 1-e^{-KI} \qquad \text{A1}$$

Where K is a constant. Figure A1.1 shows the metastable atom count rate as a function of current C(I), for a velocity of 7.6 kms^{-1}. From this the value of q can be derived, as a function of current and more importantly velocity. Equation A2 shows how q(I) is related to the count rate information of Figure A1.1:

$$q(I) = \frac{C(I) - Cmin}{Cmax - Cmin} \qquad \text{A2}$$

where, Cmin is the count rate achieved with 100% quenching, and Cmax is the count rate measured with no quenching (when the lamp is off). Equations A1 and A2 are simply rearranged to give equation A3:

$$C(I) = Cmin + [Cmax - Cmin]\, e^{-KI} \qquad \text{A3}$$

A least squares fitting program has been used to find the values of Cmin, and K. Previously Cmin has only been estimated. The values calculated are given below.

K= 0.1267 Cmin= 4192 χ^2= 0.47

The new value of K is replaced in equation A1, to find q, at 7.6 kms^{-1}, and at a quench lamp current of 28 mA (the normal operating current). The value of the quenching efficiency q is 98.3%.

By substituting the values of q and v into equations given in chapter 4.3 (4.1, 4.2, 4.3) the constants C, B and D in these equations have been calculated as C = 2.7×10^{4} ms^{-1}, B = 3.49×10^{9} ms^{-1} and D = 1.81×10^{5} ms^{-1}.

Figure A1.1

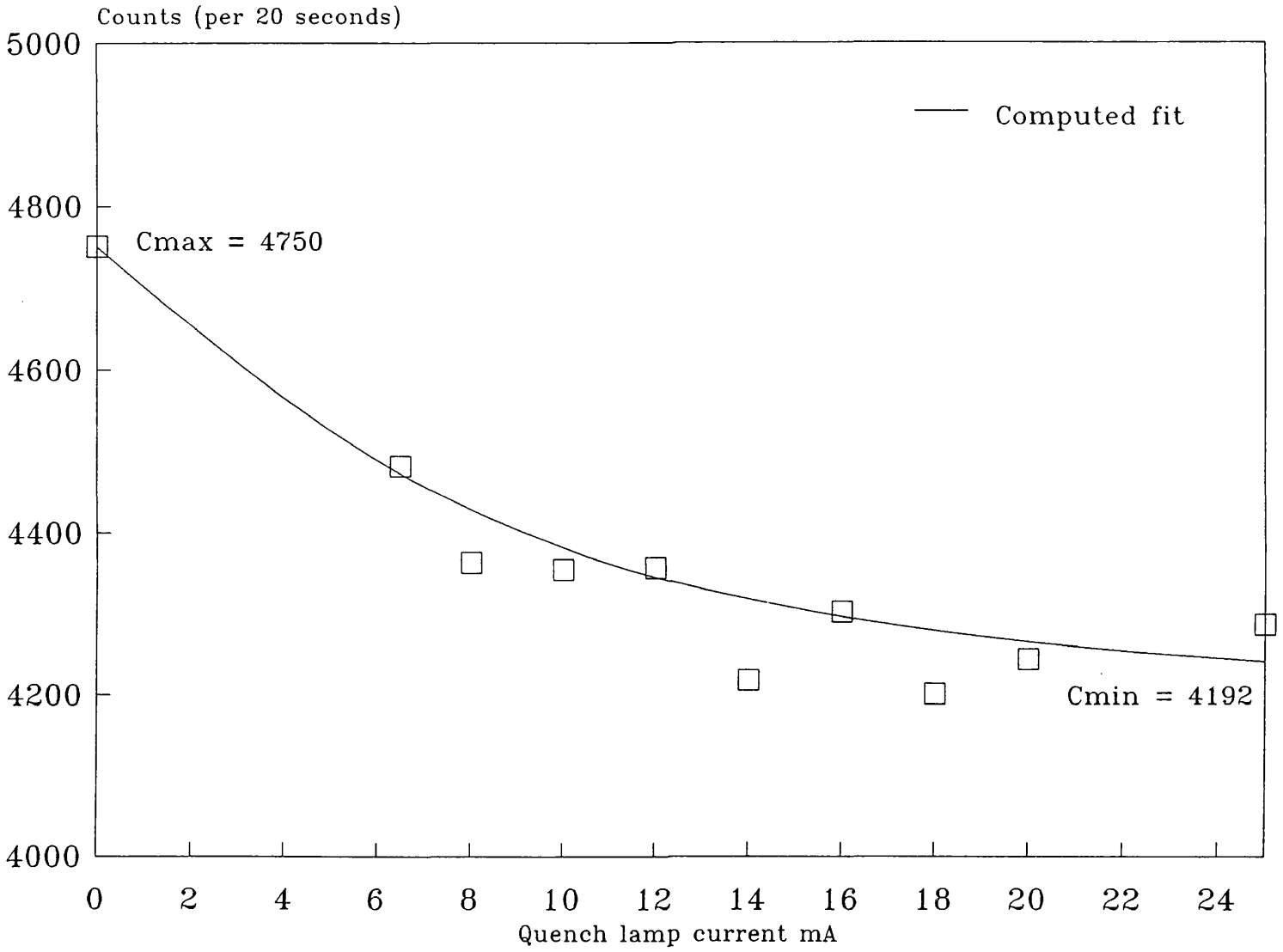
Counts (per 20 seconds)
5000
4800
4600
4400
4200
4000
Computed fit
Cmax = 4750
Cmin = 4192
0
2
4
6
8
10
12
14
16
18
20
22
24
Quench lamp current mA

Appendix 2 Relay logic circuit

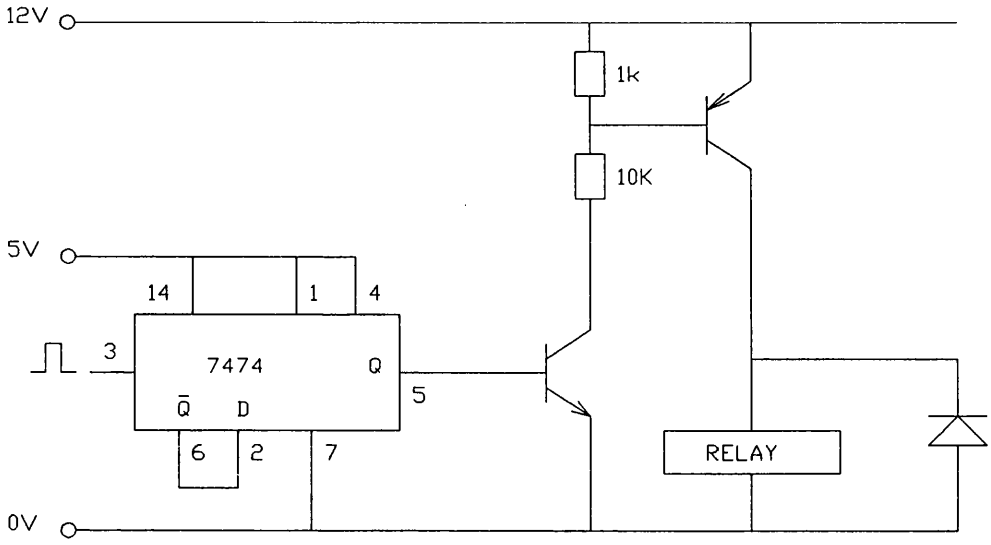

Appendix 3 Optical switch circuit

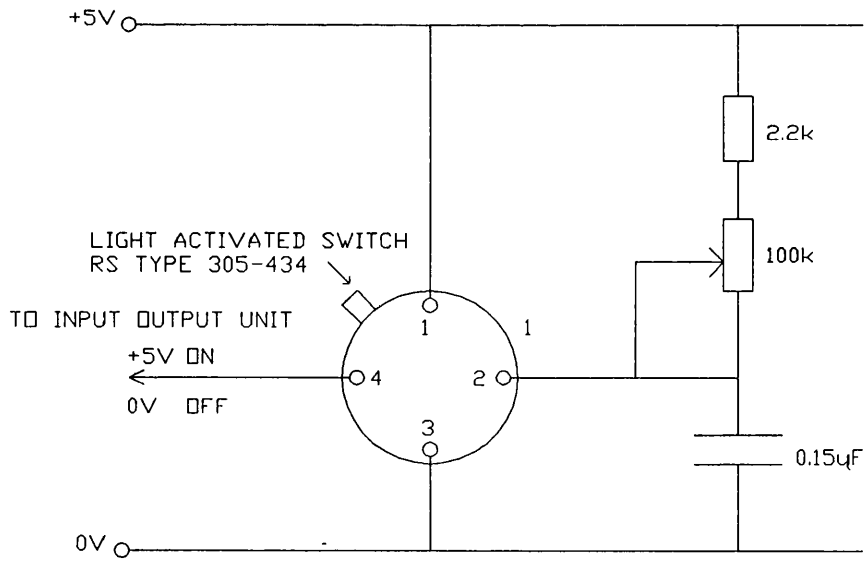

Appendix 4 TOF logic circuit with photon mask

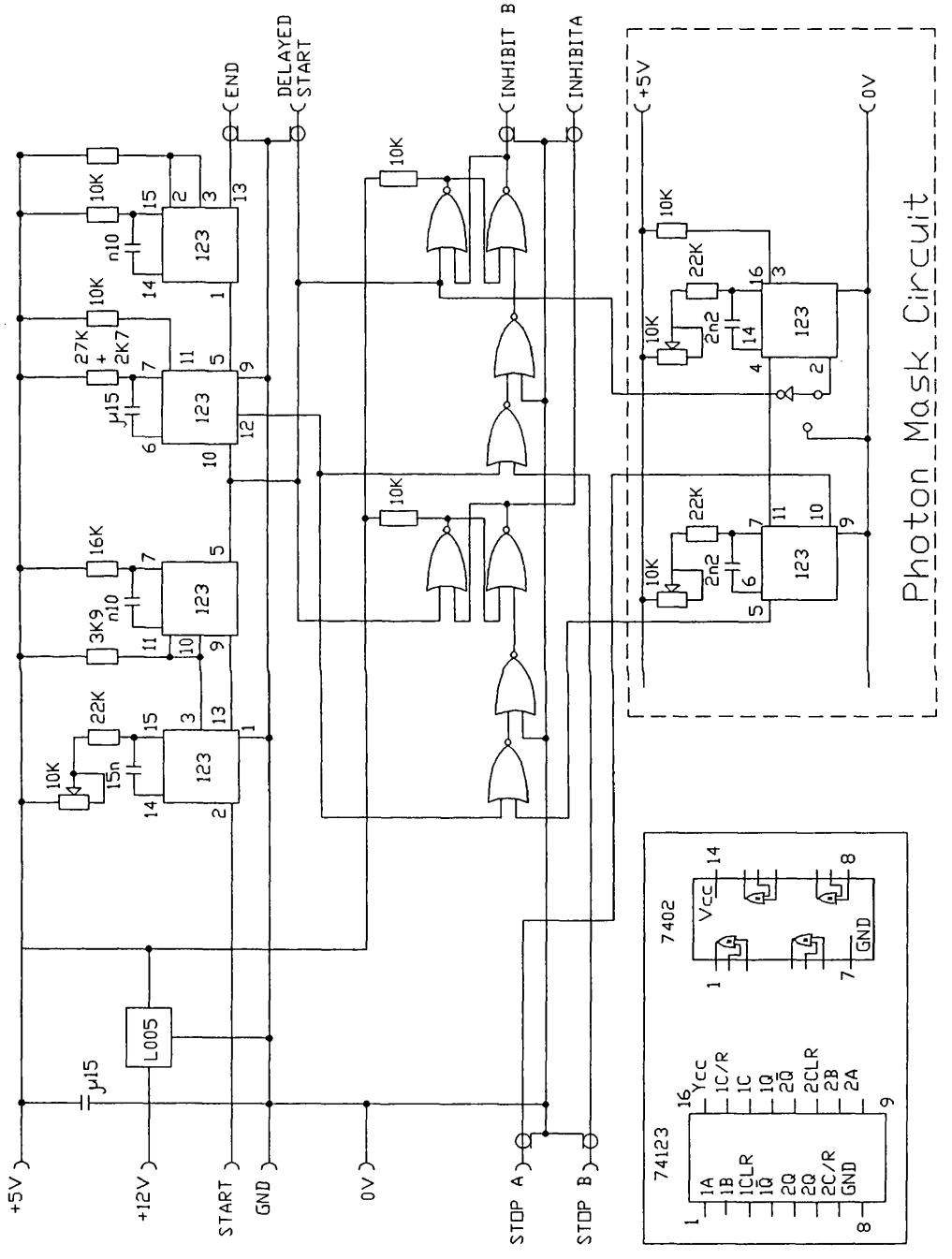

Appendix 5 Detector supply circuits

Multi-channel plate supply

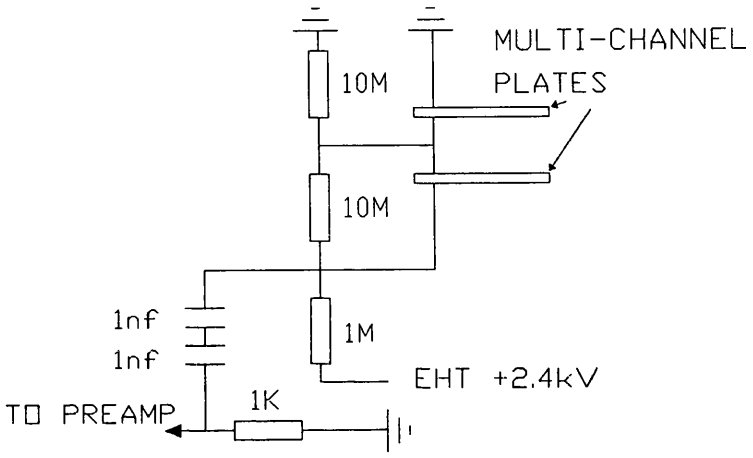

Electron multiplier supply

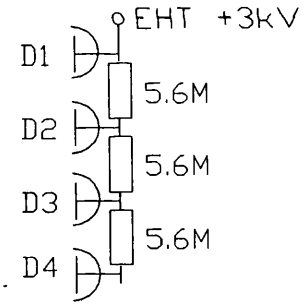

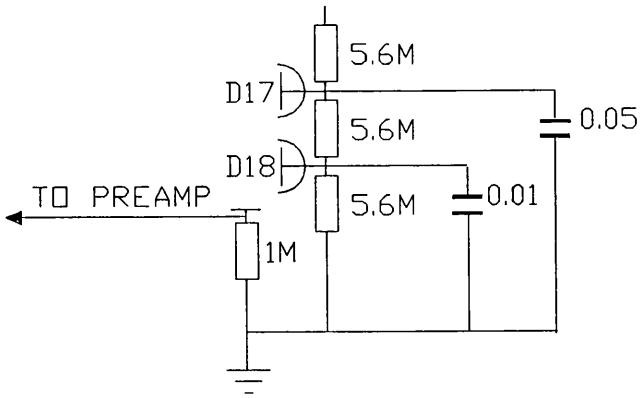

Appendix 6

TOF3 Provides data collection for total cross section experiments

```
C
C TOF3
C COLLECTS TIME OF FLIGHT DATA,PLOTS AND FILES
C LINKS WITH SUBPROGRAMS CAMCUL FOR INTERFACE WITH THE CAMAC CRATE,
C PLOT55 TO SHOW TOF SPECTRA ON THE VDU AND
C FILE TO SAVE THE DATA ON DISK
C
      COMMON FNAM(3),COM(18),PAR(18),VAL(10),DAT(520),VALON(10)
      DIMENSION DATON(520),DATI(520),DATION(520),VALI(10)
      DIMENSION IMSTOR(1001),IONSTOR(1001),IPLT(512),IONPLT(512)
      DIMENSION VALION(10)
      DATA Y/'Y'/
      NDATST=1
1     FORMAT(10I6)
2     FORMAT(18A4)
3     FORMAT(10F8.1)
C
C THE VAL* ARRAYS RECORD INFORMATION ABOUT THE DATA WHICH IS BEING COLLECTED
C 'I' INDICATES AN ION SPECTRA AND 'ON ' INDICATES THE LAMP IS ON
C
      VAL(1)=512.0
4     DO 6 I=2,10
      VAL(I)=0.0
      VALON(I)=0.0
      VALI(I)=0.0
      VALION(I)=0.0
6     CONTINUE
      NREP=0
C
C TOF SPECTRA ARE STORED IN DAT* ARRAYS
C
      DO 8 I=1,520
      DAT(I)=0.0
      DATON(I)=0.0
      DATI(I)=0.0
      DATION(I)=0.0
8     CONTINUE
C
C ONE 'CYCLE' REPRESENTS 10^4 START PULSES
C
      TYPE 10
10    FORMAT(' NUMBER OF CYCLES? '$)
      ACCEPT 1,ICYC
      NCY=1
C
C     FIRST INITIALIZE CAMAC CRATE
C
      ICOUNT=1
C
C WHEN ICOUNT = 1 THE LAMP IS OFF WHEN ICOUNT = 2 THE LAMP IS TURNED ON
C
12    DO 32 N=1,ICYC
      DO 860 L=1,20
      CALL CAMAC(11,0,0)
      CALL CAMAC(8,0,0)
      CALL CAMAC(10,0,0)
C
C     RECORD DATA WITH LAMP OFF
C
      DO 25 I=1,1001
20    CALL CAMAC(0,21,1,2,IL)
      IF(IL.EQ.0)GOTO 20
      CALL CAMAC(0,21,3,2,IL)
      CALL CAMAC(0,21,2,2,JL)
```

```
C
C DATA IS TEMPORARILY  STORED IN THE IONSTOR (IONS) AND IMSTOR (METASTABLE)
C ARRAYS
C
      IONSTOR(I)=JL
      IMSTOR(I)=IL
25     CONTINUE
C
C THE DATA IS SORTED INTO TOF SPECTRA
C FIRST THE METASTABLE  ATOMS
C
      IF(ICOUNT.EQ.2)GOTO   700
      DO 30 I=2,1001
      IF(IMSTOR(I).GE.1536)GOTO   30
      J=IFIX(IMSTOR(I)/3+1)
      DAT(J)=DAT(J)+1.0
C
C VAL2 AND VAL5 ARE THE COUNT RATE AND THE NUMBER OF THE CHANNEL WITH THE HIGHEST
C COUNT C RATE NORMALLY  THE PHOTON C PEAK,  VAL3 IS THE TOTAL METASTABLE  COUNT RATE
C
      IF(DAT(J).LE.VAL(2))GOTO   29
      VAL(2)=DAT(J)
      VAL(5)=J
29     VAL(3)=VAL(3)+1.0
30     CONTINUE
C
C SECONDLY THE IONS
C
      DO 300 I=2,1001
      IF(IONSTOR(I).GE.1536)GOTO   300
      J=IFIX(IONSTOR(I)/3+1)
      DATI(J)=DATI(J)+1.0
C
C VAL2 AND VAL5 ARE THE COUNT RATE AND THE NUMBER OF THE CHANNEL WITH THE HIGHEST
C COUNT RATE NORMALLY  THE PHOTO-C  IONISATION  PEAK,  VAL3 IS THE TOTAL ION COUNT RATE
C
      IF(DATI(J).LE.VALI(2))GOTO   290
      VALI(2)=DATI(J)
      VALI(5)=J
290    VALI(3)=VALI(3)+1.0
300    CONTINUE
      VAL(4)=VAL(4)+1.0
C
C      TURN THE QUENCH LAMP ON
C
      GOTO 1200
1100   TYPE 1102
1102   FORMAT( ' LAMP HAS FAILED TO STRIKE ' )
      CALL CAMAC(0,8,1,16,0,0)
      CALL CAMAC(0,4,0,10,)
C
C LAMP RELAY ON
C
1200   CALL CAMAC(0,8,1,16,10200,0)
      DO 100 K=1,500
100    CONTINUE
C
C TESLA RELAY ON
C
      CALL CAMAC(0,9,1,16,20400,0)
      DO 150 K=1,500
150    CONTINUE
C
C TURN TESLA RELAY OFF
C
      CALL CAMAC(0,9,1,16,0,0)
C
C WAIT
C
```

```
      DO 200 K=1,100
      DO 175 I=1,500
175    CONTINUE
200    CONTINUE
      CALL CAMAC(0,4,0,10)
      CALL CAMAC(0,4,0,26)
C
C LOOK AT LAMP WITH PHOTODIODE
C
      CALL CAMAC(0,4,0,8,DL,DH,IQ,)
      TYPE 1,IQ
C
C IF THE LAMP HAS NOT STRUCK REPEAT PROCESS AGAIN
C
      IF(IQ.EQ.1)GOTO  1100
      TYPE 170
170    FORMAT( ' LAMP ON ')
C
C RECORD DATA WITH QUENCH LAMP ON
C
      ICOUNT=2
      DO 271 I=1,100
      DO 281 K=1,500
281    CONTINUE
271    CONTINUE
      GOTO 860
700    CONTINUE
C
C SORT METASTABLE ATOM DATA INTO TOF SPECTRA
C
      DO 795 I=2,1001
      IF(IMSTOR(I).GE.1536)GOTO   795
      J=IFIX(IMSTOR(I)/3+1)
      DATON(J)=DATON(J)+1.0
      IF(DATON(J).LE.VALON(2))GOTO    790
      VALON(2)=DATON(J)
      VALON(5)=J
790    VALON(3)=VALON(3)+1.0
795    CONTINUE
C
C SORT ION DATA INTO TOF SPECTRA
C
      DO 400 I=2,1001
      IF(IONSTOR(I).GE.1536)GOTO   400
      J=IFIX(IONSTOR(I)/3+1)
      DATION(J)=DATION(J)+1.0
      IF(DATION(J).LE.VALION(2))GOTO    390
      VALION(2)=DATION(J)
      VALION(5)=J
390    VALION(3)=VALION(3)+1.0
400    CONTINUE
800    CONTINUE
      VALON(4)=VALON(4)+1.0
C
C     TURN LAMP OFF
C
      GOTO 1400
1300   CALL CAMAC(0,4,0,10,)
      TYPE 1302
1302   FORMAT( ' THE LAMP HAS FAILED TO GO OFF ' )
      CALL CAMAC(0,8,1,16,0,0)
1400   CALL CAMAC(0,8,1,16,10200,0)
      DO 850 K=1,100
      DO 825 I=1,500
825    CONTINUE
850    CONTINUE
C
C LOOK AT LAMP WITH PHOTODIODE
C
```

```
      CALL CAMAC(0,4,0,10)
      CALL CAMAC(0,4,0,26)
      CALL CAMAC(0,4,0,8,DL,DH,IQ,)
      TYPE 1,IQ
C
C IF THE LAMP HAS FAILED TO GO OFF THEN REPEAT THE PROCEDURE
C
      IF(IQ.EQ.0)GOTO  1300
      TYPE 822
822    FORMAT( ' LAMP OFF ' )
      DO 857 I=1,100
      DO 856 K=1,500
856    CONTINUE
857    CONTINUE
C
C RETURN TO BEGINNING OF CYCLE
C
      ICOUNT=1
860    CONTINUE
      TYPE 1,NCY
      NCY=NCY+1
32     CONTINUE
      NREP=NREP-1
      IF(NREP.GT.0)GOTO  12
C
C AT THE END OF A RUN OF CYCLES THE TOF SPECTRA ARE SCROLLED ON THE VDU ALONG WITH THEIR
C VAL ARRAY AND THEN THE C SPECTRA ARE PLOTTED ON THE SCREEN
C
      DO 37 I=1,512,10
      TYPE 3,(DAT(J),J=I,I+9)
37     CONTINUE
      DO 40 I=1,512,10
      TYPE 3,(DATON(J),J=I,I+9)
40     CONTINUE
      IF(VAL(2).EQ.0)VAL(2)=0.1
      SCAL=235.0/(VAL(2)*2)
      DO 41 I=1,512
      IPLT(I)=IFIX(DAT(I)*SCAL+0.5)
41     CONTINUE
      DO 42 I=1,512
      IONPLT(I)=IFIX(DATON(I)*SCAL+0.5)
42     CONTINUE
      FILPLOT=0.0
      GOTO 44
43     DO 500 I=1,512,10
      TYPE 3,(DATI(J),J=I,I+9)
500    CONTINUE
      DO 510 I=1,512,10
      TYPE 3,(DATION(J),J=I,I+9)
510    CONTINUE
      IF(VALI(2).EQ.0)VALI(2)=0.1
      SCAL=235/(VALI(2)*2)
      DO 520 I=1,512
      IPLT(I)=IFIX(DATI(I)*SCAL+0.5)
520    CONTINUE
      DO 530 I=1,512
      IONPLT(I)=IFIX(DATION(I)*SCAL+0.5)
530    CONTINUE
44     CALL PLOT55(2,1+2+4+32+512,511)
      CALL PLOT55(9,,)
      CALL PLOT55(10,,)
      IF(FILPLOT.NE.1)GOTO  52
      TYPE 3,VALI
      GOTO 51
52     TYPE 3,VAL
51     CONTINUE
      CALL PLOT55(1,0,)
      CALL PLOT55(4,1,)
      CALL PLOT55(7,,)
```

```
      CALL PLOT55(3,-512,IPLT)
      ACCEPT 2,KR
      IF(FILPLOT.NE.1)GOTO  53
      TYPE 3,VALION
      GOTO 54
53    TYPE 3,VALON
54    CONTINUE
      CALL PLOT55(1,1,)
      CALL PLOT55(3,-512,IONPLT)
      ACCEPT 2,KR
      CALL PLOT55(2,512,511)
      FILPLOT=FILPLOT+1
      IF(FILPLOT.EQ.1)  GOTO 43
C
C MORE CYCLES MAY BE PERFORMED  OR THE DATA STORED ON DISK
C
      TYPE 45
45    FORMAT(' MORE DATA(2),FILE(3)?  '$)
      ACCEPT 1, IND
      IF(IND-2)50,50,60
50    TYPE 55
55    FORMAT(' NUMBER OF REPEATS? '$)
      ACCEPT 1,NREP
      GOTO 12
C
C TO STORE THE DATA ON DISK THE FILES AR NAMED IN ORDER
C
60    TYPE 65
65    FORMAT(' IN THE ORDER METS OFF,METS ON,IONS OFF,IONS ON? '$)
63    TYPE 64
64    FORMAT(' FILENAME? ')
      ACCEPT 2,FNAM
      TYPE 70
70    FORMAT(' COMMENTS(UP TO 72 LETTERS)?')
      ACCEPT 2,COM
      TYPE 71
71    FORMAT(' FIXED PARAMETERS(UP  TO 72 LETTERS)?')
      ACCEPT 2,PAR
      CALL FILE(1,0.0)
      IF(NDATST.EQ.4)GOTO  81
      IF(NDATST-2)72,75,78
72    DO 73 I=1,512
      DAT(I)=DATON(I)
73    CONTINUE
      DO 74 I=2,10
      VAL(I)=VALON(I)
74    CONTINUE
      NDATST=NDATST+1
      GOTO 63
75    DO 76 I=1,512
      DAT(I)=DATI(I)
76    CONTINUE
      DO 77 I=2,10
      VAL(I)=VALI(I)
77    CONTINUE
      NDATST=NDATST+1
      GOTO 63
78    DO 79 I=1,512
      DAT(I)=DATION(I)
79    CONTINUE
      DO 80 I=2,10
      VAL(I)=VALION(I)
80    CONTINUE
      NDATST=NDATST+1
      GOTO 63
81    NDATST=1
      TYPE 85
C
C AFTER STORING DATA ON DISK THE PROGRAM  MAY BE RUN AGAIN
```

```
C
85    FORMAT(' RESTART(Y OR N)? '$)
      ACCEPT 2,ANS
      IF(ANS.EQ.Y)GOTO 4
      TYPE 90
C
C IF THE COMPUTER MAKES ANY MISTAKES IN FILLING THEN THE PROCEDURE IS REPEATED
C
90    FORMAT(' REMAKE LAST THREE FILES? '$)
      ACCEPT 2,ANS
      IF(ANS.EQ.Y)GOTO 72
      STOP
      END
```

Appendix 7

HIGHCOUNT Corrects TOF spectra for the effect of the high count rate

```
C
C HIGHCOUNT
C READS IN DATA FROM DISK USING FILE SUBPROGRAM
C CORRECTS FOR HIGH COUNT RATE
C PLOTS TOF SPECTRA BEFORE AND AFTER CORRECTION USING PLOT55 AND PLOT7 SUBPROGRAMS
C
  DATA Y,H/'Y','H'/
      COMMON FNAM(3),COM(18),PAR(18),VAL(10),DAT(520)
      DIMENSION SUM(180),KTF(11),VEL(180),LX(11),DIV(180)
      DIMENSION DSUM(180),ADSUM(180),DDIV(180),VELO(180)
3000   CONTINUE
      TYPE 992
C
C SCROLL AND PLOT ARE BOTH OPTIONAL
C
992    FORMAT( ' IS SCROLL REQUIRED? ' )
      ACCEPT 7,SCRO
      TYPE 991
991    FORMAT( ' IS A PLOT REQUIRED? ' )
      ACCEPT 7,GRPH
13     FORMAT(7F10.4)
8      FORMAT(3I6)
C
C LOAD TOF SPECTRUM FROM DISK
C
1      TYPE 2
2      FORMAT(' WHICH MEMORY SET? '$)
      ACCEPT 7,FNAM
      CALL FILE(0,0.0)
C
C TYPE OUT DATA AND PLOT TOF SPECTRUM
C
      TYPE 7,COM
7      FORMAT(18A4)
      TYPE 7,PAR
5      TYPE 9,VAL
      ACCEPT 7,KR
      IF(SCRO.NE.Y)GOTO  88
      DO 80,I=1,512,10
      TYPE 8,I
80     TYPE 9,(DAT(J),J=I,I+9)
9      FORMAT(10F8.1)
88     IF(GRPH.NE.Y)GOTO  27
83     TYPE 45
45     FORMAT( ' SET THE MAX VALUE '$)
      ACCEPT 13,AMAX
      IF(AMAX.LE.1.0)AMAX=VAL(2)
      TYPE 68
68     FORMAT( ' SET THE GRAPHICS (IEN,IG)  ' )
      ACCEPT 8,IEN,IG
84     CONTINUE
      CALL PLOT7(DAT,512,AMAX,IEN,IG,)
C
C CORRECT FOR HIGH COUNT RATE
C
      TYPE 1000
1000   FORMAT( ' IS A CORRECTION FOR HIGH COUNT RATE REQUIRED ' )
      ACCEPT 7,ATEL
      IF(ATEL.NE.Y)GOTO  27
C
C DAT(I) =        THE NUMBER OF COUNTS IN CHANNEL I
C IOF    =        THE PHOTON PEAK CHANNEL
```

```
C TOTS  =       RUNNING TOTAL OF COUNTS
C CYCTO =       THE NUMBER OF CYCLES IN WHICH THE DATA WAS C RECORDED (DIVIDED BY 10**4)
C CMIS  =       THE NUMBER OF CYCLES IN WHICH A CHANNEL COULD RECORD DATA

C
      TYPE 1010
1010   FORMAT( ' TYPE IN ZERO OFFSET (INTEGRAL) ' )
      ACCEPT 8,IOF
      TOTS=0.0
      DO 1015 I=1,IOF+10
      TOTS=TOTS+DAT(I)
1015   CONTINUE
      TYPE 1020
1020   FORMAT( ' HOW MANY CYCLES ' )
      ACCEPT 13,CYCTO
      IOF=IOF+10
      CYCTO=CYCTO*10000
      CMIS=0.0
      TNEW=0.0
      DO 1100 I=IOF,512
      TOTS=TOTS+DAT(I)
      CMIS=CYCTO-TOTS
      DAT(I)=DAT(I)*CYCTO/CMIS
      TNEW=TNEW+DAT(I)
      TYPE 9,  TOTS  ,TNEW
1100   CONTINUE
C
C THE TOTAL NUMBER OF COUNTS IN THE TOF SPECTRUM BEFORE AND AFTER CORRECTION ARE
C DISPLAYED
C
      TYPE 1110
1110   FORMAT( ' OLD TOTAL, NEW TOTAL ' )
      TYPE 9,   TOTS,   TNEW
C
C THE NEW TOF SPECTRUM IS PLOTTED
C
      GOTO 5
C
C THE NEW TOF SPECTRUM IS FILED ON DISK
C
27     TYPE 89
89     FORMAT( ' WHAT IS THE NEW FILE NAME? ' )
      ACCEPT 7,FNAM
      CALL FILE(1,0.0)
      GOTO 3000
      STOP
      END
```

Appendix 8

CROSCAL Calculates total ionisation cross section

```
C
C CROSCAL
C READS IN TOF SPECTRA FROM DISK, USING FILE SUBPROGRAM
C PLOTS TOF SPECTRA USING PLOT55 AND PLOT7 SUBPROGRAMS
C CORRECTS FOR HIGH COUNT RATE
C AND CALCULATES TRIPLET AND SINGLET CROSS SECTIONS
C
      DATA Y,H/'Y','H'/
      COMMON FNAM(3),COM(18),PAR(18),VAL(10),DAT(520)
      DIMENSION SUM(180),KTF(11),VEL(180),LX(11),DIV(180)
      DIMENSION DSUM(180),ADSUM(180),DDIV(180),VELO(180)
3000   CONTINUE
C
C SCROLL AND PLOT ARE BOTH OPTIONAL
C
      TYPE 992
992    FORMAT( ' IS SCROLL REQUIRED? ' )
      ACCEPT 7,SCRO
      TYPE 991
991    FORMAT( ' IS A PLOT REQUIRED? ' )
      ACCEPT 7,GRPH
13     FORMAT(7F10.4)
8      FORMAT(3I6)
      TYPE 2000
C
C ALL FOUR TOF SPECTRA ARE RED INTO THE COMPUTER Q REPRESENTS THE QUENCH LAMP
C
2000   FORMAT( ' INPUT FILES IONS QON, IONS QOFF,
     1 METS QON, METS QOFF ' )
      DO 2500 NCYC=0,90,30
1                TYPE 2
2                FORMAT(' WHICH MEMORY SET? '$)
                 ACCEPT 7,FNAM
                 CALL FILE(0,0.0)
C
C COM (COMMENTS),PAR  (PARAMETERS)  AND VAL ARE ARRAYS WHICH CONTAIN INFORMATION  ABOUT
C THE TOF SPECTRA
C
                 TYPE 7,COM
7          FORMAT(18A4)
           TYPE 7,PAR
5          TYPE 9,VAL
           ACCEPT 7,KR
           IF(SCRO.NE.Y)GOTO  88
           DO 80,I=1,512,10
           TYPE 8,I
80         TYPE 9,(DAT(J),J=I,I+9)
9          FORMAT(10F8.1)
88         IF(GRPH.NE.Y)GOTO  27
83         TYPE 45
45         FORMAT( ' SET THE MAX VALUE '$)
           ACCEPT 13,AMAX
           IF(AMAX.LE.1.0)AMAX=VAL(2)
           TYPE 68
68         FORMAT( ' SET THE GRAPHICS  (IEN,IG)  ' )
           ACCEPT 8,IEN,IG
84         CONTINUE
           CALL PLOT7(DAT,512,AMAX,IEN,IG,)
C
C A CORRECTION  FOR HIGH COUNT RATE CAN BE MADE
C
           TYPE 1000
1000       FORMAT( ' IS A CORRECTION  FOR HIGH COUNT RATE REQUIRED ' )
```

```
        ACCEPT 7,ATEL
        IF(ATEL.NE.Y)GOTO  27
C
C DAT(I) =      THE NUMBER OF COUNTS IN CHANNEL I
C IOF    =      THE PHOTON PEAK CHANNEL
C TOTS   =      RUNNING TOTAL OF COUNTS
C CYCTO  =      THE NUMBER OF CYCLES IN WHICH THE DATA WAS C RECORDED (DIVIDED BY 10^4)
C CMIS   =      THE NUMBER OF CYCLES IN WHICH A CHANNEL COULD RECORD DATA
C
        TYPE 1010
1010    FORMAT( ' TYPE IN ZERO OFFSET (INTEGRAL) ' )
        ACCEPT 8,IOF
        TOTS=0.0
        DO 1015 I=1,IOF+10
        TOTS=TOTS+DAT(I)
1015    CONTINUE
        TYPE 1020
1020    FORMAT( ' HOW MANY CYCLES ' )
        ACCEPT 13,CYCTO
        IOF=IOF+10
        CYCTO=CYCTO*10000
        CMIS=0.0
        TNEW=0.0
        DO 1100 I=IOF,512
                TOTS=TOTS+DAT(I)
                CMIS=CYCTO-TOTS
                DAT(I)=DAT(I)*CYCTO/CMIS
                TNEW=TNEW+DAT(I)
                TYPE 9,  TOTS  ,TNEW
1100    CONTINUE
C
C THE TOTAL NUMBER OF COUNTS IN THE TOF SPECTRUM BEFORE AND AFTER CORRECTION ARE
C DISPLAYED
C
        TYPE 1110
1110    FORMAT( ' OLD TOTAL, NEW TOTAL ' )
        TYPE 9,   TOTS,   TNEW
        GOTO 5
27      TYPE 89
C
C AT THIS POINT THE PROCEDURE MAY BE TERMINATED
C
89      FORMAT( ' CONTINUE ? ' )
        ACCEPT 7,ADDN
        INCI=0
        IF(ADDN.NE.Y)GOTO  177
        TYPE 106
106     FORMAT( ' TYPE IN THE ZERO OFFSET(INTEGRAL)  ' )
        ACCEPT 8,IOF
C
C TOF BIN LIMITS KTF(I) ARE READ FROM THE DATSET SUBPROGRAM TWO SETS OF KTF(I) EXIST L (LOW
C VELOCITY) AND H (HIGH VELOCITY).  THE KTFE VALUES ARE THEN CORRECTED FOR THE DIFFERENT
C PATH LENGTHS BETWEEN THE CHOPPER WHEEL AND THE METASTABLE ATOM AND ION DETECTORS
C

        TYPE 107
107     FORMAT( ' IS THIS A METASTABLE T.O.F. DISTRIBUTION? ' )
        ACCEPT 7,AMET
109     CALL DATSET(L,KTF)
        GOTO 102
101     CALL DATSET(H,KTF)
102     DO 103 I=1,11
C
C KTF VALUES ARE CONVERTED FROM MICRO SECONDS TO BIN NUMBER
C
        LX(I)=IFIX(FLOAT(KTF(I))/3.0)
103     CONTINUE
        IF(AMET.NE.Y)GOTO  119
        DO 108,I=1,11
```

```
108       LX(I)=IFIX(FLOAT(LX(I))*101.4/80.0)
119       IF(INCI.LT.20)  GOTO 105
          DO 104 I=1,11
          LX(I)=LX(I)-5
104       CONTINUE
105       CONTINUE
C
C THE TRIPLET VELOCITY SPECTRA ARE FIRST CALCULATED
C THE PHOTON PEAK CHANNEL IS SUBTRACTED TO GIVE THE ZERO OFFSET
C SUM   =         THE NUMBER OF COUNTS PER CHANNEL IN A GIVEN BIN
C DSUM  =         THE ERROR ON SUM
C VEL   =         THE WEIGHTED MEAN VELOCITY FOR A GIVEN BIN
C
          DO 110,I=1,11
          LX(I)=LX(I)+IOF-1
110       CONTINUE
          DO 120,I=1,10
                    LX(I)=LX(I)+1
                    SUM(I+INCI+NCYC)=0.0
                    TOP=0.0
                    BOT=0.0
                    VEL(I+INCI+NCYC)=0.0
                    DO 115,J=LX(I),LX(I+1)
                    SUM(I+INCI+NCYC)=SUM(I+INCI+NCYC)+DAT(J)
                    TOP=(FLOAT(J-IOF)*DAT(J))+TOP
                    BOT=BOT+DAT(J)
115                 CONTINUE
                    SUM(I+INCI+NCYC)=SUM(I+INCI+NCYC)/FLOAT(LX(I+1)-LX(I)+1)
                    DSUM(I+INCI+NCYC)=SQRT(SUM(I+INCI+NCYC))
                    DSUM(I+INCI+NCYC)=DSUM(I+INCI+NCYC)/SQRT(FLOAT(LX(I+1)+1-LX(I)))
                    AVTOF=(3.0*TOP)/BOT
                    IF(AMET.NE.Y)VEL(I+INCI+NCYC)=860.0/AVTOF
                    IF(AMET.EQ.Y)VEL(I+INCI+NCYC)=1090.0/AVTOF
120       CONTINUE
          INCI=INCI+10
          IF(INCI.LT.30)  GOTO 101
C
C SUBTRACT ANY BACKGROUND
C
          TYPE 121
121       FORMAT( ' IS A BACKGROUND SUBTRACTION REQUIRED? ' )
          ACCEPT 7,BGB
          IF(BGB.NE.Y)GOTO  129
          BGD=0.0
          DO 122 I=480,510
122       BGD=BGD+DAT(I)
          TYPE 123
123       ACCEPT13,AFT
C
C THE TRIPLET VELOCITY SPECTRA ARE SHOWN ON THE VDU
C
          DO 124 J=1,30
124       SUM(J+NCYC)=SUM(J+NCYC)-(BGD/30.0)
129       TYPE 131
131       FORMAT( ' COUNTS , ERROR , VEL  ' )
          DO 132,I=1,30
132       TYPE 9,SUM(I+NCYC),DSUM(I+NCYC),VEL(I+NCYC)
2500    CONTINUE
C
C CALCULATE THE SINGLET VELOCITY SPECTRUM
C
      ACCEPT 7,KR
      TYPE 2509
2509    FORMAT( ' SINGLET SPECTRA IONS THEN METS ' )
      DO 2700 IL=1,2
           ACCEPT 7,KR
              IF(IL.EQ.2)GOTO  2510
              IDIFF=120
              ISTOP=30
```

```
            ISTART=1
            GOTO 2600
2510        IDIFF=90
          ISTOP=90
          ISTART=61
2600        DO 2650 I=ISTART,ISTOP
            SUM(I+IDIFF)=SUM(I+30)-SUM(I)
C
C THE ERROR DSUM IS CALCULATED FROM THE COMBINATION IN QUADRETURE OF THE ERRORS OF C THE
PARENT TOF SPECTRA
C
    DSUM(I+IDIFF)=SQRT(DSUM(I+30)**2+DSUM(I)**2)
C
C AN APPROXIMATE VELOCITY IS CALCULATED, BUT BECAUSE THE VELOCITY DISTRIBUTION OF
C SINGLET AND TRIPLET METASTABLE ATOMS IS DIFFERENT THE VELOCITY MUST BE CALCULATED BY
C PRODUCING ION AND METASTABLE TOF SINGLET SPECTRA USING SUBSING AND RE-ENTERING THEM
C IN THIS PROGRAM IN THE POSITION OF THE METASTABLE ATOM AND ION TOF SPECTRA WITH QUENCH
C LAMP ON
C
        VEL(I+IDIFF)=(VEL(I+30)+VEL(I))/2
2650      CONTINUE
C
C THE SINGLET TOF SPECTRA ARE DISPLAYED ON THE VDU
C
        TYPE 2666
2666      FORMAT( ' COUNTS , ERROR , VEL ' )
        DO 2675 I=1,30
        TYPE 9,SUM(I+IDIFF),DSUM(I+IDIFF),VEL(I+IDIFF)
2675      CONTINUE
        ACCEPT 7,KR
2700  CONTINUE
C
C CALCULATE CROSS SECTIONS
C
    TYPE 140
140   FORMAT( ' CROSS SECTIONS FIRST THE TRIPLET ' )
    DO 2800 IL=1,2
                ACCEPT 7,KR
                IF(IL.EQ.2)GOTO  2850
                ISTART=1
                ISTOP=30
                IDIFF=60
                GOTO 2855
2850            ISTART=121
                ISTOP=150
                IDIFF=30
2855            CONTINUE
C
C DIV    =      THE CROSS SECTION
C ADSUM  =      THE FRACTIONAL ERROR ON SUM
C DDIV   =      THE ERROR ON DIV
C VELO   =      THE MEAN VELOCITY
C
                DO 141,I=ISTART,ISTOP
                        DIV(I)=SUM(I)/SUM(I+IDIFF)
                        ADSUM(I+IDIFF)=DSUM(I+IDIFF)/SUM(I+IDIFF)
                        ADSUM(I)=DSUM(I)/SUM(I)
                        DDIV(I)=SQRT(ADSUM(I)**2+ADSUM(I+IDIFF)**2)*DIV(I)
                        VELO(I)=(VEL(I)+VEL(I+IDIFF))/2.0
141             TYPE 13,DIV(I),DDIV(I),VELO(I),VEL(I),VEL(I+IDIFF)
290             TYPE 300
C
C THE RESULTS CAN BE NORMALISED TO ABSOLUTE DATA
C
300             FORMAT( ' MULTIPLY UP THESE RESULTS? ' )
                ACCEPT 7,AMUL
                IF(AMUL.NE.Y)GOTO  130
                TYPE 350
350             FORMAT( ' BY WHAT FACTOR? ' )
```

```
                ACCEPT 13,AMULT
                DO 400,I=ISTART,ISTOP
                DIV(I)=DIV(I)*AMULT
                DDIV(I)=DDIV(I)*AMULT
400             TYPE 13,DIV(I),DDIV(I),VELO(I)
                GOTO 290
130             CONTINUE
                TYPE 159
C
C THE CROSS SECTION DATA CAN BE PRINTED OUT AS A PERMANENT RECORD
C
159             FORMAT( ' IS A PRINT OUT REQUIRED? ' )
                ACCEPT 7,PRIO
                IF(PRIO.NE.Y)GOTO  2800
                TYPE 161
161             FORMAT( ' TYPE IN ANY COMMENTS? ' )
                ACCEPT 77,ACOM
                PRINT 77,ACOM
77              FORMAT(A48)
                ICY=ISTART
164             PRINT 167
167             FORMAT( ' ' )
                PRINT 162
162             FORMAT( '   SET 1    ERR0R     VEL     SET2     ERROR
   1            SET/SET2  ERROR ' )
                PRINT 167
                DO 163 I=ICY,9+ICY
                PRINT 13,SUM(I),DSUM(I),VELO(I),SUM(I+IDIFF),
   1            DSUM(I+IDIFF),DIV(I),DDIV(I)
163             CONTINUE
                ICY=ICY+10
                IF(ICY.LT.ISTOP)GOTO  164
                PRINT 167
2800   CONTINUE
     TYPE 2900
2900   FORMAT( ' BEGIN AGAIN ? ' )
      ACCEPT 7,REA
      IF(REA.EQ.Y)GOTO  3000
C
C CLEAR ALL PLOTS FROM THE VDU
C
177    CALL PLOT55(2,512,511)
      STOP
      END
```

Appendix 9

CROSS2 Calculates the total cross section at a velocity read into the computer

```
C
C CROSS2
C READS IN TWO TOF SPECTRA FROM DISK, PLOTS IT USING PLOT55 AND PLOT7 SUBPROGRAMS
C CROSS SECTIONS ARE CALCULATED FROM TOF BIN RANGES ENTERED BY HAND
C
      DATA Y,H/'Y','H'/
      COMMON FNAM(3),COM(18),PAR(18),VAL(10),DAT(520)
      DIMENSION SUM(2),KTF(2),VEL(2),LX(2,2)
      DIMENSION DSUM(2),ADSUM(2)
      DIMENSION DATA(2,520),IOF(2)
3000   CONTINUE
C
C SCROLL AND PLOT ARE BOTH OPTIONAL
C
      TYPE 992
992    FORMAT( ' IS SCROLL REQUIRED? ' )
      ACCEPT 7,SCRO
      TYPE 991
991    FORMAT( ' IS A PLOT REQUIRED? ' )
      ACCEPT 7,GRPH
13     FORMAT(7F10.4)
8      FORMAT(3I6)
C
C LOAD TOF SPECTRUM FROM DISK
C
      TYPE 2000
2000   FORMAT( ' INPUT FILES IONS THEN METS, ' )
      DO 2500 NCE=1,2
1               TYPE 2
2         FORMAT(' WHICH MEMORY SET? '$)
          ACCEPT 7,FNAM
                CALL FILE(0,0.0)
          TYPE 7,COM
7         FORMAT(18A4)
          TYPE 7,PAR
5         TYPE 9,VAL
          ACCEPT 7,KR
          IF(SCRO.NE.Y)GOTO  88
C
C TYPE OUT DATA AND PLOT TOF SPECTRUM
C
          DO 80,I=1,512,10
          TYPE 8,I
80        TYPE 9,(DAT(J),J=I,I+9)
9         FORMAT(10F8.1)
88        IF(GRPH.NE.Y)GOTO  900
83        TYPE 45
45        FORMAT( ' SET THE MAX VALUE '$)
          ACCEPT 13,AMAX
          IF(AMAX.LE.1.0)AMAX=VAL(2)
          TYPE 68
68        FORMAT( ' SET THE GRAPHICS (IEN,IG)  ' )
          ACCEPT 8,IEN,IG
84        CONTINUE
          CALL PLOT7(DAT,512,AMAX,IEN,IG,)
900       CONTINUE
          DO 1100 I=1,512
          DATA(NCE,I)=DAT(I)
1100      CONTINUE
2500   CONTINUE
      TYPE 106
106    FORMAT( ' TYPE IN THE ZERO OFFSETS (INTEGRAL I,M) ' )
```

```
      ACCEPT 8,IOF(1)
      ACCEPT 8,IOF(2)
C
C READ THE RANGE OF HIGH AND LOW RANGE OF THE TOF BIN AND CORRECT TIME BIN FOR THE
C DIFFERENCE IN PATH LENGTH BETWEEN THE CHOPPER WHEEL AND THE METASTABLE ATOM AND ION
C DETECTOR
C
109    TYPE 107
107    FORMAT( ' INPUT TOF RANGES, LOW,HIGH ' )
      ACCEPT 8,KTF(1)
      ACCEPT 8,KTF(2)
102    DO 103 I=1,2
      LX(1,I)=IFIX(FLOAT(KTF(I))/3.0)
103    CONTINUE
      DO 108,I=1,2
108    LX(2,I)=IFIX(FLOAT(LX(1,I))*101.4/80.0)
      DO 104,J=1,2
      DO 110,I=1,2
      LX(J,I)=LX(J,I)+IOF(J)
110    CONTINUE
104    CONTINUE
C
C SUM   =       THE NUMBER OF COUNTS PER CHANNEL IN A GIVEN BIN
C DSUM  =       THE ERROR ON SUM
C VEL   =       THE WEIGHTED MEAN VELOCITY FOR A GIVEN BIN
C
        DO 120,I=1,2
        SUM(I)=0.0
        TOP=0.0
        BOT=0.0
        VEL(I)=0.0
        DO 115,J=LX(I,1),LX(I,2)
        SUM(I)=SUM(I)+DATA(I,J)
        TOP=(FLOAT(J-IOF(I))*DATA(I,J))+TOP
        BOT=BOT+DATA(I,J)
115     CONTINUE
        SUM(I)=SUM(I)/FLOAT(LX(I,2)-LX(I,1)+1)
        DSUM(I)=SQRT(SUM(I))
        DSUM(I)=DSUM(I)/SQRT(FLOAT(LX(I,2)+1-LX(I,1)))
        AVTOF=(3.0*TOP)/BOT
        IF(I.EQ.1)VEL(I)=860.0/AVTOF
        IF(I.NE.1)VEL(I)=1090.0/AVTOF
C
C SUBTRACT ANY BACKGROUND
C
        TYPE 121
121     FORMAT( ' IS A BACKGROUND SUBTRACTION REQUIRED? ' )
        ACCEPT 7,BGB
        IF(BGB.NE.Y)GOTO  129
        BGD=0.0
        DO 122 J=480,510
122     BGD=BGD+DATA(I,J)
        TYPE 123
123     FORMAT( ' MULTIPLY THE BACKGROUND BY WHAT FRACTION? ' )
        ACCEPT13,AFT
124     SUM(I)=SUM(I)-(BGD/30.0)*AFT
C
C THE VELOCITY SPECTRA ARE SHOWN ON THE VDU
C
129     TYPE 131
131     FORMAT( ' COUNTS , ERROR , VEL ' )
132     TYPE 9,SUM(I),DSUM(I),VEL(I)
120   CONTINUE
     ACCEPT 7,KR
C
C CALCULATE CROSS SECTION
C DIV   =       THE CROSS SECTION
C ADSUM         =       THE FRACTIONAL ERROR ON SUM
C DDIV  =       THE ERROR ON DIV
```

```
C VELO =        THE MEAN VELOCITY
C
      DIV=SUM(1)/SUM(2)
      ADSUM(2)=DSUM(2)/SUM(2)
      ADSUM(1)=DSUM(1)/SUM(1)
      DDIV=SQRT(ADSUM(1)**2+ADSUM(2)**2)*DIV
      VELO=(VEL(2)+VEL(1))/2.0
      TYPE 162
162    FORMAT( '   SET 1    ERR0R     VEL     SET2     ERROR
      1   SET/SET2   ERROR ' )
      TYPE 13,SUM(1),DSUM(1),VELO,SUM(2),
     1 DSUM(2),DIV,DDIV
163    CONTINUE
      TYPE 2900
2900   FORMAT( ' BEGIN AGAIN ? ' )
      ACCEPT 7,REA
      IF(REA.EQ.Y)GOTO  109
177    CALL PLOT55(2,512,511)
      STOP
      END
```

Appendix 10

TOFM1 Collects branching ratio data

```
C
C TOFM1
C COLLECTS 20 MASS SPECTRA USING THE CAMCUL SUBPROGRAM AT 10 DIFFERENT VELOCITIES, 10 WITH
C QUENCH LAMP ON AND 10 WITH THE QUENCH LAMP OFF. THE SPECTRA ARE RECORDED
C SYMULTANIOUSLY C THE TOTAL MASS SPECTRUM IS PLOTED USING THE PLOT55 AND PLOT7
C SUBPROGRAMS
C THE SPECTRA READ INTO 20 FILES USING THE FILE SUBROGRAM
C
      COMMON FNAM(3),COM(18),PAR(18),VAL(10),DAT(256)
      DIMENSION IPLT(256)
      DIMENSION DATT(20,256),VALT(20,10),SUF(20)
      DIMENSION ISTOR(500),JSTOR(500)
      DATA Y,SUF/'Y','1','2','3','4','5','6','7','8','9','10',
     1   '11','12','13','14','15','16','17','18','19','20'/
1     FORMAT(10I6)
2     FORMAT(18A4)
3     FORMAT(10F7.1)
      VAL(1)=256.0
4     DO 5 I=2,20
      VAL(I)=0.0
5     CONTINUE
      NREP=0
C
C THE 20 SPECTRA ARE STORED IN A TWO DIMENSIONAL ARRAY DATT(I,J) I IS THE CHANNEL NUMBER
C FROM C 1 TO 256 AND J IS THE SPECTRUM NUMBER. THE VALT(I,J) ARRAY CARRIES INFORMATION
C ABOUT THE SPECTRA
C
      DO 7 I=1,20
      VALT(I,1)=256.0
      DO 6 J=2,10
      VALT(I,J)=0.0
6     CONTINUE
      DO 7 J=1,256
      DATT(I,J)=0.0
7     CONTINUE
C
C THE PHOTOIONISATION PEAK (IN MICRO SECONDS) IS RED INTO THE COMPUTER AS A VELOCITY
C OFFSET AND THE MASS SPECTRUM OFF SET WHICH ALLOWS ALL MASS PEAKS UNDER EXAMINATION
C TO BE RECORDED
C
      TYPE 8
8     FORMAT(' VELOCITY OFFSET, MASS OFFSET? '$)
      ACCEPT 1,IOF
      ACCEPT 1,JOF
      VAL(4)=FLOAT(IOF)
      TYPE 10
C
C THE NUMBER OF START PULSES RECORDED PER CYCLE CAN BE VARIED TO ALLOW FREQUENT
C DISPLAY OF THE TOTAL MASS SPECTRA IN CONDITIONS OF LOW COUNT RATE, 1000 IS NORMAL
C
10    FORMAT(' NUMBER OF START PULSES? '$)
      ACCEPT 1,NRTT
      NEV=0
      NRPTS=1
      STRT=0.0
C
C THE SUM OF ALL INDIVIDUAL MASS SPECTRA IS RECORDED IN THE DAT ARRAY
C
      DO 12 I=1,256
      DAT(I)=0.0
12    CONTINUE
14    TYPE 16
16    FORMAT(' NUMBER OF CYCLES? '$)
```

```
      ACCEPT 1,NCYC
      NCYC=NCYC*2
17     DO 18 I=1,256
      IDAT(I)=0
      JDAT(I)=0
18     CONTINUE
      IQUEN=0
C
C FIRST RECORD DATA WITH THE QUENCH LAMP OFF
C
19        DO 36 IG=1,NCYC
24        VAL(9)=VAL(9)+FLOAT(NEV)
          CALL CAMAC(11,0,0)
          CALL CAMAC(8,0,0)
          CALL CAMAC(10,0,0)
          CALL CAMAC(0,20,0,26,)
          CALL CAMAC(0,20,0,17,7,8,)
          NEV=0
          DO 28 I=1,NRTT
25                CALL CAMAC(0,21,2,2,IL)
                  IF(IL.EQ.0)GOTO  25
                  CALL CAMAC(0,21,3,2,IL1)
                  CALL CAMAC(0,20,0,2,IL2)
                  IF(IL1.GT.1050.OR.IL1.LT.45)GOTO    28
                  IF(IL2.LT.2.OR.IL2.GT.512)GOTO    28
                  NEV=NEV+1
C
C ISTOR  =        VELOCITY
C JSTOR  =        MASS
C
                  ISTOR(NEV)=IL1
                  JSTOR(NEV)=IL2-JOF
28        CONTINUE
C
C VAL5   =        THE NUMBER OF START PULSES /100
C
          VAL(5)=VAL(5)+FLOAT(NRTT)/100.0
C
C SORT THE DATA INTO ONE OF TEN MASS SPECTRA DEPENDING  ON VELOCITY
C
          DO 35 I=1,NEV
                  K=ISTOR(I)-IOF
                  M=1
                  IF(K.GE.696)GOTO  30
                  M=2
                  IF(K.GE.472)GOTO  30
                  M=3
                  IF(K.GE.372)GOTO  30
                  M=4
                  IF(K.GE.315)GOTO  30
                  M=5
                  IF(K.GE.266)GOTO  30
                  M=6
                  IF(K.GE.216)GOTO  30
                  M=7
                  IF(K.GE.170)GOTO  30
                  M=8
                  IF(K.GE.123)GOTO  30
                  M=9
                  IF(K.GE.84)GOTO  30
                  M=10
                  IF(K.GE.45)GOTO  30
                  GOTO 35
30                N=IFIX(JSTOR(I))
                  IF(N.LT.1.OR.N.GT.256)GOTO    35
                  IF(IQUEN.EQ.0)GOTO  31
                  M=M+10
31                DATT(M,N)=DATT(M,N)+1.0
                  IF(DATT(M,N).LE.VALT(M,2))GOTO    32
```

```
C
C VALT(M,2)     =       THE MAXIMUM NUMBER OF COUNTS IN ONE CHANNEL OF SPECTRUM M
C VAL2          =       THE MAXIMUM NUMBER OF COUNTS IN THE COMBINED SPECTRUM
C VALT(M,3)     =       THE TOTAL NUMBER OF COUNTS
C
                VALT(M,2)=DATT(M,N)
                IF(DATT(M,N).LE.VAL(2))GOTO   32
                VAL(2)=DATT(M,N)
32              VALT(M,3)=VALT(M,3)+1.0
                DAT(N)=DAT(N)+1
35      CONTINUE
C
C WHEN IQUEN = 0 THE LAMP IS OFF WHEN IQUEN = 1 THE LAMP IS TURNED ON
C
        IF(IQUEN.EQ.1)GOTO  355
        IQUEN=IQUEN+1
        GOTO 360
355     IQUEN=0
360     TYPE 1,NRPTS
        IF(IQUEN.EQ.0)GOTO  1500
C
C    TURN THE QUENCH LAMP ON
C
        GOTO 1010
1002    TYPE 1004
1004    FORMAT( ' LAMP HAS FAILED TO STRIKE ' )
        CALL CAMAC(0,8,1,16,0,0)
        CALL CAMAC(0,4,0,10,)
C
C LAMP RELAY ON
C
1010    CALL CAMAC(0,8,1,16,10200,0)
        DO 1050 K=1,500
1050    CONTINUE
C
C TESLA RELAY ON
C
        CALL CAMAC(0,9,1,16,20400,0)
        DO 1149 K=1,500
1149    CONTINUE
C
C TURN TESLA RELAY OFF
C
        CALL CAMAC(0,9,1,16,0,0)
C
C WAIT
C
        DO 1100 K=1,100
        DO 1150 I=1,500
1150    CONTINUE
1100    CONTINUE
        CALL CAMAC(0,4,0,10)
        CALL CAMAC(0,4,0,26)
C
C LOOK AT LAMP WITH PHOTODIODE
C
        CALL CAMAC(0,4,0,8,DL,DH,IQ,)
        TYPE 1,IQ
C
C IF THE LAMP HAS NOT STRUCK REPEAT PROCESS AGAIN
C
        IF(IQ.EQ.1)GOTO  1002
                TYPE 1160
1160  FORMAT( ' LAMP ON ' )
      DO 1170 I=1,100
      DO 1165 K=1,500
1165   CONTINUE
1170   CONTINUE
C
```

```
C RECORD DATA WITH QUENCH LAMP ON
C
      GOTO 36
1500   CONTINUE
C
C      TURN LAMP OFF
C
      GOTO 1800
1520   CALL CAMAC(0,4,0,10,)
      TYPE 1525
1525   FORMAT( ' LAMP HAS FAILED TO GO OFF ' )
      CALL CAMAC(0,8,1,16,0,0)
1800   CALL CAMAC(0,8,1,16,10200,0)
      DO 1528 I=1,100
      DO 1526 K=1,500
1526   CONTINUE
1528   CONTINUE
      CALL CAMAC(0,4,0,10,)
      CALL CAMAC(0,4,0,26)
C
C LOOK AT LAMP WITH PHOTODIODE
C
      CALL CAMAC(0,4,0,8,DL,DH,IQ,)
      TYPE 1,IQ
C
C IF THE LAMP HAS FAILED TO GO OFF THEN REPEAT THE PROCEDURE
C
      IF(IQ.EQ.0)GOTO  1520
      TYPE 1560
1560   FORMAT( ' LAMP OFF ' )
      DO 1565 I=1,100
      DO 1563 K=1,500
1563   CONTINUE
1565   CONTINUE
36     CONTINUE
      NREP=NREP-1
      IF(NREP.GT.0)GOTO  19
C
C TYPE AND PLOT DATA ON VDU
C
      DO 37 I=1,256,10
      TYPE 3,(DAT(J),J=I,I+9)
37     CONTINUE
      IF(VAL(2).EQ.0.0)VAL(2)=0.1
      SCAL=235.0/VAL(2)
      DO 41 I=1,256
      IPLT(I)=IFIX(DAT(I)*SCAL+0.5)
41     CONTINUE
      CALL PLOT55(9,,)
      CALL PLOT55(10,,)
      TYPE 3,VAL
      CALL PLOT55(1,0)
      CALL PLOT55(2,553,511)
      CALL PLOT55(4,1,)
      CALL PLOT55(7,,)
      CALL PLOT55(3,-256,IPLT)
      ACCEPT 2,KR
      CALL PLOT55(2,512,511)
50     CONTINUE
54     TYPE 55
55     FORMAT(' MORE DATA(2),FILE(3)?  '$)
      ACCEPT 1, IND
      IF(IND-2)57,57,60
57     TYPE 58
58     FORMAT(' NUMBER OF REPEATS ? '$)
      ACCEPT 1,NREP
      GOTO 19
C
C TO FILE THE DATA A SINGLE NAME IS ENTERED AND TTHE FILES ARE AUTOMATICALLY  NUMBERED
```

```
C FILE1, FILE2..TO FILE20
C
60    TYPE 65
65    FORMAT(' FILENAME? '$)
      ACCEPT 2,FNAM
C
C IF THE RETURN KEY OPERATES TWICE AND NO FILE NAME IS ENTERED, THE FILE MAY BE RENAMED
C
      TYPE 69
69    FORMAT( ' CHANGE THE NAME ? ' )
      ACCEPT 2,FC
      IF(FC.EQ.Y)GOTO60
      TYPE 70
70    FORMAT(' COMMENTS(UP TO 72 LETTERS)?')
      ACCEPT 2,COM
      TYPE 75
75    FORMAT(' FIXED PARAMETERS(UP TO 72 LETTERS)?')
      ACCEPT 2,PAR
C
C VAL(7)          =       THE NUMBER OF COUNTS RECORDED WITH THE QUENCH LAMP OFF
C VAL(8)          =       THE NUMBER OF COUNTS RECORDED WITH THE QUENCH LAMP ON
C
      DO 77 I=1,10
      VAL(7)=VAL(7)+VALT(I,3)
77    CONTINUE
      DO 79 I=11,20
      VAL(8)=VAL(8)+VALT(I,3)
79    CONTINUE
      DO 82 I=1,20
                FNAM(2)=SUF(I)
                TYPE 2,FNAM,FNAM(2)
                DO 80 J=1,256
                DAT(J)=DATT(I,J)
80              CONTINUE
C
C VAL(2)          =       THE MAXIMUM NUMBER OF COUNTS IN ANY CHANNEL
C VAL(3)          =       THE TOTAL NUMBER OF COUNTS IN THE MASS SPECTRUM
C VAL(10)         =       THE NUMBER OF THE SPECTRUM (1-20)
C
                VAL(2)=VALT(I,2)
                VAL(3)=VALT(I,3)
                VAL(10)=I
                CALL FILE(1,0.0)
82    CONTINUE
      TYPE 85
85    FORMAT(' RESTART(Y OR N)? '$)
      ACCEPT 2,ANS
      IF(ANS.EQ.Y)GOTO  4
C
C IN CASE THE COMPUTER MAKES A MISTAKE CREATING THE FILES THEY CAN BE REMADE
C
      TYPE 86
86    FORMAT( ' REMAKE FILES ' )
      ACCEPT 2,ANS
      IF(ANS.EQ.Y)GOTO  60
      STOP
      END
```

Appendix 11

BRCALC Calculates the branching ratios

```
C
C          BRCALC
C        READS IN 10 MASS SPECTRA EACH AT DIFFERENT VELOCITY, USING THE FILE SUBPROGRAM
C          THE MASS VELOCITY RANGES ARE DEFINED BY THE DATER SUBPROGRAM
C          THE SPTL SUBPROGRAM DEFINES THE MASS RANGE FOR THE PARTICLES DESIRED
C          THE NUMBER OF EACH PARTICLE PRESENT IN A MASS SPECTRUM IS CALCULATED AS IS THE
C          PERCENTAGE OF THE TOTAL NUMBER OF COUNTS WHICH IT REPRESENTS
C
      DATA BGND,VELO/'BGND','VELOCITY'/
      DATA Y,SUF/'Y','1','2','3','4','5','6','7','8','9','10',
     1     '11','12','13','14','15','16','17','18','19','20'/
      DIMENSION APC(10,8),MAX(8),MIN(8),PTL(8),BGD(10),VEL(10)
      DIMENSION AVEL(10),KTF(11)
      DIMENSION BDAT(512),ERR(10,8),AX(11),SUF(20),ATOT(10,8),TTOT(10)
      COMMON FNAM(3),COM(18),PAR(18),VAL(10),DAT(512)
1     FORMAT (2F6.2)
2     FORMAT(2I6)
C
C DEFINE THE TEN TOF RANGES
C
      TYPE 300
300    FORMAT( ' BRANCHING RACIOS FOR SINGLETS ' )
      CALL DATER(HLDAT,KTF)
      DO 500,I=1,11
      AX(I)=FLOAT(KTF(I))
500    CONTINUE
1      TYPE 4
C
C READ THE SET OF TEN MASS SPECTRA FROM DISK AND THE NUMBER OF PTLS TO BE USED.
C
4     FORMAT ( ' WHICH MEMORY SET? '$)
      ACCEPT 7,FNAM(1)
7     FORMAT(18A4)
9     FORMAT(10F8.1)
      TYPE 14
      DO 111,I=1,10
      DO 111,J=1,8
      ATOT(I,J)=0.0
111    CONTINUE
C
C A MAXIMUM OF 8 PARTICLES MAY BE USED, AND ARE REPRESENTED BY ABREVIATIONS SUCH AS AN2O,
C ANO ETC
C
14     FORMAT( ' HOW MANY PTLS ARE REQUIRED? ' )
      ACCEPT 2,IN
13     TYPE 15
15     FORMAT( ' WHAT PARTICLES ' )
      IG=0
C
C THE SUBROUTINE SPTL IS USED TO GIVE THE PREDETERMINED MASS RANGES OF THE PARTICLES
C FOR EACH PARTICLE THE RANGE IS TYPED IN THE FORM OF THE MAX AND MIN CHANNEL NUMBER
C
      DO 17,I=1,IN
      ACCEPT 7,PTL(I)
      CALL SPTL(PTL(I),MAX(I),MIN(I))
      TYPE 2,MAX(I),MIN(I)
17     CONTINUE
      DO 61,I=1,10
              TYPE 2,I
               FNAM(2)=SUF(I)
               CALL FILE(0,0.0)
               PEAK=0.0
               BGD(I)=0.0
```

```
            DO 68,K=1,IN
                        ATOT(I,K)=0.0
C
C THE MIN AND MAX VALUES ARE USED TO FIND THE NUMBER OF EACH PARTICLE IN EACH VELOCITY
C RANGE
C
                        DO 60,J=MIN(K),MAX(K)
                        ATOT(I,K)=ATOT(I,K)+DAT(J)
60                      CONTINUE
                        TTOT(I)=VAL(3)
                        IF(IN.EQ.1)GOTO  68
C
C BGD REPRESENTS  THE NO.OF BACKGROUND  COUNTS PER CHANNEL
C
68              CONTINUE
                DO 61,J=160,240
                BGD(I)=BGD(I)+DAT(J)
61    CONTINUE
      IF(IN.EQ.1)GOTO  21
      TYPE 56
56    FORMAT( ' IS A BACKGROUND  SUBTRACTOIN  REQUIRED? ' )
      ACCEPT 7,REA
      IF(REA.NE.Y)GOTO  54
      DO 71,I=1,10
      DO 71,K=1,IN
      ATOT(I,K)=ATOT(I,K)-BGD(I)*FLOAT(MAX(K)-MIN(K))/80.0
71    CONTINUE
54    CONTINUE
      TYPE 7,COM
      TYPE 7,FPAR
      TYPE 9,(VAL(I),I=1,10)
      ACCEPT 7,KR
C
C TYPE OUT THE NAMES PF EACH PTL AND THE
C NUMBERS OF EACH PTL IN EACH VEL RANGE
C
      IF(IN.GT.7)IZ=4
      IF(IN.LE.7)IZ=IN
      IV=1
107   TYPE 3,(PTL(I),I=IV,IZ),BGND,VELO
3     FORMAT(10A8)
      DO 78,I=1,10
      VEL(I)=840.0/((AX(11-I)+AX(12-I))/2.0)
      AVEL(I)=ALOG10(VEL(I))
      BGD(I)=BGD(I)/80.0
      TYPE 9,(ATOT(I,K),K=IV,IZ),BGD(I),VEL(I)
      TOT=0.0
      DO 84,K=1,IN
      TOT=TOT+ATOT(I,K)
84    CONTINUE
      DO 85,K=1,IN
      APC(I,K)=ATOT(I,K)*100.0/TOT
      IF(ATOT(I,K).EQ.0.0)GOTO   101
      ERR(I,K)=APC(I,K)*SQRT(ATOT(I,K))/ATOT(I,K)
      GOTO 85
101   ERR(I,K)=0.0
85    CONTINUE
78    CONTINUE
      IF(IV.GT.1)GOTO  109
      IF(IN.LE.7)GOTO  109
      ACCEPT 7,KR
      IV=5
      IZ=IN
      GOTO 107
109   ACCEPT 7,KR
C
C TYPE OUT THE PERCENTAGE  OF THE TOTAL COUNTS
C THAT IS DUE TO EACH PTL.
C
```

```
      TYPE 89
89     FORMAT( ' THE PERCENTAGES  OF EACH PTL ARE: ' )
5      FORMAT(6(A8,'    ERROR'))
      IF(IN.GT.4)KN=4
      IF(IN.LE.4)KN=IN
      TYPE 5,(PTL(I),I=1,KN)
      TYPE 79
      DO 83,I=1,10
      TYPE 10,((APC(I,K),ERR(I,K)),K=1,KN)
10     FORMAT(10(F6.1,'  |'))
83     CONTINUE
      IF(IN.LE.4)GOTO  104
      ACCEPT 7,KR
      TYPE 5,(PTL(I),I=5,IN)
      TYPE 79
      DO 103,I=1,10
      TYPE 10,((APC(I,K),ERR(I,K)),K=5,IN)
103    CONTINUE
104    CONTINUE
      GOTO 76
67     CONTINUE
21     TYPE 9,(ATOT(J,1),J=1,10)
76     CONTINUE
      TYPE 57
57     FORMAT(' RESTART(Y  OR N)? '$)
      ACCEPT 2,ANS
      IF(ANS.EQ.Y)GOTO  1
      STOP
      END
```

Appendix 12

Subprogram OLTP defines the interaction potential according to the theory of Olsen (1972), and can be addapted for use with singlet or triplet cases.

```
C
C     OLTP 5/4/90
C     OLSEN POTENTIAL FOR TRIPLET, OR SINGLET
C     WHEN COMPILED CALLED FVTOT
C     FUNCTION PROGRAM
C
      FUNCTION  FVTOT(R)
C
C        THE SHIELDING LENGTHS ARE GIVEN AS
C
      CM=0.98
      CK=0.057
      CL=0.18
C
C     CAB    =226 FOR TRIPLET
C            =325 FOR SINGLET
      CAB=226.
      ECS=R/CM
      IF(ECS.GE.88.)  THEN
      XCS=0.0
      ELSE
      XCS=EXP(-ECS)
      END IF
      R1=R/CM
      IF(R1.GE.88.)  THEN
      R1=0.0
      ELSE
      R1=8*EXP(-R1)
      END IF
      R2=R/CL
      IF(R2.GE.88.)  THEN
      R2=0.0
      ELSE
      R2=8*EXP(-R2)
      END IF
      R3=R/CK
      IF(R3.GE.88.)  THEN
      R3=0.0
      ELSE
      R3=2*EXP(-R3)
      END IF
      V1=2/R*(R1+R2+R3)
      V2=CAB/R**6
      V3=1-XCS*(1+ECS+ECS**2/2+ECS**3/6+ECS**4/24+ECS**5/120)
      VTOT=V1-V2*V3
      FVTOT=VTOT
      RETURN
      END
```

Appendix 13

Subprogram BRUTRP defines the interaction potential according to the work of Brutschy et al (1976)

```
C
C     BRUTRP 1976
C
      FUNCTION FVTOT(R)
      R1=4.6
      SM=0.93
      SL=0.18
      SK=0.057
      R2=5.0
      A1=-0.499
      A2=-2.35
      A3=-4.48
      A4=-4.08
      RMIN=10.7
      EPS=0.0037
      R4=1.5*RMIN
      R3=1.2*RMIN
      B1=-2.66 E-3
      B2=7.17 E-4
      B3=1.59 E-5
      B4=-5.84 E-5
C
C     DETERMINE V(R)
C
C     R LT 4.6 IMPLIES V(R)= SHIELDED COULOMB
C
      IF(R.LT.R1)THEN
       IF(R/SK.GE.44.)THEN
       RMK=0.0
       ELSE
       RMK=EXP(-R/SK)
       END IF
       IF(R/SL.GE.44.)THEN
       RML=0.0
       ELSE
       RML=EXP(-R/SL)
       END IF
      VTOT=2*27.21/R*(8*EXP(-R/SM)+8*RML+2*RMK)
      ELSE
C
C     IF R IS LT R2=5 IMPLIES VTOT=EXPONENTIAL SPLINE
C
      IF(R.LE.R2) THEN
      VTOT=EXP(A1+(R-R1)*(A2+(R-R2)*(AB+(R-R1)*A4)))
      ELSE
C
C     R LT 12.84=1.2*RMIN IMPLIES VTOT=MORSE
C
      IF(R.LE.R3)THEN
      IF(R.LE.5.37)THEN
      BETA=3.77*(1.86-0.86*EXP(-1.3*(R-5.37)**2))
      ELSE
      BETA=3.77
      END IF
      E=EXP(BETA*(1.-R/RMIN))
      VTOT=EPS*E*(E-2.)
      ELSE
C
C     IF R LT R4=16.05=1.5*RMIN IMPLIES VTOT=SPLINE
      IF(R.LE.R4)THEN
      VTOT=B1+(R-R3)*(B2+(R-R4)*(B3+(R-R3)*B4))
      ELSE
```

```
C
C     IF R GT R4 THEN VTOT=VAN DER WALL
C
      VTOT=-6173/R**6
      END IF
      END IF
      END IF
      END IF
C
C     CONVERT VTOT FROM EV TO AU
C
      FVTOT=VTOT
      RETURN
      END
```

Appendix 14

Subprogram SISKA defines the interaction potential for Ar + He(2^3S) according to the work of Siska (1979)

```
C
C   SISKA REAL PARTS OF POTENTIALS
C   SIMILAR FOR BOTH SINGLET AND TRIPLET
C
      FUNCTION FVTOT(R)
C
C   CONSTANTS DEFINED FOR TRIPLET POTENTIAL
C
      EPSTR=0.05762
      RMSTR=5.811
      B1STR=7.108
      BSTR2=5.523
      C6=3.04 E3
      C8=5.34 E4
      C10=1.224 E7
      R1STR=6.4347
      R2STR=9.8787
      EPPLS=2.673
      RMPLS=2.855
      B1PLS=3.942
      C4=273
      R1PLS=3.2843
      R2PLS=5.71
      R0=4.728
      D=0.7142
      B1S=-4.60960008E-2
      B2S=1.18563902E-2
      B3S=9.83231585E-4
      B4S=-9.59378493E-4
      B1P=-2.13898993
      B2P=0.77593273
      B3P=-0.43253151
      B4P=7.70151019E-2
C
C    CONVERT R FROM AU TO ANGSTROMS
C
     R=R*0.52917706
C
C   CALCULATE VTOT AS A FUNCTION OF R
C
C   IF R LESS THAN R1STR IMPLIES VSTR= A MORSE POTENTIAL
C
      IF(R.LE.R1STR)  THEN
      IF(R.LE.RMSTR)  THEN
      ZSTR=EXP(-B1STR*(R/RMSTR-1.))
      ELSE
      ZSTR=EXP(-B2STR*(R/RMSTR-1.))
      END IF
      VSTR=EPSTR*ZSTR*(ZSTR-2.)
      ELSE
C
C   IF R LESS THAN R2STR IMPLIES VSTR= SPLINE INTERPOLATION
C
      IF(R.LT.R2STR)THEN
      VSTR=B1S+(R-R1STR)*(B2S+(R-R2STR)*(B3S+(R-R1STR)*B4S))
      ELSE
C
C   R GREATER THAN R2STR IMPLIES VSTR= VAN DER WALL
C
C
      VSTR=-C6*R**(-6)-C8*R**(-8)-C10*R**(-10)
```

```
      END IF
      END IF
C
C   DETERMINE VPLS
C
C   IF R LESS THAN R1PLS IMPLIES VPLS= MORSE POTENTIAL
C
      IF(R.LE.R1PLS)THEN
      ZPLS=EXP(-B1PLS*(R/RMPLS-1.))
      VPLS=EPPLS*ZPLS*(ZPLS-2.)
      ELSE
C
C   IF R LESS THAN R2PLS IMPLIES VPLS= SPLINE INTERPOLATION
C
      IF(R.LT.R2PLS)THEN
      VPLS=B1P+(R-R1PLS)*(B2P+(R-R2PLS)*(B3P+(R-R1PLS)*B4P))
      ELSE
C
C   IF R GREATER THAN R2PLS IMPLIES VPLS=VAN DER WALL
C
      VPLS=-C4*R**(-4)
      END IF
      END IF
C
C   DETERMINE SWITCHING FUNCTION
C
      FR=(1.+EXP((R0-R)/D))**(-1)
      FVTOT=(1.-FR)*VPLS+FR*VSTR
      FVTOT=FVTOT*1.59477  E-3
C
C    RETURN R TO AU
C
     R=R/0.52917706
      RETURN
      END
```

Appendix 15

Subprogram HAB77 defines the interaction potential according to the work of Haberland and Schmidt (1977)

```
C
C     HAB77
C     CALCULATES V(R) FOR A RANGE OF R
C
      FUNCTION FVTOT(R)
C     SHIELDING LENGTHS
      FM=0.93
      FL=0.18
      FK=0.057
C     FIRST SPLINE PARAMETERS
      A0=-0.654
      A1=-2.49
      A2=-5.27
      A3=5.52
C     SECOND SPLINE PARAMETERS
      B0=-1.94E-3
      B1=4.44E-4
      B2=-1.06E-4
      B3=8.84E-6
      R1=4.8
      R2=5.15
C
C     R LT 4.8 IMPLIES V(R)= A SHIELDED COULOMB
C
      IF (R.LT.4.8) THEN
      VA=8*EXP(-1*R/FM)
      VB=8*EXP(-1*R/FL)
      VC=2*EXP(-1*R/FK)
      VTOT=(VA+VB+VC)*2*27.21/R
      ELSE IF(R.LT.5.15) THEN
C
C     R LT 5.15 IMPLIES V(R)= EXPONENTIAL SPLINE
C
      VTOT=EXP(A0+(R-R1)*(A1+(R-R2)*(A2-(R-R1)*A3)))
      ELSE IF(R.LT.12.84) THEN
C
C     R LT 12.84 IMPLIES V(R)= DOUBLE MORSE
C
C
C     FIRST MORSE
C
      IF (R.LT.5.96) THEN
      X=R
      BETA1=5.44*(0.873+0.127*EXP(-0.4*(R-5.96)**2))
      ELSE IF(R.LT.6.7) THEN
      X=R
      BETA1=5.44
      ELSE IF(R.LT.8.7) THEN
      X=R-0.43*SIN((R-6.71)/1.27)
      BETA1=5.44
      ELSE
      X=R-0.43*EXP(-0.85*(R-8.7)**2)
      BETA1=5.44
      END IF
      R1=10.703
      D1=0.00347
      E1=EXP(BETA1*(1-X/R1))
      V1=D1*E1*(E1-2)
C
C     SECOND MORSE
C
```

```
      IF(R.LT.5.63)  THEN
      X=R
      BETA2=8.23*(0.668+0.332*EXP(-2*(R-5.63)**2))
      ELSE IF(R.LT.6.71)  THEN
      X=R
      BETA2=8.23
      ELSE IF(R.LT.8.7)  THEN
      X=R-0.43*SIN((R-6.71)/1.27)
      BETA2=8.23
      ELSE
      X=R-0.43*EXP(-0.85*(R-8.7)**2)
      BETA2=8.23
      END IF
      R2=5.33
      D2=0.549
      E2=EXP(BETA2*(1-X/R2))
      V2=D2*E2*(E2-2)
      VTOT=V1+V2
      ELSE IF(R.LT.16.055)  THEN
C
C     R LT 1.5*R1  (R1=10.703)  IMPLIES  V(R)=  CUBIC SPLINE
C
      R1=10.703
      VP=B1+(R-1.5*R1)*(B2+(R-1.2*R1)*B3)
      VTOT=B0+(R-1.2*R1)*VP
      ELSE
      VTOT=-8875./(R**6)
      END IF
      FVTOT=VTOT/27.2
      RETURN
      END
```

Appendix 16

Subprogram MARTIN defines the interaction potentias for the Ar + He(2^1S) system according to the work of Martin et al (1978)

```
C
C   MARTIN REAL PARTS OF POTENTIALS
C   SIMILAR FOR BOTH SINGLET AND TRIPLET
C
      FUNCTION FVTOT(R)
C
C   CONSTANTS DEFINED FOR SINGLET POTENTIAL
C
      EPSTR=0.07709
      RMSTR=5.931
      B1STR=7.108
      BSTR2=5.523
      C6=4.45 E3
      C8=1.039 E5
      C10=3.115 E7
      R1STR=6.56647
      R2STR=10.081
      EPPLS=2.673
      RMPLS=2.855
      B1PLS=3.942
      C4=273
      R1PLS=3.2843
      R2PLS=5.71
      R0=4.753
      D=0.5513
      B1S=-6.16719984E-2
      B2S=1.5246608 E-2
      B3S=1.81019946 E-3
      B4S=-1.251769772 E-3
      B1P=-2.13898993
      B2P=0.77593273
      B3P=-0.43253151
      B4P=7.70151019E-2
C
C     CONVERT R FROM AU TO ANGSTROMS
C
      R=R*0.52917706
C   CALCULATE VTOT AS A FUNCTION OF R
C
C   IF R LESS THAN R1STR IMPLIES VSTR= A MORSE POTENTIAL
C
      IF(R.LE.R1STR)  THEN
      IF(R.LE.RMSTR)  THEN
      ZSTR=EXP(-B1STR*(R/RMSTR-1.))
      ELSE
      ZSTR=EXP(-B2STR*(R/RMSTR-1.))
      END IF
      VSTR=EPSTR*ZSTR*(ZSTR-2.)
      ELSE
C
C   IF R LESS THAN R2STR IMPLIES VSTR= SPLINE INTERPOLATION
C
      IF(R.LT.R2STR)THEN
      VSTR=B1S+(R-R1STR)*(B2S+(R-R2STR)*(B3S+(R-R1STR)*B4S))
      ELSE
C
C   R GREATER THAN R2STR IMPLIES VSTR= VAN DER WALL
C
C
      VSTR=-C6*R**(-6)-C8*R**(-8)-C10*R**(-10)
```

```
      END IF
      END IF
C
C   DETERMINE VPLS
C
C   IF R LESS THAN R1PLS IMPLIES VPLS= MORSE POTENTIAL
C
      IF(R.LE.R1PLS)THEN
      ZPLS=EXP(-B1PLS*(R/RMPLS-1.))
      VPLS=EPPLS*ZPLS*(ZPLS-2.)
      ELSE
C
C   IF R LESS THAN R2PLS IMPLIES VPLS= SPLINE INTERPOLATION
C
      IF(R.LT.R2PLS)THEN
      VPLS=B1P+(R-R1PLS)*(B2P+(R-R2PLS)*(B3P+(R-R1PLS)*B4P))
      ELSE
C
C   IF R GREATER THAN R2PLS IMPLIES VPLS=VAN DER WALL
C
      VPLS=-C4*R**(-4)
      END IF
      END IF
C
C   DETERMINE SWITCHING FUNCTION
C
      FR=(1.+EXP((R0-R)/D))**(-1)
      FVTOT=(1.-FR)*VPLS+FR*VSTR
      FVTOT=FVTOT*1.59477  E-3
      R=R/0.52917706
      RETURN
      END
```

Appendix 17

CRS calculates the best constants A and B in Equations 6.2 and 6.5 to fit the experimental data, using a subprogram CURFIT (Bevington 1969) this in turn links with other subprorams (FCHISQ, FDERIV, MATINV, all defined by Bevington and FUNCTN defined in Appendix 18)

```
C
C     CRS2 1/5/90
C     CALCULATES THE CROSS SECTION WITH THE
C     BEST FIT TO MY DATA, AND FINDS CHI SQUARED
C     THE VALUES OF A, AND DA ARE MODIFIED
C     LINKS WITH CURFIT, WHICH LINKS WITH FUNCTN, AND
C     FCHISQ, FDERIV, MATINV, FUNCTN LINKS WITH FVTOT AND FWTOT
C
      DIMENSION X(20),A(10),YFIT(20),Y(20),DELTAA(10),
     1 SIGMAA(10),SIGMAY(20)
      CK1=0.
      CK2=0.
C
C     FIRST INPUT THE DESIRED VELOCITIES IN KM/S
C     THE EXPERIMENTAL  Y VALUES AND THEIR ERRORS
C
      PRINT*, 'CRS CALCULATES THE THEORETICAL  CROSS SECTION'
      PRINT*, 'AND THE MINIMUM  CHI SQUARED'
      PRINT*, 'THREE MODES CAN BE USED TO WEIGHT THE RESULT'
      PRINT*,'A       MODE=+1 WEIGHT=1/DY**2'
      PRINT*,'B       MODE=0  WEIGHT=1'
      PRINT*,'C       MODE=-1 WEIGHT=1/Y'
      PRINT*
      PRINT*, 'ENTER DESIRED WEIGHTING MODE'
      PRINT*
      READ*,MODE
      PRINT*,'MODE=',MODE
      PRINT*
      PRINT*,'INPUT  THE NUMBER OF DATA POINTS '
      PRINT*
      READ*,NPTS
      PRINT*,' INPUT X(KM/S), Y(CM**2 E-16), DY'
      PRINT*
      DO 10 I=1,NPTS
      READ*,X(I),Y(I),SIGMAY(I)
10    CONTINUE
      DO 20 I=1,NPTS
      WRITE(*,*)  I,X(I),Y(I),SIGMAY(I)
20    CONTINUE
      PRINT*, ' TO CHANGE A VALUE TYPE ITS LIST NUMBER'
      PRINT*,'RETURN  THEN THE CORRECTION '
      PRINT*,'WHEN  FINISHED TYPE 100'
      PRINT*
30    READ*,I
      IF(I.EQ.100)GO  TO 40
      READ*,X(I),Y(I),SIGMAY(I)
      GO TO 30
40    CONTINUE
      PRINT*,'I,  X(I), Y(I), DY(I)'
      DO 45 I=1,NPTS
      WRITE(*,*)  I,X(I),Y(I),SIGMAY(I)
45    CONTINUE
C
C     CONVERT  Y TO AY BY MULTIPLYING  BY 3.57
C
      DO 46 I=1,NPTS
      Y(I)=Y(I)*3.57
46    CONTINUE
```

```
C
C     INPUT A PARAPETERS  AND DA INCREMENTS
C
      PRINT*,'INPUT  THE NUMBER OF PARAMETERS  '
      PRINT*
      READ*,NTERMS
      DO 47 I=1,NTERMS
      SIGMAA(I)=1.
47     CONTINUE
      PRINT*,'INPUT  PARAMETERS  A,DA'
      PRINT*
      DO 50 I=1,NTERMS
      READ*,A(I),DELTAA(I)
50     CONTINUE
      DO 60 I=1,NTERMS
      WRITE(*,*)  I,A(I),DELTAA(I)
60     CONTINUE
      PRINT*,  ' TO CHANGE A VALUE TYPE ITS LIST NUMBER'
      PRINT*,'RETURN  THEN THE CORRECTION  '
      PRINT*,'WHEN  FINISHED TYPE 100'
      PRINT*
70     READ*,I
      IF(I.EQ.100)GO  TO 80
      READ*,A(I),DELTAA(I)
      GO TO 70
80     DO 90 I=1,NTERMS
      WRITE(*,*)  I,A(I),DELTAA(I)
90     CONTINUE
      PRINT*
C
C     USE CURFIT TO MINIMISE  CHI SQUARED
C
      FLAMDA=0.001
95     CALL CURFIT(X,Y,SIGMAY,NPTS,NTERMS,MODE,A,DELTAA,
     1 SIGMAA,FLAMDA,YFIT,CHISQR)
      PRINT*,  '      I,      X,      Y,      YFIT'
      DO 100 I=1,NPTS
      WRITE(*,*)  I, X(I),  Y(I)/3.57,  YFIT(I)/3.57
      PRINT*
100    CONTINUE
      PRINT*,  'I, A, DA, SIGMAA'
      DO 105 J=1,NTERMS
      WRITE(*,*)  J,A(J),DELTAA(J),SIGMAA(I)
      PRINT*
105    CONTINUE
      PRINT*,  'CHI SQUARED=',CHISQR
      PRINT*
C
C     TEST TO SEE IF CHISQR HAS REACHED  A MINIMUM
C
      CK1=CK2
      CK2=CHISQR
      DIF=ABS(CK2-CK1)/CK2
      IF(DIF.GT.0.001)  GO TO 95
      PRINT*,'THE  FINAL VALUE OF CHI SQUARED  =',CHISQR
      STOP
      END
```

Appendix 18

subprogram FUNCTN calculates the ionisation cross section at collision velocity defined by CRS and calls the subprograms FVTOT (the real part of the interaction potential given in Appendix 12 - 16) and FWTOT (the imaginary part of the interaction potential)

```
C
C   FUNCTN 4/4/90
C   LINKS WITH GRIDLS, FVTOT, FWTOT
C   CALCULATES THE CROSS SECTION AT A GIVEN
C   VALUE OF X THE COLLISION VELOCITY
C
C   RTP IS CALCULATED FOR EACH VALUE OF L,
C   THE ANGULAR MOMENTUM, AND USED TO FIND PL
C   THE PROBABILITY OF IONISATION FOR CHANNEL L
C   THE SUM OF PL OVER L IS THE CROSS SECTION QCROS
C
      FUNCTION FUNCTN(X,I,A)
      DIMENSION X(20), A(10)
C
C     R = THE ATOMIC SEPARATION
C     IDL = THE INCREMENT OF L
C
C     DRAD = INCREMENT OF R
C     RTP  = YHE TURNING POINT WHERE VRAD=0
C     VRAD = YHE RADIAL VELOCITY FROM
C        SCHRODINGERS EQUATION
C   PLA2 =(h/2PI)**2  = 1 IN AU
C   AMU  = THE REDUCED MASS IN AU
C   XI   = COLLISION VELOCITY IN AU
C   E0   = COLLISION ENERGY IN AU
C   CK0SQ     = K ZERO SQUARED  IN AU
C   VTOT = REAL POTENTIAL  IN AU
C   WTOT = IMMAGINARY  POTENTIAL  IN AU
      PI=3.1415926
      AL=0.
      R=1.
      DL=1.
      QCROS=0.
      DRAD=0.2
      AMU=3.6364*1836.152
      PLA2=1.0
      RTP=0.
      XI=X(I)*4.5732  E-4
      E0=0.5*AMU*XI**2.
C
C   FIRST FIND THE TURNING POINTS FOR L
C
      CK0SQ=2.*AMU*E0/PLA2
10     CONTINUE
      RTP=0.
      DRAD=0.2
11     CONTINUE
      VTOT=FVTOT(R)
      CVRAD=(1.-VTOT/E0-AL*(AL+1.)/(CK0SQ*R**2.))
      IF(CVRAD.GT.0.)  THEN
      IF(DRAD.GT.1E-9)  THEN
      R=R-DRAD/2.
      DRAD=DRAD/2.
      ELSE
      RTP=R
      END IF
      ELSE
      R=R+DRAD
```

```
      ELSE
      R=R+DRAD
      END IF
      IF(RTP.EQ.0.)  GOTO 11
C
C   USE RTP TO FIND PL
C
      SUMINT=0.0
      THETA=0.001
      DTHETA=0.02
C
C   INTEGRATE  FROM 0 TO PI/2
C
15     CONTINUE
      R=RTP/COS(THETA)
      VTOT=FVTOT(R)
      WTOT=FWTOT(R,  A)
      VRAD=XI*(1.-VTOT/E0-AL*(AL+1.)/(CK0SQ*R**2))**0.5
      SINT=WTOT*R*TAN(THETA)*DTHETA/(PLA2*VRAD)
      SUMINT=SUMINT+SINT
      VUL=SINT/SUMINT
      IF(VUL.LT.1  E-10) THEN
      THETA=1.57
      ELSE
      END IF
      THETA=THETA+DTHETA
      IF(THETA.LE.1.57)  GOTO 15
      IF(SUMINT.GE.44)  THEN
      PL=1.
      ELSE
      PL=1.-EXP(-2*SUMINT)
      END IF
C
C   ADD PL TOGETHER  TO GET THE CROSS SECTION
C
      DCROSS=PI/CK0SQ*(2*AL+1.)*PL*DL
      QCROS=QCROS+DCROSS

C
C   MOVE ON TO NEXT L, BUT FOR LARGE L
C   AVERAGE  OVER A GROUP OF L BECAUSE OF SLOW
C   VARIATION  OF VTOT AT LARGE L
C
      IF(AL.LT.50.)  THEN
      DL=1.
      ELSE IF(AL.LT.100.)  THEN
      DL=2.
      ELSE IF(AL.LT.300.)  THEN
      DL=5.
      ELSE
      DL=10.
      END IF
      AL=AL+DL
      R=RTP-1.
      FRA=DCROSS/QCROS
      IF(FRA.GT.1  E-4) GOTO 10
      PRINT*,I,X(I),QCROS/3.57,AL
C     FINALY  RETURN THE CROSS SECTION TO THE
C     MAIN  PROGRAM
C
50    FUNCTN=QCROS
      RETURN
      END
```

References

Allison W. 1978 Ph.D. Thesis, University of London

Benton E E. Ferguson E E. Matsen F A. and Robertson W W. *Phys.Rev.***128**,206 (1962)

Berkling K. Helbing R. Kramer K. Pauly H.Schlier C H. and Toschek P. *Z. Phys.* **166,** 406 (1962)

Bevington P R. *Data reduction and error analysis for the physical sciences* (New York McGraw Hill) (1969)

Brehem B. and Von Puttkamer *Z. Naturforsch* **22a,** 8 (1967)

Brutschy B. and Haberland H. *J. Phys.E: Sci. Instrum.* **10,** 91 (1977)

Brutschy B. and Haberland H. *J. Phys. E: Sci Instrum.* **13,** 150 (1980)

Brutschy B. and Haberland H. and Schmidt K. *J. Phys. (B): At Mol Phys.* **9,** 2693 (1976b)

Brutschy B. and Haberland H. and Werner F. *J. Phys. (B): At Mol Phys.* **15,** 731 (1982)

Burdenski S. Feltgen R. Lichterfeld F. and Pauly H. *Chem. Phys. Lett.* **78,** 296 (1981)

Čermák V. *J. Chem. Phys.* **44,** 1318 (1966a)

Čermák V. *J. Chem. Phys.* **44,** 3774 (1966b)

Čermák V. *J. Chem. Phys.* **44,** 3781 (1966c)

Čermák V. *J. Electron Spectrosc.Relat Phenom.* **9,** 419 (1976)

Čermák V. and Yencha A L. *J. Electron Spectrosc.Relat Phenom.* **8,** 109 (1976)

Čermák V. and Yencha A L. *J. Electron Spectrosc.Relat Phenom.* **11,** 67 (1977)

Chantry P J. *J. Chem. Phys.* **55,** 2746 (1971)

Cohen S J. and Lane S F. *J. Chem. Phys.* **66,** 586 (1976)

Dunning F B. and Smith A C H. *J. Phys.* (B) **4,** 1683 (1971)

Dunning F B. Smith A C H. and Stebings R F. *J. Phys.* (B) **4,** 1683 (1971)

Eland J H D. *Photoelectron Spectroscopy.* p180 (John Wiley, New York, 1974)

Eland J H D. *Mass Spectrometry,* Special Periodical Reports, Vol 5, p91 (The Chemistry Society, London, 1979)

Fahey D W. Parks W F. and Schearer L D. *J. Phys.* (E) **13,**381 (1980)

Ferguson E E. Fehsenfeld F C. and Schmeltikopf A L. *Adv.At Mol.Phys.***5,**1 (1969)

Fuchs V and Niehaus A. *Phys.Rev.Lett.* **21,** 1136 (1968)

Haberland H. and Schmidt K. *J. Phys.* (B) **10,** 695 (1977)

Harper S F W. 1977 Ph.D. Thesis, University of London

Harper S F W. Davies G R. Smith A C H. XIIth ATMOL conference, Oxford (1980), (Institute of Physics)

Herman Z. and Čermák V. *Coll. Czech. Chem. Commun* **31,** 649 (1966)

Herce J A. Foster K D. and Muschlitz E E. *Bull. Am. Phys. Soc.* **13,** 206 (1968a)

Herce J A. Penton J R. Cross R J. and Muschlitz E E. *J. Chem. Phys.* **49,** 958 (1968b)

Hickman A P. Isaacson A D. and Miller W H. *J. Chem. Phys.* **66,** 1483 (1977a)

Hickman A P. Isaacson A D. and Miller W H. *J. Chem. Phys.* **66,** 1492 (1977b)

Hodge L A. Dunning F B. and Walters G K. *Rev. Sci. Instrum.* **50,** 1 (1979)

Hotop H. Kolb E. Lorenzen J. *J. Electron Spectrosc.Relat Phenom.* **16,** 213 (1979)

Hotop H. Niehaus A. *Z. Phys. B* **228,** 68 (1969)

Hotop H. Niehaus A. *Chem. Phys. Lett.* 3, 687 (1969)

Hotop H. Niehaus A. Schmeltekopf A L. *Z. Phys. B* **229,** 1 (1969)

Howard J S. Riola J P. Rundel R D. and Stebbings *Phys. Rev. Lett.* **29,** 321 (1972)

Glow Discharges, chapter VIII page 235

Illenberger E. and Niehaus A. *Z. Phys. B* **20,** 33 (1975)

Jerram P A. 1985 Ph.D. Thesis, University of London

Jerram P A. and Smith A C H. *J. Phys.* (B) **18,** 1747 (1985)

Katsuura K. *J. Chem. Phys.* 42, 3771 (1965)

Keliher P J. Dunning F B. O'Neill M R. Rundel R D. and Walters G K. *Phys. Rev.*(A) **11,** 1271 (1975a)

Keliher P J. Gleason R E. and Walters G K. *Phys. Rev.*(A) **11,** 1279 (1975b)

Kroon J P C. 1985 Ph.D. Thesis, Eindhoven University of Technology

Lang N C. Lilenfeld H V. and Kinsey J L. *J. Chem. Phys.* **55,** 3114 (1971)

Lindinger W. Schmeltekopf A L. and Fehsenfeld F C. *J. Chem. Phys.* **61,** 2890 (1974)

MacLennan (1966) *Phys. Rev.* **148,** 218 (1966)

Märk T D. and Oskam H J. *Phys. Rev.* (A) **4,** 1445 (1971)

Martin D W. Gregor R W. Jordan R M. and Siska P E. *J. Chem. Phys.* **69,** 2833 (1978)

Massey and Burhup *Electronic and ionic impact phenomena* (vol 3) P 1363 (Oxford University Press 1971)

Miyazaki K. Ogata Y. Fujimoto T. and Fukuda K. *Japan. J. Appl. Phys.* **13,** 1866 (1974)

Miller W H. *J. Chem. Phys.* **52,** 3563 (1970)

Miller W H. Slocomb C A. and Schaefer H F. *J. Chem. Phys.* **56,** 1347 (1972)

Miller W H. and Morgner H. *J. Chem. Phys.* **67,** 4923 (1977)

Mori M. *J. Phys. Soc. Japan* **21,** 979 (1966)

Mori M. *J. Phys. Soc. Japan* **26,** 773 (1969)

Mosely J T. Peterson J R. Rundel R D. and Stebbings R F. *Phys.* Rev. (A) **6,** 1025 (1972)

Munakata T. Kuchitsu K. and Harada Y. *Chem. Phys. Lett.* **64,** 409 (1979)

Mũnzer A. 1978 Diplomarbeit University University of Freiburg (1978)

Nakamura *J. Phys.* Soc. Japan **26,** 1473 (1969)

Nakamura *J. Phys.* Soc. Japan **31,** 574 (1971)

Nakamura *J. Phys.* (B) **8,** L489 (1975)

Nakamura *J. Phys.* (B) **9,** L59 (1976)

Niehaus A. *Ber. Bunsenges. Phys. Chem.* **77,** 632 (1973)

Ohno K. Mutoh H. Harada Y. *J. Am. Chem. Soc.* **105,** 4555 (1983)

Olsen R E. *Phys. Rev A* **6,** 1031 (1972)

Parr T P. Parr D M. and Martin R M. *J. Chem. Phys.* **76,** 1 (1982)

Pauly H. *Z. Naturforsch* **15a** 227 (1960)

Penning F M. *Naturwissenschaften* **15a,** 818 (1927)

Penning F M. *Physica* **1,** 1028 (1934)

Pesnelle A. Watel G. and Manus C. *J. Chem. Phys.* **62,** 3590 (1975)

Phelps A V. *Phys. Rev.* **114,** 1011 (1959)

Riola J P. Howard J S. Rundel R D. and Stebbings R F. *J. Phys.* (B) **7,** 376 (1974)

Rees M J. Sciama D W. and Strobbs S H. *Astrophysical Letters* **2,** 243 (1968)

Sholette W P. and Muschlitz E E. Jr *J. Chem. Phys.* **36,** 3368 (1962)

Schmeltekopf A L. and Fehsenfeld, F C. *J. Chem. Phys.* **53,** 3173 (1970)

Sidiqui H R. Bernfeld D. Siska P E. *J. Chem. Phys.* **80,** 1 (1984)

Sinda T. *Phys. Lett.* **33a,** 225 (1970)

Siska P E. *Chem. Phys. Lett.* **63,** 25 (1979)

Siska P E. *J. Chem. Phys.* **71,** 3942 (1979)

Smith F T. Marchi R P. Aberth W. Lorents D C. and Heinz O. *Phys. Rev.* **161,** 31 (1967)

Trujillo S M. 1975 Ph.D. Thesis, University of London

Theuws P G A.Beijerinck H C W. Verster N F. Schram D C. *J. Phys. E: Sci Instrum.* **15,** 573 (1982)

Tuffin F. Le Coz G. and Peresse J. *J. de Phys. Lett.* **42,** L25 (1981)

Ueno T. Yokoyama A. Takao S. and Hatano Y. *Chem. Phys.* **45,** 261 (1980)

VanDyke R S. Johnson C E. and Shugart H A. *Phys. Rev. Lett.* **25,** 1403 (1970)

Webb C E. *Inst. Phys. Conf. Ser* **29,** 1 (1976)

West W P. Cook T P. Dunning F B. Rundel R D. and Stebbings R F. *J. Chem. Phys.* **63,** 1237 (1975)

Woodard M R. Sharp R C. Seely M L. and Muschlitz E E. Jr *J. Chem. Phys.* **69,** 2968 (1978)

Woosdsworth J R. and Moos W H. *Phys. Rev. (A)* **12,** 2455 (1975)